POLITECNICO DI TORINO

UNIVERSITÀ DEGLI STUDI DI TORINO

Doctoral Dissertation
Doctoral Program in Pure and Applied Mathematics (38^{th} cycle)

Phenotype-structured integro-differential models: derivation and qualitative analysis

Author:
Emanuele BERNARDI

Supervisor:
Prof. Tommaso LORENZI
Prof. Andrea TOSIN

Politecnico di Torino - Università di Torino

October 2025

Declaration of Authorship

I hereby declare that, the contents and organization of this dissertation constitute my own original work and does not compromise in any way the rights of third parties, including those relating to the security of personal data.

Emanuele BERNARDI
December 19, 2025

Alla mia famiglia,
a chi mi è stato sempre vicino
e ai miei fallimenti

Abstract

In this thesis, we derive, analyse, and simulate several different integro-differential models, bridging the microscopic description of individual processes with mesoscopic and macroscopic representations of collective dynamics. The common thread running through the work is the use of a stochastic approach to connect individual-level mechanisms with emergent evolutionary dynamics at the population scale.

In the first chapter, we build upon and generalise kinetic theory approaches for multi-agent systems to develop a non-conservative modelling framework for phenotype-structured populations. We start from a stochastic agent-based formulation that describes individual dynamics driven by fundamental biological processes such as death, proliferation, and phenotype changes. Then, at the mesoscopic level, we formally derive the integro-differential equation governing the evolution of the population's phenotypic distribution. Subsequently, we consider a quasi-invariant regime of small and frequent phenotype changes and rigorously derive a non-local Fokker-Planck-type equation counterpart of this model.

In the second chapter, we extend this modelling framework to multi-compartmental systems structured by continuous variables representing the levels of expression of compartment-specific traits. We contextualise our construction within an epidemiological framework and, following an analogous multi-scale procedure as in the previous chapter, derive a system of integro-differential equations at the mesoscopic level and a system of ordinary differential equations at the macroscopic level. We then obtain a general formula for the basic reproduction number $\mathcal{R}_0$ for a reduced version of the previous system. This quantity is expressed directly in terms of key microscopic functions and parameters, thereby highlighting the connections between fundamental processes at the microscopic level and the resulting population-scale dynamics.

In the third chapter, we introduce a model describing the co-evolutionary dynamics of two interacting and structurally heterogeneous subsystems: nutrients and consumers. Each subsystem features its own compartmental subdivision and is endowed with a specific structural variable that characterises its internal heterogeneity. Then, we consider a suitable quasi-stationary limit and, by exploiting the conservative properties of the system, reduce the dynamics to a coupled system of integro-differential equations. Thus, we prove a well-posedness theorem ensuring existence, uniqueness, and positivity of the solutions. Finally, we investigate the

asymptotic regimes of the model, identifying the set of fittest traits and characterising the emergence of selection phenomena through both analytical and numerical results.

Finally, in the fourth chapter, we outline several future research perspectives, including, among others, the application of the techniques developed in this thesis to the context of non-convex optimisation. Preliminary numerical experiments suggest that the stochastic mechanisms underlying the models of the previous chapters may inspire new metaheuristic algorithms, offering promising directions for future interdisciplinary research.

Contents

Introduction

Mathematics is widely recognized as an interdisciplinary language, providing formal frameworks to understand phenomena in fields from physics and engineering to biology, economics, and social sciences. Its abstract formalism serves as a common language that bridges disparate disciplines and encourages the transfer of methods and ideas. Vertical developments within specific disciplines increasingly intersect with horizontal exchanges across fields, fostering a dialogue that connects distinct areas of knowledge. There are numerous cases in which mathematical formalism has been borrowed to describe phenomena far removed from its original domain. This occurs not only because such a framework provides theoretical validation, but also because it introduces a shift in perspective, often generating new insights and research directions, even in well-established areas.

Among the approaches that best exemplify this extension of mathematical formalism to heterogeneous contexts, agent-based models, and, more generally, particle-based models, occupy a prominent position. These methodological frameworks are particularly well-suited to the study of complex systems, owing to several key features. The assumptions underpinning these models are, in most cases, simple and intuitive. In applied contexts, they are often directly supported by empirical evidence. Moreover, the stochastic nature of the microscopic dynamics allows the modeller to retain the intrinsic randomness of many real-world phenomena, phenomena which, although governed by recognisable patterns, cannot be considered fully deterministic. The value of these models increases when they are not constrained to describing a specific scenario, but instead aim to identify general regularities.

The core mathematical challenge, then, lies in designing a model that not only aligns with observed data but also remains analytically tractable and suitable for rigorous mathematical analysis. In this work, we develop models that operate at the interface between microscopic, mesoscopic, and macroscopic descriptions, with particular attention to biological systems in which population structure and trait evolution play a central role. Therefore, the ultimate goal is to contribute to the mathematical understanding of the evolutionary IDEs arising in the study of biological phenomena.

Different scales

A key feature of our approach is the ability to investigate a phenomenon across multiple *scales*. These may correspond to different levels of organisation (for example, in a biomedical context: gene → protein → cell → tissue → organ → organism) or to different degrees of abstraction (see Figure A). While empirical observation typically takes place at the macroscopic level, constructing a mathematical model directly at this scale often results in overly rigid or limited representations. By contrast, starting from a microscopic description allows for greater flexibility, enabling the model to capture a wider variety of scenarios. The principal difficulty lies in translating macroscopic observations into the elementary rules that govern microscopic interactions [9]. The modelling choices made at this level must, in principle, be general, yet sufficiently structured to remain consistent with the information available at each relevant scale. This consistency is most clearly reflected in the derivation of the model's mesoscopic counterpart, which is often formulated in terms of parabolic (or elliptic) integro-differential equations (IDEs). In this framework, the unknown function typically represents the distribution of a selected property within the population under study.

Since obtaining analytical expressions for the solutions at all times is generally intractable, the investigation at this level is primarily concerned with the asymptotic behaviour of the solutions. This step proves to be crucial, especially in the final phase of validation, when one returns to the macroscopic scale, and the theoretical results obtained can be compared with empirical evidence.

Kinetic paradigm

The primary objective is to develop a formal mathematical framework that is as uniform as possible, so that it can be adapted to different problems without compromising its structure. Our approach is based on a stochastic agent-based construction which follows the kinetic paradigm introduced by Boltzmann in the second half of the 19^{th} century [33]. In recent decades, this methodology has played an increasingly central role, establishing itself as one of the most versatile tools for modelling complex and heterogeneous phenomena within a coherent mathematical framework. As a matter of fact, kinetic theory evolved into a conceptual framework to model multi-agent systems[118, 129], i.e., systems composed of a large number of interacting entities that, as a result of their interactions, give rise to an often non-trivial collective behaviour. To name just a few representative contexts in which this framework has been applied successfully, we recall the analysis of socio-economic phenomena, such as opinion formation [36, 71, 79, 141] and wealth distribution [23, 26, 54, 70], of vehicular traffic [34, 135, 142], and more recently of the spread of infectious diseases [30, 67, 68, 116–118]. Moreover, kinetic equations have also been employed to study the theoretical properties of particle-based algorithms for non-convex optimisation [20, 43]. The main strength of our perspective

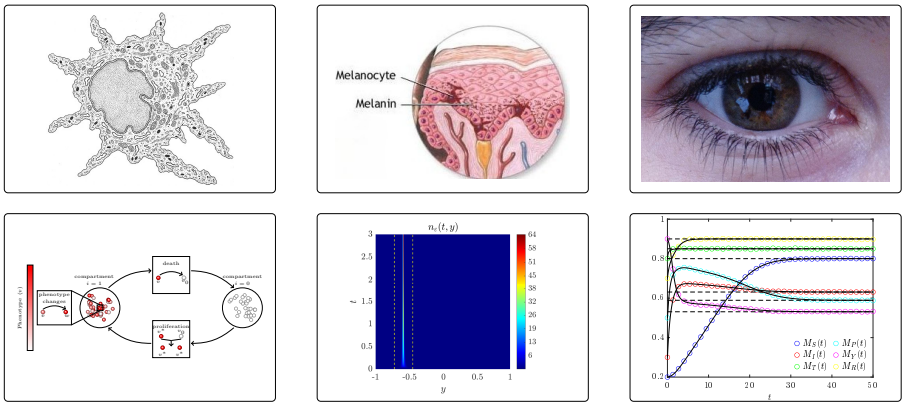

FIGURE A: Representation of the different scales that can be described through agent-based models. The first column illustrates the *microscopic* level, where each individual entity, for example, a pigmented cell such as a melanocyte (top panel; images inspired by content from [121]), is characterised by its specific phenotype. From a mathematical perspective, this level is modelled through rules governing the evolution of the phenotype of each agent (bottom panel; microscopic processes in Figure 1.1). The second column depicts the *mesoscopic* level, in which the focus shifts to the environment hosting the individuals, in our example an epithelial tissue (top panel; image inspired by content from [125]), and to the analysis of the evolution of the phenotypic trait distribution across the population (bottom panel; Selection process in Figure 3.5). Finally, the third column represents the *macroscopic* level, where the analysis concerns aggregated quantities such as the total population mass, the mean, or variance of the distribution (bottom panel; mean evolution in Figure 2.5). The temporal evolution of these quantities determines the macroscopic features of the biological system under study, in our example, skin or eye colour.

lies in its ability to bridge microscopic agent behaviour with emergent macroscopic phenomena, through well-defined intermediate (mesoscopic) representations.

Therefore, the population under consideration consists of a large number of individuals, assumed to be indistinguishable except for a continuous structural variable. Just as the particles of a rarefied gas are characterised, at each time $t \in \mathbb{R}_+$, by their position $x \in \mathbb{R}^3$ and velocity $v \in \mathbb{R}^3$, the individuals in the population are described by a *microscopic state* $x \in \mathbb{R}^d$. This variable can represent a specific trait of the agent, such as age [38, 95, 96, 140], resistance to infection or level of immunity [18, 81, 94, 110, 112], viral or pathogen load [17, 60, 110], or phenotypic [2, 7, 37, 145] and socio-economic characteristics [23, 24, 67, 68]. Trait evolution occurs as a result of interactions between agents or with the surrounding environment. Nevertheless, spontaneous transitions are also taken into account, as it is natural to expect that the intensity of the trait may evolve even in the absence of direct interactions. Taken together, these assumptions imply that the evolution of the microscopic state depends exclusively on its previous configuration, thereby giving

rise to a Markovian process.

Beyond the continuous structural trait, the microscopic state in the models considered here also includes a discrete label encoding a compartmental structure of the population. This structure is particularly useful when agents play distinct roles in the system's dynamics. Therefore, the meaning of the variable x depends on the compartment to which the individual belongs. For instance, in epidemic models, susceptible individuals can be characterized by their level of immunity, whereas for infected individuals, the variable represents the viral load.

Starting from this individual-based description, it is possible to derive mesoscopic evolution equations, such as integro-differential or partial differential equations, that describe the population-level dynamics of trait distributions.

Structured population dynamics

As a formal derivation from an underlying individual-based model, the resulting mesoscopic equations yield a faithful mean-field approximation of the microscopic dynamics and the interactions between individuals. The form of the equations at this level depends on how changes in the microscopic state are defined, which are encoded through suitable transition kernels. These operators take on different forms depending on the specific phenomenon being modelled.

The analysis then focuses on the evolution of a generic observable of the system, from which the weak formulation of the equation governing the evolution of the distribution $f(x,t)$ is derived. This procedure is analogous to that used in the derivation of the homogeneous Boltzmann equation [118, 129, 130], where binary particle interactions give rise to a bilinear integral operator. In the present setting, however, the goal is not necessarily to obtain a Boltzmann-type equation. Indeed, although an integral term is still present, it primarily models spontaneous variations in the trait and thus has a linear structure. In general, the resulting mesoscopic equation features a reaction term, accounting for proliferation and death, and a diffusion term. The latter may appear in integral form or as a differential operator.

At this point, the equation we get is characterized by the specific phenomenon under study. In Chapter 1, for instance, we analyse the phenotypic evolution of a population, driven by two main mechanisms: the selection of the trait best adapted to the environment, and the presence of small mutations, which help maintain phenotypic variability and thus facilitate adaptation to potential environmental changes (*selection–mutation* model [131, 136, 139]). Indeed, depending on the choice of the transition kernels, different modelling scenarios can emerge, such as epidemic outbreaks (Chapter 2) or a chemostat-like system involving nutrient dynamics (Chapter 3).

The next step consists of the analysis of the stationary states of the distribution, a key methodological step for understanding the system's asymptotic behaviour. In

this perspective, the main research directions include the study of long-time convergence to gain qualitative insight into the stationary state, as well as the analysis of the associated integral operator[40, 62, 108, 131, 136, 137]. More specifically, a paradigmatic example is the use of the WKB ansatz and the Hamilton–Jacobi approach, aimed at characterising the structure and properties of stationary solutions [50, 51, 66, 131].

Alternatively, by identifying an appropriate parameter choice, one can explore quasi-invariant limit regimes, in which, for example, trait variations are frequent but small, and the Boltzmann-type integral operator can be approximated by a differential operator of Fokker–Planck type[22, 110]. Such a transformation of the equation allows for simplified asymptotic approximations and provides a clearer understanding of the model's behaviour in limiting cases[22].

Finally, the linear stability analysis of stationary solutions plays a fundamental role, as it assesses the robustness of these states with respect to small perturbations and completes the theoretical picture of the system's asymptotic dynamics [58, 62, 93, 137].

Macroscopic modelling and conservation issues

It is useful to clarify the meaning attributed in this work to the expressions "macroscopic model" or "macroscopic level." In general, these refer to a class of mathematical models that describe the evolution of collective or average quantities associated with a complex system, without explicitly representing the dynamics of individual agents. In our context, we specifically consider aggregate quantities such as the total mass, the mean trait, or, more generally, the *principal moments* of the phenotype distribution. At this level, the aim is to abstract away from the detailed structure of the system-captured at the microscopic level and reformulated, in a first step, through a mesoscopic representation. Unlike what occurs, for instance, in fluid dynamics with the Euler or Navier–Stokes equations, where the macroscopic level retains a direct link to local state variables, here we focus exclusively on the time evolution of aggregated quantities.

The multi-scale nature of the Boltzmann-type kinetic paradigm is particularly suited to our applications, as it enables one to link rigorously, in a probabilistic-statistical manner, the mutual interactions taking place at the scale of the individuals to the aggregate trends that they generate at the level of the whole population of agents. On the other hand, those applications usually rely on conservation properties, such as the total number of agents of the population, which stand as pillars of the classical kinetic approach. However, this perspective appears to be at odds with the modelling of some other specific dynamics. For instance, in models describing gas mixtures possibly undergoing chemical reactions, the number of particles of a particular substance might not be conserved (as they transform into other substances).

Nevertheless, suitable reformulations have been developed to enable the application of the kinetic formalism even in such scenarios, where non-conservative phenomena occur, and thus the total mass of the system may change in time [11, 27–29, 31, 35, 85, 86].

Hence, it is natural to expect that similar issues may also emerge in biological settings, which are inherently characterised by processes of proliferation and death. Indeed, the total mass (i.e. the size of the population) is typically not conserved. This presents a challenge when deriving deterministic continuous models for the evolutionary dynamics of phenotype-structured populations from underlying stochastic agent-based models, which track proliferation, death, and phenotype changes of single population members. Such a challenge has so far been tackled through probabilistic methods [47, 49], which make it possible to rigorously derive population-level models as the limit of corresponding agent-based models when the number of population members tends to infinity, and formal limiting procedures [12, 52], which enable one to obtain the population-scale counterparts of on-lattice agent-based models when the lattice parameters tend to zero.

However, in other works built on kinetic approaches, this challenge has been addressed by considering a population that is subdivided, for example, into compartments [30, 110] or distributed across the nodes of a graph [116, 117]. In these contexts, changes in the number of individuals are not treated as variations in total mass, but rather as transitions between different subsets of the overall population. A typical example is provided by epidemiological models that include, among the compartments, a class representing deceased individuals [39]. In this way, the model structure allows for the preservation of the total number of individuals, which may also reflect a physical constraint of the system, such as the *carrying capacity*. Therefore, this construction results in the best choice also for modelling phenotype-structured populations.

Monte Carlo methods

The use of a kinetic agent-based framework to define the microscopic structure underlying our model offers an additional advantage: such systems can be efficiently implemented numerically using Monte Carlo methods [118, 127–129]. This broad class of algorithms relies on the idea of discretising only time, allowing a finite sample of particles, each identified by their microscopic state, to evolve according to stochastic rules.

These numerical schemes are particularly well-suited for simulating dynamics involving large populations. In our case, the Monte Carlo approach proves advantageous, as its stochastic and particle-based nature closely aligns with the agent-based structure of the models under consideration. On the other hand, although the convergence of these methods is theoretically guaranteed, it typically requires

large sample sizes. It is well known that this class of algorithms exhibits a convergence rate of order $O(N^{-1/2})$[129], which implies that doubling the accuracy requires quadrupling the number of samples. For this reason, it is essential to adopt implementations that minimise redundant loops and maximise computational efficiency through effective parallelisation.

Among the various implementations, the Nanbu–Babovsky scheme [15, 124] provides a particularly efficient strategy for kinetic-type systems. It approximates the system's evolution through stochastic binary interactions between sampled particles, thereby preserving key conservation properties while maintaining computational tractability. This makes it well-suited for the class of interaction-driven models analysed in this thesis, where capturing the correct statistical behaviour is often more relevant than resolving deterministic trajectories in full detail.

Outline of the thesis

In the **first chapter**, we construct a structured agent-based model for a population divided into two compartments. The dynamics involve an active compartment, which is the main focus of the analysis, and a reserve compartment, introduced to ensure the conservation of the total number of individuals and thus allow the use of kinetic formalism even for intrinsically non-conservative phenomena. Starting from the microscopic model, we derive the corresponding mesoscopic formulation, which takes the form of an integro-differential equation (IDE) governing the distribution of the microscopic structural variable (the phenotypic trait). Subsequently, the analysis focuses on the asymptotic behaviour for a quasi-invariant regime of small and frequent phenotype changes. In this limit, we rigorously derive a nonlocal Fokker–Planck-type equation counterpart of this model. We then establish the convergence of the IDE solutions and their main statistical moments towards those of the limiting PDE. The theoretical findings are illustrated through representative numerical simulations. This work has been recently submitted [22].

In the **second chapter**, we extend this modelling framework to multi-compartmental systems structured by continuous variables representing the levels of expression of compartment-specific traits. This generalisation naturally lends itself to the description of compartmental epidemiological models. After formalising the microscopic dynamics, we derive the corresponding integro-differential system and study its asymptotic limits, obtaining reduced systems for the evolution of masses and mean traits. In the homogeneous case with respect to the structural variable, we derive a general formula for the basic reproduction number $\mathcal{R}_0$ using the *Next Generation Matrix*. This quantity is expressed directly in terms of key microscopic functions and parameters, thereby highlighting the connections between fundamental processes at the microscopic level and the resulting population-scale dynamics. We also present numerical simulations of epidemiological scenarios of particular interest. This work has resulted in a scientific publication [21].

In the **third chapter**, we introduce a model describing the co-evolutionary dynamics of two interacting and structurally heterogeneous subsystems: nutrients and consumers. Each subsystem features its own compartmental subdivision and is endowed with a specific structural variable that characterises its internal heterogeneity. The mesoscopic derivation yields a conservative system of five IDEs. Then, we consider a suitable quasi-stationary limit and, by exploiting the conservative properties of the system, reduce the dynamics to a coupled system of integro-differential equations. Thus, we prove a well-posedness theorem ensuring the existence, uniqueness, and positivity of the solutions. Lastly, we investigate the asymptotic regimes of the model, identifying the set of fittest traits and characterising the emergence of selection phenomena through both analytical and numerical results.

Finally, in the **fourth chapter**, we outline several future research perspectives, including, among others, the application of the techniques developed in this thesis to the context of non-convex optimisation. Preliminary numerical experiments suggest that the stochastic mechanisms underlying the models of the previous chapters may inspire new metaheuristic algorithms, offering promising directions for future interdisciplinary research.

Chapter 1

Integro-differential model for phenotype-structured populations

Derivation and quasi-invariant asymptotics

1.1 Introduction

In this first chapter, building on kinetic theory approaches for multi-agent systems of the type advanced and adopted in [21, 110, 116, 130], and generalising them to scenarios where the total mass of the system is not conserved (i.e. mass-varying multi-agent systems), we develop a modelling framework for phenotype-structured populations that makes it possible to bridge individual-level mechanisms with population-scale evolutionary dynamics. The microscopic structuring variable $v \in \mathbb{R}$ represents a phenotypic trait of the individuals. The biological framework of reference is governed by the fundamental processes underlying epigenetic mechanisms: proliferation, death, and mutation[40, 48, 52].

These models, commonly referred to as *selection–mutation* models, capture scenarios in which only individuals with higher compatibility or *fitness* with respect to the environment are more likely to survive and reproduce[63, 131]. In such dynamics, the total number of individuals is not conserved, which hinders the direct application of standard tools from kinetic theory. To overcome this difficulty, we introduce a compartmental structure: the active population is described by compartment $i = 1$, while compartment $i = 0$ acts as a reservoir, collecting individuals that either die or provide the units required for proliferation events.

This construction ensures conservation of the total mass, in line with biological constraints that prevent unbounded population growth. Even under conditions of maximal fitness, spatial and resource limitations restrict expansion, as encapsulated

by the concept of *carrying capacity*. To account for this, compartment $i = 0$ is unstructured and aggregates all individuals with the same phenotypic trait v_0. Transitions between compartments and spontaneous phenotypic variations are modelled through random variables, consistently with the probabilistic formulation of the model.

Once the microscopic model has been defined, we derive a system oftwo integro-differential equations (IDEs) for the densities f_1 and f_0, associated with the two compartments. The equations can be decoupled, allowing the analysis to focus on f_1, which represents the dynamics of primary interest. We then consider a quasi-invariant regime for phenotypic variations, in which the transition kernel M is rescaled by a small parameter ε. This corresponds to mutations of small magnitude but occurring at high frequency. In this limit, we obtain a purely differential counterpart of Fokker–Planck type governing the evolution of f_1 [129]. After establishing a priori estimates ensuring boundedness and non-negativity of the solutions, we prove convergence of the IDE solution to that of the Fokker–Planck PDE as $\varepsilon \to 0^+$. In particular, for initial data in $L^2(\mathbb{R})$, we obtain convergence in $L^2(\mathbb{R})$ over finite time horizons. Moreover, we demonstrate convergence of the main statistical moments of the solutions, thereby establishing consistency between the two models.

In contrast to the limiting approach employed in [12, 52], which directly leads to a non-local PDE model of evolutionary dynamics analogous to the one considered here as the population-scale counterpart of an agent-based model, our approach allows one to first obtain an IDE and then derive the non-local PDE as the corresponding quasi-invariant limit. This offers a unitary method to bridge alternative representations of the evolutionary dynamics of phenotype-structured populations – from agent-based models through to IDE models to non-local PDEs. Furthermore, it makes the range of applications of our approach considerably wider, as the integral kernels comprised in IDE models permit a finer representation of the mechanisms underlying phenotype changes than the advection-diffusion terms contained in non-local PDE models. In addition, while non-local diffusion models for the evolutionary dynamics of phenotype-structured populations are usually formally derived from the corresponding IDE counterparts (see, for instance [88], and references therein), here we present a rigorous derivation under assumptions that encompass a wide spectrum of biologically relevant scenarios and lead to a non-local reaction-advection-diffusion model.

Finally, we present numerical simulations considering three scenarios corresponding to different choices of the drift coefficient. In each case, we compare the solutions of the IDE, the PDE, and the particle-based model for decreasing values of ε. The numerical results confirm the theoretical analysis, showing convergence of the integro-differential model to its differential counterpart, while also demonstrating coherence between the continuous model and the Monte Carlo approximation of the particle dynamics.

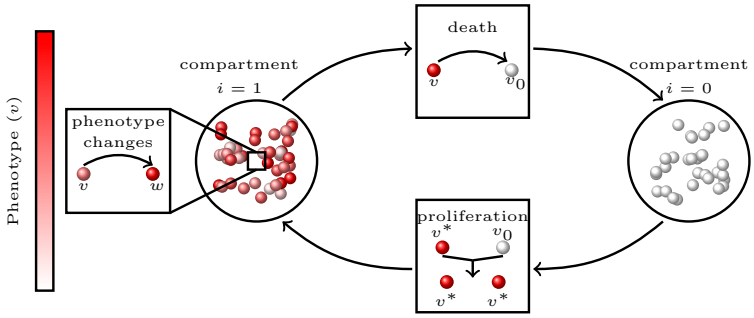

FIGURE 1.1: Schematic illustrating the conceptual framework underlying the agent-based model

The model developed in this chapter provides a first step towards constructing a microscopic agent-based framework, which will be further extended in the following chapters. Here, the focus is primarily on solution analysis and convergence results, thus establishing an initial link between kinetic theory — traditionally applied to conservative systems — and biological evolutionary dynamics, which inherently require the modelling of non-conservative phenomena.

1.2 Stochastic agent-based model

In this chapter, we consider a population structured by a continuous variable $v \in \mathbb{R}$, representing the individual phenotype and capturing variability in the proliferation and death rates of individuals. The adopted approach describes a scenario in which, in addition to spontaneous phenotypic changes, individuals can proliferate or die. This dynamics is modelled by partitioning the total population into two compartments. The first, labelled by the index 1, is structured with respect to the variable v; the second, labelled by the index 0, contains individuals characterised by an arbitrary and constant phenotypic value $v_0 \in \mathbb{R}$. As illustrated by the schematic in Figure 1.1, we conceptualise the proliferation and death of population members as *compartment switching* processes, whilst phenotypic changes undergone by population members are conceptualised as *structuring-variable switching* processes.

In more detail, between time $t \in [0, +\infty)$ and time $t + \Delta t$, with $\Delta t > 0$:

(I) The *proliferation* of a population member is modelled as an *interaction-driven compartment switching*, whereby the interaction between a focal individual in compartment $i = 0$ and an individual in compartment $i^* = 1$ with phenotype v^* leads the focal individual to transition into compartment $i^* = 1$ acquiring the phenotype v^* at rate $p(v^*)$. This results in a new individual with phenotype v^* being introduced in the population.

(II) The *death* of a population member is modelled as a *spontaneous compartment switching* (i.e. compartment switching not driven by interactions with other individuals), whereby a focal individual in compartment $i = 1$ with phenotype v spontaneously transitions into compartment $i = 0$ acquiring the phenotype v_0 at rate $d(v)$. This results in an individual with phenotype v being removed from the population.

(III) *Phenotype changes* of population members are modelled as *structuring-variable switching* processes, whereby, at rate $\mu \in \mathbb{R}_+$, a focal individual in compartment $i = 1$ switches from phenotype v to phenotype w with probability $M(w|v)$.

The functions p and d and the kernel M satisfy the following assumptions

$$p,\, d \in C(\mathbb{R}), \qquad p,\, d : \mathbb{R} \to \mathbb{R}_+, \qquad M \in \mathscr{P}(\mathbb{R};\, C(\mathbb{R})), \tag{1.1}$$

where $\mathscr{P}(\cdot)$ denotes the set of probability distributions defined on the measurable space $(\mathbb{R},\, \mathcal{B}(\mathbb{R}))$, with $\mathcal{B}(\mathbb{R})$ the Borel σ-algebra of $\mathbb{R}$.

In this conceptual framework, individuals are regarded as indistinguishable agents and their microscopic state at time t is described by the random vector $(I_t,\, V_t) \in \{0, 1\} \times \mathbb{R}$. The discrete random variable I_t specifies the compartment of an agent, while the continuous random variable V_t models the agent's phenotype at time t. We let

$$(I_t,\, V_t) \sim f(t, i, v) \tag{1.2}$$

where we use the symbol $\sim$ to indicate that a random variable is distributed according to a certain probability distribution. Moreover, we introduce the notation

$$\rho_i(t) := \int_{\mathbb{R}} f(t, i, v)\, dv. \tag{1.3}$$

The distribution function $f : \{0, 1\} \times \mathbb{R} \times [0,\, +\infty) \to \mathbb{R}_+$, being a probability density function, is such that

$$\sum_{i=0}^{1} \int_{\mathbb{R}} f(t, i, v)\, dv = \sum_{i=0}^{1} \rho_i(t) = 1, \qquad \forall\, t \geq 0. \tag{1.4}$$

Moreover, in line with (I)–(III), we let the microscopic states of the agents evolve in time due to *interaction-driven compartment switching*, *spontaneous compartment switching*, and *structure-variable switching*, which are regarded independent processes. We then model the evolution of the microscopic state $(I_t,\, V_t)$ of a focal agent between

time t and $t + \Delta t$ through the following system:

$$\begin{cases} I_{t+\Delta t} &= (1-\mathrm{S}^{\mathrm{I}})(1-\mathrm{S}^{\mathrm{II}})I_t + \mathrm{S}^{\mathrm{I}}(1-\mathrm{S}^{\mathrm{II}})I'_t + (1-\mathrm{S}^{\mathrm{I}})\mathrm{S}^{\mathrm{II}}I''_t + \mathcal{O}(\Delta t^2), \\ V_{t+\Delta t} &= (1-\mathrm{S}^{\mathrm{I}})(1-\mathrm{S}^{\mathrm{II}})\left[(1-\mathrm{S}^{\mathrm{III}})V_t + \mathrm{S}^{\mathrm{III}}W_t\right] + \mathrm{S}^{\mathrm{I}}(1-\mathrm{S}^{\mathrm{II}})V'_t \\ &\quad + (1-\mathrm{S}^{\mathrm{I}})\mathrm{S}^{\mathrm{II}}V''_t + \mathcal{O}(\Delta t^2), \end{cases} \tag{1.5}$$

where S^{I}, S^{II}, $\mathrm{S}^{\mathrm{III}} \in \{0, 1\}$ are independent Bernoulli random variables such that

$$\begin{aligned} &\mathrm{Prob}\left(\mathrm{S}^{\mathrm{I}} = 1 | I_t = i,\, V_t = v,\, I^*_t = i^*,\, V^*_t = v^*\right) = \frac{s^{\mathrm{I}}_{i,i^*}(v, v^*)\Delta t}{1 + s^{\mathrm{I}}_{i,i^*}(v, v^*)\Delta t}, \\ &\mathrm{Prob}\left(\mathrm{S}^{\mathrm{II}} = 1 | I_t = i,\, V_t = v\right) = \frac{s^{\mathrm{II}}_i(v)\Delta t}{1 + s^{\mathrm{II}}_i(v)\Delta t}, \\ &\mathrm{Prob}\left(\mathrm{S}^{\mathrm{III}} = 1 | I_t = i\right) = \frac{s^{\mathrm{III}}_i \Delta t}{1 + s^{\mathrm{III}}_i \Delta t}. \end{aligned} \tag{1.6}$$

In system (1.5), the pairs of random variables

$$(I'_t,\, V'_t | I^*_t,\, V^*_t) \sim \mathcal{T}^{\mathrm{I}}(i', v' | I^*_t,\, V^*_t) \qquad \text{and} \qquad (I''_t,\, V''_t) \sim \mathcal{T}^{\mathrm{II}}(i'',\, v'') \tag{1.7}$$

model, respectively, the new microscopic state of the focal agent when interaction-driven compartment switching and spontaneous compartment switching occurs, while the random variable

$$(W_t | V_t) \sim \mathcal{T}^{\mathrm{III}}(w | V_t) \tag{1.8}$$

models the new phenotype of the focal agent when structuring-variable switching takes place. Note also that, under assumptions (1.6), all terms related to successions of switching events (e.g. interaction-driven switching followed by spontaneous compartment switching) occurring between time t and $t + \Delta t$ are of order equal to or higher than Δt^2, and have thus been grouped into $\mathcal{O}(\Delta t^2)$, since they are negligible for Δt chosen sufficiently small. Moreover, $s^{\mathrm{I}}_{i,i^*}(v, v^*) \geq 0$ is the rate of interaction-driven compartment switching, $s^{\mathrm{II}}_i(v) \geq 0$ is the rate of spontaneous compartment switching, and $s^{\mathrm{III}}_i \geq 0$ is the rate of structuring-variable switching. In particular, to incorporate (I)–(III) into the model, we let

$$s^{\mathrm{I}}_{i,i^*}(v, v^*) \equiv s^{\mathrm{I}}_{i,i^*}(v^*) := \delta_{i,0}\delta_{i^*,1}p(v^*), \tag{1.9a}$$

$$s^{\mathrm{II}}_i(v) := \delta_{i,1}d(v), \tag{1.9b}$$

$$s^{\mathrm{III}}_i := \delta_{i,1}\mu, \tag{1.9c}$$

and

$$\mathcal{T}^{\mathrm{I}}(i', v'|i^*, v^*) := \delta_{i',i^*}\delta_{v^*}(v'), \tag{1.10a}$$

$$\mathcal{T}^{\mathrm{II}}(i'', v'') := \delta_{i'',0}\delta_{v_0}(v''), \tag{1.10b}$$

$$\mathcal{T}^{\mathrm{III}}(w|v) := M(w|v), \tag{1.10c}$$

where $\delta_{i,j}$ is the Kronecker delta and $\delta_x(y)$ is the Dirac delta centred at $y = x$.

1.3 Mesoscopic model

Starting from the system (1.5), we now formally derive the mesoscopic model corresponding to the agent-based model presented in the previous section, which consists of an evolution equation for the distribution of population members over the phenotype domain.

General evolution equation for expectations of observables We start by noting that, since the components of the pair $(I_{t+\Delta t}, V_{t+\Delta t})$ are given by (1.5), for any observable $\Phi : \{0, 1\} \times \mathbb{R} \to \mathbb{R}$, namely an arbitrary test function defined for $(i, v) \in \{0, 1\} \times \mathbb{R}$, the expectation

$$\langle \Phi(I_t, V_t) \rangle := \sum_{i=0}^{1} \int_{\mathbb{R}} \Phi(i, v) f(t, i, v)\, dv$$

satisfies (see, for instance, [129])

$$\begin{aligned}
\langle \Phi(I_{t+\Delta t}, V_{t+\Delta t}) \rangle = &\left\langle \left(1 - \frac{s^{\mathrm{I}}_{I_t,I_t^*}(V_t, V_t^*)\Delta t}{1 + s^{\mathrm{I}}_{I_t,I_t^*}(V_t, V_t^*)\Delta t}\right)\left(1 - \frac{s^{\mathrm{II}}_{I_t}(V_t)\Delta t}{1 + s^{\mathrm{II}}_{I_t}(V_t)\Delta t}\right)\left(1 - \frac{s^{\mathrm{III}}_{I_t}\Delta t}{1 + s^{\mathrm{III}}_{I_t}\Delta t}\right)\Phi(I_t, V_t)\right\rangle \\
&+ \left\langle \left(1 - \frac{s^{\mathrm{I}}_{I_t,I_t^*}(V_t, V_t^*)\Delta t}{1 + s^{\mathrm{I}}_{I_t,I_t^*}(V_t, V_t^*)\Delta t}\right)\left(1 - \frac{s^{\mathrm{II}}_{I_t}(V_t)\Delta t}{1 + s^{\mathrm{II}}_{I_t}(V_t)\Delta t}\right)\frac{s^{\mathrm{III}}_{I_t}\Delta t}{1 + s^{\mathrm{III}}_{I_t}\Delta t}\Phi(I_t, W_t)\right\rangle \\
&+ \left\langle \frac{s^{\mathrm{I}}_{I_t,I_t^*}(V_t, V_t^*)\Delta t}{1 + s^{\mathrm{I}}_{I_t,I_t^*}(V_t, V_t^*)\Delta t}\left(1 - \frac{s^{\mathrm{II}}_{I_t}(V_t)\Delta t}{1 + s^{\mathrm{II}}_{I_t}(V_t)\Delta t}\right)\Phi(I_t', V_t')\right\rangle \\
&+ \left\langle \left(1 - \frac{s^{\mathrm{I}}_{I_t,I_t^*}(V_t, V_t^*)\Delta t}{1 + s^{\mathrm{I}}_{I_t,I_t^*}(V_t, V_t^*)\Delta t}\right)\frac{s^{\mathrm{II}}_{I_t}(V_t)\Delta t}{1 + s^{\mathrm{II}}_{I_t}(V_t)\Delta t}\Phi(I_t'', V_t'')\right\rangle + \mathcal{O}(\Delta t^2).
\end{aligned}$$

From the above equation, rearranging terms, dividing through by Δt and letting $\Delta t \to 0^+$, we formally obtain the following evolution equation:

$$\begin{aligned}\frac{d}{dt}\langle\Phi(I_t,V_t)\rangle = {} & \langle s^{\mathrm{I}}_{I_t,I_t^*}(V_t,V_t^*)\left(\Phi(I_t',V_t')-\Phi(I_t,V_t)\right)\rangle \\ & + \langle s^{\mathrm{II}}_{I_t}(V_t)\left(\Phi(I_t'',V_t'')-\Phi(I_t,V_t)\right)\rangle \\ & + \langle s^{\mathrm{III}}_{I_t}\left(\Phi(I_t,W_t)-\Phi(I_t,V_t)\right)\rangle.\end{aligned} \tag{1.11}$$

Expressing the expectations $\langle\cdot\rangle$ in (1.11) in terms of sums and integrals against the probability density function f, recalling (1.7) and (1.8), and introducing the more compact notation $f_i(t,v) := f(t,i,v)$, the evolution equation (1.11) can then be rewritten as

$$\begin{aligned}\frac{d}{dt}\sum_{i=0}^{1}\int_{\mathbb{R}}\Phi(i,v)f_i(t,v)\,dv = {} & \underbrace{\sum_{i=0}^{1}\int_{\mathbb{R}}\Phi(i,v)\sum_{i'=0}^{1}\sum_{i^*=0}^{1}\int_{\mathbb{R}}\int_{\mathbb{R}}s^{\mathrm{I}}_{i',i^*}(v',v^*)\mathcal{T}^{\mathrm{I}}(i,v|i^*,v^*)}_{=:\text{(i)}} \\ & \underbrace{f_{i'}(t,v')f_{i^*}(t,v^*)\,dv'\,dv^*\,dv}_{=:\text{(i)}} \\ & \underbrace{-\sum_{i=0}^{1}\int_{\mathbb{R}}\Phi(i,v)\left(\sum_{i^*=0}^{1}\int_{\mathbb{R}}s^{\mathrm{I}}_{i,i^*}(v,v^*)f_{i^*}(t,v^*)\,dv^*\right)f_i(t,v)\,dv}_{=:\text{(ii)}} \\ & \underbrace{+\sum_{i=0}^{1}\int_{\mathbb{R}}\Phi(i,v)\left(\sum_{i''=0}^{1}\int_{\mathbb{R}}s^{\mathrm{II}}_{i''}(v'')\mathcal{T}^{\mathrm{II}}(i,v)f_{i''}(t,v'')\,dv''\right)dv}_{=:\text{(iii)}} \\ & \underbrace{-\sum_{i=0}^{1}\int_{\mathbb{R}}\Phi(i,v)s^{\mathrm{II}}_i(v)f_i(t,v)\,dv}_{=:\text{(iv)}} \\ & \underbrace{+\sum_{i=0}^{1}\int_{\mathbb{R}}\Phi(i,v)\left(\int_{\mathbb{R}}s^{\mathrm{III}}_i\mathcal{T}^{\mathrm{III}}(v|w)f_i(t,w)\,dw\right)dv}_{=:\text{(v)}} \\ & \underbrace{-\sum_{i=0}^{1}\int_{\mathbb{R}}\Phi(i,v)s^{\mathrm{III}}_i f_i(t,v)\,dv}_{=:\text{(vi)}}.\end{aligned} \tag{1.12}$$

From (1.12) we now derive the evolution equations for $f_0(t,v)$ and $f_1(t,v)$, from which we shall then derive an evolution equation for the distribution of population members over the phenotype domain, that is, the mesoscopic counterpart of the agent-based model. To do so, we choose

$$\Phi(i,v) := \delta_{i,l}\varphi(v), \tag{1.13}$$

where $l \in \{0, 1\}$ and φ is an observable quantity (test function) depending only on v. For ease of presentation, we carry out calculations for the left-hand side (LHS) of (1.12) and the terms ⓘ-ⓥⓘ on the right-hand side (RHS) of (1.12) one by one, first for $l = 0$ and then for $l = 1$.

Evolution equation for f_0 First, substituting (1.13) with $l = 0$ into the LHS of (1.12) yields

$$\frac{d}{dt}\sum_{i=0}^{1}\int_{\mathbb{R}}\Phi(i,v)f_i(t,v)\,dv = \int_{\mathbb{R}}\varphi(v)\partial_t f_0(t,v)\,dv. \tag{1.14}$$

Then, substituting (1.13) with $l = 0$ along with (1.9a) and (1.10a) into ⓘ and ⓘⓘ on the RHS of (1.12) yields

$$\begin{aligned}
ⓘ + ⓘⓘ &= \int_{\mathbb{R}}\varphi(v)\Bigg(\sum_{i'=0}^{1}\sum_{i^*=0}^{1}\int_{\mathbb{R}}\int_{\mathbb{R}} s^{\mathrm{I}}_{i',i^*}(v',v^*)\mathcal{T}^{\mathrm{I}}(0,v|i^*,v^*) \\
&\qquad \cdot f_{i'}(t,v')f_{i^*}(t,v^*)\,dv'\,dv^*\Bigg)\,dv \\
&\quad - \int_{\mathbb{R}}\varphi(v)\left(\sum_{i^*=0}^{1}\int_{\mathbb{R}} s^{\mathrm{I}}_{0,i^*}(v,v^*)f_{i^*}(t,v^*)\,dv^*\right)f_0(t,v)\,dv \\
&= -\int_{\mathbb{R}}\varphi(v)\left(\int_{\mathbb{R}} p(v^*)f_1(t,v^*)\,dv^*\right)f_0(t,v)\,dv
\end{aligned} \tag{1.15}$$

Next, substituting (1.13) with $l = 0$ along with (1.9b) and (1.10b) into ⓘⓘ and ⓘⓥ on the RHS of (1.12) yields

$$\begin{aligned}
ⓘⓘ + ⓘⓥ &= \int_{\mathbb{R}}\varphi(v)\left(\sum_{i''=0}^{1}\int_{\mathbb{R}} s^{\mathrm{II}}_{i''}(v'')\mathcal{T}^{\mathrm{II}}(0,v)f_{i''}(t,v'')\,dv''\right)dv \\
&\quad - \int_{\mathbb{R}}\varphi(v)s^{\mathrm{II}}_0(v)f_0(t,v)\,dv \\
&= \int_{\mathbb{R}}\varphi(v)\left(\int_{\mathbb{R}} d(v'')f_1(t,v'')\,dv''\right)\delta_{v^0}(v)\,dv.
\end{aligned} \tag{1.16}$$

Finally, substituting (1.13) with $l = 0$ into ⓥ and ⓥⓘ on the RHS of (1.12) and using the fact that $s^{\mathrm{III}}_0 = 0$ (cf. definition (1.9c)) yields

$$\begin{aligned}
ⓥ + ⓥⓘ &= \int_{\mathbb{R}}\varphi(v)\left(\int_{\mathbb{R}} s^{\mathrm{III}}_0\mathcal{T}^{\mathrm{III}}(v|w)f_0(t,w)\,dw\right)dv \\
&\quad - \int_{\mathbb{R}}\varphi(v)s^{\mathrm{III}}_0 f_0(t,v)\,dv = 0
\end{aligned} \tag{1.17}$$

Combining (1.14)–(1.17) and rearranging terms we obtain, owing to the arbitrariness of φ, the following evolution equation for f_0:

$$\partial_t f_0(t,v) = \int_{\mathbb{R}} d(v'') f_1(t,v'')\, dv'' \delta_{v^0}(v) - \left(\int_{\mathbb{R}} p(v^*) f_1(t,v^*)\, dv^* \right) f_0(t,v). \quad (1.18)$$

Note that integrating the differential equation (1.18) over $\mathbb{R}$ and recalling (1.3) we find

$$\frac{d\rho_0}{dt} = \int_{\mathbb{R}} d(v'') f_1(t,v'')\, dv'' - \left(\int_{\mathbb{R}} p(v^*) f_1(t,v^*)\, dv^* \right) \rho_0,$$

whence

$$\begin{aligned} \rho_0(t) = \rho_0(0) e^{-\int_0^t \int_{\mathbb{R}} p(v^*) f_1(s,v^*)\, dv^*\, ds} \\ + \int_0^t \left(\int_{\mathbb{R}} d(v'') f_1(s,v'')\, dv'' \right) e^{-\int_s^t \int_{\mathbb{R}} p(v^*) f_1(\tau,v^*)\, dv^*\, d\tau}\, ds. \end{aligned} \quad (1.19)$$

Moreover, solving the differential equation (1.18) subject to the initial condition $f_0(0,v) = \rho_0(0)\delta_{v^0}(v)$ and substituting (1.19) into the expression for f_0 so obtained yields $f_0(t,v) = \rho_0(t)\delta_{v^0}(v)$ for all $t \geq 0$, consistently with the fact that, by construction, all individuals in the compartment $i = 0$ are expected to share the same phenotype v^0 at all times.

Evolution equation for f_1 First, substituting (1.13) with $l = 1$ into the LHS of (1.12) yields

$$\frac{d}{dt} \sum_{i=0}^{1} \int_{\mathbb{R}} \Phi(i,v) f_i(t,v)\, dv = \int_{\mathbb{R}} \varphi(v) \partial_t f_1(t,v)\, dv. \quad (1.20)$$

Then, substituting (1.13) with $l = 1$ along with (1.9a) and (1.10a) into ⓘ and ⓘⓘ on the RHS of (1.12), and recalling (1.3), yields

$$\begin{aligned} \text{ⓘ} + \text{ⓘⓘ} &= \int_{\mathbb{R}} \varphi(v) \Bigg(\sum_{i'=0}^{1} \sum_{i^*=0}^{1} \int_{\mathbb{R}} \int_{\mathbb{R}} s^{\mathrm{I}}_{i',i^*}(v',v^*)\, \mathcal{T}^{\mathrm{I}}(1,v|i^*,v^*) \\ &\quad \times f_{i'}(t,v') f_{i^*}(t,v^*)\, dv'\, dv^* \Bigg) dv \\ &\quad - \int_{\mathbb{R}} \varphi(v) \left(\sum_{i^*=0}^{1} \int_{\mathbb{R}} s^{\mathrm{I}}_{1,i^*}(v,v^*) f_{i^*}(t,v^*)\, dv^* \right) f_1(t,v)\, dv \\ &= \int_{\mathbb{R}} \varphi(v) p(v) \rho_0(t) f_1(t,v)\, dv \end{aligned} \quad (1.21)$$

Next, substituting (1.13) with $l = 1$ along with (1.9b) and (1.10b) into ⓘⓘⓘ and ⓘⓥ on the RHS of (1.12) yields

$$\begin{aligned}\text{ⓘⓘⓘ} + \text{ⓘⓥ} &= \int_{\mathbb{R}} \varphi(v) \left(\sum_{i''=0}^{1} \int_{\mathbb{R}} s_{i''}^{\mathrm{II}}(v'') \mathcal{T}^{\mathrm{II}}(1, v) f_{i''}(t, v'')\, dv'' \right) dv \\ &\quad - \int_{\mathbb{R}} \varphi(v) s_1^{\mathrm{II}}(v) f_1(t, v)\, dv \\ &= - \int_{\mathbb{R}} \varphi(v) d(v) f_1(t, v)\, dv. \end{aligned} \tag{1.22}$$

Finally, substituting (1.13) with $l = 1$ along with (1.9c) and (1.10c) into ⓥ and ⓘⓥ on the RHS of (1.12) yields

$$\begin{aligned}\text{ⓥ} + \text{ⓘⓥ} &= \int_{\mathbb{R}} \varphi(v) \left(\int_{\mathbb{R}} s_1^{\mathrm{III}} \mathcal{T}^{\mathrm{III}}(v|w) f_1(t, w)\, dw \right) dv - \int_{\mathbb{R}} \varphi(v) s_1^{\mathrm{III}} f_1(t, v)\, dv \\ &= \mu \int_{\mathbb{R}} \varphi(v) \left(\int_{\mathbb{R}} M(v|w) f_1(t, w)\, dw \right) dv - \mu \int_{\mathbb{R}} \varphi(v) f_1(t, v)\, dv. \end{aligned} \tag{1.23}$$

Combining (1.20)-(1.23) and rearranging terms we obtain, invoking again the arbitrariness of φ, the following evolution equation for f_1:

$$\begin{aligned}\partial_t f_1(t, v) &= \big(p(v)\rho_0(t) - d(v)\big) f_1(t, v) \\ &\quad + \mu \left(\int_{\mathbb{R}} M(v|w) f_1(t, w)\, dw - f_1(t, v) \right) \end{aligned} \tag{1.24}$$

Mass conservation Integrating the differential equation (1.18) and the integro-differential equation (1.24) over $\mathbb{R}$, summing together the resulting differential equations, recalling (1.3), and using the fact that (cf. assumption (1.1) on the kernel M)

$$\int_{\mathbb{R}} M(v|w)\, dv = 1, \qquad \forall\, w \in \mathbb{R}$$

we find

$$\begin{aligned}\frac{d}{dt}\big(\rho_0(t) + \rho_1(t)\big) &= \int_{\mathbb{R}} d(v'') f_1(t, v'')\, dv'' - \left(\int_{\mathbb{R}} p(v^*) f_1(t, v^*)\, dv^* \right) \rho_0(t) \\ &\quad + \int_{\mathbb{R}} \big(p(v)\rho_0(t) - d(v)\big) f_1(t, v)\, dv = 0, \end{aligned}$$

which implies $\rho_0(t) + \rho_1(t) = \rho_0(0) + \rho_1(0)$ for all $t > 0$. Hence, choosing, consistently with (1.4), initial data such that $\rho_0(0) + \rho_1(0) = 1$, we have $\rho_0(t) = 1 - \rho_1(t)$

for all $t > 0$. Substituting this into the integro-differential equation (1.24) we obtain

$$\begin{aligned}\partial_t f_1(t,v) = \big(p(v)(1-\rho_1(t)) - d(v)\big) f_1(t,v) \\ + \mu \left(\int_{\mathbb{R}} M(v|w) f_1(t,w)\, dw - f_1(t,v) \right)\end{aligned} \tag{1.25}$$

Mesoscopic model In the case where p is constant, say $p(v) = p_0 \geq 0$, which is the case we investigate in this chapter, choosing, without loss of generality, $p_0 = 1$, introducing the notation below for the *net proliferation rate* (i.e. the difference between the rate of proliferation and the rate of death)

$$r(v) := 1 - d(v), \tag{1.26}$$

and renaming f_1 to f and ρ_1 to ρ, from the integro-differential equation (1.25) we obtain the following evolution equation for the distribution of population members over the phenotype domain:

$$\begin{cases} \partial_t f = \big(r(v) - \rho\big) f + \mu \left(\displaystyle\int_{\mathbb{R}} M(v|w) f(t,w)\, dw - f \right), \\ \rho(t) := \displaystyle\int_{\mathbb{R}} f(t,v)\, dv. \end{cases} \tag{1.27}$$

Notice that, owing to (1.1), the definition (1.26) implies

$$r \in C(\mathbb{R}), \qquad r : \mathbb{R} \to \mathbb{R}, \qquad r(v) \leq 1 \quad \forall\, v \in \mathbb{R}. \tag{1.28a}$$

In particular, throughout the chapter we assume

$$\sup_{v \in \mathbb{R}} r(v) = 1. \tag{1.28b}$$

1.4 Quasi-invariant phenotypic changes

In this section, we consider the regime of *small* but *frequent* phenotypic changes, which in the jargon of the kinetic theory of multi-agent systems, cf. [129], is called a *quasi-invariant regime*. In this regime, the kernel M is scaled by means of a scaling parameter $0 < \varepsilon \ll 1$ in such a way that:

(i) on the one hand, the phenotype acquired, on average, after a phenotypic change, v, is a small perturbation of the original phenotype, w;

(ii) on the other hand, the variability of the newly acquired phenotype, v, is small.

Building upon the scaling for IDE model of evolutionary dynamics in phenotype-structured populations considered in [19, 66, 113], this can be obtained by scaling M as

$$M(v|w) \to M_\varepsilon(v|w) := \frac{1}{\varepsilon}\mathcal{M}\left(\frac{v-w}{\varepsilon};\, \alpha\varepsilon, \beta\right), \tag{1.29}$$

where $\alpha \in \mathbb{R}$, $\beta \in \mathbb{R}_+$ are given model parameters and $\mathcal{M} = \mathcal{M}(z;\, \xi, \varsigma^2)$ is a two-parameter probability distribution w.r.t. $z \in \mathbb{R}$ with mean $\xi \in \mathbb{R}$ and variance $\varsigma^2 \in \mathbb{R}_+$, which we further assume to have bounded third order moment. In detail:

(H1) $\displaystyle\int_{\mathbb{R}} \mathcal{M}(z;\, \xi, \varsigma^2)\, dz = 1$ for every $(\xi,\, \varsigma^2) \in \mathbb{R} \times \mathbb{R}_+$;

(H2) $\displaystyle\int_{\mathbb{R}} z\mathcal{M}(z;\, \xi, \varsigma^2)\, dz = \xi$ for every $\varsigma^2 \in \mathbb{R}_+$;

(H3) $\displaystyle\int_{\mathbb{R}} (z-\xi)^2\mathcal{M}(z;\, \xi, \varsigma^2)\, dz = \varsigma^2$ for every $\xi \in \mathbb{R}$;

(H4) $\displaystyle\int_{\mathbb{R}} |z|^3\mathcal{M}(z;\, \xi, \varsigma^2)\, dz < +\infty$ for every $(\xi,\, \varsigma^2) \in \mathbb{R} \times \mathbb{R}_+$.

Combining (H2) and (H3) we also deduce

$$\int_{\mathbb{R}} z^2\mathcal{M}(z;\, \xi, \varsigma^2)\, dz = \varsigma^2 + \xi^2. \tag{1.30}$$

On the whole, from (1.29) and (H1)–(H3) it is not difficult to verify that, for every $\varepsilon > 0$, the following properties hold

$$\begin{aligned} \int_{\mathbb{R}} M_\varepsilon(v \mid w)\, \mathrm{d}v &= 1, \\ \int_{\mathbb{R}} v\, M_\varepsilon(v \mid w)\, \mathrm{d}v &= w + \alpha\varepsilon^2, \\ \int_{\mathbb{R}} \big(v - w - \alpha\varepsilon^2\big)^2 M_\varepsilon(v \mid w)\, \mathrm{d}v &= \beta\varepsilon^2. \end{aligned} \tag{1.31}$$

which confirm that M_ε describes a regime of small phenotypic changes as specified by (i), (ii) above. In a moment, we shall examine also the significance of assumption (H4).

Scaling M to M_ε in (1.27), we obtain

$$\partial_t f_\varepsilon = \big(r(v) - \rho_\varepsilon\big) f_\varepsilon + \mu\left(\int_{\mathbb{R}} M_\varepsilon(v|w) f_\varepsilon(t,w)\, dw - f_\varepsilon\right), \tag{1.32}$$

where we have denoted by f_ε the phenotypic distribution function parametrised by ε in consequence of the scaling (1.29) and by $\rho_\varepsilon(t) = \int_{\mathbb{R}} f_\varepsilon(t,v)\, dv$ the corresponding

density. In weak form, this reads as

$$\begin{aligned}\frac{d}{dt}\int_{\mathbb{R}}\varphi(v)f_\varepsilon(t,v)\,dv &= \int_{\mathbb{R}}\varphi(v)\big(r(v)-\rho_\varepsilon\big)f_\varepsilon(t,v)\,dv\\ &\quad+\mu\left(\int_{\mathbb{R}}\int_{\mathbb{R}}\varphi(v)M_\varepsilon(v|w)f_\varepsilon(t,w)\,dw\,dv-\int_{\mathbb{R}}\varphi(v)f_\varepsilon(t,v)\,dv\right)\\ &= \int_{\mathbb{R}}\varphi(v)\big(r(v)-\rho_\varepsilon\big)f_\varepsilon(t,v)\,dv\\ &\quad+\mu\left\{\frac{1}{\varepsilon}\int_{\mathbb{R}}\left[\int_{\mathbb{R}}\varphi(v)\mathcal{M}\left(\frac{v-w}{\varepsilon};\alpha\varepsilon,\beta\right)dv\right]f_\varepsilon(t,w)\,dw-\int_{\mathbb{R}}\varphi(v)f_\varepsilon(t,v)\,dv\right\}\end{aligned}\tag{1.33}$$

where $\varphi=\varphi(v)$ is a generic observable quantity (test function). We shall consider non-negative solutions to (1.32), (1.33), consistently with the interpretation of f_ε as the statistical distribution of the phenotype v over time. This property is ensured by the following result:

Proposition 1.1 (Non-negativity of f_ε)**.** *Under* (1.28)*, if* $f_\varepsilon(0,v)\geq 0$ *for a.e.* $v\in\mathbb{R}$ *then* $f_\varepsilon(t,v)\geq 0$ *for a.e.* $v\in\mathbb{R}$ *and every* $t>0$*.*

Proof. Let $f_\varepsilon^\pm(t,v):=\max\{0,\pm f_\varepsilon(t,v)\}\geq 0$ be the positive and negative part, respectively, of f_ε. Writing $f_\varepsilon=f_\varepsilon^+-f_\varepsilon^-$ and considering that f_ε^+, f_ε^- have essentially disjoint supports, if we multiply (1.32) by $-2f_\varepsilon^-$ we find

$$\partial_t(f_\varepsilon^-)^2=2\big(r(v)-\rho_\varepsilon\big)(f_\varepsilon^-)^2-2\mu\left(f_\varepsilon^-\int_{\mathbb{R}}M_\varepsilon(v|w)f_\varepsilon(t,w)\,dw+(f_\varepsilon^-)^2\right),$$

whence, integrating over $v\in\mathbb{R}$,

$$\begin{aligned}\frac{d}{dt}\int_{\mathbb{R}}(f_\varepsilon^-(t,v))^2\,dv &= 2\int_{\mathbb{R}}r(v)(f_\varepsilon^-(t,v))^2\,dv-2(\rho_\varepsilon+\mu)\int_{\mathbb{R}}(f_\varepsilon^-(t,v))^2\,dv\\ &\quad-2\mu\int_{\mathbb{R}}\int_{\mathbb{R}}M_\varepsilon(v|w)f_\varepsilon^+(t,w)f_\varepsilon^-(t,v)\,dw\,dv\\ &\quad+2\mu\int_{\mathbb{R}}\int_{\mathbb{R}}M_\varepsilon(v|w)f_\varepsilon^-(t,w)f_\varepsilon^-(t,v)\,dw\,dv\\ &\leq 2(1-\rho_\varepsilon-\mu)\int_{\mathbb{R}}(f_\varepsilon^-(t,v))^2\,dv\\ &\quad+2\mu\int_{\mathbb{R}}\int_{\mathbb{R}}M_\varepsilon(v|w)f_\varepsilon^-(t,w)f_\varepsilon^-(t,v)\,dw\,dv.\end{aligned}$$

Applying repeatedly the Cauchy–Schwarz inequality, first with respect to the probability measure $M_\varepsilon(v|w)dv$ and then with respect to the Lebesgue measure dw, we

obtain

$$\begin{aligned}\int_{\mathbb{R}}\int_{\mathbb{R}} M_\varepsilon(v|w) f_\varepsilon^-(t,w) f_\varepsilon^-(t,v)\,dw\,dv &= \int_{\mathbb{R}} \left(\int_{\mathbb{R}} M_\varepsilon(v|w) f_\varepsilon^-(t,v)\,dv\right) f_\varepsilon^-(t,w)\,dw \\ &\le \int_{\mathbb{R}} \left(\int_{\mathbb{R}} M_\varepsilon(v|w)(f_\varepsilon^-(t,v))^2\,dv\right)^{1/2} f_\varepsilon^-(t,w)\,dw \\ &\le \left(\int_{\mathbb{R}}\int_{\mathbb{R}} M_\varepsilon(v|w)(f_\varepsilon^-(t,v))^2\,dv\,dw\right)^{1/2} \left(\int_{\mathbb{R}} (f_\varepsilon^-(t,w))^2\,dw\right)^{1/2} \\ &= \int_{\mathbb{R}} (f_\varepsilon^-(t,v))^2\,dv,\end{aligned}$$

whence, finally,

$$\frac{d}{dt}\int_{\mathbb{R}} (f_\varepsilon^-(t,v))^2\,dv \le 2(1-\rho_\varepsilon)\int_{\mathbb{R}} (f_\varepsilon^-(t,v))^2\,dv.$$

Since $\int_{\mathbb{R}} (f_\varepsilon^-(0,v))^2\,dv = 0$ because $f_\varepsilon(0,v) \ge 0$ a.e. by assumption, the above differential inequality implies

$$\int_{\mathbb{R}} (f_\varepsilon^-(t,v))^2\,dv = 0, \qquad \forall\, t > 0.$$

Consequently, $f_\varepsilon^-(t,v) = 0$ for a.e. $v \in \mathbb{R}$ and every $t > 0$, which concludes the proof. □

The non-negativity of f_ε entails:

Proposition 1.2 (Non-negativity and boundedness of ρ_ε)**.** *Under* (1.28)*, if* $\rho_\varepsilon(0) = \rho^0 \le 1$*, where* $\rho^0 > 0$ *is taken independent of* ε*, then* $0 \le \rho_\varepsilon(t) \le 1$ *for every* $\varepsilon > 0$ *and every* $t > 0$*.*

Proof. With $\varphi(v) = 1$ in (1.33) we find

$$\frac{d\rho_\varepsilon}{dt} = \int_{\mathbb{R}} r(v) f_\varepsilon(t,v)\,dv - \rho_\varepsilon^2.$$

(i) To prove the non-negativity of ρ_ε, we multiply this equation by $-2\rho_\varepsilon^-$ to find

$$\frac{d}{dt}(\rho_\varepsilon^-)^2 = -2\rho_\varepsilon^- \int_{\mathbb{R}} r(v) f_\varepsilon(t,v)\,dv + 2(\rho_\varepsilon^-)^3 \le 2(\rho_\varepsilon^-)^3,$$

where we took advantage of the non-negativity of f_ε. Letting $u := (\rho_\varepsilon^-)^2$, this is equivalent to $\frac{du}{dt} \le 2u^{3/2}$, which, since $u(0) = (\rho_\varepsilon^-)^2(0) = 0$ and $\frac{3}{2} > 1$, implies $u(t) \le 0$ for all $t > 0$. Thus, $(\rho_\varepsilon^-)^2(t) = 0$ for every $t > 0$ and the thesis follows.

(ii) To prove the boundedness from above of ρ_ε we observe that

$$\frac{d\rho_\varepsilon}{dt} \leq \rho_\varepsilon - \rho_\varepsilon^2,$$

due again to the non-negativity of f_ε. Integrating this differential inequality gives

$$\rho_\varepsilon(t) \leq \frac{\rho^0}{(1-\rho^0)e^{-t} + \rho^0},$$

whence the thesis follows as $1 - \rho^0 \geq 0$ by assumption. □

Performing now the change of variable $z := \frac{v-w}{\varepsilon}$ in the v-integral containing $\mathcal{M}$ on the right-hand side of (1.33) gives

$$\begin{aligned}\frac{d}{dt}\int_{\mathbb{R}} \varphi(v) f_\varepsilon(t,v)\,dv = &\int_{\mathbb{R}} \varphi(v)\big(r(v) - \rho_\varepsilon\big) f_\varepsilon(t,v)\,dv \\ &+ \mu\left\{ \int_{\mathbb{R}} \left[\int_{\mathbb{R}} \varphi(w+\varepsilon z)\mathcal{M}(z;\,\alpha\varepsilon,\beta)\,dz\right] f_\varepsilon(t,w)\,dw \right. \\ &\left. - \int_{\mathbb{R}} \varphi(v) f_\varepsilon(t,v)\,dv \right\}.\end{aligned} \tag{1.34}$$

For a sufficiently smooth test function, say $\varphi \in C^{2,1}(\mathbb{R})$ with bounded second derivative, considering that ε is small we can Taylor-expand $\varphi(w+\varepsilon z)$ up to the second order with centre in w and Lagrange remainder:

$$\varphi(w+\varepsilon z) = \varphi(w) + \varphi'(w)\varepsilon z + \frac{1}{2}\varphi''(w)\varepsilon^2 z^2 + \frac{1}{2}\big(\varphi''(\tilde{v}) - \varphi''(w)\big)\varepsilon^2 z^2,$$

where $\tilde{v} = (1-\theta)w + \theta(w+\varepsilon z) = w + \theta\varepsilon z$ for some $\theta \in [0,1]$. Substituting into (1.34) and recalling (H1), (H2), and (1.30) yields

$$\begin{aligned}\frac{d}{dt}\int_{\mathbb{R}} \varphi(v) f_\varepsilon(t,v)\,dv = &\int_{\mathbb{R}} \varphi(v)\big(r(v) - \rho_\varepsilon\big) f_\varepsilon(t,v)\,dv \\ &+ \mu\varepsilon^2\left(\alpha\int_{\mathbb{R}} \varphi'(w) f_\varepsilon(t,w)\,dw + \frac{1}{2}(\beta + \alpha^2\varepsilon^2)\int_{\mathbb{R}} \varphi''(w) f_\varepsilon(t,w)\,dw \right. \\ &\left. + \frac{1}{2}\int_{\mathbb{R}}\int_{\mathbb{R}} (\varphi''(\tilde{v}) - \varphi''(w)) z^2 \mathcal{M}(z;\,\alpha\varepsilon,\beta) f_\varepsilon(t,w)\,dz\,dw\right),\end{aligned} \tag{1.35}$$

which suggests to fix

$$\mu = \frac{1}{\varepsilon^2}, \tag{1.36}$$

so as to observe the effect of phenotypic changes despite the fact that they are small.

Notice that this is in line with the idea that, in the quasi-invariant regime, phenotypic changes are frequent. With this scaling of μ, we rewrite (1.35) as

$$\begin{aligned}\frac{d}{dt}\int_{\mathbb{R}}\varphi(v)f_\varepsilon(t,v)\,dv = \int_{\mathbb{R}}\varphi(v)\big(r(v)-\rho_\varepsilon\big)f_\varepsilon(t,v)\,dv \\ +\alpha\int_{\mathbb{R}}\varphi'(v)f_\varepsilon(t,v)\,dv+\frac{\beta}{2}\int_{\mathbb{R}}\varphi''(v)f_\varepsilon(t,v)\,dv+R_\varepsilon(f_\varepsilon,\varphi),\end{aligned} \tag{1.37}$$

where we have set

$$R_\varepsilon(f_\varepsilon,\varphi)(t) := \alpha^2\varepsilon^2\int_{\mathbb{R}}\varphi''(v)f_\varepsilon(t,v)\,dv+\frac{1}{2}\int_{\mathbb{R}}\int_{\mathbb{R}}(\varphi''(\tilde v)-\varphi''(w))z^2\mathcal{M}(z;\,\alpha\varepsilon,\beta)f_\varepsilon(t,w)\,dz\,dw.$$

Owing to Proposition 1.2 and to the assumed smoothness of φ, we observe that

$$\begin{aligned}|R_\varepsilon(f_\varepsilon,\varphi)(t)| &\le \alpha^2\varepsilon^2\|\varphi''\|_\infty+\frac{\beta}{2}\operatorname{Lip}(\varphi'')\int_{\mathbb{R}}\int_{\mathbb{R}}|\tilde v-w|z^2\mathcal{M}(z;\,\alpha\varepsilon,\beta)f_\varepsilon(t,w)\,dz\,dw\\ &\le \alpha^2\varepsilon^2\|\varphi''\|_\infty+\frac{\beta\varepsilon}{2}\operatorname{Lip}(\varphi'')\int_{\mathbb{R}}|z|^3\mathcal{M}(z;\,\alpha\varepsilon,\beta)\,dz,\end{aligned}$$

where $\operatorname{Lip}(\varphi'')>0$ is the Lipschitz constant of φ''. In particular, we have used $|\tilde v-w|=\theta\varepsilon|z|\le\varepsilon|z|$ because $0\le\theta\le1$.

To estimate the last integral term on the right-hand side, let Z_ε be a random variable with law $\mathcal{M}(z;\,\alpha\varepsilon,\beta)$, so that

$$\int_{\mathbb{R}}|z|^3\mathcal{M}(z;\,\alpha\varepsilon,\beta)\,dz=\langle|Z_\varepsilon|^3\rangle,$$

where, like in Section 1.3, $\langle\cdot\rangle$ denotes expectation. Then $\langle Z_\varepsilon\rangle=\alpha\varepsilon$, $\operatorname{Var}(Z_\varepsilon)=\beta$, and Z_ε can be standardised as $Z_\varepsilon=\sqrt{\beta}\tilde Z+\alpha\varepsilon$, where $\tilde Z$ is a random variable with $\langle\tilde Z\rangle=0$, $\langle\tilde Z^2\rangle=1$, and $\langle|\tilde Z|^3\rangle<+\infty$ owing to (H4). Then,

$$\begin{aligned}\langle|Z_\varepsilon|^3\rangle=\langle\left|\sqrt{\beta}\tilde Z+\alpha\varepsilon\right|^3\rangle &\le \beta^{3/2}\langle|\tilde Z|^3\rangle+3|\alpha|\beta\varepsilon+3\alpha^2\sqrt{\beta}\varepsilon^2\langle|\tilde Z|\rangle+|\alpha|^3\varepsilon^3\\ &\le \beta^{3/2}\langle|\tilde Z|^3\rangle+1\end{aligned} \tag{1.38}$$

for ε small enough, considering that $\langle|\tilde Z|\rangle\le\langle\tilde Z^2\rangle^{1/2}=1$ by Jensen's inequality.

On the whole, we bound $|R_\varepsilon(f_\varepsilon,\varphi)(t)|$ in such a way that $|R_\varepsilon(f_\varepsilon,\varphi)(t)|\to0$ as $\varepsilon\to0^+$. Consequently, we see that, for ε small, equation (1.37) solved by f_ε approaches the following equation solved by a new distribution function g

$$\begin{aligned}\frac{d}{dt}\int_{\mathbb{R}}\varphi(v)g(t,v)\,dv = \int_{\mathbb{R}}\varphi(v)\big(r(v)-\varrho\big)g(t,v)\,dv \\ +\alpha\int_{\mathbb{R}}\varphi'(v)g(t,v)\,dv+\frac{\beta}{2}\int_{\mathbb{R}}\varphi''(v)g(t,v)\,dv\end{aligned} \tag{1.39}$$

with $\varrho(t) := \int_{\mathbb{R}} g(t,v)\,dv$.

Equation (1.39) can be fruitfully written in strong form by integrating by parts the last two terms on the right-hand side. This yields

$$\partial_t g = \big(r(v) - \varrho\big)g - \alpha\partial_v g + \frac{\beta}{2}\partial_v^2 g, \tag{1.40}$$

provided that suitable conditions are imposed for $|v| \to \infty$. Such conditions involve, in general, the test function φ but, as we shall see, only test functions in the form of powers of v will be relevant for our next purposes. In more detail, for φ such that $|\varphi(v)| \sim |v|^p$ when $|v| \to \infty$ with $0 \le p \le 2$, (1.40) is obtained from (1.39) by prescribing the "boundary" conditions

$$g(t,v),\ \partial_v g(t,v) \xrightarrow{|v|\to\infty} 0 \quad \forall\, t > 0, \quad \text{infinitesimals of order} > 2. \tag{1.41}$$

Notice that (1.40) is a Fokker–Planck-type equation with non-local reaction term. Also in this case, we shall consider non-negative solutions to (1.39), (1.40), which are provided by

Proposition 1.3 (Non-negativity of g)**.** *Under* (1.28) *and* (1.41), *if* $g(0,v) \ge 0$ *for a.e.* $v \in \mathbb{R}$ *then* $g(t,v) \ge 0$ *for a.e.* $v \in \mathbb{R}$ *and every* $t > 0$.

Proof. We multiply (1.40) by $-2g^-$, where g^- denotes the negative part of g, to obtain

$$\partial_t (g^-)^2 = 2\big(r(v) - \varrho\big)(g^-)^2 - \alpha\partial_v (g^-)^2 - \beta g^- \partial_v^2 g.$$

Next, we integrate over $v \in \mathbb{R}$ and use integration by parts to find

$$\begin{aligned}\frac{d}{dt}\int_{\mathbb{R}} (g^-(t,v))^2\,dv = 2\int_{\mathbb{R}} r(v)(g^-(t,v))^2\,dv - 2\varrho\int_{\mathbb{R}} (g^-(t,v))^2\,dv \\ - \alpha\Big((g^-(t,v))^2\Big|_{v=-\infty}^{v=+\infty} \\ - \beta\left(-\int_{\mathbb{R}} \partial_v g(t,v)\partial_v g^-(t,v)\,dv + \Big(g^-(t,v)\partial_v g(t,v)\Big|_{v=-\infty}^{v=+\infty}\right).\end{aligned}$$

Owing to (1.41), the boundary terms vanish. Moreover, writing $g = g^+ - g^-$ and using that g^+, g^- have essentially disjoint supports we deduce $\int_{\mathbb{R}} \partial_v g(t,v)\partial_v g^-(t,v)\,dv = -\int_{\mathbb{R}} (\partial_v g^-(t,v))^2\,dv \le 0$, whence, finally,

$$\frac{d}{dt}\int_{\mathbb{R}} (g^-(t,v))^2\,dv \le 2(1-\varrho)\int_{\mathbb{R}} (g^-(t,v))^2\,dv,$$

which, since $\int_{\mathbb{R}} (g^-(0,v))^2\,dv = 0$ because $g(0,v) \ge 0$ a.e. by assumption, implies

$$\int_{\mathbb{R}} (g^-(t,v))^2\,dv = 0, \qquad \forall\, t > 0.$$

Therefore, $g^-(t,v) = 0$ for a.e. $v \in \mathbb{R}$ and every $t > 0$, which concludes the proof. □

1.4.1 Convergence of f_ε to g as $\varepsilon \to 0^+$

In this section, we prove the convergence of the solution f_ε of the integro-differential model (1.32) to the solution g of the differential model (1.40)-(1.41) in the quasi-invariant limit $\varepsilon \to 0^+$. This will provide a mathematical justification of the fact that the differential model, often used in the literature as the starting point of further investigations, is the exact counterpart of the agent-based model in the quasi-invariant regime.

Preliminary results

Here, before the formal analysis, we report two generalisations of the classical Grönwall's inequality, which we exploit for the development of our theory.

Lemma 1.4. *For $T > 0$, let a, b, $u : [0, T] \to \mathbb{R}$ be real-valued continuous functions such that a is differentiable in $(0, T)$, b is non-negative in $[0, T]$, and also*

$$u(t) \le a(t) + \int_0^t b(s)u(s)\,ds, \qquad \forall\, t \in [0, T].$$

Then

$$u(t) \le a(0)e^{\int_0^t b(s)\,ds} + \int_0^t a'(s)e^{\int_s^t b(\tau)\,d\tau}\,ds, \qquad \forall\, t \in [0, T].$$

Proof. In the said hypotheses, the classical Grönwall's inequality implies (cf. e.g., [123])

$$u(t) \le a(t) + \int_0^t a(s)b(s)e^{\int_s^t b(\tau)\,d\tau}\,ds = a(t) - \int_0^t a(s)\frac{d}{ds}e^{\int_s^t b(\tau)\,d\tau}\,ds,$$

whence, integrating by parts,

$$\begin{aligned} &= a(t) - \Big(a(s)e^{\int_s^t b(\tau)\,d\tau}\Big|_0^t + \int_0^t a'(s)e^{\int_s^t b(\tau)\,d\tau}\,ds \\ &= a(0)e^{\int_0^t b(\tau)\,d\tau} + \int_0^t a'(s)e^{\int_s^t b(\tau)\,d\tau}\,ds, \end{aligned}$$

which gives the thesis. □

Lemma 1.5. *For $T > 0$, let a, b, $u : [0, T] \to \mathbb{R}$ be real-valued continuous functions with b non-negative and a, b non-decreasing. Assume moreover that*

$$u(t) \le a(t) + b(t)\int_0^t u(s)\,ds, \qquad \forall\, t \in [0, T]. \tag{1.42}$$

Then

$$u(t) \leq a(t)e^{b(t)t}, \qquad \forall\, t \in [0,\, T].$$

Remark 1.6. This result is a variation of the classical Grönwall's inequality in that the function b is neither constant nor s-dependent within the integral on the right-hand side of (1.42).

Proof of Lemma 1.5. We introduce the auxiliary function

$$v(s) := e^{-\int_0^s b(\tau)\,d\tau} \int_0^s u(\tau)\,d\tau,$$

which is such that

$$v'(s) = e^{-\int_0^s b(\tau)\,d\tau} \left(u(s) - b(s) \int_0^s u(\tau)\,d\tau \right) \leq a(s)e^{-\int_0^s b(\tau)\,d\tau},$$

the last inequality following from (1.42). Integrating on $[0,\, t]$, with $0 < t \leq T$, and considering that $v(0) = 0$ by definition, we find

$$v(t) \leq \int_0^t a(s)e^{-\int_0^s b(\tau)\,d\tau}\,ds \leq a(t) \int_0^t e^{-\int_0^s b(\tau)\,d\tau}\,ds,$$

where we have used that $a(s) \leq a(t)$ for all $s \leq t$, because a is non-decreasing. Hence, recalling the definition of v,

$$\begin{aligned} b(t)e^{\int_0^t b(\tau)\,d\tau} v(t) &= b(t) \int_0^t u(r)\,dt \\ &\leq a(t)b(t) \int_0^t e^{\int_s^t b(\tau)\,d\tau}\,ds \\ &\leq a(t)b(t) \int_0^t e^{b(t)(t-s)}\,ds, \end{aligned}$$

where we have considered that $b(r) \leq b(t)$ for all $r \leq t$, because also b is non-decreasing. Then,

$$\begin{aligned} b(t) \int_0^t u(\tau)\,d\tau &\leq a(t)e^{b(t)t} \int_0^t b(t)e^{-b(t)s}\,ds \\ &= a(t)e^{b(t)t} \left(-e^{-b(t)s} \Big|_0^t \right. \\ &= a(t) \left(e^{b(t)t} - 1 \right). \end{aligned}$$

Substituting this into (1.42) yields the thesis. □

1.4.1.1 *A priori* estimates

To begin with, we establish some *a priori* estimates that will be useful in the sequel.

Proposition 1.7 (Non-negativity and boundedness of ϱ)**.** *Under the same assumptions as in Proposition 1.2, if* $\varrho(0) = \varrho^0 \leq 1$ *then* $0 \leq \varrho(t) \leq 1$ *for every* $t > 0$.

Proof. From (1.39), we obtain the evolution equation of ϱ by taking $\varphi(v) = 1$:

$$\frac{d\varrho}{dt} = \int_{\mathbb{R}} r(v) g(t,v)\, dv - \varrho^2.$$

The thesis follows then by arguing like in the proof of Proposition 1.2, since ϱ fulfills the same equation as ρ_ε with f_ε replaced by the non-negative distribution function g. □

From now on, we shall invariably make the following assumptions on the function r and the initial phenotypic distribution $f^0 = f^0(v)$:

$$\begin{aligned} &r,\, f^0 \in L^2(\mathbb{R}) \cap W^{3,\infty}(\mathbb{R}), \\ &f^0,\, \partial_v f^0 \to 0 \quad \text{as} \quad |v| \to \infty, \qquad f^0(v) \geq 0 \quad \text{a.e.} \end{aligned} \tag{1.43}$$

The assumption on the trend of f^0, $\partial_v f^0$ for $|v| \to \infty$ is motivated by the similar request on g, cf. (1.41). More specifically, we prescribe f^0 as the common initial condition to both (1.32) for every $\varepsilon > 0$ and (1.40):

$$f_\varepsilon(0,\cdot) = g(0,\cdot) = f^0, \qquad \forall\, \varepsilon > 0. \tag{1.44}$$

Notice that the results of Propositions 1.2, 1.7 hold using, in particular, $\|r\|_\infty$ as an upper bound on r, since $\|r\|_\infty \geq 1$ due to (1.28).

Remark 1.8. The framework developed up to this point does not encompass the case of constant r, cf. the assumption $r \in L^2(\mathbb{R})$ in (1.43). The reason is that such a case, though simpler, is structurally quite different from the general case of non-constant r. Specifically, it gives rise to self-consistent equations for the densities ρ_ε, ϱ with also $\rho_\varepsilon(t) = \varrho(t)$ for every ε, $t > 0$. This impacts on the estimates needed to achieve the quasi-invariant limit in a way which cannot be dealt with simply as a particular instance of the case of non-constant r.

While throughout the chapter we focus on the biologically more significant case of a net proliferation rate, r, depending on the phenotype of the individuals, in subsection 1.4.2 we provide for completeness technical details about the case of constant r.

Proposition 1.9 (L^2 estimate on f_ε)**.** *Under* (1.43), $f_\varepsilon(t,\cdot) \in L^2(\mathbb{R})$ *for every* $\varepsilon > 0$ *and every* $t \in (0,\, T]$*, where* $T > 0$ *is arbitrary.*

Proof. We multiply (1.32) by $2f_\varepsilon$ and integrate both sides w.r.t. $v \in \mathbb{R}$ to find

$$\begin{aligned}\frac{d}{dt}\|f_\varepsilon(t)\|_{L^2}^2 &= 2\int_{\mathbb{R}} \big(r(v)-\rho_\varepsilon\big) f_\varepsilon^2(t,v)\,dv \\ &\quad + \frac{2}{\varepsilon^2}\int_{\mathbb{R}}\int_{\mathbb{R}} M_\varepsilon(v|w) f_\varepsilon(t,w) f_\varepsilon(t,v)\,dv\,dw - \frac{2}{\varepsilon^2}\|f_\varepsilon\|_{L^2}^2 \\ &\le 2\left(\|r\|_\infty - \frac{1}{\varepsilon^2}\right)\|f_\varepsilon(t)\|_{L^2}^2 + \frac{2}{\varepsilon^2}\int_{\mathbb{R}}\left(\int_{\mathbb{R}} M_\varepsilon(v|w) f_\varepsilon(t,v)\,dv\right) f_\varepsilon(t,w)\,dw.\end{aligned}$$

Since $\int_{\mathbb{R}} M_\varepsilon(v|w) f_\varepsilon(t,v)\,dv \le \big(\int_{\mathbb{R}} M_\varepsilon(v|w) f_\varepsilon^2(t,v)\,dv\big)^{1/2}$ by Cauchy–Schwarz inequality w.r.t. the integration probability measure $M_\varepsilon(v|w)dv$, then

$$\le 2\left(\|r\|_\infty - \frac{1}{\varepsilon^2}\right)\|f_\varepsilon(t)\|_{L^2}^2 + \frac{2}{\varepsilon^2}\int_{\mathbb{R}}\left(\int_{\mathbb{R}} M_\varepsilon(v|w) f_\varepsilon^2(t,v)\,dv\right)^{1/2} f_\varepsilon(t,w)\,dw.$$

A further application of Cauchy–Schwarz inequality to the integral in dw produces

$$\le 2\left(\|r\|_\infty - \frac{1}{\varepsilon^2}\right)\|f_\varepsilon(t)\|_{L^2}^2 + \frac{2}{\varepsilon^2}\|f_\varepsilon(t)\|_{L^2}\left(\int_{\mathbb{R}}\int_{\mathbb{R}} M_\varepsilon(v|w) f_\varepsilon^2(t,v)\,dv\,dw\right)^{1/2},$$

whence, invoking the first formula in (1.31),

$$= 2\|r\|_\infty \|f_\varepsilon(t)\|_{L^2}^2.$$

Finally,

$$\|f_\varepsilon(t)\|_{L^2} \le \left\|f^0\right\|_{L^2} e^{t\|r\|_\infty},$$

which shows that $\|f_\varepsilon(t)\|_{L^2}$ is bounded for every $t \in (0,\, T]$ with arbitrary $T > 0$, whence the thesis follows. □

Proposition 1.10 (L^∞ estimates of f_ε and its derivatives)**.** *Under* (1.43), $f_\varepsilon(t,\cdot) \in W^{3,\infty}(\mathbb{R})$ *for every* $\varepsilon > 0$ *and every* $t \in (0,\, T]$*, where* $T > 0$ *is arbitrary.*

Proof. (i) We begin by estimating $\|f_\varepsilon(t)\|_\infty$. From (1.32) with the scaling (1.29), (1.36) and the change of variable $z := \frac{v-w}{\varepsilon}$ we have

$$\partial_t f_\varepsilon + \frac{1}{\varepsilon^2} f_\varepsilon = \big(r(v)-\rho_\varepsilon\big) f_\varepsilon + \frac{1}{\varepsilon^2}\int_{\mathbb{R}} \mathcal{M}(z;\, \alpha\varepsilon, \beta) f_\varepsilon(t, v-\varepsilon z)\,dz, \qquad (1.45)$$

whence, using the non-negativity of f_ε, ρ_ε and multiplying both sides by e^{t/ε^2},

$$\partial_t \left(e^{t/\varepsilon^2} f_\varepsilon \right) \leq \left(\|r\|_\infty + \frac{1}{\varepsilon^2} \right) e^{t/\varepsilon^2} \|f_\varepsilon(t)\|_\infty.$$

We integrate now both sides on $[0,\, t]$, $t > 0$, to find

$$e^{t/\varepsilon^2} f_\varepsilon(t,v) \leq f^0(v) + \left(\|r\|_\infty + \frac{1}{\varepsilon^2} \right) \int_0^t e^{s/\varepsilon^2} \|f_\varepsilon(s)\|_\infty \, ds$$

for every $v \in \mathbb{R}$. Therefore

$$e^{t/\varepsilon^2} \|f_\varepsilon(t)\|_\infty \leq \left\| f^0 \right\|_\infty + \left(\|r\|_\infty + \frac{1}{\varepsilon^2} \right) \int_0^t e^{s/\varepsilon^2} \|f_\varepsilon(s)\|_\infty \, ds$$

and, finally, applying Grönwall's inequality to the function $e^{t/\varepsilon^2} \|f_\varepsilon(t)\|_\infty$,

$$\|f_\varepsilon(t)\|_\infty \leq \left\| f^0 \right\|_\infty e^{\|r\|_\infty t},$$

which ensures that $\|f_\varepsilon(t)\|_\infty$ is bounded for every $t \in (0,\, T]$ with arbitrary $T > 0$.

(ii) We estimate now $\|\partial_v f_\varepsilon(t)\|_\infty$. For this, we differentiate (1.45) w.r.t. v to find

$$\begin{aligned} \partial_t(\partial_v f_\varepsilon) + \frac{1}{\varepsilon^2} \partial_v f_\varepsilon = r'(v) f_\varepsilon + \big(r(v) - \rho_\varepsilon\big) \partial_v f_\varepsilon \\ + \frac{1}{\varepsilon^2} \int_{\mathbb{R}} \mathcal{M}(z;\, \alpha\varepsilon, \beta) \partial_v f_\varepsilon(t, v - \varepsilon z) \, dz, \end{aligned} \tag{1.46}$$

then we multiply both sides by e^{t/ε^2} and estimate:

$$\partial_t \left(e^{t/\varepsilon^2} \partial_v f_\varepsilon \right) \leq \|r'\|_\infty e^{t/\varepsilon^2} \|f_\varepsilon(t)\|_\infty + \left(2\|r\|_\infty + \frac{1}{\varepsilon^2} \right) e^{t/\varepsilon^2} \|\partial_v f_\varepsilon(t)\|_\infty,$$

whence, integrating both sides on $[0,\, t]$, $t > 0$, and arguing like in the previous step,

$$\begin{aligned} e^{t/\varepsilon^2} \|\partial_v f_\varepsilon(t)\|_\infty \leq \left\| \partial_v f^0 \right\|_\infty + \|r'\|_\infty \int_0^t e^{s/\varepsilon^2} \|f_\varepsilon(s)\|_\infty \, ds \\ + \left(2\|r\|_\infty + \frac{1}{\varepsilon^2} \right) \int_0^t e^{s/\varepsilon^2} \|\partial_v f_\varepsilon(s)\|_\infty \, ds. \end{aligned}$$

Finally, applying Lemma 1.4 to the function $u(t) = e^{t/\varepsilon^2} \|\partial_v f_\varepsilon(t)\|_\infty$ with

$$a(t) = \left\| \partial_v f^0 \right\|_\infty + \|r'\|_\infty \int_0^t e^{s/\varepsilon^2} \|f_\varepsilon(s)\|_\infty \, ds, \qquad b(t) = 2\|r\|_\infty + \frac{1}{\varepsilon^2},$$

we obtain

$$\begin{aligned}\|\partial_v f_\varepsilon(t)\|_\infty &\le \left\|\partial_v f^0\right\|_\infty e^{2\|r\|_\infty t} + \|r'\|_\infty \int_0^t \|f_\varepsilon(s)\|_\infty e^{2\|r\|_\infty (t-s)}\, ds \\ &\le \left(\left\|\partial_v f^0\right\|_\infty + \|r'\|_\infty \left\|f^0\right\|_\infty t\right) e^{2\|r\|_\infty t},\end{aligned}$$

where we have used the estimate of $\|f_\varepsilon(t)\|_\infty$ established in the previous step. This shows that $\|\partial_v f_\varepsilon(t)\|_\infty$ is bounded for every $t \in (0, T]$ for an arbitrary $T > 0$.

(iii) We continue by estimating $\left\|\partial_v^2 f_\varepsilon(t)\right\|_\infty$. Differentiating (1.46) w.r.t. v gives

$$\begin{aligned}\partial_t(\partial_v^2 f_\varepsilon) + \frac{1}{\varepsilon^2}\partial_v^2 f_\varepsilon &= r''(v) f_\varepsilon + 2r'(v)\partial_v f_\varepsilon + \big(r(v) - \rho_\varepsilon\big)\partial_v^2 f_\varepsilon \\ &\quad + \frac{1}{\varepsilon^2}\int_{\mathbb{R}} \mathcal{M}(z;\, \alpha\varepsilon, \beta)\partial_v^2 f_\varepsilon(t, v - \varepsilon z)\, dz, \qquad (1.47)\end{aligned}$$

whence, proceeding analogously to the previous steps, we find

$$\begin{aligned}\partial_t\left(e^{t/\varepsilon^2}\partial_v^2 f_\varepsilon\right) &\le \|r''\|_\infty e^{t/\varepsilon^2}\|f_\varepsilon(t)\|_\infty + 2\|r'\|_\infty e^{t/\varepsilon^2}\|\partial_v f_\varepsilon(t)\|_\infty \\ &\quad + \left(2\|r\|_\infty + \frac{1}{\varepsilon^2}\right) e^{t/\varepsilon^2}\left\|\partial_v^2 f_\varepsilon(t)\right\|_\infty\end{aligned}$$

and further

$$\begin{aligned}e^{t/\varepsilon^2}\left\|\partial_v^2 f_\varepsilon(t)\right\|_\infty &\le \left\|\partial_v^2 f^0\right\|_\infty + \int_0^t e^{s/\varepsilon^2}\left(\|r''\|_\infty\|f_\varepsilon(s)\|_\infty + 2\|r'\|_\infty\|\partial_v f_\varepsilon(s)\|_\infty\right) ds \\ &\quad + \left(2\|r\|_\infty + \frac{1}{\varepsilon^2}\right)\int_0^t e^{s/\varepsilon^2}\left\|\partial_v^2 f_\varepsilon(s)\right\|_\infty ds\end{aligned}$$

for $t > 0$. Applying now Lemma 1.4 to the function $u(t) = e^{t/\varepsilon^2}\left\|\partial_v^2 f_\varepsilon(t)\right\|_\infty$ with

$$\begin{aligned}a(t) &= \left\|\partial_v^2 f^0\right\|_\infty + \int_0^t e^{s/\varepsilon^2}\left(\|r''\|_\infty\|f_\varepsilon(s)\|_\infty + 2\|r'\|_\infty\|\partial_v f_\varepsilon(s)\|_\infty\right) ds, \\ b(t) &= 2\|r\|_\infty + \frac{1}{\varepsilon^2}\end{aligned}$$

yields

$$\begin{aligned}\left\|\partial_v^2 f_\varepsilon(t)\right\|_\infty &\le \left\|\partial_v^2 f^0\right\|_\infty e^{2\|r\|_\infty t} \\ &\quad + \int_0^t \left(\|r''\|_\infty\|f_\varepsilon(s)\|_\infty + 2\|r'\|_\infty\|\partial_v f_\varepsilon(s)\|_\infty\right) e^{2\|r\|_\infty (t-s)}\, ds,\end{aligned}$$

whence the boundedness of $\left\|\partial_v^2 f_\varepsilon(t)\right\|_\infty$ for every $t \in (0, T]$ and arbitrary

$T > 0$ follows owing to the boundedness of $\|f_\varepsilon(t)\|_\infty$, $\|\partial_v f_\varepsilon(t)\|_\infty$ established in the previous steps.

(iv) We conclude by estimating $\left\|\partial_v^3 f_\varepsilon(t)\right\|_\infty$. For this, we differentiate (1.47) w.r.t. v obtaining:

$$\begin{aligned}\partial_t(\partial_v^3 f_\varepsilon) + \frac{1}{\varepsilon^2}\partial_v^3 f_\varepsilon &= r'''(v) f_\varepsilon + 3r''(v)\partial_v f_\varepsilon + 3r'(v)\partial_v^2 f_\varepsilon + \big(r(v) - \rho_\varepsilon\big)\partial_v^3 f_\varepsilon \\ &\quad + \frac{1}{\varepsilon^2}\int_{\mathbb{R}} \mathcal{M}(z;\, \alpha\varepsilon, \beta)\partial_v^3 f_\varepsilon(t, v - \varepsilon z)\, dz \\ &\le \|r'''\|_\infty \|f_\varepsilon(t)\|_\infty + 3\|r''\|_\infty \|\partial_v f_\varepsilon(t)\|_\infty + 3\|r'\|_\infty \left\|\partial_v^2 f_\varepsilon(t)\right\|_\infty \\ &\quad + \left(2\|r\|_\infty + \frac{1}{\varepsilon^2}\right)\left\|\partial_v^3 f_\varepsilon(t)\right\|_\infty,\end{aligned}$$

whence, multiplying both sides by e^{t/ε^2} and integrating on $[0,\, t]$, $t > 0$, we find

$$\begin{aligned}e^{t/\varepsilon^2}\left\|\partial_v^3 f_\varepsilon(t)\right\|_\infty &\le \left\|\partial_v^3 f^0\right\|_\infty \\ &\quad + \int_0^t e^{s/\varepsilon^2}(\|r'''\|_\infty \|f_\varepsilon(s)\|_\infty + 3\|r''\|_\infty \|\partial_v f_\varepsilon(s)\|_\infty + 3\|r'\|_\infty \left\|\partial_v^2 f_\varepsilon(s)\right\|_\infty)\, ds \\ &\quad + \left(2\|r\|_\infty + \frac{1}{\varepsilon^2}\right)\int_0^t e^{s/\varepsilon^2}\left\|\partial_v^3 f_\varepsilon(s)\right\|_\infty ds.\end{aligned}$$

We now apply Lemma 1.4 to the function $u(t) = e^{t/\varepsilon^2}\left\|\partial_v^3 f_\varepsilon(t)\right\|_\infty$ with

$$\begin{aligned}a(t) &= \left\|\partial_v^3 f^0\right\|_\infty + \int_0^t e^{s/\varepsilon^2}(\|r'''\|_\infty \|f_\varepsilon(s)\|_\infty + 3\|r''\|_\infty \|\partial_v f_\varepsilon(s)\|_\infty + 3\|r'\|_\infty \left\|\partial_v^2 f_\varepsilon(s)\right\|_\infty)\, ds \\ b(t) &= 2\|r\|_\infty + \frac{1}{\varepsilon^2}\end{aligned}$$

to find

$$\begin{aligned}\left\|\partial_v^3 f_\varepsilon(t)\right\|_\infty &\le \left\|\partial_v^3 f^0\right\|_\infty e^{2\|r\|_\infty t} \\ &\quad + \int_0^t (\|r'''\|_\infty \|f_\varepsilon(s)\|_\infty + 3\|r''\|_\infty \|\partial_v f_\varepsilon(s)\|_\infty \\ &\qquad + 3\|r'\|_\infty \left\|\partial_v^2 f_\varepsilon(s)\right\|_\infty) e^{2\|r\|_\infty (t-s)}\, ds.\end{aligned}$$

The boundedness of $\left\|\partial_v^3 f_\varepsilon(t)\right\|_\infty$ for every $t \in (0,\, T]$ and arbitrary $T > 0$ follows then from the analogous property of $\|f_\varepsilon(t)\|_\infty$, $\|\partial_v f_\varepsilon(t)\|_\infty$, and $\left\|\partial_v^2 f_\varepsilon(t)\right\|_\infty$ obtained in the previous steps. □

Remark 1.11. As a by-product of Proposition 1.10, we notice that $\|f_\varepsilon(t)\|_\infty$, $\|\partial_v f_\varepsilon(t)\|_\infty$, $\left\|\partial_v^2 f_\varepsilon(t)\right\|_\infty$, and $\left\|\partial_v^3 f_\varepsilon(t)\right\|_\infty$ are all bounded *uniformly* in ε in every bounded interval $(0,\, T]$, $T > 0$.

Unlike (1.40), the integro-differential equation (1.32) does not require the prescription of boundary conditions. Nevertheless, soon a clue to the trend of $f_\varepsilon(t,\cdot)$, $\partial_v f_\varepsilon(t,\cdot)$ for $|v| \to \infty$ will be needed, which is provided by

Proposition 1.12. *Under* (1.43), $f_\varepsilon(t,v)$, $\partial_v f_\varepsilon(t,v) \to 0$ *for* $|v| \to \infty$ *for every* $t > 0$ *and every* $\varepsilon > 0$.

Proof. (i) Let $u_\varepsilon(t) := \lim_{v\to+\infty} f_\varepsilon(t,v)$. Passing to the limit $v \to +\infty$ in (1.45) we obtain

$$u_\varepsilon' + \frac{1}{\varepsilon^2} u_\varepsilon \le 2\|r\|_\infty u_\varepsilon + \frac{1}{\varepsilon^2} u_\varepsilon,$$

where we observed that, owing to Proposition 1.10, the mapping $z \mapsto \mathcal{M}(z;\alpha\varepsilon,\beta) f_\varepsilon(t,v-\varepsilon z)$ is bounded for every $v \in \mathbb{R}$ by the integrable mapping $z \mapsto \|f_\varepsilon(t)\|_\infty \mathcal{M}(z;\alpha\varepsilon,\beta)$, cf. (H1), therefore we could pass the limit through the integral by dominated convergence. The inequality above is equivalent to

$$u_\varepsilon' \le 2\|r\|_\infty u_\varepsilon,$$

which, along with $u_\varepsilon(0) = \lim_{v\to+\infty} f^0(v) = 0$ by assumption, implies $u_\varepsilon(t) \le 0$ for all $t > 0$. But $u_\varepsilon(t) \ge 0$, because f_ε is non-negative; thus, ultimately, $u_\varepsilon(t) = 0$ for all $t > 0$.

The very same argument proves also that $\lim_{v\to-\infty} f_\varepsilon(t,v) = 0$ for all $t > 0$.

(ii) Let now $w_\varepsilon(t) := \lim_{v\to+\infty} |\partial_v f_\varepsilon(t,v)| \ge 0$. From (1.46) we deduce preliminarily

$$\partial_t |\partial_v f_\varepsilon| \le \|r'\|_\infty f_\varepsilon + 2\|r\|_\infty |\partial_v f_\varepsilon| + \frac{1}{\varepsilon^2}\left(\int_{\mathbb{R}} \mathcal{M}(z;\alpha\varepsilon,\beta) |\partial_v f_\varepsilon(t,v-\varepsilon z)|\, dz + |\partial_v f_\varepsilon| \right),$$

whence, taking the limit $v \to +\infty$ and invoking again the dominated convergence,

$$w_\varepsilon' \le 2\left(\|r\|_\infty + \frac{1}{\varepsilon^2} \right) w_\varepsilon,$$

where we have used that $f_\varepsilon(t,\cdot) \to 0$ for $v \to +\infty$ as proved in the previous step. Since $w_\varepsilon(0) = \lim_{v\to+\infty} \left|\partial_v f^0(v)\right| = 0$ by assumption, we conclude $w_\varepsilon(t) = 0$ for all $t > 0$.

The same argument shows also that $\lim_{v\to-\infty} |\partial_v f_\varepsilon(t,v)| = 0$ for all $t > 0$. □

We end this section by showing that also the differential model (1.40) preserves the boundedness in time of the L^2 norm of its solution:

Proposition 1.13 (L^2 estimate on g)**.** *Under* (1.43), $g(t,\cdot) \in L^2(\mathbb{R})$ *for every* $t \in (0,\, T]$, *where* $T > 0$ *is arbitrary.*

Proof. We multiply (1.40) by $2g$ and integrate both sides w.r.t. $v \in \mathbb{R}$ to find:

$$\frac{d}{dt}\|g(t)\|_{L^2}^2 = 2\int_{\mathbb{R}} (r(v) - \varrho) g^2(t,v)\, dv - 2\alpha \int_{\mathbb{R}} g(t,v)\partial_v g(t,v)\, dv + \beta \int_{\mathbb{R}} g(t,v)\partial_v^2 g(t,v)\, dv.$$

Observing that $2g\partial_v g = \partial_v g^2$ and integrating by parts the last term on the right-hand side we further obtain:

$$\begin{aligned}\frac{d}{dt}\|g(t)\|_{L^2}^2 = 2\int_{\mathbb{R}} (r(v) - \varrho) g^2(t,v)\, dv - \alpha\Big(g^2(t,v)\Big|_{v=-\infty}^{v=+\infty} \\ - \beta \int_{\mathbb{R}} (\partial_v g(t,v))^2\, dv + \beta\Big(g(t,v)\partial_v g(t,v)\Big|_{v=-\infty}^{v=+\infty}.\end{aligned}$$

Finally, the boundary conditions (1.41) together with the non-negativity of $(\partial_v g)^2$, ϱ yield

$$\leq 2\|r\|_\infty \|g(t)\|_{L^2}^2,$$

therefore

$$\|g(t)\|_{L^2} \leq \left\|f^0\right\|_{L^2} e^{\|r\|_\infty t},$$

whence the thesis follows. □

1.4.1.2 L^2 convergence

Propositions 1.9, 1.13 indicate that, for L^2-integrable initial data, $L^2(\mathbb{R})$ is a space the solutions $f_\varepsilon(t,\cdot)$, $g(t,\cdot)$ to (1.32), (1.40) belong to for t in bounded intervals of the form $(0,\, T]$, $T > 0$ arbitrary. It is therefore reasonable to ascertain the convergence of f_ε to g in that space as $\varepsilon \to 0^+$.

To this purpose, we preliminarily establish:

Proposition 1.14. *Under* (1.43), (1.44)*, the following estimate holds:*

$$|(\rho_\varepsilon - \varrho)(t)| \leq \|r\|_{L^2} e^{2\|r\|_\infty t} \int_0^t \|(f_\varepsilon - g)(s)\|_{L^2}\, ds, \qquad t > 0.$$

Proof. Subtracting (1.33) and (1.39) with $\varphi(v) = 1$ gives

$$\frac{d}{dt}(\rho_\varepsilon - \varrho) = \int_{\mathbb{R}} r(v)\big(f_\varepsilon(t,v) - g(t,v)\big)\, dv - \big(\rho_\varepsilon^2 - \varrho^2\big).$$

Using the Cauchy–Schwarz inquality in the first term on the right-hand side and writing $\rho_\varepsilon^2 - \varrho^2 = (\rho_\varepsilon + \varrho)(\rho_\varepsilon - \varrho)$, we estimate

$$\frac{d}{dt}|\rho_\varepsilon - \varrho| \le \|r\|_{L^2}\|(f_\varepsilon - g)(t)\|_{L^2} + 2\|r\|_\infty|\rho_\varepsilon - \varrho|,$$

whence, integrating over $[0,\, t]$, $t > 0$, and using that $\rho_\varepsilon(0) = \varrho(0)$ owing to (1.44),

$$|(\rho_\varepsilon - \varrho)(t)| \le \|r\|_{L^2}\int_0^t \|(f_\varepsilon - g)(s)\|_{L^2}\,ds + 2\|r\|_\infty\int_0^t |(\rho_\varepsilon - \varrho)(s)|\,ds.$$

Grönwall's inequality yields then the thesis. □

We are now in a position to prove:

Theorem 1.15 (Quasi-invariant limit)**.** *Under* (1.43), (1.44), $f_\varepsilon(t,\cdot) \to g(t,\cdot)$ *in* $L^2(\mathbb{R})$ *for every* $t \in (0,\, T]$ *with arbitrary* $T > 0$ *when* $\varepsilon \to 0^+$.

Proof. Subtracting (1.32) – with the scaling (1.29), (1.36) – and (1.40) we find:

$$\begin{aligned}\partial_t(f_\varepsilon - g) = {}& \big(r(v) - \rho_\varepsilon\big)(f_\varepsilon - g) - (\rho_\varepsilon - \varrho)g \\ & + \frac{1}{\varepsilon^2}\left(\int_{\mathbb{R}} \mathcal{M}(z;\, \alpha\varepsilon, \beta) f_\varepsilon(t, v - \varepsilon z)\,dz - f_\varepsilon\right) + \alpha\partial_v g - \frac{\beta}{2}\partial_v^2 g,\end{aligned}$$

where we have performed the change of variable from w to $z := \frac{v-w}{\varepsilon}$ in the integral. Expanding

$$f_\varepsilon(t, v - \varepsilon z) = f_\varepsilon(t,v) - \varepsilon\partial_v f_\varepsilon(t,v)z + \frac{\varepsilon^2}{2}\partial_v^2 f_\varepsilon(t,v)z^2 - \frac{\varepsilon^3}{6}\partial_v^3 f_\varepsilon(\tilde v, t)z^3,$$

where $\tilde v := (1-\theta)v + \theta(v - \varepsilon z) = v - \theta\varepsilon z$ for some $\theta \in [0,\, 1]$, and recalling (H1)–(H4) we further find

$$\begin{aligned}\partial_t(f_\varepsilon - g) = {}& \big(r(v) - \rho_\varepsilon\big)(f_\varepsilon - g) - (\rho_\varepsilon - \varrho)g - \alpha\partial_v(f_\varepsilon - g) + \frac{\beta}{2}\partial_v^2(f_\varepsilon - g) \\ & + \frac{\alpha^2\varepsilon^2}{2}\partial_v^2 f_\varepsilon - \frac{\varepsilon}{6}\int_{\mathbb{R}} z^3\mathcal{M}(z;\, \alpha\varepsilon, \beta)\partial_v^3 f_\varepsilon(\tilde v, t)\,dz.\end{aligned}$$

We now multiply both sides by $2(f_\varepsilon - g)$ and integrate w.r.t. $v \in \mathbb{R}$ to obtain:

$$\begin{aligned}\frac{d}{dt}\|(f_\varepsilon - g)(t)\|_{L^2}^2 &= 2\int_{\mathbb{R}} (r(v) - \rho_\varepsilon)(f_\varepsilon(t,v) - g(t,v))^2\, dv \\ &\quad - 2(\rho_\varepsilon - \varrho)\int_{\mathbb{R}} g(t,v)(f_\varepsilon(t,v) - g(t,v))\, dv \\ &\quad - 2\alpha\int_{\mathbb{R}} \partial_v(f_\varepsilon(t,v) - g(t,v))(f_\varepsilon(t,v) - g(t,v))\, dv \\ &\quad + \beta\int_{\mathbb{R}} \partial_v^2(f_\varepsilon(t,v) - g(t,v))(f_\varepsilon(t,v) - g(t,v))\, dv \\ &\quad + \alpha^2\varepsilon^2\int_{\mathbb{R}} \partial_v^2 f_\varepsilon(t,v)(f_\varepsilon(t,v) - g(t,v))\, dv \\ &\quad - \frac{\varepsilon}{3}\int_{\mathbb{R}}\int_{\mathbb{R}} z^3\mathcal{M}(z;\alpha\varepsilon,\beta)\partial_v^3 f_\varepsilon(\tilde{v},t)(f_\varepsilon(t,v) - g(t,v))\, dz\, dv.\end{aligned}$$

Next, we notice that $2(f_\varepsilon - g)\partial_v(f_\varepsilon - g) = \partial_v(f_\varepsilon - g)^2$ and we exploit Cauchy–Schwarz inequality and integration-by-parts to further elaborate this as:

$$\begin{aligned}&\leq 2\|r\|_\infty\|(f_\varepsilon - g)(t)\|_{L^2}^2 + 2|(\rho_\varepsilon - \varrho)(t)| \cdot \|g(t)\|_{L^2}\|(f_\varepsilon - g)(t)\|_{L^2} \\ &\quad - \alpha\Big((f_\varepsilon(t,v) - g(t,v))^2\Big|_{v=-\infty}^{v=+\infty} \\ &\quad + \beta\Big(\partial_v(f_\varepsilon(t,v) - g(t,v))(f_\varepsilon(t,v) - g(t,v))\Big|_{v=-\infty}^{v=+\infty} \\ &\qquad - \beta\int_{\mathbb{R}}\big(\partial_v(f_\varepsilon(t,v) - g(t,v)\big)^2 dv \\ &\quad + 2\varepsilon\left(\alpha\varepsilon\Big\|\partial_v^2 f_\varepsilon(t)\Big\|_\infty + \frac{1}{3}\Big\|\partial_v^3 f_\varepsilon(t)\Big\|_\infty\big(\beta^{3/2}\langle\Big|\tilde{Z}^3\Big|\rangle + 1\big)\right)(\rho_\varepsilon + \varrho)(t),\end{aligned}$$

where $\tilde{Z}$ is the random variable introduced in (1.38).

Applying Proposition 1.12 together with the boundary conditions (1.41) along with Propositions 1.2, 1.7, 1.13, 1.14, we arrive at

$$\begin{aligned}&\leq 2\|r\|_\infty\|(f_\varepsilon - g)(t)\|_{L^2}^2 \\ &\quad + 2\|r\|_{L^2}\Big\|f^0\Big\|_{L^2} e^{3\|r\|_\infty t}\|(f_\varepsilon - g)(t)\|_{L^2}\int_0^t \|(f_\varepsilon - g)(\tau)\|_{L^2}\, d\tau \\ &\quad + 4\varepsilon\|r\|_\infty\left(\alpha\varepsilon\Big\|\partial_v^2 f_\varepsilon(t)\Big\|_\infty + \frac{1}{3}\big(\beta^{3/2}\langle\Big|\tilde{Z}^3\Big|\rangle + 1\big)\Big\|\partial_v^3 f_\varepsilon(t)\Big\|_\infty\right).\end{aligned}$$

Next, we integrate both sides on $[0,\, t]$, $t > 0$, and use the fact that $f_\varepsilon(0,v) = g(0,v) = f^0(v)$ to deduce:

$$\begin{aligned}
\|(f_\varepsilon - g)(t)\|_{L^2}^2 &\le 2\|r\|_\infty \int_0^t \|(f_\varepsilon - g)(s)\|_{L^2}^2\, ds \\
&\quad + 2\|r\|_{L^2}\left\|f^0\right\|_{L^2} \int_0^t e^{3\|r\|_\infty s}\|(f_\varepsilon - g)(s)\|_{L^2} \int_0^s \|(f_\varepsilon - g)(\tau)\|_{L^2}\, d\tau\, ds \\
&\quad + 4\varepsilon\|r\|_\infty \left(\alpha\varepsilon \int_0^t \left\|\partial_v^2 f_\varepsilon(s)\right\|_\infty ds + \frac{1}{3}\left(\beta^{3/2}\langle\left|\tilde{Z}^3\right|\rangle + 1\right) \int_0^t \left\|\partial_v^3 f_\varepsilon(s)\right\|_\infty ds\right) \\
&\le 2\|r\|_\infty \int_0^t \|(f_\varepsilon - g)(s)\|_{L^2}^2\, ds \\
&\quad + 2\|r\|_{L^2}\left\|f^0\right\|_{L^2} e^{3\|r\|_\infty t}\left(\int_0^t \|(f_\varepsilon - g)(s)\|_{L^2}\, ds\right)^2 \\
&\quad + 4\varepsilon\|r\|_\infty \left(\alpha\varepsilon \int_0^t \left\|\partial_v^2 f_\varepsilon(s)\right\|_\infty ds + \frac{1}{3}\left(\beta^{3/2}\langle\left|\tilde{Z}^3\right|\rangle + 1\right) \int_0^t \left\|\partial_v^3 f_\varepsilon(s)\right\|_\infty ds\right),
\end{aligned}$$

whence, applying Cauchy–Schwarz inequality to the second term on the right-hand side,

$$\begin{aligned}
&\le 2\left(\|r\|_\infty + \|r\|_{L^2}\left\|f^0\right\|_{L^2} t e^{3\|r\|_\infty t}\right) \int_0^t \|(f_\varepsilon - g)(s)\|_{L^2}^2\, ds \\
&\quad + 4\varepsilon\|r\|_\infty \left(\alpha\varepsilon \int_0^t \left\|\partial_v^2 f_\varepsilon(s)\right\|_\infty ds + \frac{1}{3}\left(\beta^{3/2}\langle\left|\tilde{Z}^3\right|\rangle + 1\right) \int_0^t \left\|\partial_v^3 f_\varepsilon(s)\right\|_\infty ds\right).
\end{aligned}$$

Proposition 1.10 implies that $\left\|\partial_v^2 f_\varepsilon(t)\right\|_\infty$ and $\left\|\partial_v^3 f_\varepsilon(t)\right\|_\infty$ are ε-uniformly bounded in $(0,\, T]$ by a constant $C_T > 0$, thus

$$\begin{aligned}
&\le 2\left(\|r\|_\infty + \|r\|_{L^2}\left\|f^0\right\|_{L^2} t e^{3\|r\|_\infty t}\right) \int_0^t \|(f_\varepsilon - g)(s)\|_{L^2}^2\, ds \\
&\quad + 4\varepsilon\|r\|_\infty C_T \left(\alpha\varepsilon + \frac{1}{3}\left(\beta^{3/2}\langle\left|\tilde{Z}^3\right|\rangle + 1\right)\right) t.
\end{aligned}$$

Finally, Lemma 1.5 applied to $u(t) = \|(f_\varepsilon - g)(t)\|_{L^2}^2$ with

$$a(t) = 4\varepsilon\|r\|_\infty C_T \left(\alpha\varepsilon + \tfrac{1}{3}\left(\beta^{3/2}\langle|\tilde{Z}^3|\rangle + 1\right)\right) t, \qquad b(t) = 2\left(\|r\|_\infty + \|r\|_{L^2}\left\|f^0\right\|_{L^2} t e^{3\|r\|_\infty t}\right),$$

which are non-decreasing non-negative functions in $[0,\, T]$, yields

$$\|(f_\varepsilon - g)(t)\|_{L^2}^2 \le 4\varepsilon\|r\|_\infty C_T \left(\alpha\varepsilon + \frac{1}{3}\left(\beta^{3/2}\langle\left|\tilde{Z}^3\right|\rangle + 1\right)\right) t e^{b(t)t} \xrightarrow{\varepsilon\to 0^+} 0,$$

which concludes the proof. □

1.4.1.3 Convergence of the statistical moments

To grasp the big picture of a multi-agent system, one usually refers to aggregate macroscopic quantities represented by the statistical moments of the distribution function. We recall, in particular, the most significant low-order ones:

- $\rho_\varepsilon(t) := \int_{\mathbb{R}} f_\varepsilon(t,v)\,dv$, i.e. the density of the agents at time $t > 0$ (zeroth order moment),
- $p_\varepsilon(t) := \int_{\mathbb{R}} v f_\varepsilon(t,v)\,dv$, i.e. the phenotypic "momentum" at time $t > 0$ (first order moment),
- $E_\varepsilon(t) := \int_{\mathbb{R}} v^2 f_\varepsilon(t,v)\,dv$, i.e. the phenotypic "bulk energy" at time $t > 0$ (second order moment).

In this section, we show that in the quasi-invariant limit $\varepsilon \to 0^+$ these quantities converge to the corresponding moments of the limit phenotypic distribution function g:

$$\varrho(t) := \int_{\mathbb{R}} g(t,v)\,dv, \qquad p(t) := \int_{\mathbb{R}} v g(t,v)\,dv, \qquad E(t) := \int_{\mathbb{R}} v^2 g(t,v)\,dv,$$

thereby establishing that the differential model (1.40) inherits in the limit also the exact main statistical moments of the agent distribution. For this, besides (1.43) we shall need the following additional assumption on the function r:

$$v^2 r \in L^2(\mathbb{R}). \tag{1.48}$$

The first result is a straightforward consequence of the theory developed in Section 1.4.1.2.

Theorem 1.16 (Convergence of the density)**.** *Under* (1.43), (1.44), $\rho_\varepsilon(t) \to \varrho(t)$ *for every* $t \in (0,\, T]$ *and arbitrary* $T > 0$ *as* $\varepsilon \to 0^+$.

Proof. The thesis follows from the fact that Proposition 1.14 and the proof of Theorem 1.15 imply jointly[1] $|\rho_\varepsilon(t) - \varrho(t)| \lesssim \sqrt{\varepsilon}$ for all $t \in (0,\, T]$. □

We proceed now with the other two moments.

Theorem 1.17 (Convergence of the phenotypic momentum and bulk energy)**.** *Under* (1.43), (1.44), *and* (1.48), $p_\varepsilon(t) \to p(t)$ *and* $E_\varepsilon(t) \to E(t)$ *for every* $t \in (0,\, T]$ *and arbitrary* $T > 0$ *as* $\varepsilon \to 0^+$.

[1]The symbol $\lesssim$ indicates that there exists a constant $C > 0$, independent of ε, t and the specific value of which is not relevant, such that $|\rho_\varepsilon(t) - \varrho(t)| \le C\sqrt{\varepsilon}$ for every $t \in (0,\, T]$. From the proof of Theorem 1.15, it can be seen that such a constant instead depends on T.

Proof. (i) We begin with the convergence of the phenotypic momentum. We observe preliminarily that from (1.48) it follows also $vr \in L^2(\mathbb{R})$; in fact:

$$\|vr\|_{L^2}^2 = \int_{\mathbb{R}} v^2 r^2(v)\,dv = \int_{\{|v|\le 1\}} v^2 r^2(v)\,dv + \int_{\{|v|>1\}} v^2 r^2(v)\,dv,$$

whence, since $v^2 \le 1$ for $|v| \le 1$ and $v^2 < v^4$ for $|v| > 1$,

$$\begin{aligned} &\le \int_{\{|v|\le 1\}} r^2(v)\,dv + \int_{\{|v|>1\}} v^4 r^2(v)\,dv \\ &\le \|r\|_{L^2}^2 + \left\|v^2 r\right\|_{L^2}^2 < +\infty. \end{aligned}$$

Letting now $\varphi(v) = v$ in (1.33) with (1.36) and recalling (1.31), we obtain

$$\frac{dp_\varepsilon}{dt} = \int_{\mathbb{R}} vr(v) f_\varepsilon(t,v)\,dv - \rho_\varepsilon p_\varepsilon + \alpha\rho_\varepsilon;$$

likewise, substituting $\varphi(v) = v$ into (1.39) we find

$$\frac{dp}{dt} = \int_{\mathbb{R}} vr(v) g(t,v)\,dv - \varrho p + \alpha\varrho. \tag{1.49}$$

Subtracting these two equations produces

$$\frac{d}{dt}(p_\varepsilon - p) = \int_{\mathbb{R}} vr(v)\big(f_\varepsilon(t,v) - g(t,v)\big)\,dv - \rho_\varepsilon(p_\varepsilon - p) + (\alpha - p)(\rho_\varepsilon - \varrho),$$

whence

$$\frac{d}{dt}|p_\varepsilon - p| \le \|vr\|_{L^2}\|(f_\varepsilon - g)(t)\|_{L^2} + \|r\|_\infty |p_\varepsilon - p| + (|p| + |\alpha|)|\rho_\varepsilon - \varrho|. \tag{1.50}$$

Notice that from (1.49) it follows that p is bounded on every bounded time interval; in fact:

$$\frac{d}{dt}|p| \le \|vr\|_{L^2}\|g(t)\|_{L^2} + \|r\|_\infty |p| + |\alpha| \cdot \|r\|_\infty,$$

thus, by Grönwall's inequality after bounding $\|g(t)\|_{L^2}$ by means of Proposition 1.13, $|p(t)|$ is bounded by a non-negative non-decreasing function, say $h = h(t)$. Using this in (1.50) after integrating on $[0,\, t]$, $t > 0$, yields

$$\begin{aligned} |(p_\varepsilon - p)(t)| \le \|rv\|_{L^2} \int_0^t \|(f_\varepsilon - g)(s)\|_{L^2}\,ds + \int_0^t (h(s) + |\alpha|)|(\rho_\varepsilon - \varrho)(s)|\,ds \\ + \|r\|_\infty \int_0^t |(p_\varepsilon - p)(s)|\,ds, \end{aligned}$$

where we have taken into account that $p_\varepsilon(0) = p(0)$ because of (1.44).

At this stage, Lemma 1.4 applied to the function $u(t) = |(p_\varepsilon - p)(t)|$ with

$$a(t) = \|rv\|_{L^2} \int_0^t \|(f_\varepsilon - g)(s)\|_{L^2}\, ds + \int_0^t (h(s) + |\alpha|)|(\rho_\varepsilon - \varrho)(s)|\, ds, \quad b(t) = \|r\|_\infty$$

produces

$$|(p_\varepsilon - p)(t)| \le \int_0^t \big(\|vr\|_{L^2}\|(f_\varepsilon - g)(s)\|_{L^2} + (h(s) + |\alpha|)|(\rho_\varepsilon - \varrho)(s)|\big) e^{\|r\|_\infty (t-s)}\, ds.$$

The thesis follows then passing the limit $\varepsilon \to 0^+$ through the integral by dominated convergence – notice that, owing to Propositions 1.2, 1.7, 1.9, 1.13, the integrand is bounded by the integrable mapping $t \mapsto 2\|vr\|_{L^2}\|f^0\|_{L^2} e^{\|r\|_\infty t} + 2(|\alpha| + h(s))\|r\|_\infty$ – and invoking Theorems 1.15, 1.16.

(ii) As for the convergence of the phenotypic bulk energy, we proceed analogously to the previous step by substituting $\varphi(v) = v^2$ into (1.33) with (1.36) and into (1.39) to find, respectively,

$$\begin{aligned} \frac{dE_\varepsilon}{dt} &= \int_{\mathbb{R}} v^2 r(v) f_\varepsilon(t,v)\, dv - \rho_\varepsilon E_\varepsilon + 2\alpha p_\varepsilon + (\beta + \alpha^2\varepsilon^2)\rho_\varepsilon, \\ \frac{dE}{dt} &= \int_{\mathbb{R}} v^2 r(v) g(t,v)\, dv - \varrho E + 2\alpha p + \beta\varrho. \end{aligned}$$

Subtracting these equations yields

$$\begin{aligned} \frac{d}{dt}|E_\varepsilon - E| \le \left\|v^2 r\right\|_{L^2} &\|(f_\varepsilon - g)(t)\|_{L^2} \\ &+ \|r\|_\infty |E_\varepsilon - E| + (|E| + \beta)|\rho_\varepsilon - \varrho| \\ &+ 2|\alpha| \cdot |p_\varepsilon - p| + \alpha^2 \|r\|_\infty \varepsilon^2. \end{aligned}$$

In particular, the equation of E shows that the latter is bounded by a non-negative non-decreasing function, say $k = k(t)$, because

$$\frac{d}{dt}|E| \le \left\|v^2 r\right\|_{L^2} \|g(t)\|_{L^2} + \|r\|_\infty |E| + 2|\alpha| \cdot |p| + \beta\|r\|_\infty,$$

where $\|g(t)\|_{L^2}$ can be bounded by means of Proposition 1.13 while $|p|$ is bounded by the function h introduced in the previous step.

On the whole, we have then:

$$\begin{aligned}|(E_\varepsilon - E)(t)| \leq \left\|v^2 r\right\|_{L^2} \int_0^t \|(f_\varepsilon - g)(s)\|_{L^2}\, ds + \int_0^t (k(s)+\beta)|(\rho_\varepsilon - \varrho)(s)|\, ds \\ + 2|\alpha| \int_0^t |(p_\varepsilon - p)(s)|\, ds + \alpha^2 \|r\|_\infty \varepsilon^2 t \\ + \|r\|_\infty \int_0^t |(E_\varepsilon - E)(s)|\, ds,\end{aligned}$$

which, invoking Lemma 1.4 for the function $u(t) = |(E_\varepsilon - E)(t)|$ with

$$\begin{aligned}a(t) &= \left\|v^2 r\right\|_{L^2} \int_0^t \|(f_\varepsilon - g)(s)\|_{L^2}\, ds + \int_0^t (k(s)+\beta)|(\rho_\varepsilon - \varrho)(s)|\, ds \\ &\quad + 2|\alpha| \int_0^t |(p_\varepsilon - p)(s)|\, ds + \alpha^2 \|r\|_\infty \varepsilon^2 t, \\ b(t) &= \|r\|_\infty,\end{aligned}$$

implies

$$\begin{aligned}|(E_\varepsilon - E)(t)| \leq \int_0^t \Big(\left\|v^2 r\right\|_{L^2} \|(f_\varepsilon - g)(s)\|_{L^2} + (k(s)+\beta)|(\rho_\varepsilon - \varrho)(s)| \\ + 2|\alpha| \cdot |(p_\varepsilon - p)(s)| + \alpha^2 \|r\|_\infty \varepsilon^2 s \Big) e^{\|r\|_\infty (t-s)}\, ds.\end{aligned}$$

The thesis follows then from Theorems 1.15, 1.16 along with the result proved in the previous step, passing the limit $\varepsilon \to 0^+$ through the integral by dominated convergence. □

Remark 1.18. From the statistical moments above, one can compute two other aggregate quantities of interest, such as the mean phenotype:

$$\bar{v}_\varepsilon := \frac{p_\varepsilon}{\rho_\varepsilon}$$

and the variance of the phenotypic distribution:

$$\sigma_\varepsilon^2 := \frac{E_\varepsilon}{\rho_\varepsilon} - \bar{v}_\varepsilon^2.$$

In the quasi-invariant regime, the corresponding quantities $\bar{v}$, σ^2 are defined analogously using ϱ, p, and E.

1.4.2 The case of constant r

As stated in Remark 1.8, the theory developed in this chapter does not cover the case of constant r. For the sake of theoretical speculation and completeness, in

this subsection we provide the technical details needed to also address the simpler quasi-invariant limit with constant $r \leq 1$.

In the following, we keep assumptions (1.43), (1.44), except that we drop the request $r \in L^2(\mathbb{R})$.

The main simplification that occurs with a constant r is that the density ρ_ε obeys a self-consistent equation independent of ε. In fact, substituting $\varphi(v) = 1$ into (1.33) we obtain

$$\frac{d\rho_\varepsilon}{dt} = (r - \rho_\varepsilon)\rho_\varepsilon,$$

which is a logistic equation admitting the ε-free solution

$$\rho_\varepsilon(t) = \frac{r\rho^0}{(r-\rho^0)e^{-rt} + \rho^0}.$$

If $0 \leq \rho^0 \leq r$, the result of Proposition 1.2 still holds true qualitatively, and we have, in particular, $0 \leq \rho_\varepsilon(t) \leq r$ for all $t > 0$.

The same reasoning applied to (1.39) with $\varphi(v) = 1$ shows that the density ϱ fulfills the very same equation as ρ_ε:

$$\frac{d\varrho}{dt} = (r - \varrho)\varrho,$$

whence $\rho_\varepsilon(t) = \varrho(t)$ for every $\varepsilon > 0$ and every $t \geq 0$. In practice, there exists a unique density, say ρ, which is independent of ε and is the same for both distribution functions f_ε, g. Therefore, there is no need to pass to the limit $\varepsilon \to 0^+$ in the density.

On the other hand, Propositions 1.1, 1.3, 1.9, 1.10, 1.12, 1.13 still hold true because none of their proofs uses the L^2-integrability of r, as it can be ascertained by direct inspection.

The consequence of these facts is that Theorem 1.15 also holds when r is constant. In fact, the term $|(\rho_\varepsilon - \varrho)(t)|$, which in the proof of the theorem carries the dependence on $\|r\|L^2$, vanishes whereas the rest of the proof remains unchanged due to the boundedness of $\partial_v^2 f_\varepsilon$ and $\partial_v^3 f_\varepsilon$. Specifically, the L^2-estimate on $f_\varepsilon - g$ provided in the proof modifies as

$$\|(f_\varepsilon - g)(t)\|L^2{}^2 \leq 2r \int_0^t \|(f_\varepsilon - g)(s)\|L^2{}^2 \, ds + 4\varepsilon r C_T \left(\alpha\varepsilon + \frac{1}{3}(\beta^{3/2}\langle|\tilde{Z}|^3\rangle + 1)\right) t,$$

whence one obtains the convergence $f_\varepsilon(t) \to g(t)$ in $L^2(\mathbb{R})$ for every $t > 0$ as $\varepsilon \to 0^+$ by applying the standard Grönwall's inequality.

As far as the convergence of the statistical moments is concerned, we notice that also the phenotypic momentum of f_ε does not depend on ε. In fact, substituting

TABLE 1.1: Parameters used in the numerical simulations of Figures 1.2, 1.3, 1.4

Parameter	Description	Value
N	Number of agents in MC simulations	10^5
Δv	Phenotypic mesh size	$2.5 \cdot 10^{-2}$
Δt	Numerical time step	10^{-4}
T	Final time of simulations	10
	Computational phenotypic domain	$[-15, 15]$
R	Radius of the mollifier ψ	5
δ	Amplitude of the transition layer of the mollifier ψ	0.5
v_m	Fittest trait (i.e. maximum point of the function r)	1.5
α	Drift coefficient	-0.3, 0, 0.3
β	Diffusion coefficient	0.4
ε	Scaling parameter for the quasi-invariant regime	1, $10^{-1/2}$, 10^{-1}

$\varphi(v) = v$ into (1.33) with (1.36) we find

$$\frac{dp_\varepsilon}{dt} = (r - \rho)p_\varepsilon + \alpha\rho,$$

which is the very same equation satisfied by the phenotypic momentum p of g, as it can be checked by substituting $\varphi(v) = v$ into (1.39). Thus, $p_\varepsilon(t) = p(t)$ for every $\varepsilon > 0$ and every $t \geq 0$, which makes it needless to pass to the limit $\varepsilon \to 0^+$. Conversely, the phenotypic bulk energies E_ε, E satisfy

$$\frac{dE_\varepsilon}{dt} = (r - \rho)E_\varepsilon + 2\alpha p + (\beta + \alpha^2\varepsilon^2)\rho, \qquad \frac{dE}{dt} = (r - \rho)E + 2\alpha p + \beta\rho,$$

whence

$$\frac{d}{dt}(E_\varepsilon - E) = (r - \rho)(E_\varepsilon - E) + \alpha^2\varepsilon^2\rho$$

and, finally,

$$|(E_\varepsilon - E)(t)| \leq 2r \int_0^t |(E_\varepsilon - E)(s)|\, ds + \alpha^2 r\varepsilon^2 t.$$

From here, Grönwall's inequality provides the convergence $E_\varepsilon(t) \to E(t)$ for all $t > 0$ when $\varepsilon \to 0^+$, in particular without assumption (1.48) which, with constant r, could not be met.

1.5 Main results of numerical simulations

We now illustrate, by means of a sample of results of numerical simulations, the theoretical results proved in the previous sections. In more detail, we present the results of numerical simulations carried out for:

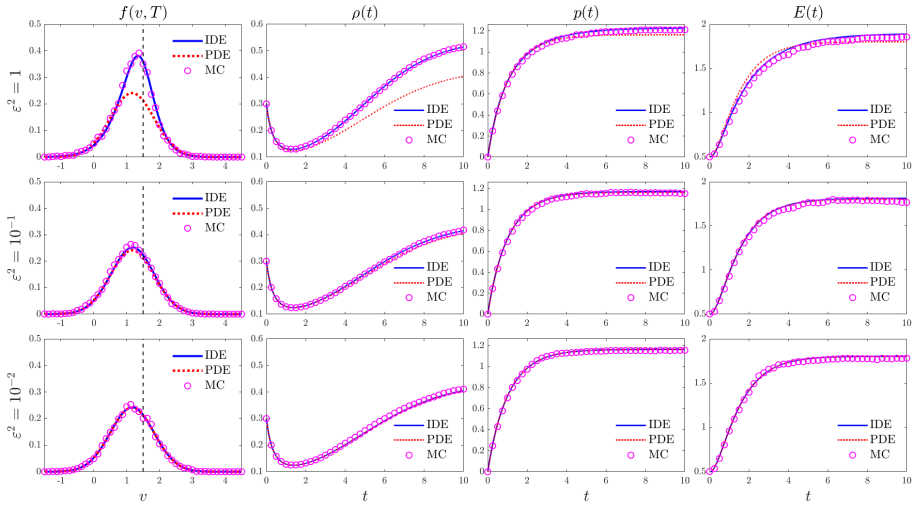

FIGURE 1.2: Results of numerical simulations of the stochastic agent-based model (1.5) (MC), the integro-differential model (1.32) (IDE), and the limit differential model (1.40) (PDE), for the drift coefficient $\alpha < 0$. The dashed vertical line in the panels of the first column highlights the fittest trait v_m

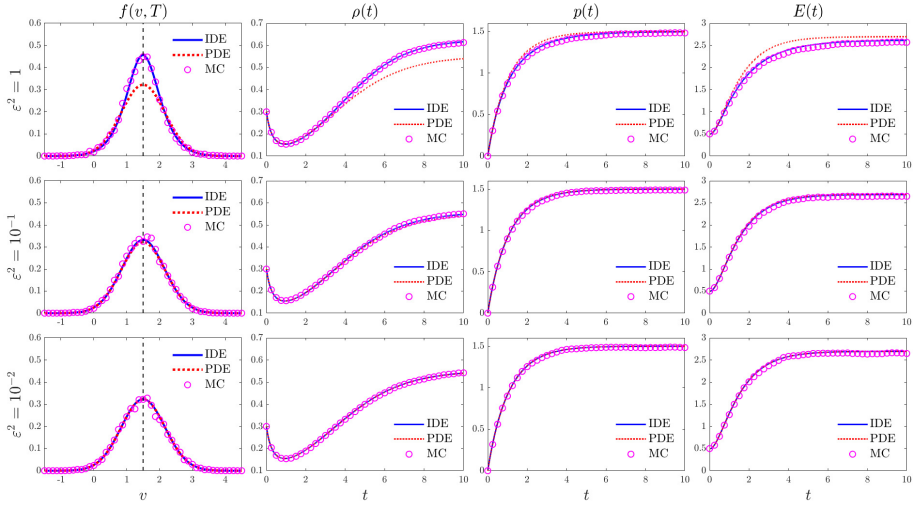

FIGURE 1.3: Results of numerical simulations of the stochastic agent-based model (1.5) (MC), the integro-differential model (1.32) (IDE), and the limit differential model (1.40) (PDE), for the drift coefficient $\alpha = 0$. The dashed vertical line in the panels of the first column highlights the fittest trait v_m

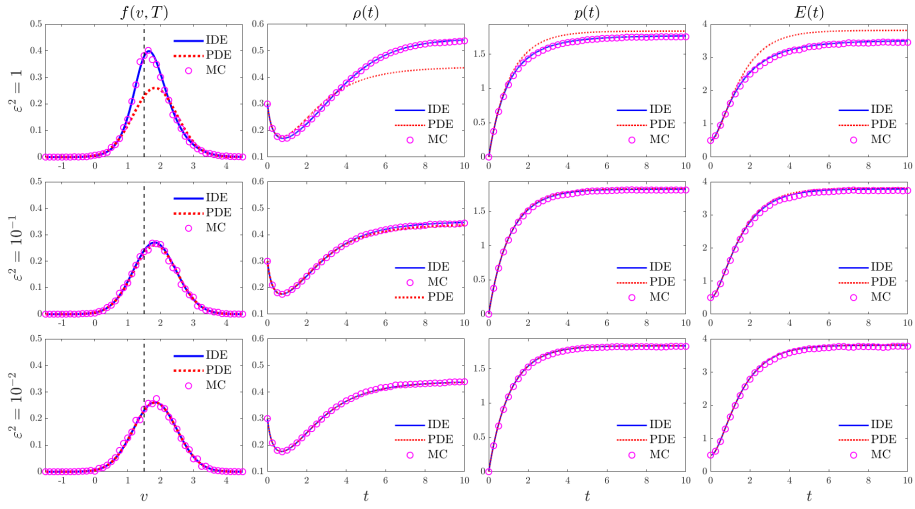

FIGURE 1.4: Results of numerical simulations of the stochastic agent-based model (1.5) (MC), the integro-differential model (1.32) (IDE), and the limit differential model (1.40) (PDE), for the drift coefficient $\alpha > 0$. The dashed vertical line in the panels of the first column indicates the fittest trait v_m

- the stochastic agent-based model (1.5) through a direct Monte Carlo method, cf. [129];
- the integro-differential model (1.32), for three decreasing values of the scaling parameter ε, through an explicit-in-time Euler scheme complemented with a numerical approximation of the integral term based on the trapezium rule;
- the limit differential model (1.40) through an explicit-in-time Euler scheme complemented with finite difference schemes for the approximation of the v-derivatives.

We compare and contrast these results in terms of distribution functions and low-order statistical moments. Specifically, the objective is to verify that there is quantitative agreement between the numerical solutions of the stochastic agent-based and integro-differential models for all the values of the scaling parameter, ε, thus corroborating the formal derivation presented in Section 1.3. Moreover, we aim at showing the convergence of the solution of the integro-differential model, and of its low-order statistical moments, to the solution of the differential model, and to the corresponding low-order moments, as the scaling parameter gets smaller, in order to provide numerical evidence for the quasi-invariant limit analytically studied in Section 1.4.

The parameter values employed in numerical simulations are summarised in Table 1.1.

As an initial condition, common to all simulations and to equations (1.32), (1.40), cf. (1.44), we prescribe

$$f^0(v) := \frac{3}{10\sqrt{\pi}} e^{-v^2},$$

namely a normal distribution with mass $\rho^0 = 0.3$, null mean, and variance equal to 0.5, which complies with assumptions (1.43). This is also the distribution from which the agents are initially sampled for the Monte Carlo method used for the stochastic agent-based model (1.5).

Concerning the net proliferation rate, r, we choose

$$r(v) := \Big(1 - (v - v_m)^2\Big)\, \psi(v).$$

The parabolic profile $1 - (v - v_m)^2$ is maximum at $v = v_m$ with $r(v_m) = 1$, cf. (1.28), which represents the so-called *fittest trait*, i.e. the phenotype corresponding to the maximum net proliferation rate. The factor $\psi : \mathbb{R} \to [0, 1]$ is a C^∞-mollifier, which is needed to adjust the trend of r at infinity, in compliance with assumptions (1.43), while allowing r to coincide with the desired parabolic profile at finite points. In more detail, ψ is defined by first introducing the functions

$$\zeta(v) := \frac{1}{2}\left[1 + \tanh\left(\frac{2v}{1 - v^2}\right)\right] \chi_{(-1,1)}(v), \qquad \hat{\psi}(v) := 1 - \zeta\left(\frac{2(v - R)}{\delta} - 1\right),$$

where $\chi_{(-1,1)}$ denotes the characteristic function of the interval $(-1, 1)$, and then letting

$$\psi(v) := \begin{cases} \hat{\psi}(-v) & \text{if } -R - \delta < v < -R \\ 1 & \text{if } -R \le v \le R \\ \hat{\psi}(v) & \text{if } R < v < R + \delta \\ 0 & \text{otherwise,} \end{cases}$$

where δ, $R > 0$ are real parameters, cf. Table 1.1. Notice that $\psi \equiv 1$, and thus $r(v) = 1 - (v - v_m)^2$, for $v \in [-R, R]$. In contrast, in the two layers $(-R - \delta, -R)$ and $(R, R + \delta)$ of amplitude δ the function $\hat{\psi}$ produces a C^∞-transition of ψ from 0 to 1 and from 1 to 0, respectively.

Figures 1.2, 1.3, 1.4 display the results of numerical simulations for three different values of the drift coefficient, α, that is, $\alpha < 0$ (Figure 1.2), $\alpha = 0$ (Figure 1.3), and $\alpha > 0$ (Figure 1.4) – see Table 1.1 for further details on the parameter values. In summary, the rows of each figure display, from left to right, the distribution function at the final time of simulations, $T = 10$, and the time evolution from $t = 0$ to $t = T$ of the density of agents, the phenotypic momentum, and the phenotypic bulk energy, computed for the three models for a given value of the scaling parameter ε, which decreases, from row to row, from $\varepsilon = 1$ through to $\varepsilon = \frac{1}{\sqrt{10}}$ to $\varepsilon = \frac{1}{10}$. In all cases, it is evident that, while there is excellent quantitative agreement between numerical solutions of the agent-based model (1.5) and the integro-differential models (1.32)

at all times and for all values of ε, the agreement with the solution of the differential model (1.40) improves as ε decreases, as expected from the quasi-invariant asymptotics. Note that, for the employed simulation set-up, a good qualitative agreement with the solution of the differential model (1.40) is already observed for a value of ε as moderately small as $\frac{1}{\sqrt{10}} \approx 0.32$.

1.6 Concluding remarks

In this chapter, we have advanced and employed a derivation method for aggregate mathematical descriptions of evolutionary dynamics in phenotype-structured populations, where population members undergo proliferation, death, and phenotype changes. This method is rooted in kinetic theory approaches for mass-varying multi-agent systems and makes it possible to bridge, in a consistent manner, three types of models for phenotype-structured populations commonly found in the literature: agent-based models tracking the dynamics of single population members, wherein phenotype changes and proliferation and death are represented as stochastic particle processes; IDE models governing the dynamics of phenotype distribution functions, in which phenotype changes are described by an integral operator encoding a mutation kernel, whereas proliferation and death are encapsulated in a non-local reaction term; and non-local PDEs for phenotype density functions, in which phenotype changes are taken into account by an advection-diffusion term, while proliferation and death are still represented by a non-local reaction term.

Our approach incorporates, from the very beginning, that is, from the agent-based level of representation, non-conservative phenomena (i.e. proliferation and death of population members). This has required special care in passing to the IDE model through the kinetic paradigm for multi-agent systems, since non-conservation of the number of agents, and thus of the mass of the system, is non-routine within such a paradigm. Moreover, this approach has shed light on the mutual relations among the aforementioned alternative types of models, which in the literature are usually addressed separately. In particular, we have shown that the IDE model is the aggregate counterpart of the agent-based model in every regime of the parameters driving the evolutionary dynamics of the population, whereas the non-local PDE model provides a faithful representation of the underlying evolutionary dynamics only in the regime of small and frequent phenotype changes.

Chapter 2

A multi-compartmental integro-differential model for phenotype structured population

Derivation and applications in epidemiology

2.1 Introduction

In the previous chapter, we developed a microscopic model that leverages the kinetic formalism to describe the phenotypic evolution of a population composed of a large number of individuals. To this end, we partitioned the population into two compartments, labelled 0 and 1, treating the former as a reservoir in which the microscopic structure is not explicitly modelled, and the latter as the population under investigation. This scheme proved useful for maintaining consistency with the biological nature of the system, as it explicitly incorporates proliferation and death processes. The resulting dynamics fall within the class of *selection–mutation* models, but the formulation involved only a single compartment. In fact, since the dynamics of the passive compartment can be derived from those of the active one (section 1.3), it was sufficient to isolate a single evolution equation.

However, the microscopic construction introduced is conceived in a simplified form, and it is therefore natural to extend it to scenarios in which a greater number of compartments play a dynamically relevant role. A classical example is the SIR model proposed by Kermack and McKendrick [103], which partitions the population into three compartments and generates a simple yet sufficiently rich dynamic

The results presented in this chapter are based on [21].

to describe the outbreak of a virus in an immunologically naive population. Another well-known case is provided by the Lotka–Volterra models, in which the population is composed of two species which interact within the same environment and mutually influence their evolutionary dynamics.

In this regard, although working with a system composed of a large number of equations entails greater analytical complexity, it also allows for a more faithful representation of the dynamics under investigation. Striking a balance between these two aspects is therefore essential for constructing a model that is as accurate as possible but still feasible. Following this logic, those examples considered above are typically formulated as systems of ordinary differential equations (ODEs), which clearly result in a significantly lower level of complexity.

In recent years, compartmental models have been the focus of significant research efforts aimed at enhancing their descriptive power through the introduction of heterogeneous structural properties. In epidemiology, this has led, for instance, to the inclusion of features such as viral load for infected individuals, or resistance to infection for susceptible and recovered ones [110]. At the same time, there has been growing interest in increasing the number of compartments to more accurately represent the diversity of behaviours and scenarios observed in infections with specific characteristics.

This chapter focuses on the formulation of a model capable of describing a multi-compartmental dynamic, in which each compartment is further structured by a continuous variable. The purpose of this variable is to represent the variability of relevant traits within the population, following and generalising the modelling approach proposed for SI systems in [110]. The model accounts for both the evolution of traits within each compartment and the transitions of individuals between different compartments. Therefore, this chapter starts by introducing an abstract and general formulation of the system, and then presents an implementation in an epidemiological setting. In this context, specific assumptions are introduced to adapt the general framework to different applied scenarios.

The mesoscopic counterpart of the model takes the form of a system of integro-differential equations (IDEs) for the population densities in each compartment. These densities describe the distributions of individuals over the domains of the structural variables associated with each compartment (cf. the schemtic Figure 2.1) . Through an appropriate rescaling procedure, the corresponding macroscopic model is finally derived, consisting of a system of ordinary differential equations (ODEs): one for the evolution of the fractions of individuals in each compartment, and another for the mean values of the structural traits. Moreover, in the second part, we employ a reduced version of the macroscopic model to obtain a general formula for the basic reproduction number $\mathcal{R}_0$.

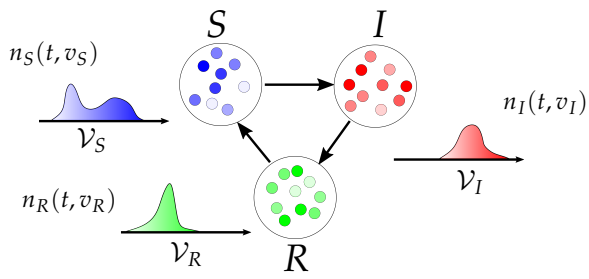

FIGURE 2.1: Schematic flow diagram of a heterogeneous SIRS system, along with its representation in terms of population density functions $n_i(t, v_i)$. Each function describes the distribution of individuals within compartment $i \in \mathcal{I} := \{S, I, R\}$ over the corresponding structuring variable $v_i \in \mathcal{V}_i$ at time t.

2.2 Stochastic agent-based model

As in the previous chapter, we consider a system of $N > 1$ interacting compartments, indexed by $i \in \mathcal{I} := \{1, \dots, N\}$. Each compartment is structured by a specific continuous variable $v_i \in \mathcal{V}_i \subset \mathbb{R}$, where $\mathcal{V}_i$ is a bounded interval. At time $t \in [0, \infty)$, we describe the microscopic state of individuals in the system, regarded as being indistinguishable, by the random vector $(I_t, \mathbf{V}_t)$, where $I_t \in \mathcal{I}$ and $\mathbf{V}_t \equiv (V_{1,t}, \dots, V_{N,t}) \in \mathcal{V} := \mathcal{V}_1 \times \dots \times \mathcal{V}_N \subset \mathbb{R}^N$. The discrete random variable I_t specifies the compartment of an individual at time t (i.e. individuals belonging to compartment i at time t will have $I_t = i$), while the continuous random variable $V_{i,t}$ models the level of expression of the trait represented by the i^{th} structuring variable at time t.

We let

$$(I_t, \mathbf{V}_t) \sim f(t, i, \mathbf{v}). \tag{2.1}$$

The distribution function $f : [0, \infty) \times \mathcal{I} \times \mathcal{V} \to \mathbb{R}_+$, being a probability density function, is such that

$$\sum_{i \in \mathcal{I}} \int_{\mathcal{V}} f(t, i, \mathbf{v}) \mathrm{d}\mathbf{v} = 1 \quad \forall\, t \in [0, \infty). \tag{2.2}$$

We focus on a scenario where between time t and time $t + \Delta t$, with $\Delta t > 0$:

(I) At rate $\theta_i \in \mathbb{R}_+^*$, *structuring-variable switching* may occur, whereby an individual in compartment i with expression level v_i of the trait represented by the structuring variable may spontaneously acquire a new expression level v_i', with probability $K_i(v_i'|v_i)$.

(II) At rate $\zeta \in \mathbb{R}_+^*$, *compartment switching* may take place, whereby an individual in compartment i with expression level v_i of the trait represented by the structuring variable may transition into compartment j. Compartment switching

can either be spontaneous (i.e. not driven by interactions with other individuals) with probability $r \in [0, 1]$, or driven by intra-/inter-compartment interactions (i.e. interactions between individuals of the same compartment/different compartments) with probability $1 - r$. In more detail:

(IIa) when *spontaneous compartment switching* occurs, the individual transitions into compartment j, with probability $p(j|i, v_i)$, and acquires a value v_j'' of the structuring variable of the new compartment, with probability $P(v_j''|j, i, v_i)$. This is the case, for example, of the switch $I \to R$ in the SIRWS model presented in Section 2.4.3, whereby an infected individual spontaneously recovers and becomes immune;

(IIb) when *interaction-driven compartment switching* occurs, the interaction with an individual in compartment k with value v_k^* of the structuring variable leads the individual to transition into compartment j, with probability $q(j|i, v_i, k, v_k^*)$, and acquire value v_j'' of the structuring variable of the new compartment, with probability $Q(v_j''|j, i, v_i, k, v_k^*)$. Considering again the SIRWS model presented in Section 2.4.3, this is the case, for example, of: the switch $S + I \to I + I$, whereby a susceptible individual interacts with an infected individual and contracts the disease (i.e. $k = j$); or the switch $W + I \to R + I$, whereby an individual with waning immunity interacts with an infected individual and receives a boost of immunity, becoming recovered and thus immune (i.e. $k \neq j$).

The aforementioned kernels K_i, P, and Q and the functions p and q satisfy the following assumptions for all $i, j, k \in \mathcal{I}$:

$$K_i(\cdot|\cdot) \in \mathscr{P}(\mathcal{V}_i; C(\mathcal{V}_i)), \quad P(\cdot|j, i, \cdot) \in \mathscr{P}(\mathcal{V}_j; C(\mathcal{V}_i)), \quad p(j|i, \cdot) \in C(\mathcal{V}_i),$$

$$Q(\cdot|j, i, \cdot, k, \cdot) \in \mathscr{P}(\mathcal{V}_j; C(\mathcal{V}_i \times \mathcal{V}_k)), \quad q(j|i, \cdot, k, \cdot) \in C(\mathcal{V}_i \times \mathcal{V}_k),$$

$$\mathrm{Supp}(K_i) \subseteq \mathcal{V}_i \times \mathcal{V}_i, \quad K_i \geq 0 \text{ a.e.}, \tag{2.3a}$$

$$\int_{\mathcal{V}_i} K_i(v_i'|v_i)\mathrm{d}v_i' = 1 \text{ and } \int_{\mathcal{V}_i} v_i' K_i(v_i'|v_i)\mathrm{d}v_i' \in \mathcal{V}_i \quad \forall v_i \in \mathcal{V}_i, \tag{2.3b}$$

$$\int_{\mathcal{V}_i} (v_i')^2 K_i(v_i'|v_i)\mathrm{d}v_i' - \left(\int_{\mathcal{V}_i} v_i' K_i(v_i'|v_i)\mathrm{d}v_i'\right)^2 > 0 \ \ \forall v_i \in \mathring{\mathcal{V}}_i, \tag{2.3c}$$

$$\mathrm{Supp}(P(\cdot|j, i, \cdot)) \subseteq \mathcal{V}_j \times \mathcal{V}_i, \quad P(\cdot|j, i, \cdot) \geq 0 \text{ a.e.},$$

$$\int_{\mathcal{V}_j} P(v_j''|j, i, v_i)\mathrm{d}v_j'' = 1, \ \int_{\mathcal{V}_j} v_j'' P(v_j''|j, i, v_i)\mathrm{d}v_j'' \in \mathcal{V}_j \quad \forall v_i \in \mathcal{V}_i,$$

$$\mathrm{Supp}(Q(\cdot|j,i,\cdot,k,\cdot)) \subseteq \mathcal{V}_j \times \mathcal{V}_i \times \mathcal{V}_k, \quad Q(\cdot|j,i,\cdot,k,\cdot) \geq 0 \text{ a.e.},$$

$$\int_{\mathcal{V}_j} Q(v_j''|j,i,v_i,k,v_k^*)\mathrm{d}v_j'' = 1, \quad \int_{\mathcal{V}_j} v_j'' Q(v_j''|j,i,v_i,k,v_k^*)\mathrm{d}v_j'' \in \mathcal{V}_j \quad \forall (v_i,v_k) \in \mathcal{V}_i \times \mathcal{V}_k,$$

$$\mathrm{Supp}(p(j|i,\cdot)) \subseteq \mathcal{V}_i, \quad 0 \leq p(j|i,\cdot) \leq 1,$$

$$\mathrm{Supp}(q(j|i,\cdot,k,\cdot)) \subseteq \mathcal{V}_i \times \mathcal{V}_k, \quad 0 \leq q(j|i,\cdot,k,\cdot) \leq 1,$$

$$\sum_{j\in\mathcal{I}} p(j|i,v_i) = 1 \ \ \forall v_i \in \mathcal{V}_i, \tag{2.4a}$$

$$\sum_{j\in\mathcal{I}} q(j|i,v_i,k,v_k^*) = 1 \ \ \forall (v_i,v_k^*) \in \mathcal{V}_i \times \mathcal{V}_k, \tag{2.4b}$$

where $\mathscr{P}(\mathcal{V}_i)$ denotes the set of probability distributions defined on the measurable space $(\mathcal{V}_i, \mathcal{B})$, with $\mathcal{B}$ the Borel σ-algebra, $C(\mathcal{V}_i)$ denotes the set of continuous functions defined on $\mathcal{V}_i$, and $\mathrm{Supp}(\cdot)$ denotes the support of $(\cdot)$. Note that the normalisation conditions (2.4a) and (2.4b) imply that

$$p(i|i,v_i) = 1 - \sum_{\substack{j\in\mathcal{I}\\ j\neq i}} p(j|i,v_i) \ \ \forall v_i \in \mathcal{V}_i, \tag{2.5a}$$

$$q(i|i,v_i,k,v_k^*) = 1 - \sum_{\substack{j\in\mathcal{I}\\ j\neq i}} q(j|i,v_i,k,v_k^*) \ \ \forall (v_i,v_k^*) \in \mathcal{V}_i \times \mathcal{V}_k. \tag{2.5b}$$

Under these conditions, the random process which governs the evolution of the microscopic state $(I_t, \mathbf{V}_t)$ takes the following form

$$\begin{cases} I_{t+\Delta t} = (1-Z)\, I_t + Z\, [\Xi I_t' + (1-\Xi) I_t''], \\ V_{i,t+\Delta t} = (1-Z)\Big[(1-\Theta_i)\, V_{i,t} + \Theta_i\, V_{i,t}'\Big] + Z\, V_{i,t}'', \quad i \in \mathcal{I}, \end{cases} \tag{2.6}$$

where Z, Ξ, and $\Theta_1, \ldots, \Theta_N$ are independent Bernoulli random variables with parameters $\zeta\Delta t$, r, and $\theta_1\Delta t, \ldots, \theta_N\Delta t$, respectively. Note that, unlike in equation (1.6), in this case the coefficients are assumed to be constant. As a result, the time step Δt must be sufficiently small so that $\max(\zeta, \theta_1, \ldots, \theta_N)\,\Delta t \leq 1$. In the system (2.6), the random variables $I_t' \in \mathcal{I}$ and $I_t'' \in \mathcal{I}$ model, respectively, the index of the new compartment an individual belongs to if spontaneous and interaction-driven compartment switching occurs, while the random variable $V_{i,t}'' \in \mathcal{V}_i$ models the corresponding value of the structuring variable that is acquired by the individual. Moreover, the random variable $V_{i,t}' \in \mathcal{V}_i$ models the new value of the structuring

variable that is acquired by an individual in compartment i if structuring-variable switching occurs.

For ease of presentation, in the remainder of this chapter we use the notation

$$ {}^{i}\hat{\mathcal{V}} := \mathcal{V}_1 \times \ldots \times \mathcal{V}_{i-1} \times \mathcal{V}_{i+1} \times \ldots \times \mathcal{V}_N, \quad {}^{i}\hat{\mathbf{v}} \equiv (v_1, \ldots, v_{i-1}, v_{i+1}, \ldots, v_N). \tag{2.7} $$

To incorporate (I) into (2.6), for all i, $h \in \mathcal{I}$ we let

$$ (V'_{i,t} | I_t, \mathbf{V}_t) \sim T(v'_i | I_t, \mathbf{V}_t), \tag{2.8a} $$

$$ T(v'_i | h, \mathbf{v}) := \begin{cases} K_i(v'_i | v_i) & \text{if } i = h, \\ \delta_{v_i}(v'_i) & \text{if } i \neq h, \end{cases} \tag{2.8b} $$

where $\delta_x(y)$ is the Dirac delta centred at $y = x$. Moreover, recalling the notation (2.7), to incorporate (IIa) into (2.6), for all $i, i' \in \mathcal{I}$ we let

$$ (I'_t, \mathbf{V}''_t | I_t, \mathbf{V}_t) \sim \mathcal{T}(i', \mathbf{v}'' | I_t, \mathbf{V}_t), \tag{2.9a} $$

$$ \mathcal{T}(i', \mathbf{v}'' | i, \mathbf{v}) := \delta_{i', {}^{i'}\hat{\mathbf{v}}}({}^{i'}\hat{\mathbf{v}}'') p(i' | i, v_i) P(v''_{i'} | i', i, v_i), \tag{2.9b} $$

while to incorporate (IIb) for all $i, i'', k \in \mathcal{I}$ we let

$$ (I''_t, \mathbf{V}''_t | I_t, \mathbf{V}_t, I^*_t, \mathbf{V}^*_t) \sim \mathcal{T}_k(i'', \mathbf{v}'' | I_t, \mathbf{V}_t, I^*_t, \mathbf{V}^*_t), \tag{2.10a} $$

$$ \mathcal{T}_k(i'', \mathbf{v}'' | i, \mathbf{v}, i^*, \mathbf{v}^*) := \delta_{i'', {}^{i''}\hat{\mathbf{v}}}({}^{i''}\hat{\mathbf{v}}'') q(i'' | i, v_i, k, v^*_k) Q(v''_{i''} | i'', i, v_i, k, v^*_k). \tag{2.10b} $$

In summary, the definition (2.8b) translates in mathematical terms the idea that only individuals in compartment i undergo changes in the trait represented by the structuring variable v_i due to structuring-variable switching, according to the kernel K_i. Moreover, the definition (2.9b) (resp. the definition (2.10b)) captures the fact that spontaneous compartment switching (resp. interaction-driven compartment switching) leads individuals in compartment i with expression level v_i of the trait represented by the structuring variable to transition into compartment i' (resp. compartment i''), with probability $p(i' | i, v_i)$ (resp. with probability $q(i'' | i, v_i, k, v^*_k)$, where k and v^*_k are the compartment and the value of the structuring variable of the individual with which/whom the interaction occurs), and acquire the expression level $v''_{i'}$ (resp. $v''_{i''}$) of the trait represented by the structuring variable of the new compartment, according to the kernel $P(v''_{i'} | i', i, v_i)$ (resp. the kernel $Q(v''_{i''} | i'', i, v_i, k, v^*_k)$).

2.3 Mesoscopic model

Starting from the system (2.6), we now formally derive the mesoscopic model corresponding to the microscopic model presented in the previous section, which comprises a system of balance equations for the population density functions

$$n_i(t, v_i) \equiv n(t, i, v_i) \coloneqq \int_{{}^i\hat{\mathcal{V}}} f(t, i, \mathbf{v}) \mathrm{d}^i\hat{\mathbf{v}}, \quad i \in \mathcal{I}, \tag{2.11}$$

where $f(t, i, \mathbf{v})$ is the probability density function given in (2.1), and ${}^i\hat{\mathcal{V}}$ and ${}^i\hat{\mathbf{v}}$ are defined via (2.7). The population density function $n_i(t, v_i)$ represents the distribution of individuals in compartment i over the corresponding structuring-variable domain $\mathcal{V}_i$ at time t (cf. the schematic in Figure 2.1). Specifically, we will formally show that the dynamics of the population density functions $n_i(t, v_i)$ with $i \in \mathcal{I}$ are governed by the following IDE system

$$\begin{aligned}
\partial_t n_i(t, v_i) = \theta_i \Big[\int_{\mathcal{V}_i} K_i(v_i|v_i') n_i(t, v_i') \mathrm{d}v_i' - n_i(t, v_i) \Big] \\
+ \zeta\, r \Big[\sum_{\substack{j \in \mathcal{I} \\ j \neq i}} \int_{\mathcal{V}_j} p(i|j, v_j) P(v_i|i, j, v_j) n_j(t, v_j) \mathrm{d}v_j - \sum_{\substack{j \in \mathcal{I} \\ j \neq i}} p(j|i, v_i)\; n_i(t, v_i) \Big] \\
+ \zeta\, (1 - r) \Big[\sum_{k \in \mathcal{I}} \sum_{\substack{j \in \mathcal{I} \\ j \neq i}} \int_{\mathcal{V}_j} \int_{\mathcal{V}_k} q(i|j, v_j, k, v_k) Q(v_i|i, j, v_j, k, v_k) n_k(t, v_k) n_j(t, v_j) \mathrm{d}v_k \mathrm{d}v_j \\
- \sum_{k \in \mathcal{I}} \sum_{\substack{j \in \mathcal{I} \\ j \neq i}} \int_{\mathcal{V}_k} q(j|i, v_i, k, v_k) n_k(t, v_k) \mathrm{d}v_k\; n_i(t, v_i) \Big], \quad v_i \in \mathcal{V}_i, \quad i \in \mathcal{I}.
\end{aligned} \tag{2.12}$$

Before proceeding with the formal derivation, we introduce the following lemma, which will prove useful in the subsequent steps.

Lemma 2.1. *Let $\{\Theta_i\}_{i \in \mathcal{I}}$ be independent Bernoulli random variables with parameters $\theta_i \Delta t$. Define*

$$\mathfrak{S} \coloneqq \sum_{i \in \mathcal{I}} \Theta_i.$$

Then, as $\Delta t \to 0^+$, it holds

$$\mathbb{P}(\mathfrak{S} \geq 2) = o(\Delta t).$$

Proof. Clearly,

$$\mathbb{P}(\mathfrak{S} \geq 2) = 1 - \Big(\mathbb{P}(\mathfrak{S} = 0) + \mathbb{P}(\mathfrak{S} = 1) \Big).$$

Moreover,

$$\mathbb{P}(\mathfrak{S} = 0) = \prod_{i \in \mathcal{I}} (1 - \theta_i \Delta t), \qquad \mathbb{P}(\mathfrak{S} = 1) = \sum_{i \in \mathcal{I}} \theta_i \Delta t \prod_{\substack{j \in \mathcal{I} \\ j \neq i}} (1 - \theta_j \Delta t).$$

Let

$$p := \prod_{i\in\mathcal{I}}(1-\theta_i\Delta t).$$

Then

$$\log p = \sum_{i\in\mathcal{I}}\log(1-\theta_i\Delta t) = -\sum_{i\in\mathcal{I}}\theta_i\Delta t + o(\Delta t), \quad \Delta t \to 0^+,$$

so that

$$p = 1 - \sum_{i\in\mathcal{I}}\theta_i\Delta t + o(\Delta t).$$

Hence,

$$\begin{aligned}\mathbb{P}(\mathfrak{S}=1) &= \sum_{i\in\mathcal{I}}\theta_i\Delta t\left(1-\sum_{j\neq i}\theta_j\Delta t + o(\Delta t)\right)\\ &= \sum_{i\in\mathcal{I}}\theta_i\Delta t - \sum_{i\in\mathcal{I}}\sum_{\substack{j\in\mathcal{I}\\ j\neq i}}\theta_i\theta_j\Delta t^2 + o(\Delta t^2)\\ &= \sum_{i\in\mathcal{I}}\theta_i\Delta t + o(\Delta t^2).\end{aligned}$$

Therefore,

$$\mathbb{P}(\mathfrak{S}\geq 2) = 1 - \Big(1 - \sum_{i\in\mathcal{I}}\theta_i\Delta t + o(\Delta t) + \sum_{i\in\mathcal{I}}\theta_i\Delta t + o(\Delta t^2)\Big) = o(\Delta t),$$

which proves the claim. □

General evolution equation for expectations of observables. We start by noting that, since the components of the random vector $(I_{t+\Delta t}, \mathbf{V}_{t+\Delta t})$ are given by (2.6), for any observable $\Phi : \mathcal{I}\times\mathcal{V}\to\mathbb{R}$ the expectation

$$\langle\Phi(I_t,\mathbf{V}_t)\rangle := \sum_{l\in\mathcal{I}}\int_{\mathcal{V}}\Phi(l,\mathbf{v})f(t,l,\mathbf{v})\mathrm{d}\mathbf{v}$$

satisfies (see, for instance, [129])

$$\begin{aligned}\langle\Phi(I_{t+\Delta t},\mathbf{V}_{t+\Delta t})\rangle = &\langle\Phi(I_t,\mathbf{W}_t)\rangle\,(1-\zeta)\,\Delta t\\ &+ r\,\langle\Phi(I_t',\mathbf{V}_t'')\rangle\,\zeta\,\Delta t\\ &+ (1-r)\,\langle\Phi(I_t'',\mathbf{V}_t'')\rangle\,\zeta\,\Delta t,\end{aligned} \tag{2.13}$$

where

$$\mathbf{W}_t \equiv (W_{1,t},\ldots,W_{N,t}) \;\text{ with }\; W_{i,t} := (1-\Theta_i)\,V_{i,t} + \Theta_i\,V_{i,t}' \;\text{ for }\; i=1,\ldots,N \tag{2.13}$$

and $\mathbf{V}''_t \equiv \left(V''_{1,t}, \ldots, V''_{N,t}\right)$. Recalling that Z and $\Theta_1, \ldots, \Theta_N$ are independent Bernoulli random variables with parameters $\zeta\Delta t$ and $\theta_1\Delta t, \ldots, \theta_N\Delta t$, respectively, introducing the diagonal matrix

$$\mathbf{\Theta} \coloneqq \mathrm{diag}\left(\Theta_1, \ldots, \Theta_N\right)$$

and rewriting the vector $\mathbf{W}_t$ as

$$\mathbf{W}_t = \left(\mathbf{I} - \mathbf{\Theta}\right)\, \mathbf{V}_t + \mathbf{\Theta}\, \mathbf{V}'_t,$$

where $\mathbf{I}$ is the identity matrix, yields

$$\begin{aligned}\left\langle \Phi\left(I_t, \mathbf{W}_t\right)\right\rangle = {} & \left\langle \Phi\left(I_t, \mathbf{V}_t\right)\right\rangle \mathrm{P}(\mathbf{\Theta} = \mathbf{0}) \\ & + \sum_{h\in\mathcal{I}} \left\langle \Phi\left(I_t, \mathbf{V}'^{,h}_t\right)\right\rangle \mathrm{P}(\Theta_h = 1 \ \wedge\ \Theta_j = 0\, \forall j \neq h) \\ & + \ o.t.\,, \end{aligned} \tag{2.14}$$

In (2.14), $\mathrm{P}(\cdot)$ is the notation that we will be using for probability, $\mathbf{0}$ is the null matrix,

$$\mathbf{V}'^{,h}_t \coloneqq \left(V_{1,t}, \ldots, V_{h-1,t}, V'_{h,t}, V_{h+1,t}, \ldots, V_{N,t}\right), \tag{2.15}$$

and $o.t.$ are all the other terms accounting for the remaining cases in which multiple diagonal elements of the matrix $\mathbf{\Theta}$ are equal to 1, i.e. higher order terms in Δt which will formally vanish in the limit $\Delta t \to 0$. Using (2.14), we rewrite (2.13) as

$$\begin{aligned}\left\langle \Phi\left(I_{t+\Delta t}, \mathbf{V}_{t+\Delta t}\right)\right\rangle = {} & \Big[\sum_{h\in\mathcal{I}} \left\langle \Phi\left(I_t, \mathbf{V}'^{,h}_t\right)\right\rangle \mathrm{P}(\Theta_h = 1 \wedge \Theta_j = 0\, \forall j \neq h) \\ & + \left\langle \Phi\left(I_t, \mathbf{V}_t\right)\right\rangle \mathrm{P}(\mathbf{\Theta} = \mathbf{0}) + \ o.t.\Big] \left(1 - \zeta\Delta t\right) \\ & + r \left\langle \Phi\left(I'_t, \mathbf{V}''_t\right)\right\rangle \zeta\Delta t + \left(1 - r\right) \left\langle \Phi\left(I''_t, \mathbf{V}''_t\right)\right\rangle \zeta\Delta t \end{aligned} \tag{2.16}$$

and then, using the fact that, as proved in Lemma 2.1,

$$\mathrm{P}(\mathbf{\Theta} = \mathbf{0}) = \prod_{h\in\mathcal{I}} (1 - \theta_h\Delta t) = 1 - \Delta t \sum_{h\in\mathcal{I}} \theta_h + o(\Delta t), \tag{2.17}$$

$$\mathrm{P}(\Theta_h = 1 \wedge \Theta_j = 0\, \forall j \neq h) = \theta_h\Delta t \prod_{\substack{j\in\mathcal{I} \\ j\neq h}} (1 - \theta_j\Delta t) = \theta_h\Delta t + o(\Delta t)$$

and

$$o.t. = o(\Delta t), \tag{2.18}$$

with a little algebra we rewrite (2.16) as

$$\begin{aligned}\langle \Phi\left(I_{t+\Delta t}, \mathbf{V}_{t+\Delta t}\right)\rangle = \langle \Phi\left(I_t, \mathbf{V}_t\right)\rangle \\ + \Delta t \sum_{h\in\mathcal{I}} \theta_h \Big(\Big\langle \Phi\left(I_t, \mathbf{V}_t'^{,h}\right)\Big\rangle - \langle \Phi\left(I_t, \mathbf{V}_t\right)\rangle \Big) \\ + \Delta t\, \zeta \Big(r \left\langle \Phi\left(I_t', \mathbf{V}_t''\right)\right\rangle + (1-r)\left\langle \Phi\left(I_t'', \mathbf{V}_t''\right)\right\rangle - \langle \Phi\left(I_t, \mathbf{V}_t\right)\rangle \Big) \\ + o(\Delta t).\end{aligned} \tag{2.19}$$

From (2.19), rearranging terms, dividing through by Δt and letting $\Delta t \to 0^+$, we formally obtain the following evolution equation

$$\begin{aligned}\frac{\mathrm{d}}{\mathrm{d}t}\langle \Phi\left(I_t, \mathbf{V}_t\right)\rangle = \sum_{h\in\mathcal{I}} \theta_h \Big(\Big\langle \Phi\left(I_t, \mathbf{V}_t'^{,h}\right)\Big\rangle - \langle \Phi\left(I_t, \mathbf{V}_t\right)\rangle \Big) \\ + \zeta \Big(r \left\langle \Phi\left(I_t', \mathbf{V}_t''\right)\right\rangle + (1-r)\left\langle \Phi\left(I_t'', \mathbf{V}_t''\right)\right\rangle - \langle \Phi\left(I_t, \mathbf{V}_t\right)\rangle \Big),\end{aligned} \tag{2.20}$$

which can be regarded as a weak form of the conservation equation for the probability density function $f(t, i, \mathbf{v})$. Expressing the expectations $\langle\cdot\rangle$ in (2.20) in terms of sums and integrals against the probability density function f, and using (2.8a), (2.9a), and (2.10a), the evolution equation (2.20) can then be rewritten as

$$\begin{aligned}&\frac{\mathrm{d}}{\mathrm{d}t}\sum_{l\in\mathcal{I}}\int_{\mathcal{V}} \Phi(l,\mathbf{v})\, f(t,l,\mathbf{v})\mathrm{d}\mathbf{v} = \\ &= \underbrace{\sum_{h\in\mathcal{I}} \theta_h \left[\sum_{l\in\mathcal{I}} \int_{\mathcal{V}} \Phi(l,\mathbf{v}'^{,h}) \left(\int_{\mathcal{V}_h} T(v_h'|l,\mathbf{v})\, f(t,l,\mathbf{v})\mathrm{d}v_h \right) \mathrm{d}\mathbf{v}'^{,h} - \sum_{l\in\mathcal{I}}\int_{\mathcal{V}} \Phi(l,\mathbf{v})\, f(t,l,\mathbf{v})\mathrm{d}\mathbf{v} \right]}_{=:\textcircled{i}} \\ &\quad + \underbrace{\zeta\, r \sum_{l\in\mathcal{I}} \int_{\mathcal{V}} \Phi(l,\mathbf{v}'') \left(\sum_{j\in\mathcal{I}} \int_{\mathcal{V}} \mathcal{T}(l,\mathbf{v}''|j,\mathbf{v}) f(t,j,\mathbf{v})\mathrm{d}\mathbf{v} \right) \mathrm{d}\mathbf{v}''}_{=:\textcircled{ii}} \\ &\quad + \underbrace{\zeta\,(1-r) \sum_{l\in\mathcal{I}} \int_{\mathcal{V}} \Phi(l,\mathbf{v}'') \left(\sum_{k\in\mathcal{I}} \sum_{j\in\mathcal{I}} \int_{\mathcal{V}}\int_{\mathcal{V}} \mathcal{T}_k(l,\mathbf{v}''|j,\mathbf{v},k,v_k^*) f(t,j,\mathbf{v}) f(t,k,\mathbf{v}^*)\mathrm{d}\mathbf{v}\mathrm{d}\mathbf{v}^* \right) \mathrm{d}\mathbf{v}''}_{=:\textcircled{iii}} \\ &\quad - \underbrace{\zeta \sum_{l\in\mathcal{I}} \int_{\mathcal{V}} \Phi(l,\mathbf{v})\, f(t,l,\mathbf{v})\mathrm{d}\mathbf{v}}_{=:\textcircled{iv}},\end{aligned} \tag{2.21}$$

where, recalling the notation (2.15), $\mathbf{v}'^{,h} = (v_1, \ldots, v_{h-1}, v_h', v_{h+1}, \ldots, v_N)$.

From (2.21) we now derive a weak form of the IDE system (2.12). To do so, we choose

$$\Phi(l,\mathbf{v}) := \delta_{i,l}\, \phi(v_i)\, \mathbb{1}_{i\hat{\mathcal{V}}}({}^{i}\hat{\mathbf{v}}), \tag{2.22}$$

where ${}^{i}\hat{\mathcal{V}}$ and ${}^{i}\hat{\mathbf{v}}$ are defined via (2.7), δ is the Kronecker delta, $\mathbb{1}_{i\hat{\mathcal{V}}}$ is the indicator

function of the set ${}^i\hat{\mathcal{V}}$, and $\phi \in C^\infty(\mathcal{V}_i)$ is a smooth test function. We then substitute (2.22) into (2.21) and, for ease of presentation, carry out calculations for the left-hand side (LHS) of (2.21) and the terms ⓘ-ⓘⓥ on the right-hand side (RHS) of (2.21) one by one.

LHS of (2.21) Recalling (2.11), substituting (2.22) into the LHS of (2.21) yields

$$\frac{\mathrm{d}}{\mathrm{d}t}\sum_{l\in\mathcal{I}}\int_{\mathcal{V}}\Phi(l,\mathbf{v})\,f(t,l,\mathbf{v})\mathrm{d}\mathbf{v}=\int_{\mathcal{V}_i}\phi(v_i)\,\partial_t n_i(t,v_i)\,\mathrm{d}v_i. \tag{2.23}$$

ⓘ on the RHS of (2.21) Recalling (2.11), substituting (2.22) along with (2.8b) into ⓘ yields

$$\begin{aligned}
ⓘ &= \theta_i\left[\int_{\mathcal{V}_i}\int_{\mathcal{V}_i}\phi(v_i')K_i(v_i'|v_i)n_i(t,v_i)\mathrm{d}v_i'\mathrm{d}v_i-\int_{\mathcal{V}_i}\phi(v_i)n_i(t,v_i)\mathrm{d}v_i\right]\\
&\quad+\sum_{\substack{h\in\mathcal{I}\\h\neq i}}\theta_h\left[\int_{\mathcal{V}_i}\int_{\mathcal{V}_h}\phi(v_i)\delta_{v_h}(v_h')\,n_i(t,v_i)\mathrm{d}v_h'\mathrm{d}v_i-\int_{\mathcal{V}_i}\phi(v_i)n_i(t,v_i)\mathrm{d}v_i\right]\\
&=\theta_i\left[\int_{\mathcal{V}_i}\int_{\mathcal{V}_i}\phi(v_i')K_i(v_i'|v_i)n_i(t,v_i)\mathrm{d}v_i'\mathrm{d}v_i-\int_{\mathcal{V}_i}\phi(v_i)n_i(t,v_i)\mathrm{d}v_i\right],
\end{aligned}$$

from which, swapping v_i' and v_i in the first integral and then rearranging terms, we find

$$ⓘ=\int_{\mathcal{V}_i}\phi(v_i)\left\{\theta_i\left[\int_{\mathcal{V}_i}K_i(v_i|v_i')n_i(t,v_i')\mathrm{d}v_i'-n_i(t,v_i)\right]\right\}\mathrm{d}v_i. \tag{2.24}$$

ⓘⓘ on the RHS of (2.21) Substituting first (2.22) and then (2.9b) into ⓘⓘ and rearranging terms yields

$$\begin{aligned}
ⓘⓘ &= \int_{\mathcal{V}_i}\phi(v_i'')\left(\sum_{j\in\mathcal{I}}\int_{{}^i\hat{\mathcal{V}}}\int_{\mathcal{V}}\mathcal{T}(i,\mathbf{v}''|j,\mathbf{v})f(t,j,\mathbf{v})\mathrm{d}\mathbf{v}\mathrm{d}^i\hat{\mathbf{v}}''\right)\mathrm{d}v_i''\\
&=\int_{\mathcal{V}_i}\phi(v_i'')\left(\sum_{\substack{j\in\mathcal{I}\\j\neq i}}\int_{{}^i\hat{\mathcal{V}}}\int_{\mathcal{V}}\delta_{{}^i\hat{\mathbf{v}}''}({}^i\hat{\mathbf{v}})p(i|j,v_j)P(v_i''|i,j,v_j)f(t,j,\mathbf{v})\mathrm{d}\mathbf{v}\mathrm{d}^i\hat{\mathbf{v}}''\right)\mathrm{d}v_i''\\
&\quad+\int_{\mathcal{V}_i}\phi(v_i'')\left(\int_{{}^i\hat{\mathcal{V}}}\int_{\mathcal{V}}\delta_{{}^i\hat{\mathbf{v}}''}({}^i\hat{\mathbf{v}})p(i|i,v_i)\delta_{v_i''}(v_i)f(t,i,\mathbf{v})\mathrm{d}\mathbf{v}\mathrm{d}^i\hat{\mathbf{v}}''\right)\mathrm{d}v_i''\\
&=\int_{\mathcal{V}_i}\phi(v_i'')\left(\sum_{\substack{j\in\mathcal{I}\\j\neq i}}\int_{\mathcal{V}}p(i|j,v_j)P(v_i''|i,j,v_j)f(t,j,\mathbf{v})\mathrm{d}\mathbf{v}\right)\mathrm{d}v_i''
\end{aligned}$$

$$+\int_{\mathcal{V}_i}\phi(v_i'')\left(\int_{\mathcal{V}}p(i|i,v_i)\delta_{v_i}(v_i'')f(t,i,\mathbf{v})\mathrm{d}\mathbf{v}\right)\mathrm{d}v_i'',$$

from which, recalling (2.11), using the relation (2.5a) and renaming v_i'' to v_i, we find

$$\begin{aligned}\textcircled{ii} = \int_{\mathcal{V}_i}\phi(v_i)\Bigg\{&\sum_{\substack{j\in\mathcal{I}\\ j\neq i}}\int_{\mathcal{V}_j}p(i\mid j,v_j)\,P(v_i\mid i,j,v_j)\,n_j(t,v_j)\,\mathrm{d}v_j\\ &+\left(1-\sum_{\substack{j\in\mathcal{I}\\ j\neq i}}p(j\mid i,v_i)\right)n_i(t,v_i)\Bigg\}\,\mathrm{d}v_i.\end{aligned}\tag{2.25}$$

ⓘⓘ on the RHS of (2.21) Substituting first (2.22) and then (2.10b) into ⓘⓘ and rearranging terms yields

$$\begin{aligned}\textcircled{ii} &= \int_{\mathcal{V}_i}\phi(v_i'')\left(\sum_{k\in\mathcal{I}}\sum_{j\in\mathcal{I}}\int_{i\hat{\mathcal{V}}}\int_{\mathcal{V}}\int_{\mathcal{V}}\mathcal{T}_k(i,\mathbf{v}''|j,\mathbf{v},k,v_k^*)f(t,j,\mathbf{v})f(t,k,\mathbf{v}^*)\mathrm{d}\mathbf{v}\mathrm{d}\mathbf{v}^*\mathrm{d}^i\hat{\mathbf{v}}''\right)\mathrm{d}v_i''\\
&= \int_{\mathcal{V}_i}\phi(v_i'')\left(\sum_{k\in\mathcal{I}}\sum_{\substack{j\in\mathcal{I}\\ j\neq i}}\int_{i\hat{\mathcal{V}}}\int_{\mathcal{V}}\int_{\mathcal{V}}\delta_{i\hat{\mathbf{v}}''}({}^i\hat{\mathbf{v}})q(i|j,v_j,k,v_k^*)Q(v_i''|i,j,v_j,k,v_k^*)f(t,j,\mathbf{v})f(t,k,\mathbf{v}^*)\mathrm{d}\mathbf{v}\mathrm{d}\mathbf{v}^*\mathrm{d}^i\hat{\mathbf{v}}''\right)\mathrm{d}v_i''\\
&\quad+\int_{\mathcal{V}_i}\phi(v_i'')\left(\sum_{k\in\mathcal{I}}\int_{i\hat{\mathcal{V}}}\int_{\mathcal{V}}\int_{\mathcal{V}}\delta_{i\hat{\mathbf{v}}''}({}^i\hat{\mathbf{v}})q(i|i,v_i,k,v_k^*)\delta_{v_i''}(v_i)f(t,i,\mathbf{v})f(t,k,\mathbf{v}^*)\mathrm{d}\mathbf{v}\mathrm{d}\mathbf{v}^*\mathrm{d}^i\hat{\mathbf{v}}''\right)\mathrm{d}v_i''\\
&= \int_{\mathcal{V}_i}\phi(v_i'')\left(\sum_{k\in\mathcal{I}}\sum_{\substack{j\in\mathcal{I}\\ j\neq i}}\int_{\mathcal{V}}\int_{\mathcal{V}}q(i|j,v_j,k,v_k^*)Q(v_i''|i,j,v_j,k,v_k^*)f(t,j,\mathbf{v})f(t,k,\mathbf{v}^*)\mathrm{d}\mathbf{v}\mathrm{d}\mathbf{v}^*\right)\mathrm{d}v_i''\\
&\quad+\int_{\mathcal{V}_i}\phi(v_i'')\left(\sum_{k\in\mathcal{I}}\int_{\mathcal{V}}\int_{\mathcal{V}}q(i|i,v_i,k,v_k^*)\delta_{v_i}(v_i'')f(t,i,\mathbf{v})f(t,k,\mathbf{v}^*)\mathrm{d}\mathbf{v}\mathrm{d}\mathbf{v}^*\right)\mathrm{d}v_i''.\end{aligned}$$

Then, recalling (2.11), computing the integrals with respect to all the components of $\mathbf{v}$ except v_j and all the components of $\mathbf{v}^*$ except v_k^*, using the relation (2.5b) along with the fact that (cf. the integral identity (2.2))

$$\sum_{k\in\mathcal{I}}\int_{\mathcal{V}_k}n_k(t,v_k^*)\mathrm{d}v_k^*=1\ \ \forall\, t\in[0,\infty),$$

and renaming v_i'' to v_i and v_k^* to v_k, we find

$$\begin{aligned}\text{(iii)} = &\int_{\mathcal{V}_i} \phi(v_i) \left\{ \sum_{k\in\mathcal{I}} \sum_{\substack{j\in\mathcal{I}\\ j\neq i}} \int_{\mathcal{V}_k} \int_{\mathcal{V}_j} q(i|j,v_j,k,v_k) Q(v_i|i,j,v_j,k,v_k) n_j(t,v_j) n_k(t,v_k) \mathrm{d}v_j \mathrm{d}v_k \right\} \mathrm{d}v_i \\ &+ \int_{\mathcal{V}_i} \phi(v_i) \left\{ \left(1 - \sum_{k\in\mathcal{I}} \sum_{\substack{j\in\mathcal{I}\\ j\neq i}} \int_{\mathcal{V}_k} q(j|i,v_i,k,v_k) n_k(t,v_k) \mathrm{d}v_k \right) n_i(t,v_i) \right\} \mathrm{d}v_i.\end{aligned} \tag{2.26}$$

(iv) on the RHS of (2.21) Recalling (2.11), substituting (2.22) into (iv) yields

$$\text{(iv)} = \int_{\mathcal{V}_i} \phi(v_i)\, n_i(t,v_i)\, \mathrm{d}v_i. \tag{2.27}$$

Substituting (2.23), (2.24), (2.25), (2.26), and (2.27) into (2.21), after a little algebra one obtains a weak formulation of the IDE system (2.12).

2.3.1 Macroscopic model

In this section, we aim to recover a macroscopic representation of heterogeneously structured compartmental epidemiological systems starting from the mesoscopic representation provided by the IDE system (2.12), i.e. to obtain a set of equations describing the time evolution of macroscopic quantities such as the fractions of individuals in the various compartments

$$N_i(t) := \int_{\mathcal{V}_i} n_i(t,v_i) \mathrm{d}v_i, \qquad i \in \mathcal{I},$$

and the mean values of the compartment-specific structuring variables

$$M_i(t) := \frac{1}{N_i(t)} \int_{\mathcal{V}_i} v_i n_i(t,v_i) \mathrm{d}v_i, \qquad i \in \mathcal{I}.$$

Integrating directly the IDE system (2.12) does not produce closed equations for these quantities. For instance, in the case of the N_i's, noticing that

$$\int_{\mathcal{V}_i} \left(\int_{\mathcal{V}_i} K_i(v_i|v_i') n_i(t,v_i') \mathrm{d}v_i' - n_i(t,v_i) \right) \mathrm{d}v_i = 0 \tag{2.28}$$

because of (2.3b), one finds

$$\begin{aligned}\frac{\mathrm{d}N_i}{\mathrm{d}t} &= \zeta r \sum_{\substack{j\in\mathcal{I}\\ j\neq i}} \left(\int_{\mathcal{V}_i}\int_{\mathcal{V}_j} p(i|j,v_j)P(v_i|i,j,v_j)n_j(t,v_j)\mathrm{d}v_j\mathrm{d}v_i - \int_{\mathcal{V}_i} p(j|i,v_i)n_i(t,v_i)\mathrm{d}v_i \right) \\ &\quad + \zeta(1-r)\sum_{k\in\mathcal{I}}\sum_{\substack{j\in\mathcal{I}\\ j\neq i}} \left(\int_{\mathcal{V}_i}\int_{\mathcal{V}_j}\int_{\mathcal{V}_k} q(i|j,v_j,k,v_k)Q(v_i|i,j,v_j,k,v_k)n_k(t,v_k)n_j(t,v_j)\mathrm{d}v_k\mathrm{d}v_j\mathrm{d}v_i \right. \\ &\qquad \left. - \int_{\mathcal{V}_i}\int_{\mathcal{V}_k} q(j|i,v_i,k,v_k)n_k(t,v_k)n_i(t,v_i)\mathrm{d}v_k\mathrm{d}v_i \right),\end{aligned}$$

which still requires the knowledge of the population density functions. To circumvent this difficulty, we adopt a procedure reminiscent of the *hydrodynamic limit*. In statistical mechanics, this approach allows one to derive macroscopic evolution PDEs for quantities such as bulk density, velocity, and energy from the underlying microscopic representation, in the limit of a small hydrodynamic parameter—typically the Knudsen number.

We introduce a small scaling parameter $0 < \varepsilon \ll 1$ and let $\zeta = \varepsilon$ in (2.12). Since ζ is the rate at which compartment switching occurs, this amounts to assuming a *quasi-invariant* regime of transitions across the compartments. In other words, the probability that individuals leave their compartments over time is small. To compensate for such a smallness, thereby enabling the observation of significant time trends, we scale simultaneously the time variable as $t \to t/\varepsilon$. Upon introducing the scaled population density functions

$$n_i^\varepsilon(t,v_i) \coloneqq n_i\left(\tfrac{t}{\varepsilon},v_i\right), \qquad i\in\mathcal{I},$$

whence $\partial_t n_i^\varepsilon = \frac{1}{\varepsilon}\partial_t n_i$, we rewrite (2.12) as

$$\begin{aligned}\varepsilon\partial_t n_i^\varepsilon(t,v_i) &= \theta_i\left(\int_{\mathcal{V}_i} K_i(v_i|v_i')n_i^\varepsilon(t,v_i')\mathrm{d}v_i' - n_i^\varepsilon(t,v_i)\right) \\ &\quad + \varepsilon r\sum_{\substack{j\in\mathcal{I}\\ j\neq i}}\left(\int_{\mathcal{V}_j} p(i|j,v_j)P(v_i|i,j,v_j)n_j^\varepsilon(t,v_j)\mathrm{d}v_j - p(j|i,v_i)n_i^\varepsilon(t,v_i)\right) \\ &\quad + \varepsilon(1-r)\sum_{k\in\mathcal{I}}\sum_{\substack{j\in\mathcal{I}\\ j\neq i}}\left(\int_{\mathcal{V}_j}\int_{\mathcal{V}_k} q(i|j,v_j,k,v_k)Q(v_i|i,j,v_j,k,v_k)n_k^\varepsilon(t,v_k)n_j^\varepsilon(t,v_j)\mathrm{d}v_k\mathrm{d}v_j \right. \\ &\qquad \left. - n_i^\varepsilon(t,v_i)\int_{\mathcal{V}_k} q(j|i,v_i,k,v_k)n_k^\varepsilon(t,v_k)\mathrm{d}v_k\right). \qquad (2.29)\end{aligned}$$

Integrating both sides with respect to v_i and recalling (2.28), we obtain

$$\begin{aligned}\frac{\mathrm{d}}{\mathrm{d}t}\int_{\mathcal{V}_i} n_i^\varepsilon(t,v_i)\mathrm{d}v_i = r\sum_{\substack{j\in\mathcal{I}\\ j\neq i}}\int_{\mathcal{V}_i}\left(\int_{\mathcal{V}_j} p(i|j,v_j)P(v_i|i,j,v_j)n_j^\varepsilon(t,v_j)\mathrm{d}v_j - p(j|i,v_i)n_i^\varepsilon(t,v_i)\right)\mathrm{d}v_i\\ + (1-r)\sum_{k\in\mathcal{I}}\sum_{\substack{j\in\mathcal{I}\\ j\neq i}}\int_{\mathcal{V}_i}\left(\int_{\mathcal{V}_j}\int_{\mathcal{V}_k} q(i|j,v_j,k,v_k)Q(v_i|i,j,v_j,k,v_k)\right.\\ \times n_k^\varepsilon(t,v_k)n_j^\varepsilon(t,v_j)\mathrm{d}v_k\mathrm{d}v_j\\ \left. - n_i^\varepsilon(t,v_i)\int_{\mathcal{V}_k} q(j|i,v_i,k,v_k)n_k^\varepsilon(t,v_k)\mathrm{d}v_k\right)\mathrm{d}v_i \qquad (2.30)\end{aligned}$$

for all $\varepsilon > 0$. To proceed further, we assume that the K_i's are conservative also on average, i.e.

$$\int_{\mathcal{V}_i} v_i K_i(v_i|v_i')\mathrm{d}v_i = v_i' \qquad \forall\, v_i' \in \mathcal{V}_i, \quad \forall\, i \in \mathcal{I}, \qquad (2.31)$$

so that

$$\int_{\mathcal{V}_i} v_i\left(\int_{\mathcal{V}_i} K_i(v_i|v_i')n_i^\varepsilon(t,v_i')\mathrm{d}v_i' - n_i^\varepsilon(t,v_i)\right)\mathrm{d}v_i = 0.$$

Hence, multiplying (2.29) by v_i and integrating with respect to v_i itself we find

$$\begin{aligned}\frac{\mathrm{d}}{\mathrm{d}t}\int_{\mathcal{V}_i} v_i n_i^\varepsilon(t,v_i)\mathrm{d}v_i = r\sum_{\substack{j\in\mathcal{I}\\ j\neq i}}\left(\int_{\mathcal{V}_j} p(i|j,v_j)\bar{P}(i,j,v_j)n_j^\varepsilon(t,v_j)\mathrm{d}v_j - \int_{\mathcal{V}_i} p(j|i,v_i)v_i n_i^\varepsilon(t,v_i)\mathrm{d}v_i\right)\\ + (1-r)\sum_{k\in\mathcal{I}}\sum_{\substack{j\in\mathcal{I}\\ j\neq i}}\left(\int_{\mathcal{V}_j}\int_{\mathcal{V}_k} q(i|j,v_j,k,v_k)\bar{Q}(i,j,v_j,k,v_k)\right.\\ \times n_k^\varepsilon(t,v_k)n_j^\varepsilon(t,v_j)\mathrm{d}v_k\mathrm{d}v_j\\ \left. - \int_{\mathcal{V}_i} v_i n_i^\varepsilon(t,v_i)\int_{\mathcal{V}_k} q(j|i,v_i,k,v_k)n_k^\varepsilon(t,v_k)\mathrm{d}v_k\mathrm{d}v_i\right) \qquad (2.32)\end{aligned}$$

for all $\varepsilon > 0$, where we have used the following definitions:

$$\bar{P}(i,j,v_j) \coloneqq \int_{\mathcal{V}_i} v_i P(v_i|i,j,v_j)\mathrm{d}v_i, \qquad \bar{Q}(i,j,v_j,k,v_k) \coloneqq \int_{\mathcal{V}_i} v_i Q(v_i|i,j,v_j,k,v_k)\mathrm{d}v_i.$$

To discover a universal trend valid in the regime of small ε we pass now to the limit $\varepsilon \to 0^+$. To do so, we assume that n_i^ε converges to some n_i^0, $i \in \mathcal{I}$, which, owing to (2.29), formally satisfies

$$\int_{\mathcal{V}_i} K_i(v_i|v_i')n_i^0(t,v_i')\mathrm{d}v_i' - n_i^0(t,v_i) = 0.$$

Therefore, n_i^0 is an eigenfunction of the integral operator $\psi \mapsto \int_{\mathcal{V}_i} K(v_i|v_i')\psi(t,v_i')\mathrm{d}v_i'$ associated with the eigenvalue 1 and such that

$$\int_{\mathcal{V}_i} n_i^0(t,v_i)\mathrm{d}v_i = N_i^0(t), \qquad \int_{\mathcal{V}_i} v_i n_i^0(t,v_i)\mathrm{d}v_i = N_i^0(t)M_i^0(t),$$

N_i^0, M_i^0 being the limit values of the scaled fraction and mean compartment-specific structuring variable of the individuals in compartment $i \in \mathcal{I}$. Following [110], we let $n_i^0(t,v_i) = N_i^0(t)\psi_i(t,v_i)$, where ψ_i fulfills

$$\int_{\mathcal{V}_i} \psi_i(t,v_i)\mathrm{d}v_i = 1, \qquad \int_{\mathcal{V}_i} v_i\psi_i(t,v_i)\mathrm{d}v_i = M_i^0(t).$$

Then, letting, without loss of generality, $\mathcal{V}_i = [\underline{v}_i, \bar{v}_i]$ with $\underline{v}_i < \bar{v}_i$, under assumptions (2.3a), (2.3b), (2.3c), and (2.31), it is possible to prove, see again [110], that there exists a unique ψ_i, which is in the form

$$\psi_i(t,v_i) = (1 - M_i^0(t))\delta_{\underline{v}_i}(v_i) + M_i^0(t)\delta_{\bar{v}_i}(v_i), \qquad i \in \mathcal{I},$$

so that finally there exists a unique n_i^0, which is in the form

$$n_i^0(t,v_i) = N_i^0(t)(1 - M_i^0(t))\delta_{\underline{v}_i}(v_i) + N_i^0(t)M_i^0(t)\delta_{\bar{v}_i}(v_i), \qquad i \in \mathcal{I}.$$

In the following, without loss of generality, we set $\underline{v}_i = 0$ and $\bar{v}_i = 1$, that is,

$$\mathcal{V}_i = [0,\,1] \qquad \forall\, i \in \mathcal{I}. \tag{2.33}$$

Substituting the expressions for the n_i^0's just found into (2.30), after passing there to the limit $\varepsilon \to 0^+$, and dropping the superscripts "0" for convenience, yields

$$\begin{aligned}
\frac{\mathrm{d}N_i}{\mathrm{d}t} = {} & r\sum_{\substack{j\in\mathcal{I}\\ j\neq i}}\Big[\Big(p(i|j,0)(1-M_j) + p(i|j,1)M_j\Big)N_j - \Big(p(j|i,0)(1-M_i) + p(j|i,1)M_i\Big)N_i\Big] \\
& + (1-r)\sum_{k\in\mathcal{I}}\sum_{\substack{j\in\mathcal{I}\\ j\neq i}}\Big[\Big(q(i|j,0,k,0)(1-M_j)(1-M_k) + q(i|j,1,k,0)M_j(1-M_k) \\
& \qquad + q(i|j,0,k,1)(1-M_j)M_k + q(i|j,1,k,1)M_jM_k\Big)N_j \\
& \qquad - \Big(q(j|i,0,k,0)(1-M_i)(1-M_k) + q(j|i,1,k,0)M_i(1-M_k) \\
& \qquad + q(j|i,0,k,1)(1-M_i)M_k + q(j|i,1,k,1)M_iM_k\Big)N_i\Big]N_k.
\end{aligned} \tag{2.34}$$

Note that, as expected, the ODE system (2.34) is mass-preserving, that is,

$$\frac{\mathrm{d}}{\mathrm{d}t}\sum_{i\in\mathcal{I}} N_i(t) = 0 \;\; \forall\, t > 0 \quad \Longrightarrow \quad \sum_{i\in\mathcal{I}} N_i(t) = \sum_{i\in\mathcal{I}} N_i(0) \;\; \forall\, t > 0. \tag{2.35}$$

Similarly, substituting the expressions for the n_i^0's found above into (2.32), after passing also there to the limit $\varepsilon \to 0^+$, and dropping again the superscripts "0", gives

$$\begin{aligned}\frac{\mathrm{d}}{\mathrm{d}t}(N_iM_i) = r\sum_{\substack{j\in\mathcal{I}\\ j\neq i}}\Big[\Big(p(i|j,0)\bar{P}(i,j,0)(1-M_j) + p(i|j,1)\bar{P}(i,j,1)M_j\Big)N_j - p(j|i,1)N_iM_i\Big]\\ + (1-r)\sum_{k\in\mathcal{I}}\sum_{\substack{j\in\mathcal{I}\\ j\neq i}}\Big[\Big(q(i|j,0,k,0)\bar{Q}(i,j,0,k,0)(1-M_j)(1-M_k)\\ + q(i|j,1,k,0)\bar{Q}(i,j,1,k,0)M_j(1-M_k)\\ + q(i|j,0,k,1)\bar{Q}(i,j,0,k,1)(1-M_j)M_k\\ + q(i|j,1,k,1)\bar{Q}(i,j,1,k,1)M_jM_k\Big)N_j\\ - \Big(q(j|i,1,k,0)M_i(1-M_k) + q(j|i,1,k,1)M_iM_k\Big)N_i\Big]N_k. \quad (2.36)\end{aligned}$$

The ODE system (2.34),(2.36) constitutes, for $i \in \mathcal{I}$, a self-consistent compartmental model describing the evolution in time of the macroscopic quantities N_i, M_i in terms of the microscopic information contained in the model parameter r and functions p, q, $\bar{P}$, and $\bar{Q}$.

2.3.2 The homogeneous case

A considerable simplification of the ODE system (2.34),(2.36) is obtained in the *homogeneous* case, i.e. when one assumes that the functions p, q, $\bar{P}$, and $\bar{Q}$ depend on the compartment indices but are independent of the structuring variables, that is,

$$\begin{aligned} &p(j|i,v_i) \equiv p(j|i), && \bar{P}(i,j,v_j) \equiv \bar{P}(i,j),\\ &q(j|i,v_i,k,v_k) \equiv q(j|i,k), && \bar{Q}(i,j,v_j,k,v_k) \equiv \bar{Q}(i,j,k).\end{aligned}$$

In this case, recalling (2.4), we then find that (2.34) can be written in the form

$$\begin{aligned}\frac{\mathrm{d}N_i}{\mathrm{d}t} = r\sum_{\substack{j\in\mathcal{I}\\ j\neq i}}\big(p(i\mid j)N_j - p(j\mid i)N_i\big)\\ + (1-r)\sum_{k\in\mathcal{I}}\sum_{\substack{j\in\mathcal{I}\\ j\neq i}}\big(q(i\mid j,k)N_j - q(j\mid i,k)N_i\big)N_k, \qquad i\in\mathcal{I}. \quad (2.37)\end{aligned}$$

Notice that (2.37) is a self-consistent system in the unknowns N_i, $i \in \mathcal{I}$. In other words, in the homogeneous case the evolution of the fractions of individuals is independent of that of the mean values of the compartment-specific structuring variables. The same is not true in the general case (2.34), owing to the coupling produced by the inhomogeneous coefficients p and q. This result makes it possible

to assimilate (2.37) to a classical compartmental model of population dynamics. On the other hand, unlike a classical compartmental model, the framework defined by (2.34),(2.36) still allows one to track the evolution in time of the mean values of the compartment-specific structuring variables in consequence of the transitions of the individuals between the various compartments. In fact, from (2.36), under the homogeneity assumption, we find

$$\frac{\mathrm{d}}{\mathrm{d}t}(N_iM_i) = r\left(\sum_{\substack{j\in\mathcal{I}\\ j\neq i}} p(i|j)\bar{P}(i,j)N_j - (1-p(i|i))N_iM_i\right) + (1-r)\sum_{k\in\mathcal{I}}\sum_{\substack{j\in\mathcal{I}\\ j\neq i}}\big(q(i|j,k)\bar{Q}(i,j,k)N_j - q(j|i,k)N_iM_i\big)N_k, \qquad i\in\mathcal{I},$$

which, developing the time derivative on the left-hand side and using (2.37), further becomes

$$\frac{\mathrm{d}M_i}{\mathrm{d}t} = \frac{r}{N_i}\sum_{\substack{j\in\mathcal{I}\\ j\neq i}} p(i|j)\big(\bar{P}(i,j) - M_i\big)N_j + \frac{1-r}{N_i}\sum_{k\in\mathcal{I}}\sum_{\substack{j\in\mathcal{I}\\ j\neq i}} q(i|j,k)\big(\bar{Q}(i,j,k) - M_i\big)N_jN_k, \qquad i\in\mathcal{I}. \tag{2.38}$$

We notice that when N_i approaches 0 a singularity in (2.38) has to be expected. Moreover, we observe that the right-hand side of (2.38) is linear in M_i and, therefore, the existence of an endemic equilibrium $(N_i^*)_{i\in\mathcal{I}} \in (0,1)^N$ of (2.37) implies straightforwardly the existence of a corresponding equilibrium $(M_i^*)_{i\in\mathcal{I}} \in [0,1]^N$. In such a case, if $(N_i^*)_{i\in\mathcal{I}}$ is asymptotically stable then $(M_i^*)_{i\in\mathcal{I}}$ inherits the same stability property.

2.3.2.1 Basic reproduction number $\mathcal{R}_0$

In this section, we apply the Next Generation Matrix method [64, 65, 144] to derive the basic reproduction number $\mathcal{R}_0$ of the ODE system (2.37). We remark that the construction presented here reduces the method to its most elementary building blocks, which are the probabilities of leaving each infectious compartments and the probabilities of contaminating a susceptible individual upon interacting with them. This way, we elucidate the structural microscopic origin of an aggregate parameter as significant as $\mathcal{R}_0$ in the context of compartmental epidemiological models.

Without loss of generality, we assume that $i = 1$ corresponds to the Susceptible compartment. We focus on systems of ODEs of type (2.37) which possess only one

Disease Free Equilibrium (DFE) of the form

$$(N_1, N_2, \ldots, N_N) = (1, 0, \ldots, 0). \tag{2.39}$$

Such systems are quite common in the literature, see Section 2.4 for specific case studies.

The entry (i, j) of the Jacobian matrix $\mathbf{J}$ of (2.37) is given by

$$\begin{aligned} J_{ij} &= r\big(p(i|j) - \delta_{i,j}\big) \\ &\quad + (1-r)\left(\sum_{\substack{l\in\mathcal{I}\\ l\neq i}} \big(q(i|l,j)N_l - q(l|i,j)N_i\big) + \sum_{k\in\mathcal{I}} q(i|j,k)N_k(1-\delta_{i,j}) - \sum_{k\in\mathcal{I}}\sum_{\substack{l\in\mathcal{I}\\ l\neq i}} q(l|i,k)N_k\delta_{i,j}\right), \end{aligned}$$

where δ is the Kronecker delta, cf. (2.22). Evaluating at the DFE (2.39), this produces

$$\begin{aligned} J_{ij}(\mathrm{DFE}) &= r\big(p(i|j) - \delta_{i,j}\big) \\ &\quad + (1-r)\left(q(i|1,j)(1-\delta_{i,1}) - \sum_{\substack{l\in\mathcal{I}\\ l\neq i}} q(l|i,j)\delta_{i,1} + q(i|j,1)(1-\delta_{i,j}) - \sum_{\substack{l\in\mathcal{I}\\ l\neq i}} q(l|i,1)\delta_{i,j}\right). \end{aligned}$$

Next, we consider the sub-matrix $\mathbf{J}^*(\mathrm{DFE})$ of $\mathbf{J}(\mathrm{DFE})$ determined by infectious or infection-related (such as, for instance, Exposed, Asymptomatic, etc) compartments and we seek a decomposition of the form

$$\mathbf{J}^*(\mathrm{DFE}) = \mathbf{A} - \mathbf{B},$$

where the matrix $\mathbf{A}$ has non-negative entries and represents *transmission*, whereas the matrix $\mathbf{B}$ is invertible and represents *transitions*. There is not a unique way to define these two matrices. However, considering their respective interpretations, natural definitions for their entries are

$$\begin{aligned} A_{ij} &\coloneqq (1-r)\Big(q(i \mid 1,j)(1-\delta_{i,1}) - \sum_{\substack{l\in\mathcal{I}\\ l\neq i}} q(l \mid i,j)\delta_{i,1} \\ &\qquad + q(i \mid j,1)(1-\delta_{i,j}) - \sum_{\substack{l\in\mathcal{I}\\ l\neq i}} q(l \mid i,1)\delta_{i,j}\Big), \\ B_{ij} &\coloneqq r\big(\delta_{i,j} - p(i \mid j)\big) \end{aligned} \tag{2.40}$$

for all $i, j \in \mathcal{I}$ associated with infectious or infection-related compartments. Notice that, owing to (2.4a), Gershgorin first theorem applied to the columns of $\mathbf{B}$ ensures that all the eigenvalues of $\mathbf{B}$ have strictly non-negative real parts. Nevertheless, the origin of the complex plane may be contained in each of the Gershgorin discs; hence, we do not know in general whether $\mathbf{B}$ is invertible or not. A simple criterion ensuring invertibility is that there exists at least one non-infectious compartment

that can be reached with a spontaneous flow from each infectious compartment. This will be the case in all the specific models we shall present in Section 2.4.

Assuming that $\mathbf{B}$ in (2.40) is invertible, the Next Generation Matrix method provides the basic reproduction number $\mathcal{R}_0$ as

$$\mathcal{R}_0 = \rho(\mathbf{A}\mathbf{B}^{-1}), \tag{2.41}$$

where ρ denotes the spectral radius.

One of the most classical results on compartmental models is the global stability of the DFE under the condition $\mathcal{R}_0 < 1$. In addition to this, the modelling framework based on (2.37) allows one to build compartmental models which exhibit both forward and backward bifurcations at $\mathcal{R}_0 = 1$. In the former case, the DFE usually loses stability as $\mathcal{R}_0$ becomes greater than 1, in favour of the stability of a (unique) Endemic Equilibrium (EE). In the latter case, there exists a value $\mathcal{R}_0^* \in (0, 1)$ such that for $\mathcal{R}_0^* < \mathcal{R}_0 < 1$ the system exhibits bi-stability of DFE and EE as well as the existence of an unstable EE at the boundary of the corresponding basins of attraction.

Another classical result is the existence of at least one EE when $\mathcal{R}_0 > 1$. However, the modelling framework based on (2.37) presented here can easily be adapted to at least one system which does not possess this characteristic, namely the celebrated SIR model. Under the assumption $\mathcal{R}_0 > 1$, SIR orbits are indeed heteroclinic to the set of null infection (see e.g. [98, Lemma 1] for a proof) and the system does not possess any EE. Consequently, we cannot conclude, in general, the existence of any EE for system (2.37) without referring to specific cases or enforcing additional assumptions on the model functions p, q, $\bar{P}$, and $\bar{Q}$.

2.4 Case studies

In this section, we demonstrate, through a few case studies, how different classical compartmental epidemiological models can be derived from the ODE system (2.37), under appropriate choices of the microscopic parameter functions p, q, $\bar{P}$, and $\bar{Q}$. In contrast to their classical counterparts, the models here derived comprise also a system of ODEs for the mean values of the corresponding compartment-specific structuring variables, which is obtained from the ODE system (2.38), thus providing a richer description of the dynamics of the epidemiological system considered.

For every case study, we specify the choices of the microscopic parameter functions p, q, $\bar{P}$, and $\bar{Q}$ under which (2.37) reduces to the ODE system of the classical model. Moreover, we compare numerical solutions and analytical results of the ODEs of the macroscopic model with the results of Monte Carlo simulations of the underlying individual-based model, and show that there is excellent agreement between them. This provides validation of the formal procedures employed in Sections 2.3

and 2.3.1 to obtain first the IDE system (2.12) and then the ODE systems (2.37) and (2.38) from the individual-based model governed by the system (2.6). Simulations were performed in Matlab (version 2023a). The macroscopic ODE systems were solved using standard numerical routines (i.e. `ode45` in MATLAB 2023a), as they are low-dimensional and not stiff. By contrast, due to large number of agents, Monte Carlo simulations of the individual-based model required more attention. In particular, algorithms were implemented avoiding unnecessary loops and making use of vectorised operations, which significantly improved efficiency. As a result, we were able to carry out simulations involving up to 10^6 agents per run on a standard personal computer (12th Gen Intel(R) Core(TM) i7-1260P, 2.10 GHz, 12 cores, 16 logical processors, 16 GB RAM). We note that more complex scenarios may require larger numbers of agents to ensure statistical convergence, in which case additional computational resources would be beneficial.

For consistency with the extant literature, in each case study we use an alphabetic index set $\mathcal{I}$ rather than a numerical one. For instance, in the case of three compartments of Susceptible, Infectious, and Recovered individuals, we set $\mathcal{I} = \{S, I, R\}$ instead of $\mathcal{I} = \{1, 2, 3\}$. Moreover, for consistency with (2.33), we choose $\mathcal{V}_i = [0, 1]$ for all $i \in \mathcal{I}$. The values of key parameters of the macroscopic models used in numerical simulations are provided in the captions of Figures 2.3, 2.5, 2.7, while the definitions of the model parameters and functions that are used to carry out Monte Carlo simulations of the individual-based models are specify in the relative sections. Finally, the initial conditions for the fractions of individuals in the various compartments are such that, consistently with (2.2), the following normalisation condition holds:

$$\sum_{i\in\mathcal{I}} N_i(0) = 1.$$

Since the macroscopic model and the underlying microscopic model are mass-preserving, cf. (2.35), such a normalisation condition then holds for all $t > 0$, i.e.

$$\sum_{i\in\mathcal{I}} N_i(t) = 1 \ \ \forall\, t > 0.$$

We notice that in all cases considered here the components of the unique DFE, cf. (2.39), are $N_S = 1$ and $N_j = 0$ for all $j \in \mathcal{I}$ with $j \neq S$.

2.4.1 SIRS model

Considering an SIRS system, we take $N = 3$ and $\mathcal{I} = \{S, I, R\}$. As per the diagram displayed in Figure 2.2, only the following types of compartment switching occur: $S \to I$ (driven by the interaction between a susceptible and an infectious individual), $I \to R$ (spontaneous), and $R \to S$ (spontaneous). Therefore, the non-vanishing transition probabilities are $q(I|S, I)$, $p(R|I)$, and $p(S|R)$, whereas all the

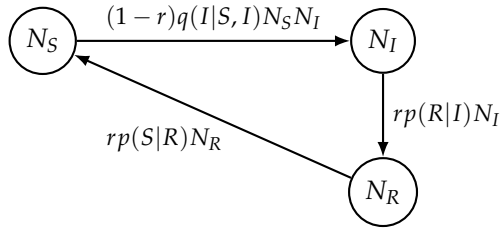

FIGURE 2.2: Flow diagram of the SIRS model

remaining p's and q's are zero. The ODE system (2.37) then reduces to

$$\begin{cases} \dfrac{\mathrm{d}N_S}{\mathrm{d}t} = rp(S|R)N_R - (1-r)q(I|S,I)N_SN_I, \\ \dfrac{\mathrm{d}N_I}{\mathrm{d}t} = -rp(R|I)N_I + (1-r)q(I|S,I)N_SN_I, \\ \dfrac{\mathrm{d}N_R}{\mathrm{d}t} = r\big(p(R|I)N_I - p(S|R)N_R\big). \end{cases} \tag{2.42}$$

In particular, the matrices defined via (2.40) are scalar quantities, i.e.

$$\mathbf{A} \equiv A = (1-r)q(I|S,I), \qquad \mathbf{B} \equiv B = r(1-p(I|I)) = rp(R|I),$$

where the above expression for B follows from (2.4a), recalling that in this case $p(S|I) = 0$. Finally, through (2.41), we find

$$\mathcal{R}_0 = \frac{A}{B} = \frac{(1-r)q(I|S,I)}{rp(R|I)}.$$

This coincides with the basic reproduction number classically computed as the ratio between the rate at which susceptible individuals become infectious and that at which infectious individuals become recovered, which from (2.42) are indeed $(1-r)q(I|S,I)$ and $rp(R|I)$, respectively.

The DFE $(N_S, N_I, N_R) = (1, 0, 0)$ is globally asymptotically stable when $\mathcal{R}_0 < 1$, cf. [42]. Conversely, when $\mathcal{R}_0 > 1$ there is a unique EE of components

$$N_S^* = \frac{1}{\mathcal{R}_0}, \qquad N_I^* = \frac{p(S|R)}{p(S|R)+p(R|I)}\left(1-\frac{1}{\mathcal{R}_0}\right), \qquad N_R^* = 1 - N_S^* - N_I^*,$$

which is globally stable, cf. [126].

Moreover, in this case the compartment-specific structuring variables can be interpreted as: (i) the level of *resistance to infection* in compartment $i = S$; (ii) the level of *viral load* in compartment $i = I$; (iii) the level of *immunity* in compartment

$i = R$. The evolution of their mean values is governed by the following ODE system, which is derived from (2.38):

$$\begin{cases} \dfrac{\mathrm{d}M_S}{\mathrm{d}t} = r\dfrac{p(S|R)(\bar{P}(S,R) - M_S)}{N_S}N_R, \\ \dfrac{\mathrm{d}M_I}{\mathrm{d}t} = (1-r)q(I|S,I)(\bar{Q}(I,S,I) - M_I)N_S, \\ \dfrac{\mathrm{d}M_R}{\mathrm{d}t} = r\dfrac{p(R|I)(\bar{P}(R,I) - M_R)}{N_R}N_I, \end{cases} \tag{2.43}$$

the equilibrium of which corresponding to the EE of (2.42) is

$$M_S^* = \bar{P}(S,R), \qquad M_I^* = \bar{Q}(I,S,I), \qquad M_R^* = \bar{P}(R,I).$$

Simulation set-up. For the Monte Carlo simulations of the individual-based model, the following parameters and functions are used:

$$\Delta t = 10^{-2}, \quad r = 0.5, \quad \theta_i = 0.5 \ \ \forall\, i \in \mathcal{I},$$

$$K_i(v_i'|v_i) \coloneqq \delta(v_i' - v_i) \ \ \forall\, i \in \mathcal{I},$$

$$p(j|i,v_i) \equiv p(j|i) \coloneqq \begin{cases} \delta_{jS} & \text{for} \quad i = S, \\ 0.2\,\delta_{jR} + 0.8\,\delta_{jI} & \text{for} \quad i = I, \\ 0.1\,\delta_{jS} + 0.9\,\delta_{jR} & \text{for} \quad i = R, \end{cases}$$

$$q(j|i,v_i,k,v_k^*) \equiv q(j|i,k) \coloneqq \begin{cases} 0.4\,\delta_{jI} + 0.6\,\delta_{jS} & \text{for} \quad i = S,\ k = I, \\ \delta_{ji} & \text{otherwise.} \end{cases}$$

Moreover, the relevant terms P and Q are

$$P(v_j''|j,i) \coloneqq \begin{cases} \mathbb{1}_{[0,1]}(v_j''), & \text{for} \quad j = R,\ i = I, \\ \frac{5}{3}\,\mathbb{1}_{[0,0.6]}(v_j'') & \text{for} \quad j = S,\ i = R, \end{cases}$$

$$Q(v_j''|j,i,k) \coloneqq \tfrac{5}{4}\,\mathbb{1}_{[0,0.8]}(v_j'') \quad \text{for} \quad j = k = I,\ i = S.$$

At the initial time $t = 0$, the individuals in the various compartments are distributed according to

$$n_i(0,v_i) \coloneqq \frac{N_i(0)}{2M_i(0)}\,\mathbb{1}_{[0,2M_i(0)]}(v_i), \qquad i \in \mathcal{I},$$

where the values of $N_i(0)$ and $M_i(0)$ are reported in the caption of Figure 2.3.

The plots in Figure 2.3 show a comparison between numerical solutions of the ODE

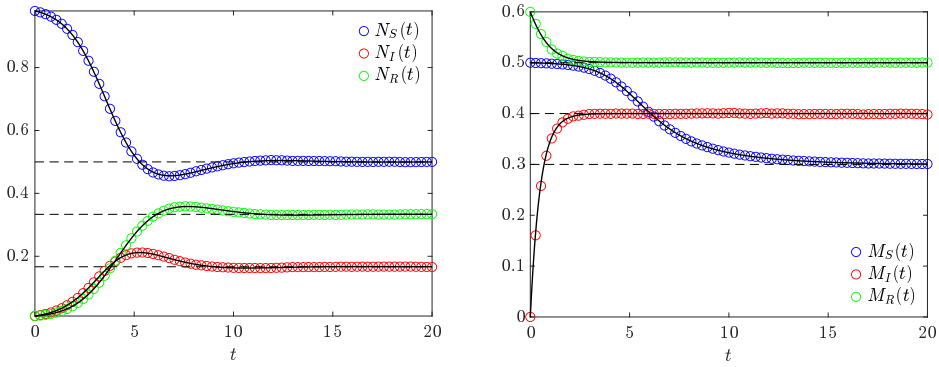

(a) (b)

FIGURE 2.3: SIRS model. Solid lines: numerical solutions of (2.42) (panel (a)) and (2.43) (panel (b)); circles: results of Monte Carlo simulations of the individual-based model; dashed lines: analytical equilibria. Relevant parameters: $\mathcal{R}_0 = 2$, $rp(S|R) = 0.05$, $(1-r)q(I|S,I) = 0.2$, $rp(R|I) = 0.1$, $\bar{P}(S,R) = 0.3$, $\bar{Q}(I,S,I) = 0.4$, $\bar{P}(R,I) = 0.5$. Initial condition: $(N_S(0), N_I(0), N_R(0), M_S(0), M_I(0), M_R(0)) = (0.98, 0.01, 0.01, 0.5, 0, 0.6)$. Simulations are carried out using 10^6 agents.

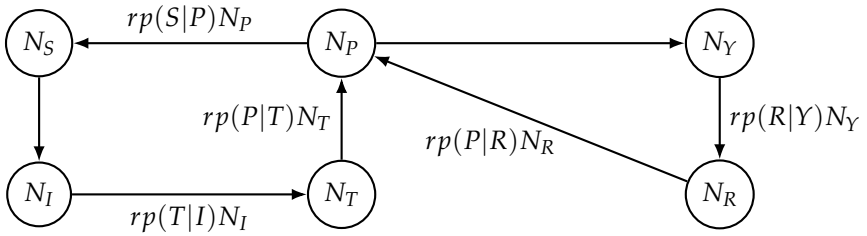

FIGURE 2.4: Flow diagram of the SIRS model with secondary infections. The infection rates between N_S and N_I (primary) and between N_P and N_Y (secondary) are omitted to avoid overcrowding

systems (2.42) and (2.43) and the results of Monte Carlo simulations of the corresponding individual-based model for the case where $\mathcal{R}_0 > 1$.

2.4.2 SIRS model with secondary infections

Within the general formulation provided by (2.37), we can model systems exhibiting either *forward* bifurcations when $\mathcal{R}_0 = 1$, such as the SIRS model presented in Section 2.4.1, or *backward* bifurcations. In the former case, one usually expects global asymptotic stability of the DFE when $\mathcal{R}_0 < 1$, and global asymptotic stability of the EE when $\mathcal{R}_0 > 1$. On the contrary, in the latter case there exists a value $\mathcal{R}_0^* \in (0, 1)$ of the basic reproduction number such that for $\mathcal{R}_0^* < \mathcal{R}_0 < 1$

the system exhibits bi-stability between the DFE and one EE along with a second unstable EE. This happens, for instance, in the SIRS model with secondary infections [99], which can be recast in the form (2.37) with $N = 6$ compartments and $\mathcal{I} = \{S, I, T, P, Y, R\}$. Specifically, besides the compartments $i = S, I, R$, three additional compartments are introduced: (i) $i = T$, comprising the individuals that are temporarily immune after recovering from a primary infection; (ii) $i = P$, comprising partly susceptible individuals that lost their transient immunity after recovering from a primary infection; (iii) and $i = Y$, comprising the individuals that undergo a secondary infection. On the basis of the diagram of Figure 2.4, the ODE system (2.37) particularises to

$$\begin{cases} \frac{\mathrm{d}N_S}{\mathrm{d}t} = rp(S|P)N_P - (1-r)\big(q(I|S,I)N_I + q(I|S,Y)N_Y\big)N_S, \\ \frac{\mathrm{d}N_I}{\mathrm{d}t} = -rp(T|I)N_I + (1-r)\big(q(I|S,I)N_I + q(I|S,Y)N_Y\big)N_S, \\ \frac{\mathrm{d}N_T}{\mathrm{d}t} = r\big(p(T|I)N_I - p(P|T)N_T\big), \\ \frac{\mathrm{d}N_P}{\mathrm{d}t} = r\big(p(P|T)N_T - p(S|P)N_P + p(P|R)N_R\big) - (1-r)\big(q(Y|P,I)N_I + q(Y|P,Y)N_Y\big)N_P, \\ \frac{\mathrm{d}N_Y}{\mathrm{d}t} = -rp(R|Y)N_Y + (1-r)\big(q(Y|P,I)N_I + q(Y|P,Y)N_Y\big)N_P, \\ \frac{\mathrm{d}N_R}{\mathrm{d}t} = r\big(p(R|Y)N_Y - p(P|R)N_R\big). \end{cases} \tag{2.44}$$

Since both $i = I$ and $i = Y$ are infectious compartment, in this case the matrices defined via (2.40) are

$$\mathbf{A} = \begin{pmatrix} (1-r)q(I|S,I) & (1-r)q(I|S,Y) \\ 0 & 0 \end{pmatrix}, \qquad \mathbf{B} = \begin{pmatrix} rp(T|I) & 0 \\ 0 & rp(R|Y) \end{pmatrix},$$

whence

$$\mathbf{AB}^{-1} = \begin{pmatrix} \frac{(1-r)q(I|S,I)}{rp(T|I)} & \frac{(1-r)q(I|S,Y)}{rp(R|Y)} \\ 0 & 0 \end{pmatrix},$$

and consequently, through (2.41), we find

$$\mathcal{R}_0 = \frac{(1-r)q(I|S,I)}{rp(T|I)}.$$

Notice that the above expression of $\mathcal{R}_0$ does not depend directly on any transition probability related to secondary infections.

Moreover, in this case the additional compartment-specific structuring variables can be interpreted as: (i) the level of *temporary immunity* in compartment $i = T$; (ii) the level of *partial immunity* in compartment $i = P$; (iii) the level of *viral load* following a secondary infection in compartment $i = Y$. The evolution of the mean values of the compartment-specific structuring variables is in this case governed by

the following ODE system, which is derived from (2.38):

$$\begin{cases} \frac{\mathrm{d}M_S}{\mathrm{d}t} = r\frac{p(S|P)(\bar{P}(S,P) - M_S)N_P}{N_S}, \\ \frac{\mathrm{d}M_I}{\mathrm{d}t} = (1-r)\frac{q(I|S,I)\big(\bar{Q}(I,S,I) - M_I\big)N_I + q(I|S,Y)\big(\bar{Q}(I,S,Y) - M_I\big)N_Y}{N_I}N_S, \\ \frac{\mathrm{d}M_T}{\mathrm{d}t} = r\frac{p(T|I)\big(\bar{P}(T,I) - M_T\big)}{N_T}N_I, \\ \frac{\mathrm{d}M_P}{\mathrm{d}t} = r\frac{p(P|T)(\bar{P}(P,T) - M_P)N_T + p(P|R)(\bar{P}(P,R) - M_P)N_R}{N_P}, \\ \frac{\mathrm{d}M_Y}{\mathrm{d}t} = (1-r)\frac{q(Y|P,I)\big(\bar{Q}(Y,P,I) - M_Y\big)N_I + q(Y|P,Y)\big(\bar{Q}(Y,P,Y) - M_Y\big)N_Y}{N_Y}N_P, \\ \frac{\mathrm{d}M_R}{\mathrm{d}t} = r\frac{p(R|Y)\big(\bar{P}(R,Y) - M_R\big)}{N_R}N_Y. \end{cases} \tag{2.45}$$

Simulation set-up. For the Monte Carlo simulations, the following parameters and functions are used:

$$\Delta t = 10^{-2}, \quad r = 0.5, \quad \theta_i = 0.5 \ \ \forall\, i \in \mathcal{I},$$

$$K_i(v_i'|v_i) \coloneqq \delta(v_i' - v_i) \ \ \forall\, i \in \mathcal{I},$$

$$p(j|i,v_i) \equiv p(j|i) \coloneqq \begin{cases} \delta_{jS} & \text{for} \quad i = S, \\ 0.25\,\delta_{jT} + 0.75\,\delta_{jI} & \text{for} \quad i = I, \\ 0.30\,\delta_{jP} + 0.70\,\delta_{jT} & \text{for} \quad i = T, \\ 0.15\,\delta_{jS} + 0.85\,\delta_{jP} & \text{for} \quad i = P, \\ 0.25\,\delta_{jR} + 0.75\,\delta_{jY} & \text{for} \quad i = Y, \\ 0.15\,\delta_{jP} + 0.85\,\delta_{jR} & \text{for} \quad i = R, \end{cases}$$

$$q(j|i,v_i,k,v_k^*) \equiv q(j|i,k) \coloneqq \begin{cases} 0.245\delta_{jI} + 0.755\delta_{jS} & \text{for} \quad i = S,\ k = I, \\ 0.490\delta_{jI} + 0.510\delta_{jS} & \text{for} \quad i = S,\ k = Y, \\ 0.490\delta_{jY} + 0.510\delta_{jP} & \text{for} \quad i = P,\ k = I, \\ 0.980\delta_{jY} + 0.020\delta_{jP} & \text{for} \quad i = P,\ k = Y, \\ \delta_{ji} & \text{otherwise.} \end{cases}$$

The relevant terms P and Q are

$$P(v_j''|j,i) \coloneqq \begin{cases} \frac{10}{17}\mathbb{1}_{[0,1.7]}(v_j'') & \text{for} \quad j = T,\ i = I, \\ \frac{5}{8}\mathbb{1}_{[0,1.6]}(v_j'') & \text{for} \quad j = P,\ i = T, \\ \frac{5}{8}\mathbb{1}_{[0,1.6]}(v_j'') & \text{for} \quad j = S,\ i = P, \\ \frac{5}{9}\mathbb{1}_{[0,1.8]}(v_j'') & \text{for} \quad j = R,\ i = Y, \\ \frac{5}{4}\mathbb{1}_{[0,0.8]}(v_j'') & \text{for} \quad j = P,\ i = R, \end{cases}$$

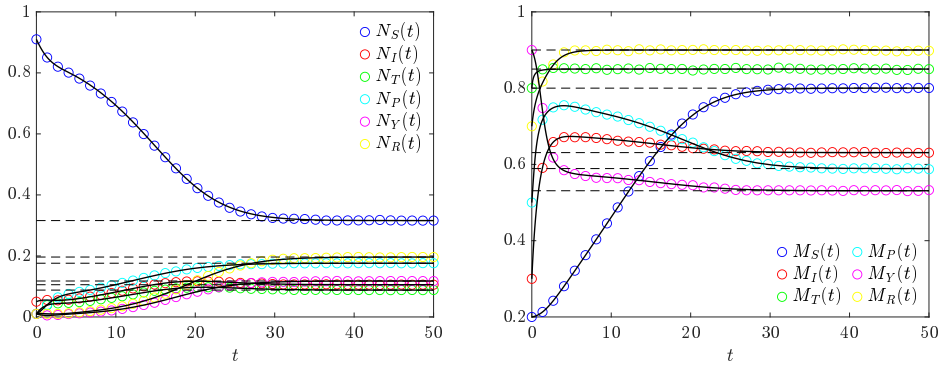

FIGURE 2.5: SIRS model with secondary infections. Solid lines: numerical solutions of (2.44) (panel (a)) and (2.45) (panel (b)); circles: results of Monte Carlo simulations of the individual-based model; dashed lines: analytical equilibria. Relevant parameters: $p(S|P) = p(P|R) = 0.5p(P|T)$, $rp(P|T) = 0.15$, $(1-r)q(I|S,I) = 0.1225$, $q(I|S,Y) = 2q(I|S,I)$, $rp(T|I) = 0.125$, $q(Y|P,I) = 2q(I|S,I)$, $rp(R|Y) = 0.125$, $\bar{P}(S,P) = 0.8$, $\bar{Q}(I,S,I) = 0.7$, $\bar{Q}(I,S,Y) = 0.6$, $\bar{P}(T,I) = 0.85$, $\bar{P}(P,T) = 0.8$, $\bar{P}(P,R) = 0.4$, $\bar{Q}(Y,P,I) = 0.6$, $\bar{Q}(Y,P,Y) = 0.5$, $\bar{P}(R,Y) = 0.9$. Initial condition: $(N_S(0), N_I(0), N_T(0), N_P(0), N_Y(0), N_R(0), M_S(0), M_I(0), M_T(0), M_P(0), M_Y(0), M_R(0)) = (0.91, 0.05, 0.01, 0.01, 0.01, 0.01, 0.2, 0.3, 0.8, 0.5, 0.9, 0.7)$. Simulations are carried out using 10^6 agents.

$$Q(v_j''|j,i,k) := \begin{cases} \frac{5}{7}\mathbb{1}_{[0,1.4]}(v_j'') & \text{for} \quad j=k=I,\ i=S, \\ \frac{5}{6}\mathbb{1}_{[0,1.2]}(v_j'') & \text{for} \quad j=I,\ i=S,\ k=Y, \\ \frac{5}{6}\mathbb{1}_{[0,1.2]}(v_j'') & \text{for} \quad j=Y,\ i=P,\ k=I, \\ \mathbb{1}_{[0,1]}(v_j'') & \text{for} \quad j=k=Y,\ i=P. \end{cases}$$

At the initial time $t = 0$, the distributions are

$$n_i(0,v_i) := \frac{N_i(0)}{2M_i(0)}\mathbb{1}_{[0,2M_i(0)]}(v_i), \qquad i \in \mathcal{I},$$

with $N_i(0)$ and $M_i(0)$ given in the caption of Figure 2.5.

The plots in Figure 2.5 show a comparison between numerical solutions of the ODE systems (2.44) and (2.45) and the results of Monte Carlo simulations, which indicate that convergence to the EE occurs even though $\mathcal{R}_0 < 1$.

2.4.3 SIRWS model

We present now a model, also included in the framework (2.37), wherein interaction-driven compartmental switching does not lead individuals to enter an infectious

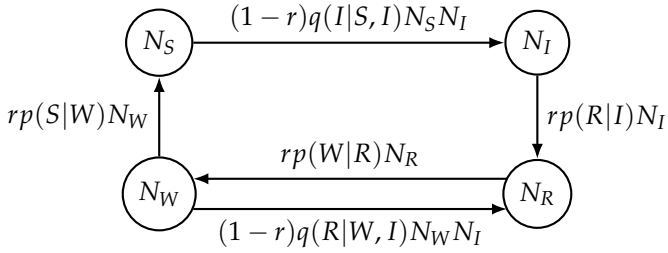

FIGURE 2.6: Flow diagram of the SIRWS model

compartment. Specifically, to consider the SIRWS model [57, 98], we choose $N = 4$ and $\mathcal{I} = \{S, I, R, W\}$, where the compartment $i = W$ comprises individuals undergoing a "waning immunity" phase: while in this compartment, interacting with an infectious individual boosts the immunity, which induces a switch back to compartment $i = R$. Otherwise, an individual will eventually lose immunity completely and move to compartment $i = S$.

In [57, 98] the authors include demography, which we neglect here so as to recast their model in our framework. Following the diagram depicted in Figure 2.6, we derive from (2.37) the following ODE system:

$$\begin{cases} \dfrac{\mathrm{d}N_S}{\mathrm{d}t} = rp(S|W)N_W - (1-r)q(I|S,I)N_SN_I, \\ \dfrac{\mathrm{d}N_I}{\mathrm{d}t} = -rp(R|I)N_I + (1-r)q(I|S,I)N_SN_I, \\ \dfrac{\mathrm{d}N_R}{\mathrm{d}t} = r\big(p(R|I)N_I - p(W|R)N_R\big) + (1-r)q(R|W,I)N_WN_I, \\ \dfrac{\mathrm{d}N_W}{\mathrm{d}t} = r\big(p(W|R)N_R - p(S|W)N_W\big) - (1-r)q(R|W,I)N_WN_I. \end{cases} \tag{2.46}$$

The matrices $\mathbf{A}$ and $\mathbf{B}$ of this system are again scalar quantities, as it is the case for the ODE system (2.42), because only one infectious compartment is present, that is,

$$\mathbf{A} \equiv A = (1-r)q(I|S,I), \qquad \mathbf{B} \equiv B = r\big(1-p(I|I)\big) = rp(R|I).$$

The above expression for B follows from (2.4a) together with the fact that, in this model, $p(S|I) = p(W|I) = 0$. Through (2.41) we find

$$\mathcal{R}_0 = \frac{A}{B} = \frac{(1-r)q(I|S,I)}{rp(R|I)},$$

i.e. the same basic reproduction number as that of the SIRS model.

Moreover, in this case the additional compartment-specific structuring variable can be interpreted as the level of *immunity* in compartment $i = W$. The evolution of the

mean values of the compartment-specific structuring variables is now governed by the following ODE system, which is again derived from (2.38):

$$\begin{cases} \dfrac{\mathrm{d}M_S}{\mathrm{d}t} = r\dfrac{p(S|W)(\bar{P}(S,W) - M_S)}{N_S}N_W, \\ \dfrac{\mathrm{d}M_I}{\mathrm{d}t} = (1-r)q(I|S,I)(\bar{Q}(I,S,I) - M_I)N_S, \\ \dfrac{\mathrm{d}M_R}{\mathrm{d}t} = \dfrac{rp(R|I)(\bar{P}(R,I) - M_R) + (1-r)q(R|W,I)(\bar{Q}(R,W,I) - M_R)N_W}{N_R}N_I, \\ \dfrac{\mathrm{d}M_W}{\mathrm{d}t} = r\dfrac{p(W|R)(\bar{P}(W,R) - M_W)}{N_W}N_R. \end{cases} \quad d \tag{2.47}$$

Assuming that the fractions of individuals in each compartment tend asymptotically in time to the EE, say $(N_S^*, N_I^*, N_R^*, N_W^*)$, we see from (2.47) that the corresponding mean compartment-specific structuring variables tend to $M_S^* = \bar{P}(S,R)$, $M_I^* = \bar{Q}(I,S,I)$, $M_W^* = \bar{P}(W,R)$, and

$$M_R^* = \frac{rp(R|I)\bar{P}(R,I) + (1-r)q(R|W,I)\bar{Q}(R,W,I)N_W^*}{rp(R|I) + (1-r)q(R|W,I)N_W^*}.$$

Since the SIRWS model admits periodic limit cycles, see [57, 98], we might observe periodic fluctuations in M_R, which depend on N_W, while the mean values of all the other compartment-specific structuring variables, which are independent of the fractions of individuals in the various compartments, converge to an equilibrium. To better investigate this possibility, we look at the equilibrium value of M_R as a function of N_W

$$M_R(N_W) = \frac{rp(R|I)\bar{P}(R,I) + (1-r)q(R|W,I)\bar{Q}(R,W,I)N_W}{rp(R|I) + (1-r)q(R|W,I)N_W}$$

and we compute

$$\frac{\mathrm{d}M_R}{\mathrm{d}N_W} = r(1-r)p(R|I)q(R|W,I)\frac{\bar{Q}(R,W,I) - \bar{P}(R,I)}{(rp(R|I) + (1-r)q(R|W,I)N_W)^2},$$

whence we discover that M_R is strictly increasing or decreasing with respect to N_W depending on the sign of $\bar{Q}(R,W,I) - \bar{P}(R,I)$. In particular, $\bar{Q}(R,W,I) > \bar{P}(R,I)$ results in peaks of M_R while $\bar{Q}(R,W,I) < \bar{P}(R,I)$ in dips of M_R. If instead $\bar{Q}(R,W,I) = \bar{P}(R,I)$ then M_R does not oscillate. Moreover, large values of $\bar{Q}(R,W,I) - \bar{P}(R,I)$ result in large excursions of M_R away from the equilibrium value M_R^*. Nevertheless, we observe that the term N_I in the equation for M_R in (2.47) makes the evolution of M_R quite slow if the epidemic is dormant, i.e. $N_I \approx 0$. Therefore, excursions away from M_R^* can be clearly observed only when N_I grows sufficiently far from 0.

Simulation set-up. For the Monte Carlo simulations, the following parameters and functions are used:

$$\Delta t = 0.0032, \quad r = 0.05, \quad \theta_i = 0.5 \ \ \forall\, i \in \mathcal{I},$$

$$K_i(v_i'|v_i) := \delta(v_i' - v_i) \ \ \forall\, i \in \mathcal{I}, \ \ \forall\, i \in \mathcal{I},$$

$$p(j|i, v_i) \equiv p(j|i) := \begin{cases} \delta_{ji} & \text{for} \quad i = S, \\ 0.5806\,\delta_{jR} + 0.4194\,\delta_{jI} & \text{for} \quad i = I, \\ 0.0323\,\delta_{jW} + 0.9677\,\delta_{jR} & \text{for} \quad i = R, \\ 0.0323\,\delta_{jS} + 0.9677\,\delta_{jW} & \text{for} \quad i = W, \end{cases}$$

$$q(j|i, v_i, k, v_k^*) \equiv q(j|i, k) := \begin{cases} 0.1019\,\delta_{jI} + 0.8981\,\delta_{jS} & \text{for} \quad i = S, \ k = I, \\ 0.5093\,\delta_{jR} + 0.4907\,\delta_{jW} & \text{for} \quad i = W, \ k = I, \\ \delta_{ji} & \text{otherwise.} \end{cases}$$

Moreover, the terms $P(v_j''|j, i, v_i) \equiv P(v_j''|j, i)$ and $Q(v_j''|j, i, v_i, k, v_k^*) \equiv Q(v_j''|j, i, k)$ which are relevant (i.e. either different from zero or with $j \neq i$) for the present case study are defined as

$$P(v_j''|j, i) := \begin{cases} \frac{5}{4}\mathbb{1}_{[0,\,0.8]}(v_j'') & \text{for} \quad j = R, \ i = I, \\ \frac{5}{2}\mathbb{1}_{[0,\,0.4]}(v_j'') & \text{for} \quad j = W, \ i = R, \\ \frac{5}{3}\mathbb{1}_{[0,\,0.6]}(v_j'') & \text{for} \quad j = S, \ i = W, \end{cases}$$

$$Q(v_j''|j, i, k) := \begin{cases} \frac{5}{4}\mathbb{1}_{[0,\,0.8]}(v_j'') & \text{for} \quad j = k = I, \ i = S, \\ \frac{5}{9}\mathbb{1}_{[0,\,1.8]}(v_j'') & \text{for} \quad j = R, \ i = W, \ k = I. \end{cases}$$

At the initial time $t = 0$, the individuals in the various compartments are distributed according to the following distributions:

$$n_i(0, v_i) := \frac{N_i(0)}{2M_i(0)}\,\mathbb{1}_{[0,\,2M_i(0)]}(v_i), \qquad i \in \mathcal{I},$$

where the values of $N_i(0)$ and $M_i(0)$ are reported in the caption of Figure 2.7.

The plots in Figure 2.7 show a comparison between numerical solutions of the ODE systems (2.46) and (2.47) and the results of Monte Carlo simulations of the corresponding individual-based model. Notice how M_R reacts to the dips of N_W, which coincide with the spikes of N_I representing consequent epidemic waves.

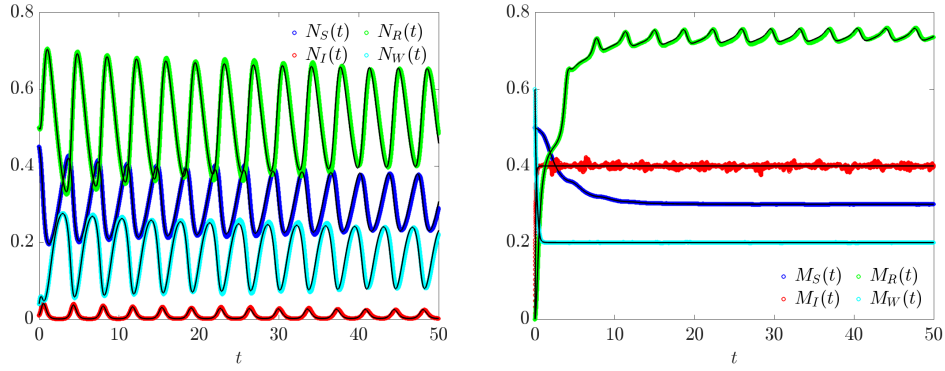

FIGURE 2.7: SIRWS model (without demography). Solid lines: numerical solutions of (2.46) (panel (a)) and (2.47) (panel (b)); circles: results of Monte Carlo simulations of the individual-based model governed by (2.6) adapted to this case. Relevant parameters: $rp(S|W) = rp(W|R) = 1/3100$, $(1-r)q(I|S,I) = 3/31$, $rp(R|I) = 17/310$, $q(R|W,I) = 10q(I|S,I)$, $(1-r)q(R|W,I) = 30/31$, $\bar{P}(S,W) = 0.3$, $\bar{Q}(I,S,I) = 0.4$, $\bar{Q}(R,W,I) = 0.9$, $\bar{P}(R,I) = 0.4$, $\bar{P}(W,R) = 0.2$. Hence, $\mathcal{R}_0 = 30/17$. Initial condition: $(N_S(0), N_I(0), N_R(0), N_W(0), M_S(0), M_I(0), M_R(0), M_W(0)) = (0.97, 0.01, 0.01, 0.01, 0.5, 0, 0.6, 0)$. Monte Carlo simulations are carried out using 10^6 agents.

2.5 Concluding remarks

This chapter is part of the construction of a general framework aimed at systematically bridging the different scales. In particular, we have developed a framework for modelling heterogeneous, compartmental, and structured epidemiological systems, following an approach already partially introduced in the previous chapter. The construction reintroduces labels for the compartments ($i \in \mathcal{I}$) and continuous structural variables $v_i \in \mathcal{V}_i$ for each $i \in \mathcal{I}$. In this context, these variables represent the expression level of a specific trait associated with each compartment. This structure allows for a more detailed depiction of the individual profile and is particularly well suited to epidemiological models, where, for instance, infected individuals can be represented by a viral load parameter, while recovered individuals are characterised by a resistance parameter to infection.

For the evolution of the microscopic state, we once again rely on the study of the random vector $(I_t, \mathbf{V}_t)$. The random variables, respectively, provide information on the compartment to which the individual belongs and the value of the expressed traits. Changes in the microscopic state thus correspond to the evolution of these random variables: on the one hand, the expression levels of specific traits evolve

over time; on the other hand, individuals may transition between different compartments. These transitions may occur either spontaneously or as a result of interactions with other individuals, whether from the same compartment or from different ones.

We first formulated a stochastic individual-based model that tracks the dynamics of single individuals, from which we formally derived the corresponding mesoscopic model, which consists of the IDE system (2.12) for the population density functions, $n_i(t, v_i)$, of the various compartments at time t.

So far, this construction reflects the aim of providing a representation as comprehensive as possible of the interactions across the different descriptive scales. However, such a structure makes the model extremely difficult to analyse in its full generality. For this reason, a number of simplifying assumptions are introduced.

First, we consider an appropriately rescaled version of the system, given by the IDE system (2.29), and perform formal asymptotic analyses to derive the corresponding macroscopic model. The resulting macroscopic formulation consists of the ODE system (2.34), (2.36), which governs the fractions $N_i(t)$ of individuals in the different compartments and the mean values $M_i(t)$ of the compartment-specific structuring variables. In this ODE system, the evolution of these macroscopic quantities is expressed in terms of the microscopic information encoded in the model parameters and functions.

Second, in order to restrict attention to a class of models more directly applicable to epidemiology, we introduce a homogeneity assumption in the dynamics. Specifically, we assume that the model functions depend on the compartment indices but are independent of the structuring variables. Under this assumption, the ODE system (2.34), (2.36) reduces to the simpler systems (2.37) and (2.38). Employing the Next Generation Matrix approach, we then derive a general expression for the basic reproduction number $\mathcal{R}_0$, in terms of key parameters and functions of the underlying microscopic model. This illustrates how the framework developed here allows one to establish explicit connections between fundamental individual-level processes and population-scale dynamics.

Moreover, in this chapter we applied the modelling framework to case studies from classical compartmental epidemiological systems (i.e. the SIRS model, the SIRS model with secondary infections, and the SIRWS model) and, for each of them, we showed that there is excellent agreement between the results of Monte Carlo simulations of the individual-based model and both numerical solutions and analytical results of the macroscopic model. This validates the internal consistency of the modelling framework and the formal limiting procedures employed to obtain the mesoscopic and macroscopic models from the underlying individual-based model.

Chapter 3

A phenotype structured integro-differential model for nutrient-consumer dynamics

Derivation and asymptotic analysis

3.1 Introduction

In the previous chapters, we developed and analysed models describing the evolutionary dynamics of structured populations divided into multiple compartments. In this chapter, we extend the framework to study the co-evolutionary dynamics of two distinct but interacting subsystems, each organised into compartments and endowed with its own structural heterogeneity. Unlike the setting of Chapter 1, where effective analysis was restricted to a single compartment, or that of Chapter 2, where a single population was distributed across N compartments, here we consider two different populations. Consequently, only two structuring variables are required, one for each subsystem, treating the population as a whole rather than with heterogeneity at the compartment level.

We focus on the biologically relevant case in which the two subsystems correspond to *nutrients* and *consumer agents*. The first subsystem describes nutrients which are not treated as a homogeneous substrate, as often assumed in the literature (cf. [12–14, 59, 66, 115, 122]), but are modelled with a structural variable $x \in \Omega_x \subset \mathbb{R}$ that captures internal heterogeneity. To enforce conservation of the total amount of nutrients, we distinguish between two compartments: *substrate* of available resources and *reserve* of consumed units, which can be regenerated and reintroduced into the substrate.

The second subsystem consists of consumer agents, characterised by a structural variable $y \in \Omega_y \subset \mathbb{R}$. They are divided into three compartments: *non-reproductive* individuals that accumulate resources, *reproductive* individuals ready to generate

offspring, and a *reservoir* that collects naturally dying agents and provides the mass required for reproduction.

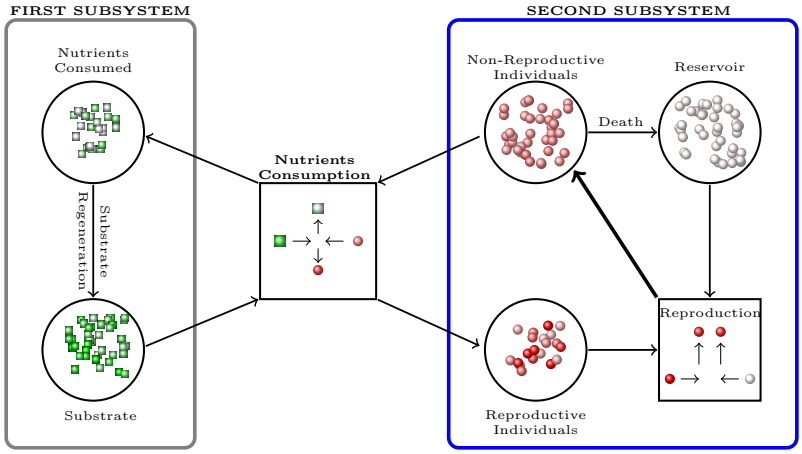

FIGURE 3.1: Modelling strategies used to describe the underlying biological processes.

This organisation, summarized in Figure 3.1, guarantees a twofold conservation property: the total mass of the system is preserved, and within it the amounts of nutrients and agents are conserved separately. Thus, the framework describes the joint dynamics of two interacting populations, each with its own structural variable and compartmental organisation.

Transitions between compartments are mediated by suitable kernels, which govern changes in the microscopic state due to binary interactions. Following the approach introduced in Chapter 1 and Chapter 2, the transition probabilities are expressed through the realisation parameters associated with Bernoulli random variables depending on the initial microscopic state. Moreover, unlike the abstract construction introduced in the previous chapter, in the present model, the trait acquired after a compartmental switch is determined purely deterministic. In particular, the counterparts of the kernels P and Q defined in the points (IIa) and (IIb) of Section 2.2 are here represented by Dirac distributions. This implies that, at the moment of the switch, the individual assumes a new trait fully determined by its initial state and by the type of transition, without the involvement of stochastic mechanisms representing spontaneous variations. The only exception to this *Markovian* setting occurs in the spontaneous transition to the reserve compartment, which represents, as in Chapter 1, the death of an individual. In this case, the structural variable is not preserved, so that the compartment can be treated as unstructured.

The resulting model is a framework that unifies the conceptual tools of the previous chapters while extending them to capture the coupled evolution of nutrients and consumers in a single, analytically tractable system. To this end, we exploit the conservative nature of the model and consider a fast-proliferation limit, which

allows us to reduce the system to a pair of integro-differential equations. For this reduced system, we first establish a well-posedness theorem, providing the a priori estimates required to investigate the asymptotic dynamics. Then, we identify the survival set of traits, that is, the unique region of the domain where a positive net growth rate is attainable. This enables us to characterise the long-term behaviour of the two subsystems, distinguishing between regimes leading to saturation, extinction, or selection. Interestingly, although the model is formally based on an indirect interaction mechanism between consumers, its structure still gives rise to emergent behaviours that resemble those of direct competition models, as observed in related ecological frameworks [122]. These theoretical scenarios are illustrated and validated through dedicated numerical simulations.

3.2 Stochastic agent-based model

We consider $N = 5$ interacting compartments, indexed by $i \in \mathcal{I} := \{1, \dots, 5\}$. In this case, however, only two structuring variables are introduced, since the system consists of two subsystems: the nutrients and the consumer agents. We denote respectively these variables by $x \in \Omega_x \subset \mathbb{R}$ and $y \in \Omega_y \subset \mathbb{R}$, where both Ω_x and Ω_y are bounded intervals. Here, x represents the structuring variable for nutrients, while y represents the structuring variable for agents.

At each time $t \in [0, \infty)$, all units are regarded as indistinguishable except for their microscopic state, represented by the random variables $(I_t, \mathbf{V}_t)$. The discrete random variable $I_t \in \mathcal{I}$ identifies the compartment to which a given individual belongs at time t, while the continuous random variable $\mathbf{V}_t := (V_{x,t}, V_{y,t}) \in \Omega := \Omega_x \times \Omega_y \subset \mathbb{R}^2$ describes the expression levels of the traits across the two subsystems. We write

$$(I_t, \mathbf{V}_t) \sim f(t, i, x, y), \tag{3.1}$$

where the symbol $\sim$ indicates that the random vector is distributed according to the probability distribution f. Such a function $f : [0, \infty) \times \mathcal{I} \times \Omega \to \mathbb{R}_+$ is a probability density, therefore we have

$$\sum_{i=1}^{5} \int_{\Omega} f(t, i, \mathbf{v}) \mathrm{d}\mathbf{v} = 1 \quad \forall t \in [0, \infty), \tag{3.2}$$

where we denote $\mathbf{v} = (x, y)$.

In the present model, we neglect intra-compartment mutations. This assumption reflects the goal of focusing the analysis on the interactions between the two subsystems rather than on variations occurring within each compartment. However, we note that including such mutations would not entail substantial complications in the microscopic derivation and would be a natural extension of the present work.

Compartment switches are allowed with rate ζ. A fraction $r(i)$ of these transitions occurs spontaneously, while the remaining fraction $1 - r(i)$ results from pairwise

interactions.
In summary, the processes included in our model are of two types.

Interaction-driven processes:

(I) **Nutrient consumption.** A binary interaction occurs between a nutrient unit available in the substrate (compartment $i = 2$, trait x) and a consumer not yet capable of proliferation (compartment $i = 3$, trait y). The interaction produces a new individual that has reached reproductive maturity (compartment $i = 4$, trait y) and a corresponding consumed nutrient unit (compartment $i = 1$, trait x).

(II) **Proliferation.** This process involves an interaction between a reserve individual (compartment $i = 5$, trait y_0) and a mature individual (compartment $i = 4$, trait y). The outcome is the production of two new agents in compartment $i = 3$, both inheriting the parental trait y.

Spontaneous processes:

(III) **Substrate regeneration.** Consumed nutrient units (compartment $i = 1$, trait x) are spontaneously regenerated into available substrate (compartment $i = 2$, trait x).

(IV) **Death.** A fraction of individuals not in a proliferation stage (compartment $i = 3$, trait y) die spontaneously, moving to the reserve compartment (compartment $i = 5$, trait y_0).

Remark 3.1. For notational convenience, in this section, we may denote the domains of continuous structural variables by Ω_j, as if each compartment were associated with a distinct structural domain, while in fact there are only two: Ω_x and Ω_y. Specifically, we set $\Omega_j = \Omega_x$ for $j \in \{1, 2\}$ and $\Omega_j = \Omega_y$ for $j \in \{3, 4, 5\}$. This convention reflects the distinction between the compartments related to nutrient units (the first two) and those related to consumers (the remaining three). Accordingly, we may denote by $\mathbf{v}$ the pair (x, y) and by v_j the continuous variable associated with compartment j, with $v_j = x$ for $j \in \{1, 2\}$ and $v_j = y$ for $j \in \{3, 4, 5\}$. This notation provides a uniform description while preserving the distinction between the two subsystems.

Under these assumptions, the random process that governs the evolution of the microscopic state $(I_t, \mathbf{V}_t)$ takes the following form

$$\begin{cases} I_{t+\Delta t} = (1 - Z)\, I_t + Z\, [\Xi I'_t + (1 - \Xi) I''_t]\,, \\ V_{x,t+\Delta t} = (1 - Z) V_{x,t} + Z\, V'_{x,t}\,, \\ V_{y,t+\Delta t} = (1 - Z) V_{y,t} + Z\, V'_{y,t}\,, \end{cases} \tag{3.3}$$

where Z and Ξ are independent Bernoulli random variables such that:

$$\begin{aligned} &\text{Prob}\left(Z = 1 \mid I_t = i, V_{x,t} = x_i, V_{y,t} = y_i\right) = \zeta \Delta t, \\ &\text{Prob}\left(\Xi = 1 \mid I_t = i, V_{x,t} = x_i, V_{y,i} = y_i\right) = r(i), \end{aligned} \tag{3.4}$$

We assume $\Delta t\, \zeta \leq 1$, while no analogous restriction is needed for $r(i)$, since $r(i) \in [0,1]$ for all $i \in \mathcal{I}$. In system (3.3), the random variables $I'_t, I''_t \in \mathcal{I}$ model, respectively, the index of the new compartment reached following a spontaneous or interaction-driven transition. The random variable $\mathbf{V}'_t = (V'_{x,t}, V'_{y,t}) \in \Omega$ represents the corresponding structural trait acquired by the individual. To complete the description of the dynamics, we let

$$\begin{aligned} (I'_t, \mathbf{V}'_t \mid I_t, \mathbf{V}_t) &\sim \mathcal{P}(i', x', y' \mid i, x, y), \\ (I''_t, \mathbf{V}'_t \mid I_t, \mathbf{V}_t, I^*_t, \mathbf{V}^*_t) &\sim \mathcal{Q}(i'', x', y' \mid i, x, y, i^*, x^*, y^*), \end{aligned} \tag{3.5}$$

where $\mathcal{P}$ and $\mathcal{Q}$ represent the transition kernels for spontaneous and interaction-driven processes, respectively. We now let

$$\mathcal{P}(i', \mathbf{v}' \mid i, \mathbf{v}) := \begin{cases} \left(p_1^2(x)\, \delta_{i',2} + (1 - p_1^2(x))\, \delta_{i',1}\right) \delta_x(x')\, \delta_y(y') & \text{if } i = 1, \\ \left(p_3^5(y)\, \delta_{i',5} \delta_{y_0}(y') + (1 - p_3^5(y))\, \delta_{i',3} \delta_y(y')\right) \delta_x(x') & \text{if } i = 3, \\ \delta_{i',i}\, \delta_x(x')\, \delta_y(y') & \text{otherwise.} \end{cases} \tag{3.6}$$

Here, the functions $p_i^j(v_i)$ denote the probability that an individual in compartment i with trait v_i spontaneously transitions to compartment j. The first line corresponds to the process (III), *substrate regeneration*: a consumed nutrient unit ($i = 1$) may return to the available substrate ($i' = 2$) with probability $p_1^2(x)$, keeping its trait x unchanged. The second line describes the process (IV), *death*: non-reproductive agents ($i = 3$) may be transferred to the reserve compartment ($i' = 5$) with probability $p_3^5(y)$ and assigned the fixed trait y_0, representing the loss of structural information associated with death. For the *interaction-driven* transitions, we set:

$$\mathcal{Q}(i'', \mathbf{v}' \mid i, \mathbf{v}, i^*, \mathbf{v}^*) := \begin{cases} \left(q_{2,3}^1(x, y^*) \delta_{i'',1} + (1 - q_{2,3}^1(x, y^*)) \delta_{i'',2}\right) \delta_y(y') \delta_x(x') & \text{if } i = 2,\ i^* = 3, \\ \left(q_{3,2}^4(y, x^*) \delta_{i'',4} + (1 - q_{3,2}^4(y, x^*)) \delta_{i'',3}\right) \delta_y(y') \delta_x(x') & \text{if } i = 3,\ i^* = 2, \\ \left(q_{4,5}^3(y, y^*) \delta_{i'',3} + (1 - q_{4,5}^3(y, y^*)) \delta_{i'',4}\right) \delta_y(y') \delta_x(x') & \text{if } i = 4,\ i^* = 5, \\ \left(q_{5,4}^3(y, y^*) \delta_{i'',3} + (1 - q_{5,4}^3(y, y^*)) \delta_{i'',5}\right) \delta_{y^*}(y') \delta_x(x') & \text{if } i = 5,\ i^* = 4, \\ \delta_{i'',i} \delta_y(y') \delta_x(x') & \text{otherwise.} \end{cases} \tag{3.7}$$

The functions $q_{i,j}^{i''}(v_i, v_j)$ denote the probability that an individual initially in compartment i with trait v_i, interacting with another individual in compartment j with trait v_j, transitions to compartment i''. The first two lines describe the *substrate*

consumption process (I): the first from the perspective of the nutrient unit, which may be transferred to the consumed nutrient compartment ($i'' = 1$) or remain in the available substrate ($i'' = 2$); the second from the perspective of the consumer, which may acquire reproductive capability ($i'' = 4$) or remain in its initial compartment ($i'' = 3$). The third and fourth lines describe the process of *proliferation* (II): the third from the perspective of the parental individual ($i = 4$), which returns to compartment $i'' = 3$; the fourth from the perspective of the reserve agent ($i = 5$), which may give birth in compartment $i = 3$. In both equations (3.6) and (3.7), the Dirac measures $\delta_{v_i}(v'_j)$ ensure that the trait is preserved or modified according to the nature of the process. Finally, $\delta_{i,j}$ denotes the Kronecker delta, equal to 1 if $i = j$ and 0 otherwise.

3.3 Mesoscopic model

Starting from system (3.3), our objective is to derive the mesoscopic model corresponding to the microscopic formulation introduced in the previous section. In particular, we are not interested in the fully general representation of the density $f(t, i, x, y)$ defined in (3.1), but rather in the marginal densities associated with the five compartments under consideration:

$$\begin{aligned}
c(t,x) &:= \int_{\Omega_y} f(t,1,x,y)\,\mathrm{d}y \qquad \text{(consumed nutrients)},\\
s(t,x) &:= \int_{\Omega_y} f(t,2,x,y)\,\mathrm{d}y \qquad \text{(substrate)},\\
n(t,y) &:= \int_{\Omega_x} f(t,3,x,y)\,\mathrm{d}x \qquad \text{(non-reproductive agents)},\\
m(t,y) &:= \int_{\Omega_x} f(t,4,x,y)\,\mathrm{d}x \qquad \text{(reproductive agents)},\\
h(t,y) &:= \int_{\Omega_x} f(t,5,x,y)\,\mathrm{d}x \qquad \text{(reserve)}.
\end{aligned} \tag{3.8}$$

Hence, we also define the corresponding masses as

$$\begin{aligned}
C(t) &:= \int_{\Omega_x} c(t,x)\,\mathrm{d}x,\\
S(t) &:= \int_{\Omega_x} s(t,x)\,\mathrm{d}x,\\
N(t) &:= \int_{\Omega_y} n(t,y)\,\mathrm{d}y,\\
M(t) &:= \int_{\Omega_y} m(t,y)\,\mathrm{d}y,\\
H(t) &:= \int_{\Omega_y} h(t,y)\,\mathrm{d}y.
\end{aligned} \tag{3.9}$$

General evolution for the expectation of observables The components of the pair $(I_{t+\Delta t}, \mathbf{V}_{t+\Delta t})$ are fully determined by system (3.3). Consequently, for any observable $\Phi : \mathcal{I} \times \Omega \to \mathbb{R}$, namely a generic test function defined on $(i, \mathbf{v}) \in \mathcal{I} \times \Omega$, the expectation

$$\langle \Phi(I_t, \mathbf{V}_t) \rangle := \sum_{i \in \mathcal{I}} \int_\Omega \Phi(i, \mathbf{v})\, f(t, i, \mathbf{v})\, \mathrm{d}\mathbf{v}, \tag{3.10}$$

satisfies

$$\begin{aligned} \langle \Phi\left(I_{t+\Delta t}, \mathbf{V}_{t+\Delta t}\right) \rangle = \langle \Phi\left(I_t, \mathbf{V}_t\right) \rangle \\ + \Delta t\, \zeta \Big(\langle r(I_t) \Phi\left(I_t', \mathbf{V}_t'\right) \rangle + \langle (1 - r(I_t)) \Phi\left(I_t'', \mathbf{V}_t'\right) \rangle - \langle \Phi\left(I_t, \mathbf{V}_t\right) \rangle \Big) \\ + o(\Delta t). \end{aligned} \tag{3.11}$$

From the above equation, rearranging terms, dividing by Δt and letting $\Delta t \to 0^+$, we formally obtain the following evolution equation:

$$\frac{\mathrm{d}}{\mathrm{d}t} \langle \Phi\left(I_t, \mathbf{V}_t\right) \rangle = \zeta \Big(\langle r(I_t) \Phi\left(I_t', \mathbf{V}_t'\right) \rangle + \langle (1 - r(I_t)) \Phi\left(I_t'', \mathbf{V}_t'\right) \rangle - \langle \Phi\left(I_t, \mathbf{V}_t\right) \rangle \Big). \tag{3.12}$$

Remark 3.1. In equation (3.12), the coefficient $r(I_t)$ represents the fraction of individuals that, upon changing compartment, do so through spontaneous transitions rather than binary interactions. Each compartment in the model is subject exclusively to one of the two mechanisms, except for the compartment of non-reproductive individuals ($i = 3$). For that, a spontaneous transition corresponds to death, whereas interaction-driven transitions represent the attainment of reproductive maturity. Therefore, $r(3)$ acquires a biological meaning: it can be interpreted as an indicator of population health: lower values suggest growth-oriented dynamics, while higher ones signal a tendency towards decline. To avoid introducing any bias at this stage of the derivation, we adopt the neutral value $r(3) = 0.5$, together with the following set of parameters:

Compartment i	**Value** $r(i)$
1	1
2	0
3	0.5
4	0
5	0

(3.13)

Equation (3.12) can be interpreted as the weak formulation of the conservation law for the distribution $f(t, i, \mathbf{v})$. To derive its explicit form, we use definitions (3.6), (3.7), (3.10), and (3.13). The expectations $\langle \cdot \rangle$ in (3.12) can be expressed in terms of sums and integrals against the probability density function f and consequently rewritten as

$$
\begin{aligned}
&\frac{\mathrm{d}}{\mathrm{d}t}\sum_{k\in\mathcal{I}}\int_\Omega \Phi(k,\mathbf{v})\, f(t,k,\mathbf{v})\mathrm{d}\mathbf{v} = \\
&\quad = \zeta \underbrace{\sum_{k\in\mathcal{I}}\int_\Omega \Phi(k,\mathbf{v}'')\left(\sum_{j\in\mathcal{I}} r(j)\int_\Omega \mathcal{P}(k,\mathbf{v}''|j,\mathbf{v}) f(t,j,\mathbf{v})\mathrm{d}\mathbf{v}\right)\mathrm{d}\mathbf{v}''}_{=:\textcircled{i}} \\
&\qquad + \zeta \underbrace{\sum_{k\in\mathcal{I}}\int_\Omega \Phi(k,\mathbf{v}'')\left(\sum_{i'\in\mathcal{I}}\sum_{j\in\mathcal{I}}(1-r(j))\int_\Omega\int_{\Omega'} \mathcal{Q}(k,\mathbf{v}''|j,\mathbf{v},i',\mathbf{v}') f(t,j,\mathbf{v}) f(t,i',\mathbf{v}')\mathrm{d}\mathbf{v}\mathrm{d}\mathbf{v}'\right)\mathrm{d}\mathbf{v}''}_{=:\textcircled{ii}} \\
&\quad . \qquad - \zeta \underbrace{\sum_{k\in\mathcal{I}}\int_\Omega \Phi(k,\mathbf{v})\, f(t,k,\mathbf{v})\mathrm{d}\mathbf{v}}_{=:\textcircled{iii}}.
\end{aligned}
\tag{3.14}
$$

Starting from equation (3.14), we now derive the weak formulation of the system of equations describing the evolution of the distributions introduced in (3.8). To this end, we define the following test function:

$$
\Phi(k,\mathbf{v}) := \begin{cases} \delta_{i,k}\,\varphi(x)\,\mathbb{1}_{\Omega_y}(y) & \text{if } i\in\{1,2\}, \\ \delta_{i,k}\,\varphi(y)\,\mathbb{1}_{\Omega_x}(x) & \text{if } i\in\{3,4,5\}, \end{cases}
\tag{3.15}
$$

where δ is the Kronecker delta, $\mathbb{1}_{\Omega_j}$ is the indicator function of the set Ω_j, and $\varphi \in C^\infty(\Omega_j)$ is a smooth test function. In the following, we carry out the calculations in detail for the first compartment, while for the remaining four, we adopt a more concise presentation, since the procedure is analogous.

Consumed nutrients ($i = 1$) The first compartment represents the consumed nutrients. Using definition (3.15) with $i = 1$, we immediately obtain:

$$
\frac{d}{dt}\sum_{k\in\mathcal{I}}\int_\Omega \Phi(k,\mathbf{v})\, f(t,k,\mathbf{v})\,\mathrm{d}\mathbf{v} = \int_{\Omega_y} \varphi(y)\,\partial_t c(t,y)\,\mathrm{d}y.
\tag{3.16}
$$

For the term ① on the right-hand side of (3.14) we first substitute (3.13) and (3.6):

$$\begin{aligned}
① &= \sum_{k\in\mathcal{I}}\int_\Omega \Phi(k,\mathbf{v}'')\Bigg(\underbrace{1}_{r(1)}\int_\Omega \mathcal{P}(k,\mathbf{v}''|1,\mathbf{v})f(t,1,\mathbf{v})\mathrm{d}\mathbf{v}\\
&\quad+\underbrace{\tfrac{1}{2}}_{r(3)}\int_\Omega \mathcal{P}(k,\mathbf{v}''|3,\mathbf{v})f(t,3,\mathbf{v})\mathrm{d}\mathbf{v}\Bigg)\mathrm{d}\mathbf{v}''\\
&= \sum_{k\in\mathcal{I}}\int_\Omega \Phi(k,\mathbf{v}'')\Bigg(\int_{\Omega_x}\left(p_1^2(x)\,\delta_{k,2}+(1-p_1^2(x))\,\delta_{k,1}\right)\delta_x(x'')\,\delta_y(y'')f(t,1,x,y)\mathrm{d}x\mathrm{d}y\\
&\quad+\tfrac{1}{2}\int_\Omega\left(p_3^5(y)\,\delta_{k,5}\,\delta_{y_0}(y'')+(1-p_3^5(y))\,\delta_{k,3}\delta_y(y'')\right)\delta_x(x'')f(t,3,x,y)\mathrm{d}\mathbf{v}\Bigg)\mathrm{d}\mathbf{v}''.
\end{aligned}\tag{3.17}$$

Now integrating, substituting (3.15) in (3.17) for $i=1$, and recalling (3.8) we get

$$① = \int_{\Omega_{x''}}\varphi(x'')\left(1-p_1^2(x'')\right)c(t,x'')\,\mathrm{d}x''. \tag{3.18}$$

For the term ② on the right-hand side of (3.14) we first substitute (3.13), (3.7), and using (3.9) we get:

$$\begin{aligned}
② = \sum_{k\in\mathcal{I}}\int_\Omega \Phi(k,\mathbf{v}'')\Bigg[&\underbrace{1}_{(1-r(2))}\Big(\int_\Omega\int_{\Omega'}\left(q_{2,3}^1(x,y')\delta_{k,1}+(1-q_{2,3}^1(x,y'))\delta_{k,2}\right)\delta_y(y'')\delta_x(x'')f(t,2,x,y)f(t,3,\mathbf{v}')\mathrm{d}\mathbf{v}\mathrm{d}\mathbf{v}'\\
&+\delta_{k,2}f(t,2,x'',y'')[1-N(t)]\Big)\\
&+\underbrace{\tfrac{1}{2}}_{(1-r(3))}\Big(\int_\Omega\int_{\Omega'}\left(q_{3,2}^4(y,x')\delta_{k,4}+(1-q_{3,2}^4(y,x'))\delta_{k,3}\right)\delta_y(y'')\delta_x(x'')f(t,3,x,y)f(t,2,\mathbf{v}')\mathrm{d}\mathbf{v}\mathrm{d}\mathbf{v}'\\
&+\delta_{k,3}f(t,3,x'',y'')[1-S(t)]\Big)\\
&+\underbrace{1}_{(1-r(4))}\Big(\int_\Omega\int_{\Omega'}\left(q_{4,5}^3(y,y')\delta_{k,3}+(1-q_{4,5}^3(y,y'))\delta_{k,4}\right)\delta_y(y'')\delta_x(x'')f(t,4,x,y)f(t,5,\mathbf{v}')\mathrm{d}\mathbf{v}\mathrm{d}\mathbf{v}'\\
&+\delta_{k,4}f(t,4,x'',y'')[1-H(t)]\Big)\\
&+\underbrace{1}_{(1-r(5))}\Big(\int_\Omega\int_{\Omega'}\left(q_{5,4}^3(y,y')\delta_{k,3}+(1-q_{5,4}^3(y,y'))\delta_{k,5}\right)\delta_y(y'')\delta_x(x'')f(t,5,x,y)f(t,4,\mathbf{v}')\mathrm{d}\mathbf{v}\mathrm{d}\mathbf{v}'\\
&+\delta_{k,5}f(t,5,x'',y'')[1-M(t)]\Big)\Bigg]\mathrm{d}v''.
\end{aligned}\tag{3.19}$$

Now integrating, substituting (3.15) in (3.19) for $i = 1$, and recalling (3.8) we get

$$\textcircled{ii} = \int_{\Omega_{x''}} \int_{\Omega_{y'}} \varphi(x'') q^1_{2,3}(x'', y') n(t, y') s(t, x'') \, \mathrm{d}y' \mathrm{d}x''. \tag{3.20}$$

Then, for term (ii) in (3.14) using definition (3.15) for $i = 1$ we easily get

$$\textcircled{iii} = \int_{\Omega_x} \varphi(x) c(t, x) \mathrm{d}x. \tag{3.21}$$

Finally, combining equations (3.16), (3.18), (3.20), and (3.21) we obtain

$$\begin{aligned} \int_{\Omega_y} \varphi(x) \, \partial_t c(t, x) \, \mathrm{d}x = {} & \zeta \int_{\Omega_x} \varphi(x) \left(1 - p^2_1(x)\right) c(t, x) \, \mathrm{d}x + \zeta \int_{\Omega_x} \int_{\Omega_y} \varphi(x) q^1_{2,3}(x, y) n(t, y) s(t, x) \, \mathrm{d}y \mathrm{d}x \\ & - \zeta \int_{\Omega_x} \varphi(x) c(t, x) \mathrm{d}x \\ = {} & \zeta \int_{\Omega_x} \varphi(x) \left(\int_{\Omega_y} q^1_{2,3}(x, y) n(t, y) \, \mathrm{d}y \; s(t, x) - p^2_1(x) c(t, x) \right) \mathrm{d}x. \end{aligned} \tag{3.22}$$

In equation (3.22), we obtained the weak formulation for the evolution of the distribution associated with compartment $i = 1$, corresponding to consumed nutrients. Proceeding in an entirely analogous way, it is possible to derive the weak formulations for the distributions associated with the other compartments. These equations are given by:

$$\begin{aligned} & \int_{\Omega_x} \varphi(x) \, \partial_t c(t, x) \, \mathrm{d}x = \zeta \int_{\Omega_x} \varphi(x) \left(\int_{\Omega_y} q^1_{2,3}(x, y) n(t, y) \, \mathrm{d}y \; s(t, x) - p^2_1(x) c(t, x) \right) \mathrm{d}x, \\ & \int_{\Omega_x} \varphi(x) \, \partial_t s(t, x) \, \mathrm{d}x = \zeta \int_{\Omega_x} \varphi(x) \left(p^2_1(x) c(t, x) - \int_{\Omega_y} q^1_{2,3}(x, y) n(t, y) \, \mathrm{d}y \; s(t, x) \right) \mathrm{d}x, \\ & \int_{\Omega_y} \varphi(y) \, \partial_t n(t, y) \, \mathrm{d}y = \zeta \int_{\Omega_y} \varphi(y) \left[2 \, q^3_{4,5}(y) m(t, y) \; H(t) - \frac{1}{2} \left(\int_{\Omega_x} q^4_{3,2}(y, x) s(t, x) \, \mathrm{d}x \; n(t, y) + p^5_3(y) n(t, y) \right) \right] \mathrm{d}y, \\ & \int_{\Omega_y} \varphi(y) \, \partial_t m(t, y) \, \mathrm{d}y = \zeta \int_{\Omega_y} \varphi(y) \left(\frac{1}{2} \int_{\Omega_x} q^4_{3,2}(y, x) s(t, x) \, \mathrm{d}x \; n(t, y) - q^3_{4,5}(y) m(t, y) \; H(t) \right) \mathrm{d}y, \\ & \int_{\Omega_y} \varphi(y) \, \partial_t h(t, y) \, \mathrm{d}y = \zeta \int_{\Omega_y} \varphi(y) \left(\delta_{y_0}(y) \int_{\Omega'} p^5_3(y') n(t, y') \mathrm{d}y' \; - H(t) \int_{\Omega^*} q^3_{4,5}(y^*) m(t, y^*) \mathrm{d}y^* \right) \mathrm{d}y. \end{aligned} \tag{3.23}$$

We set $q^3_{4,5}(y, y') \equiv q^3_{4,5}(y)$ and $q^3_{5,4}(y, y') \equiv q^3_{5,4}(y')$, further imposing $q^3_{4,5}(y) = q^3_{5,4}(y')$. These assumptions reflect the modelling choice of not endowing agents in compartment $i = 5$ with a structural variable, thereby making it natural to assume that the transition probability is independent of the specific trait of individuals in this compartment. We observe that the fifth equation of system (3.23) has a structure analogous to that presented in (1.18) for f_0. Hence, by assuming $h(0, y) = H(0)\delta_{y_0}(y)$, one obtains $h(t, y) = H(t)\delta_{y_0}(y)$ for all $t > 0$. This property is consistent with the modelling assumption that all individuals in compartment $i = 5$ share the same trait y_0.

Mass conservation By setting $\varphi(x) = 1$ in the equations of system (3.23) and integrating over the corresponding domains, one obtains a system describing the evolution of the masses associated with each compartment. Summing the five resulting equations, and using the definition (3.9), we observe that

$$\frac{d}{dt}\big(C(t) + S(t) + N(t) + M(t) + H(t)\big) = 0 \qquad \forall\, t > 0. \tag{3.24}$$

It follows that the system conserves the total mass: the overall quantity of agents and nutrients remains constant in time. Moreover, summing the first two equations of system (3.23), we obtain

$$\int_{\Omega_x} \varphi(x)\, \partial_t \big(c(t,x) + s(t,x)\big)\, \mathrm{d}x = 0. \tag{3.25}$$

This implies that there is mass preservation within the subsystem of nutrient units, as so

$$c(t,x) + s(t,x) =: \gamma(x). \tag{3.26}$$

Consequently, the first two equations of system (3.23) can be summarised into a single equation for the substrate density alone:

$$\int_{\Omega_x} \varphi(x)\, \partial_t s(t,x)\, \mathrm{d}x = \zeta \int_{\Omega_x} \varphi(x) \left[p_1^2(x)\big(\gamma(x) - s(t,x)\big) - \left(\int_{\Omega_y} q_{2,3}^1(x,y)\, n(t,y)\, \mathrm{d}y \right) s(t,x) \right] \mathrm{d}x. \tag{3.27}$$

In light of the previous observations, the system can be rewritten in a reduced form, where the overall dynamics are described by the following three evolution equations:

$$\begin{cases} \partial_t s(t,x) = & p_1^2(x)\, \gamma(x) - s(t,x) \left(p_1^2(x) + \displaystyle\int_{\Omega_y} q_{2,3}^1(x,y)\, n(t,y)\, \mathrm{d}y \right), \\ \partial_t n(t,y) = & 2\, q_{4,5}^3(y)\, m(t,y)\, H(t) - \frac{1}{2}\, n(t,y) \left(p_3^5(y) + \displaystyle\int_{\Omega_x} q_{3,2}^4(y,x)\, s(t,x)\, \mathrm{d}x \right), \\ \partial_t m(t,y) = & \frac{1}{2}\, n(t,y) \displaystyle\int_{\Omega_x} q_{3,2}^4(y,x)\, s(t,x)\, \mathrm{d}x - q_{4,5}^3(y)\, m(t,y)\, H(t), \end{cases} \tag{3.28}$$

where we have set $\zeta \equiv 1$, as it represents a scale coefficient at this level of analysis. Since the evolution of $h(t,y)$ occurs only through its aggregate mass, we omit the corresponding equation for the density while keeping $H(t)$ explicit for clarity, as this term will be simplified in the following section.

3.4 Fast reproduction limit

To proceed with the analytical study of the system (3.28), an additional assumption is required to reduce the system to only two equations. Hence, we assume that the dynamics of $m(t,y)$ evolve on a much faster time scale compared to those of $n(t,y)$ and $s(t,x)$. This reflects the idea that the reproductive process reaches equilibrium

almost instantaneously with respect to maturation and nutrient uptake. Formally, this corresponds to imposing a quasi-stationarity condition on the evolution of m, that is,

$$\partial_t m(t,y) = 0.$$

This assumption implicitly requires that the reservoir compartment is large enough so that reproduction is always possible, provided that a sufficient amount of resources is available. Under this assumption, the third equation of (3.28) reduces to

$$0 = \tfrac{1}{2}\, n(t,y) \int_{\Omega_x} q^4_{3,2}(y,x)\, s(t,x)\, \mathrm{d}x - q^3_{4,5}(y)\, m(t,y)\, H(t),$$

which gives

$$m(t,y) = \frac{n(t,y) \int_{\Omega_x} q^4_{3,2}(y,x)\, s(t,x)\, \mathrm{d}x}{2\, q^3_{4,5}(y)\, H(t)}.$$

Substituting this expression into the second equation of system (3.28), we obtain the following for $n(t,y)$:

$$\partial_t n(t,y) = \left(\tfrac{3}{2} \int_{\Omega} q^4_{3,2}(y,x) s(t,x)\, \mathrm{d}x - p^5_3(y) \right) n(t,y).$$

Therefore, the resulting reduced system reads:

$$\begin{cases} \partial_t s(t,x) = & p^2_1(x)\, \gamma(x) - s(t,x) \left(p^2_1(x) + \displaystyle\int_{\Omega_y} q^1_{2,3}(x,y)\, n(t,y)\, \mathrm{d}y \right), \\ \partial_t n(t,y) & = \left(\tfrac{1}{2} \displaystyle\int_{\Omega} q^4_{3,2}(y,x) s(t,x)\, \mathrm{d}x - p^5_3(y) \right) n(t,y). \end{cases} \tag{3.29}$$

We note that the system derived above retains notation tied to the original five-compartment microscopic model. In particular, rate functions such as $p^2_1(x)$, $q^1_{2,3}(x,y)$, $q^4_{3,2}(y,x)$, and $p^5_3(y)$ reflect compartment indices, which are no longer explicit in the reduced system. To improve clarity and align terminology with biological meaning, we introduce a new notation for the rate functions in Table 3.1.

With this new notation, the system 3.29 can be written as:

$$\begin{cases} \partial_t s(t,x) & = \alpha(x)\gamma(x) - \Lambda(x, \mathcal{N}_\eta) s(t,x), \\ \partial_t n(t,y) & = R(y, \mathcal{S}_\beta)\, n(t,y), \end{cases} \tag{3.30}$$

where

$$\begin{aligned} \Lambda(x, \mathcal{N}_\eta) &= \alpha(x) + \mathcal{N}_\eta(t,x) \qquad & \mathcal{N}_\eta(t,x) &:= \int_{\Omega_y} \eta(x,y)\, n(t,y)\, \mathrm{d}y, \\ R(y, \mathcal{S}_\beta) &= \mathcal{S}_\beta(t,y) - \kappa(y) \qquad & \mathcal{S}_\beta(t,y) &:= \int_{\Omega_x} \beta(x,y)\, s(t,x)\, \mathrm{d}x. \end{aligned} \tag{3.31}$$

The system is complemented by the initial conditions $s(0,x) = s^0(x)$ and $n(0,y) = n^0(y)$.

TABLE 3.1: Correspondence between original and updated notation for rate functions.

Old notation	New notation	Biological interpretation
$p_1^2(x)$	$\alpha(x)$	Regeneration rate of nutrients
$q_{2,3}^1(x,y)$	$\eta(x,y)$	Uptake rate of nutrients by individuals
$p_3^5(y)$	$\kappa(y)$	Mortality rate of individuals
$\frac{1}{2}q_{3,2}^4(y,x)$	$\beta(x,y)$	Reproduction rate via nutrient intake

3.4.1 Well-posedness

We now establish the existence of solutions to system (3.30)- 3.31. At this stage, we may still consider a bounded $\Omega \subset \mathbb{R}^2$; however, for the asymptotic analysis, it is preferable to assume that the domain is compact. The key ingredients, reported below, are suitable assumptions on the regularity and positivity of the coefficients, as well as L^1–L^∞ bounds on the initial data.

Hypothesis 1. Let the rate functions and initial data satisfy:

(H1) $\alpha \in W^{1,\infty}(\Omega_x)$ and $\alpha(x) \geq \underline{\alpha} > 0 \; \forall\, x \in \Omega_x$, $\kappa \in W^{1,\infty}(\Omega_y)$ and $\kappa(y) \geq \underline{\kappa} > 0$ $\forall\, y \in \Omega_y$;

(H2) $\gamma \in L^\infty(\Omega_x)$, with $\gamma(x)$ nonnegative;

(H3) η, $\beta \in W^{1,\infty}(\Omega_x \times \Omega_y)$ and strictly positive;

(H4) $\eta = \chi\beta$, where $\chi > 1$, $\chi \in \mathbb{N}$, represents the number of nutrient units required for the proliferation of one individual;

(H5) $s^0 \in C(\Omega_x)$ nonnegative and $n^0 \in C(\Omega_y)$ with $n^0(y) > 0$ for all $y \in \Omega_y$.

Theorem 3.1 (Well-posedness)**.** *Let all the above hypotheses hold, then the Cauchy problem* (3.30)-(3.31) *admits a unique nonnegative solution* (s,n) *with* $s \in C(\mathbb{R}_+, L^1(\Omega_x))$ *and* $n \in C(\mathbb{R}_+, L^1(\Omega_y))$*. Moreover, there exists* $\overline{M} > 0$ *such that*

$$||n(t,\cdot)||_{L^1(\Omega)} + ||s(t,\cdot)||_{L^1(\Omega)} \leq \overline{M} \quad \forall t > 0. \tag{3.32}$$

Proof. **Notation.** Let us recall the notation $\mathbf{v} = (x, y) \in \Omega_x \times \Omega_y =: \Omega$ and $z = (s, n)$, and consider the Banach spaces

$$(P, ||\cdot||_P), \quad P := \left\{ z = (s, n) : s \in L^1(\Omega_x),\ n \in L^1(\Omega_y) \right\},$$

$$||z(t,\cdot)||_P = ||s(t,\cdot)||_{L^1} + ||n(t,\cdot)||_{L^1},$$

$$(B, ||\cdot||), \quad B := C([0,T], P), ||z||_B = \sup_{t\in[0,T]} ||z(t,\cdot)||_P,$$

where $T \in \mathbb{R}_+$. Now, we consider

$$F_s[z](t,x) = \gamma(x)\alpha(x) - s(t,x)\left(\alpha(x) + \int_\Omega \eta(x,y)n(t,y)\mathrm{d}y\right),$$

$$F_n[z](t,y) = \left(\int_\Omega \beta(x,y)s(t,x)\mathrm{d}x - \kappa(y)\right) n(t,y).$$

Therefore, we can write

$$\begin{cases} \partial_t z(t,\mathbf{v}) = F[z](t,\mathbf{v}), \\ z(\mathbf{v},0) = z^0(\mathbf{v}) := (s^0, n^0), \end{cases} \qquad (t,\mathbf{v}) \in [0,T]\times\Omega, \tag{3.33}$$

where $F[z](t,\mathbf{v}) = (F_s[z](t,x), F_n[z](t,y))$. We also note that

$$z(t,\mathbf{v}) = G[z](t,\mathbf{v}), \quad \text{with} \quad G[z](t,\mathbf{v}) = z(0,\mathbf{v}) + \int_0^t F[z](s,\mathbf{v})\mathrm{d}s. \tag{3.34}$$

Local well posedness. Let all the previous hypotheses hold. Then, for any $z, \mu \in B$ with $z(0,\mathbf{v}) = \mu(0,\mathbf{v}) = z^0(\mathbf{v})$, the operator G satisfies the following estimates

$$\begin{aligned} ||G[z]||_B \le T\Big[& 2\Big(\max\{||\kappa||_{L^\infty}, ||\alpha||_{L^\infty}\} + \max\{||\eta||_{L^\infty}, ||\beta||_{L^\infty}\}||z||_B\Big)||z||_B \\ & + ||\gamma||_{L^1}||\alpha||_{L^\infty}\Big] + ||z^0||_P, \end{aligned} \tag{3.35}$$

$$\begin{aligned} \|G[z] - G[\mu]\|_B \le 2T\Big(& \max\left\{\|\kappa\|_{L^\infty}, \|\alpha\|_{L^\infty}\right\} \\ & + \max\left\{\|\eta\|_{L^\infty}, \|\beta\|_{L^\infty}\right\}\left(\|z\|_B + \|\mu\|_B\right)\Big)\|z-\mu\|_B. \end{aligned} \tag{3.36}$$

We note that the second estimate (3.36) is a consequence of the estimate (3.35). Therefore, we provide the proof of (3.35). Considering hypothesis 1 we derive

$$||F_s[z](t,x)||_{L^1} \le ||\gamma||_{L^1}||\alpha||_{L^\infty} + ||\alpha||_{L^\infty}||s(t,\cdot)||_{L^1} + ||\eta||_{L^\infty}||s(t,\cdot)||_{L^1}||n(t,\cdot)||_{L^1},$$

$$||F_n[z](t,y)||_{L^1} \leq ||\kappa||_{L^\infty}||n(t,\cdot)||_{L^1} + ||\beta||_{L^\infty}||s(t,\cdot)||_{L^1}||n(t,\cdot)||_{L^1}.$$

Hence,

$$\begin{aligned}\|F[z]\|_P &= \|F_s[z](t,x)\|_{L^1} + \|F_n[z](t,y)\|_{L^1} \\ &\leq \Bigg[\|\gamma\|_{L^\infty}\|\alpha\|_{L^1} + 2\Big(\max\{\|\kappa\|_{L^\infty}, \|\alpha\|_{L^\infty}\} \\ &\quad + \max\{\|\eta\|_{L^\infty}, \|\beta\|_{L^\infty}\}\,\|z\|_P\Big)\|z\|_P\Bigg].\end{aligned} \tag{3.37}$$

Now, recalling G defined in (3.34) we have

$$||G[z]||_P \leq ||z^0||_P + \int_0^t ||F[z]||_P \mathrm{d}s,$$

which combined with (3.37) gives us (3.35) and guarantees that G maps B into itself. Moreover, thanks to (3.36) there exists a $T^* > 0$ such that G is a contraction on B. Consequently, the Banach–Caccioppoli fixed-point theorem implies that, for any $T < T^*$, the operator $G : B \to B$ admits a unique fixed point $z \in B$. Therefore, the Cauchy problem (3.33) admits a unique solution with components $s \in C([0,T], L^1(\Omega_x))$ and $n \in C([0,T], L^1(\Omega_y))$.

Non-negativity of s and n Solving the IDE (3.30) for $s(t,x)$ subject to the initial condition a_0 yields the semi-explicit formula

$$s(t,x) = s^0(x)\, e^{-\int_0^t \Lambda(x,\mathcal{N}_\eta(\theta))\,\mathrm{d}\theta} + \alpha(x)\gamma(x)\int_0^t e^{-\int_\sigma^t \Lambda(x,\mathcal{N}_\eta(\tau))\,\mathrm{d}\tau}\,\mathrm{d}\sigma. \tag{3.38}$$

Since the functions $\alpha(x)$ and $\gamma(x)$ are positive and $s^0(x)$ is nonnegative, the above formula implies that s is nonnegative. On the other hand, the semi-explicit solution of (3.30) for $n(t,y)$ given the initial condition $n^0(y)$ is

$$n(t,y) = n^0(y) e^{\int_0^t R(y,\mathcal{S}_\beta(\theta))\mathrm{d}\theta}, \tag{3.39}$$

from which we conclude that n is nonnegative due to the fact that the function $n^0(y)$ is nonnegative.

Uniform bound on $||z(t,\cdot)||_P$ and on $||z||_B$ First, we integrate and sum the two equations of (3.30) and we get

$$\begin{aligned}\frac{\mathrm{d}}{\mathrm{d}t}\left(\int_{\Omega_x} s(t,x)\,\mathrm{d}x + \int_{\Omega_y} n(t,y)\,\mathrm{d}y\right) &= \int_{\Omega_x} \alpha(x)\gamma(x)\,\mathrm{d}x \\ &- \int_{\Omega_x} \alpha(x)s(t,x)\,\mathrm{d}x - \int_{\Omega_y} \kappa(y)n(t,y)\,\mathrm{d}y \\ &+ \int_{\Omega} \beta(x,y)(1/\chi - 1)n(t,y)s(t,x)\,\mathrm{d}y\,\mathrm{d}x.\end{aligned} \tag{3.40}$$

Now, we note that, since the number of nutrient units needed for proliferation is greater than 1 ($\chi > 1$), the last right-hand side term is negative. Hence, we have

$$A(t) + N(t) \leq \max\left\{A(0) + N(0), \frac{\overline{\alpha}}{\min\{\underline{\alpha}, \underline{\kappa}\}}\int_{\Omega_x}\gamma(x)\mathrm{d}x\right\} := \overline{M}. \tag{3.41}$$

Therefore, given the positivity of the solutions s and n, we have

$$||z(t,\cdot)||_P \leq \overline{M}, \tag{3.42}$$

and the bound is uniform in time, so we also have $||z||_B \leq \overline{M}$. The uniform bound (3.42) guarantees that we can iterate the process performed locally in the first part of the proof on new time intervals of the form $[iT, (i+1)T]$ with $i \in \mathbb{N}$ and therefore, conclude our proof. □

Corollary 3.2. *Under the hypotheses of Theorem 3.1, assume in addition that*

$$0 \leq s^0(x) \leq \gamma(x) \qquad \text{for a.e. } x \in \Omega_x. \tag{3.43}$$

Then, for every $t \geq 0$, it holds

$$0 \leq s(t,x) \leq \gamma(x) \qquad \text{for a.e. } x \in \Omega_x.$$

Proof. From the first equation of system (3.30),

$$\partial_t s(t,x) = \alpha(x)\gamma(x) - s(t,x)\Big(\alpha(x) + \int_{\Omega_y}\eta(x,y)\,n(t,y)\,\mathrm{d}y\Big).$$

Since $n(t,y) \geq 0$ and $\eta(x,y) \geq 0$, we have

$$\partial_t s(t,x) \leq \alpha(x)\gamma(x) - \alpha(x)s(t,x) = \alpha(x)\big(\gamma(x) - s(t,x)\big),$$

which can be rewritten as

$$\partial_t\big(e^{\alpha(x)t}s(t,x)\big) \leq \alpha(x)\gamma(x)e^{\alpha(x)t}.$$

Integrating in time and dividing by $e^{\alpha(x)t}$, we obtain the explicit upper bound

$$s(t,x) \leq \gamma(x) + \big(s^0(x) - \gamma(x)\big)e^{-\alpha(x)t}.$$

Since $s^0(x) \leq \gamma(x)$, the right–hand side is bounded above by $\gamma(x)$. □

The dynamics presented in (3.30) entail a form of indirect competition within the consumer population. Indeed, examining the fitness term $R(y, \mathcal{S}_\beta)$, it becomes clear that it depends on n neither locally nor through any integral functional.
In [122], a model analogous to the one proposed here, motivated by specific biological systems, such as those arising in phytoplankton ecology [131], was analysed. There, an appropriate rescaling of the variables allows the system to be reformulated as a direct-competition model. It is therefore reasonable to expect that, even within the structure considered in this work, a formally indirect mechanism may still exhibit emergent behaviour typical of direct competitive dynamics. In the following section, we show that convergence results consistent with this intuition naturally emerge in the asymptotic regime of the system, without the need to introduce any formal transformation of the model.

3.4.2 Asymptotic results

The well-posedness result allows us to investigate the asymptotic behaviour through a suitable time rescaling. In fact, based on previous studies on the long-term behaviour of a continuously structured population model [59, 62, 66, 108], we introduce a small parameter $\varepsilon > 0$ and use the time scaling $t \to \frac{t}{\varepsilon}$, thus, considering the asymptotic regime $\varepsilon \to 0$ amounts to studying the behaviour of solutions to the IDEs of the model on long time scales. With this scaling, the system (3.30) reads as

$$\begin{cases} \varepsilon \partial_t s_\varepsilon(t,x) &= \alpha(x)\gamma(x) - \Lambda_\varepsilon(x, \mathcal{N}_\eta^\varepsilon) s_\varepsilon(t,x), \\ \varepsilon \partial_t n_\varepsilon(t,y) &= R_\varepsilon(y, \mathcal{S}_\beta^\varepsilon)\, n_\varepsilon(t,y), \\ s_\varepsilon(0,x) = s^0(x) \quad & n_\varepsilon(0,y) = n^0(y), \end{cases} \tag{3.44}$$

where

$$\begin{aligned} \Lambda_\varepsilon(x, \mathcal{N}_\eta^\varepsilon(t,x)) &= \alpha(x) + \mathcal{N}_\eta^\varepsilon(t,x) \qquad \mathcal{N}_\eta^\varepsilon(t,x) := \int_{\Omega_y} \eta(x,y)\, n_\varepsilon(t,y)\, \mathrm{d}y, \\ R_\varepsilon(y, \mathcal{S}_\beta^\varepsilon(t,y)) &= \mathcal{S}_\beta^\varepsilon(t,y) - \kappa(y) \qquad \mathcal{S}_\beta^\varepsilon(t,y) := \int_{\Omega_x} \beta(x,y)\, s_\varepsilon(t,x) \mathrm{d}x. \end{aligned} \tag{3.45}$$

Well-posedness and existence for the Cauchy problem (3.44)–(3.45) with fixed $\varepsilon > 0$ follow directly from Theorem 3.1. Therefore, no further elaboration is required. In particular, estimate (3.42) provides the key tool for the following compactness result.

Proposition 3.3. *Under assumption (H1)-(H5), the solutions to the Cauchy problem* (3.44)–(3.45) *satisfy, up to extraction of subsequences,*

$$z_\varepsilon = (s_\varepsilon, n_\varepsilon) \overset{*}{\underset{\varepsilon\to 0}{\rightharpoonup}} (s,n) =: z \quad in \quad E', \tag{3.46}$$

where

$$E' = L^\infty([0,T];\, \mathcal{M}(\Omega_x \times \Omega_y)). \tag{3.47}$$

Let us define operators

$$I_{\varepsilon,\Lambda}(t,x) := \int_0^t \Lambda_\varepsilon(x, \mathcal{N}_\eta^\varepsilon(\tau,x))\mathrm{d}\tau, \qquad I_{\varepsilon,R}(t,y) := \int_0^t R_\varepsilon(y, \mathcal{S}_\beta^\varepsilon(\tau,y))\mathrm{d}\tau. \tag{3.48}$$

Then, we have

$$\begin{aligned} I_{\varepsilon,\Lambda} &\underset{\varepsilon\to 0}{\longrightarrow} I_\Lambda \quad \textit{uniformly in} \quad [0,T]\times\Omega_x, \\ I_{\varepsilon,R} &\underset{\varepsilon\to 0}{\longrightarrow} I_R \quad \textit{uniformly in} \quad [0,T]\times\Omega_y, \end{aligned} \tag{3.49}$$

where

$$I_\Lambda(t,x) := \int_0^t \Lambda(x,\tau)\mathrm{d}\tau, \qquad I_R(t,y) := \int_0^t R(y,\tau)\mathrm{d}\tau. \tag{3.50}$$

and

$$\begin{aligned} \Lambda(x, \mathcal{N}_\eta(\tau,x)) &:= \alpha(x) + \mathcal{N}_\eta(\tau,x) \qquad \mathcal{N}_\eta(\tau,x) := \int_{\Omega_y} \eta(x,y)\, n(\tau,y)\, \mathrm{d}y, \\ R(y, \mathcal{S}_\beta(\tau,y)) &:= \mathcal{S}_\beta(\tau,y) - \kappa(y) \qquad \mathcal{S}_\beta(\tau,y) := \int_{\Omega_x} \beta(x,y)\, s(\tau,x)\, \mathrm{d}x. \end{aligned} \tag{3.51}$$

Proof. First, we write the equivalent of the inequality (3.40) for system (3.44), which reads

$$\frac{\mathrm{d}}{\mathrm{d}t}\Big(\|s_\varepsilon(t,\cdot)\|_{L^1} + \|n_\varepsilon(t,\cdot)\|_{L^1}\Big) \le \frac{1}{\varepsilon}\Big(\overline{\alpha}\,\|\gamma\|_{L^1} - \min\{\underline{\alpha},\underline{\kappa}\}\,(\|s_\varepsilon(t,\cdot)\|_{L^1} + \|n_\varepsilon(t,\cdot)\|_{L^1})\Big). \tag{3.52}$$

As a consequence, we deduce that

$$\|s_\varepsilon(t,\cdot)\|_{L^1} + \|n_\varepsilon(t,\cdot)\|_{L^1} \le \max\left\{\frac{\overline{\alpha}\,\|\gamma\|_{L^1}}{\min\{\underline{\alpha},\underline{\kappa}\}}, \|s^0\|_{L^1} + \|n^0\|_{L^1}\right\}. \tag{3.53}$$

Therefore, (3.42) also holds for system (3.44) independently of ε, and it allows us to use the Banach-Alaoglu theorem to conclude that, up to extraction of subsequences,

the asymptotic result (3.46) is verified. Moreover, these results guarantee

$$\begin{aligned} \Lambda_\varepsilon(x, \mathcal{N}_\eta^\varepsilon) \to \Lambda(x, \mathcal{N}_\eta) &:= \alpha(x) + \int_{\Omega_y} \eta(x,y)\, n(t,y)\, \mathrm{d}y \quad \varepsilon \to 0, \\ R_\varepsilon(y, \mathcal{S}_\beta^\varepsilon) \to R(y, \mathcal{S}_\beta) &:= \int_{\Omega_x} \beta(x,y)\, s(t,x)\, \mathrm{d}x - \kappa(y) \quad \varepsilon \to 0, \end{aligned} \tag{3.54}$$

since β, $\eta \in C(\Omega_x \times \Omega_y)$. Therefore, thanks to (3.54) and (3.42), there exist subsequences of (3.48), that we still denote as $I_{\varepsilon,\Lambda}$, $I_{\varepsilon,R}$, such that

$$\begin{aligned} &\text{for all} \quad (t,x) \in [0,+\infty) \times \Omega_x \quad I_{\varepsilon,\Lambda}(t,x) \underset{\varepsilon\to 0}{\longrightarrow} I_\Lambda(t,x), \\ &\text{for all} \quad (t,y) \in [0,+\infty) \times \Omega_y \quad I_{\varepsilon,R}(t,y) \underset{\varepsilon\to 0}{\longrightarrow} I_R(t,y), \end{aligned} \tag{3.55}$$

Moreover, the hypotheses on α and κ in (H1)-(H5) ensure that, for any $\varepsilon > 0$, the functions $I_{\varepsilon,\Lambda}$, $I_{\varepsilon,R}$ and their first derivatives with respect to t and x or y are bounded in $L^\infty((0,T) \times \Omega_x)$ and $L^\infty((0,T) \times \Omega_y)$ respectively. Hence, since $W^{1,\infty}((0,T) \times \Omega)$ is compactly embedded in $C([0,T] \times \Omega)$, we conclude that

$$I_{\varepsilon,\Lambda}(t,x) \underset{\varepsilon\to 0}{\longrightarrow} I_\Lambda(t,x) \qquad \text{and} \qquad I_{\varepsilon,R}(t,y) \underset{\varepsilon\to 0}{\longrightarrow} I_R(t,y), \tag{3.56}$$

uniformly in $[0,T] \times \Omega_x$ and $[0,T] \times \Omega_y$ respectively.

□

Remark 3.4. The convergence in Proposition 3.3 is understood in the weak-* topology of

$$E' = L^\infty([0,T]; \mathcal{M}(\Omega_x \times \Omega_y)),$$

with pre-dual

$$E = L^1([0,T]; C(\Omega_x \times \Omega_y)).$$

Explicitly,

$$z_\varepsilon \rightharpoonup^* z \quad \Longleftrightarrow \quad \int_0^T \langle \varphi(t), z_\varepsilon(t) \rangle \, \mathrm{d}t \to \int_0^T \langle \varphi(t), z(t) \rangle \, \mathrm{d}t \quad \forall\, \varphi \in L^1([0,T]; C(\Omega_x \times \Omega_y)).$$

This identification relies on the compactness (or local compactness) of the spatial domains $\Omega_x, \Omega_y \subset \mathbb{R}^d$, which ensures that $(C_0(\Omega))' = \mathcal{M}(\Omega)$, the space of finite Radon measures. For simplicity, we take Ω compact, so that $(C(\Omega))' = \mathcal{M}(\Omega)$. In this framework, functions in $L^1(\Omega)$ correspond to absolutely continuous measures in $\mathcal{M}(\Omega)$, and the family $\{z_\varepsilon\}_\varepsilon$, originally bounded in $L^1(\Omega)$, can equivalently be viewed as taking values in $\mathcal{M}(\Omega)$. This justifies working in the Bochner space $L^\infty([0,T]; \mathcal{M}(\Omega))$, where compactness and weak-* convergence of subsequences follow from the Banach-Alaoglu theorem.

The previous convergence result ensures the existence of limiting quantities (s, n) satisfying weak convergence (3.46), and we want to characterize this limit. First, we report the following Lemma:

Lemma 3.5 (Saturation of nutrients)**.** *Let the assumptions of Theorem 3.1 hold, and suppose that for some interval $(t_1, t_2) \subset (0, T)$ and for some $\sigma > 0$ we have*

$$\int_{t_1}^{t_2} \int_{\Omega_y} n_\varepsilon(t, y) \mathrm{d}y \mathrm{d}t = O\left(e^{-\sigma/\varepsilon}\right) \quad \text{as } \varepsilon \to 0. \tag{3.57}$$

Then, for a.e. $t \in (t_1, t_2)$, the limiting nutrient density $s(t, x)$ obtained in (3.46) *attains the maximal level $\gamma(x)$, that is,*

$$s(t, x) = \gamma(x) \quad \text{a.e. on } \Omega_x \quad \text{and for a.e. } t \in (t_1, t_2). \tag{3.58}$$

Proof. We note that since $\eta \in L^\infty(\Omega_x \times \Omega_y)$ for every $(\tau_0, t) \subset (t_1, t_2)$ and for every $x \in \Omega_x$

$$\begin{aligned} \int_{\tau_0}^{t} \mathcal{N}_\eta^\varepsilon(\tau, x) \mathrm{d}\tau &= \int_{\tau_0}^{t} \int_{\Omega_y} \eta(x, y) n_\varepsilon(\tau, y) \mathrm{d}y \mathrm{d}\tau \\ &\leq \|\eta\|_{L^\infty} \int_{t_1}^{t_2} \int_{\Omega_y} n(\tau, y) \mathrm{d}\tau \leq C e^{-\sigma/\varepsilon}, \end{aligned} \tag{3.59}$$

for some $C > 0$. Hence, for all $t \in (t_1, t_2)$ we can choose $\tau_0 \in (t_1, t)$ such that

$$I_{\varepsilon,\Lambda}(t, x) - I_{\varepsilon,\Lambda}(\tau_0, x) = \int_{\tau_0}^{t} \Lambda_\varepsilon(x, \mathcal{N}_\eta^\varepsilon) \mathrm{d}\tau = \alpha(x)(t - \tau_0) + r_\varepsilon(\tau_0, t, x), \tag{3.60}$$

with $r_\varepsilon \leq C(t - \tau_0) e^{-\sigma/\varepsilon}$.
To prove the limit (3.58) we study the semi-explicit formula

$$s_\varepsilon(t, x) = s^0(x) e^{-I_{\varepsilon,\Lambda}(t,x)/\varepsilon} + \frac{\alpha(x)\gamma(x)}{\varepsilon} \int_0^t \exp\Big(-\tfrac{1}{\varepsilon}\big(I_{\varepsilon,\Lambda}(t, x) - I_{\varepsilon,\Lambda}(\tau, x)\big)\Big) d\tau.$$

First, we use the fact that $\Lambda_\varepsilon \geq \alpha(x)$ and obtain

$$s^0(x) e^{-I_{\varepsilon,\Lambda}(t,x)/\varepsilon} \leq s^0(x) e^{-\alpha(x)t/\varepsilon} \xrightarrow{\varepsilon \to 0} 0.$$

To evaluate the second term on the right-hand side, we take $\tau_0 \in (t_1, t)$ and split the interval $[0, t]$ into $[0, \tau_0] \cup (\tau_0, t]$. For $\tau \in [0, \tau_0]$, we have

$$\frac{\alpha(x)\gamma(x)}{\varepsilon} \int_0^{\tau_0} \exp\Big(-\tfrac{1}{\varepsilon}\big(I_{\varepsilon,\Lambda}(t, x) - I_{\varepsilon,\Lambda}(\tau, x)\big)\Big) \mathrm{d}\tau \leq \gamma(x) e^{-\alpha(x)(t-\tau_0)/\varepsilon} \xrightarrow{\varepsilon \to 0} 0.$$

Finally, for $\tau \in [\tau_0, t]$, we use the estimate (3.60) to write

$$\exp\Big(-\tfrac{1}{\varepsilon}\big(I_{\varepsilon,\Lambda}(t, x) - I_{\varepsilon,\Lambda}(\tau, x)\big)\Big) = e^{-\alpha(x)(t-\tau)/\varepsilon - r_\varepsilon/\varepsilon}.$$

Hence

$$\lim_{\varepsilon\to 0}\frac{\alpha(x)\gamma(x)}{\varepsilon}\int_{\tau_0}^{t}\exp\Big(-\tfrac{1}{\varepsilon}\big(I_{\varepsilon,\Lambda}(t,x)-I_{\varepsilon,\Lambda}(\tau,x)\big)\Big)\mathrm{d}\tau =$$

$$\lim_{\varepsilon\to 0}\gamma(x)e^{-r_\varepsilon/\varepsilon}\big(1-e^{-\alpha(x)(t-\tau_0)/\varepsilon}\big)=\gamma(x).$$

Therefore, for a.e. $t\in(t_1,t_2)$ we have $s_\varepsilon(t,x)\to\gamma(x)$ and, thanks to the uniqueness of the limit (3.46), it also holds that $s(t,\cdot)=\gamma(\cdot)$ a.e. on. Ω_x. □

Now, let us define the function

$$g(y)=\int_{\Omega_x}\beta(x,y)\gamma(x)\mathrm{d}x-\kappa(y)\quad\forall\, y\in\Omega_y, \tag{3.61}$$

and introduce the sets:

$$\mathcal{O}\coloneqq\Big\{y\in\Omega_y\,\Big|\,g(y)>0\Big\}, \tag{3.62a}$$

$$\overline{\mathcal{O}}\coloneqq\Big\{y\in\Omega_y\,\Big|\,g(y)\geq 0\Big\}, \tag{3.62b}$$

$$\mathcal{A}(t)\coloneqq\operatorname*{argmax}_{y\in\Omega_y} I_R(t,y), \tag{3.62c}$$

for which the following holds:

Corollary 3.6. *As long as all the hypotheses of Theorem 3.1 and of Corollary 3.2 hold, if there exists* $\hat{t}\in[0,T]$ *such that* $\max\limits_{y\in\Omega_y} I_R(\hat{t},y)\geq 0$ *then*

$$\mathcal{A}(\hat{t})\subset\overline{\mathcal{O}}. \tag{3.63}$$

Proof. First we note that Corollary 3.2 is verified also for s_ε, i.e. $0\leq s_\varepsilon\leq\gamma$ a.e., therefore

$$s_\varepsilon(t,x)\overset{*}{\underset{\varepsilon\to 0}{\rightharpoonup}} s(t,x)\leq\gamma(x)\qquad\text{a.e. in}\quad[0,T]\times\Omega_x.$$

then $\forall\, y\in\mathcal{A}(\hat{t})$ we have

$$0\leq I_R(\hat{t},y)\leq\hat{t}g(y), \tag{3.64}$$

which proves (3.63). □

We can now provide a first characterization of the limiting behaviour of the solutions to system (3.44)–(3.45) as $\varepsilon\to 0$.

Lemma 3.7 (Asymptotic behaviour of $n(t,y)$)**.** *Let the assumptions of Proposition 3.3 and assumption* (3.43) *hold. Then*

- *(**Survival**) if $\mathcal{O} \neq \emptyset$ the limit function $I_R(t,y)$ defined in* (3.51) *is such that*

$$\begin{aligned} \max_{y\in\Omega_y} I_R(t,y) = 0 \quad \textit{for any} \quad t \in [0,T], \\ N(t) > 0, \quad \operatorname{supp} n(t,\cdot) = \mathcal{A}(t), \quad \textit{for a.e. } t \in [0,T]; \end{aligned} \tag{3.65}$$

- *(**Extinction**) if $\mathcal{O} = \emptyset$ we have two possible scenarios:*
  1. *(Fast extinction) if $\overline{\mathcal{O}} = \emptyset$ the limit function $I_R(t,y)$ defined in* (3.51) *is such that*

$$\begin{aligned} &\max_{y\in\Omega_y} I_R(t,y) < 0 \quad \forall\, t \in [0,T] \quad \textit{and for some } c > 0, \\ &\int_{\Omega_y} n_\varepsilon(t,y)\mathrm{d}y = O(e^{-c/\varepsilon}) \quad \textit{as } \varepsilon \to 0 \quad \textit{a.e. on } [0,T]; \end{aligned} \tag{3.66}$$

  2. *(Slow extinction) if $\overline{\mathcal{O}} \neq \emptyset$ the limit function $I_R(t,y)$ defined in* (3.51) *is such that*

$$\begin{aligned} &\max_{y\in\Omega_y} I_R(t,y) = 0 \quad \forall\, t \in [0,T], \quad \textit{and} \\ &\int_{\Omega_y} n_\varepsilon(t,y)\mathrm{d}y = o(\varepsilon) \quad \textit{as } \varepsilon \to 0 \quad \textit{a.e. on } [0,T]. \end{aligned} \tag{3.67}$$

In both cases

$$s_\varepsilon(t,x) \underset{\varepsilon\to 0}{\overset{*}{\rightharpoonup}} \gamma(x) \quad \textit{for a.e. } (t,x) \in [0,T]\times\Omega_x. \tag{3.68}$$

Proof. Step 1.
We first prove that

$$I_R(t,y) \leq 0 \quad \text{for all} \quad (t,y) \in (0,T)\times\Omega_y. \tag{3.69}$$

From the rescaled system (3.44) we have

$$\varepsilon\partial_t n_\varepsilon(t,y) = R_\varepsilon(y,\mathcal{S}^\varepsilon_\beta) n_\varepsilon(t,y),$$

which yields, for any $t > 0$,

$$n_\varepsilon(t,y) = n_\varepsilon(0,y)\exp\left(\frac{1}{\varepsilon}\int_0^t R_\varepsilon(y,\mathcal{S}^\varepsilon_\beta(\tau),y)\,\mathrm{d}\tau\right) = n^0(y)\exp\left(\frac{1}{\varepsilon} I_{\varepsilon,R}(t,y)\right). \tag{3.70}$$

By contradiction, assume that there exists $(\hat{t}, \hat{y}) \in [0, T] \times \Omega_y$ such that $I_R(\hat{t}, \hat{y}) > 0$ and the uniform convergence (3.49) guarantees that there exists $\sigma > 0$ such that

$$I_{\varepsilon,R}(t, y) \geq \sigma,$$

whenever $|t - \hat{t}| \leq \sigma$, $|y - \hat{y}| \leq \sigma$, and $0 < \varepsilon \leq \sigma$. Hence, for every $t \in [\hat{t} - \sigma, \hat{t} + \sigma]$,

$$\int_{\Omega_y} n_\varepsilon(t, y)\, \mathrm{d}y \;\geq\; e^{\sigma/\varepsilon} \int_{\hat{y}-\sigma}^{\hat{y}+\sigma} n^0(y)\, \mathrm{d}y \;\underset{\varepsilon \to 0}{\longrightarrow}\; \infty,$$

where we have used (3.70) and the fact that $n^0(y) > 0$. This contradicts the result of uniform boundedness (3.53). Consequently, we conclude that

$$I_R(t, y) \leq 0 \qquad \forall (t, y) \in [0, T] \times \Omega_y. \tag{3.71}$$

Step 2.
We now show that if there exists $\hat{t} \in [0, T]$

$$I_R(\hat{t}, \cdot) < 0 \quad \text{on } \Omega_y, \tag{3.72a}$$

then

$$\int_{\hat{t}-\sigma}^{\hat{t}+\sigma} \int_{\Omega_y} n_\varepsilon(t, y)\, \mathrm{d}y\, \mathrm{d}t = O\left(e^{-\sigma/\varepsilon}\right) \quad \text{for } \varepsilon \to 0, \tag{3.72b}$$

$$\text{and} \quad n(\hat{t}, \cdot) = 0 \quad \text{a.e. on} \quad \Omega_y, \tag{3.72c}$$

for some $\sigma > 0$. Let $\hat{t} \in [0, T]$ be such that $I_R(\hat{t}, \cdot) < 0$. The uniform convergence result (3.49) ensures the existence of $\sigma > 0$ such that

$$I_R(t, \cdot) \leq -\sigma \qquad \text{for } |t - \hat{t}| \leq \sigma, \quad \text{on} \quad \Omega_y,$$

with $\sigma \geq \varepsilon > 0$. It follows that

$$\begin{aligned} \lim_{\varepsilon \to 0} \int_{\hat{t}-\sigma}^{\hat{t}+\sigma} \int_{\Omega_y} n_\varepsilon(t, y)\, \mathrm{d}y\, \mathrm{d}t &= \lim_{\varepsilon \to 0} \int_{\hat{t}-\sigma}^{\hat{t}+\sigma} \int_{\Omega_y} n^0(y)\, e^{\frac{I_{R,\varepsilon}(t,y)}{\varepsilon}}\, \mathrm{d}y\, \mathrm{d}t \\ &\leq 2\sigma \lim_{\varepsilon \to 0} e^{-\frac{\sigma}{\varepsilon}} \int_{\Omega_y} n^0(y)\, \mathrm{d}y. \end{aligned} \tag{3.73}$$

Moreover, the weak convergence result (3.46)–(3.47) for $n(t, y)$ implies that

$$\int_{\hat{t}-\sigma}^{\hat{t}+\sigma} \int_{\Omega_y} \varphi(y)\, n(t, y)\, \mathrm{d}y\, \mathrm{d}t = \lim_{\varepsilon \to 0} \int_{\hat{t}-\sigma}^{\hat{t}+\sigma} \int_{\Omega_y} \varphi(y)\, n_\varepsilon(t, y)\, \mathrm{d}y\, \mathrm{d}t, \tag{3.74}$$

for every smooth test function $\varphi : \Omega_y \to \mathbb{R}$. Choose φ such that

$$\varphi \;=\; \mathbb{1}_{\Omega_y}, \tag{3.75}$$

where $\mathbb{1}$ denotes the indicator function. Since $n_\varepsilon \geq 0$, we obtain

$$\int_{\hat{t}-\sigma}^{\hat{t}+\sigma} \int_{\Omega_y} n(t,y)\,\mathrm{d}y\,\mathrm{d}t = \lim_{\varepsilon\to 0} \int_{\hat{t}-\sigma}^{\hat{t}+\sigma} \int_{\Omega_y} n_\varepsilon(t,y)\,\mathrm{d}y\,\mathrm{d}t = O\left(e^{-\sigma/\varepsilon}\right). \tag{3.76}$$

This proves both (3.72b) and (3.72c). Note that condition (3.72b) coincides with the assumption of Lemma 3.5, which can therefore be applied directly when (3.72a) holds.

Step 3.

Now, we prove (3.65).

Consider $\mathcal{O} \neq \emptyset$ and assume that there exist $\hat{t} \in [0,T)$ and $\sigma > 0$ with $\hat{t}+\sigma \leq T$ such that

$$\max_{y\in\Omega_y} I_R(t,y) = 0 \quad \forall\, t \in [0,\hat{t}] \quad \text{and} \quad N(t) > 0 \quad \text{a.e. on } [0,\hat{t}], \tag{3.77}$$

whereas

$$\max_{y\in\Omega_y} I_R(t,y) < 0 \quad \forall\, t \in (\hat{t},\hat{t}+\sigma). \tag{3.78}$$

Assumptions (3.77) and (3.78) allow us to use the results of *Step 2*. In particular, (3.72b) along with Lemma 3.5 ensure that $s_\varepsilon(t,x) \overset{*}{\underset{\varepsilon\to 0}{\rightharpoonup}} \gamma(x)$ for a.e. $t \in (\hat{t},\hat{t}+\sigma)$. Now we take $\hat{y} \in \mathcal{A}(\hat{t})$ and we write

$$\begin{aligned} I_R(\hat{t}+\sigma,\hat{y}) &= \int_0^{\hat{t}+\sigma} R(\hat{y},\mathcal{N}_\eta(\tau,\hat{y}))\mathrm{d}\tau \\ &= I_R(\hat{t},\hat{y}) + \int_{\hat{t}}^{\hat{t}+\sigma} R(\hat{y},\mathcal{N}_\eta(\tau,\hat{y}))\mathrm{d}\tau \\ &= 0 + \int_{\hat{t}}^{\hat{t}+\sigma} \left(\int_{\Omega_x} \beta(x,\hat{y})\gamma(x)\mathrm{d}x - \kappa(\hat{y}) \right) \mathrm{d}\tau \geq 0, \end{aligned} \tag{3.79}$$

where the last inequality is given by the facts that $\sigma > 0$ and $\hat{y} \in \overline{\mathcal{O}}$ due to Corollary 3.6. Then we have $I_R(\hat{t}+\sigma,\hat{y}) \geq 0$ which contradicts (3.78). Hence,

$$\max_{y\in\Omega_y} I_R(t,y) = 0 \;\forall\; t \in (\hat{t},\hat{t}+\sigma) \quad \text{and} \quad N(t) > 0 \quad \text{a.e. on } (\hat{t},\hat{t}+\sigma). \tag{3.80}$$

as well. Therefore, result (3.65) is verified.

Step 4.

First, we consider the case of $\overline{\mathcal{O}} = \emptyset$. By contradiction we suppose there exists

$\hat{t} \in [0, T]$ such that

$$\max_{y \in \Omega_y} I_R(\hat{t}, y) = 0. \tag{3.81}$$

By definition, we have

$$0 = \max_{y \in \Omega_y} I_R(\hat{t}, y) = \max_{y \in \Omega_y} \int_0^{\hat{t}} \left(\int_{\Omega_x} \beta(x, y) s(\tau, x) \mathrm{d}x - \kappa(y) \right) \mathrm{d}\tau \leq \max_{y \in \Omega_y} \left(\int_{\Omega_x} \beta(x, y) \gamma(x) \mathrm{d}x - \kappa(y) \right) \hat{t}. \tag{3.82}$$

Since $\overline{\mathcal{O}} = \emptyset$, we have $\int_{\Omega_x} \beta(x, y)\gamma(x), dx - \kappa(y) < 0$ for all $y \in \Omega_y$, and thus $I_R(\hat{t}, \cdot) < 0$ which contradicts with 3.81 and proves (3.66). To prove (3.68) we observe that, since $I_R(t, \cdot) < 0$ for every $t \in [0, T]$, (3.72b) and (3.72c) guarantee that $N(t) = 0$ a.e. on $[0, T]$ and there exists $\sigma \geq \varepsilon > 0$ such that

$$\int_{\hat{t}-\sigma}^{\hat{t}+\sigma} \int_{\Omega_y} n_\varepsilon(t, y) \, \mathrm{d}y \, \mathrm{d}t = O\left(e^{-\sigma/\varepsilon}\right) \quad \text{for} \quad \varepsilon \to 0.$$

Hence, all the hypotheses of the lemma 3.5 hold and we conclude the proof for (3.66). Finally, we consider the case of $\overline{\mathcal{O}} \neq \emptyset$.

Following the same strategy used in *Step 3* we can prove that

$$\max_{y \in \Omega_y} I_R(t, y) = 0 \quad \forall \, t \in [0, T]. \tag{3.83}$$

However, in this case, since $\mathcal{O} = \emptyset$, equation (3.83) implies

$$0 = \max_{y \in \Omega_y} I_R(t, y) \leq \max_{y \in \Omega_y} \int_0^t g(y) \mathrm{d}\tau = 0, \tag{3.84}$$

which means

$$\int_0^t \int_{\Omega_x} |\gamma(x) - s(\tau, x)| \max_{y \in \Omega_y} \beta(x, y) \mathrm{d}x \mathrm{d}\tau = 0. \tag{3.85}$$

Therefore, since $\beta(x, y) > 0$ we have $s(t, x) = \gamma(x)$ for a.e. $(t, x) \in [0, T] \times \Omega_x$. Lastly, to prove that $\int_{\Omega_y} n_\varepsilon(t, y) \mathrm{d}y = o(\varepsilon)$ as $\varepsilon \to 0$, we suppose by contradiction that

$$\lim_{\varepsilon \to 0} \frac{\int_{\Omega_y} n_\varepsilon(t, y) \mathrm{d}y}{\varepsilon} > 0 \quad \text{for a.e.} \quad t \in [0, T]. \tag{3.86}$$

But if that is the case, following the proof steps for Lemma 3.5, we find

$$\lim_{\varepsilon \to 0} s_\varepsilon(t, x) = \lim_{\varepsilon \to 0} \gamma(x) e^{-r_\varepsilon/\varepsilon} \left(1 - e^{-\alpha(x)(t-\tau_0)/\varepsilon}\right), \tag{3.87}$$

where, thanks to hypothesis (H4) for β, we have

$$r_\varepsilon \geq C(t-\tau_0)\int_{\Omega_y} n_\varepsilon(t,y)\mathrm{d}y.$$

Hence, if (3.86) holds, we get $s_\varepsilon(t,x) \nrightarrow \gamma(x)$ which contradicts the previous result and finally proves (3.67). □

Remark 3.8. The previous lemma provides sufficient conditions to characterise the asymptotic behaviour of the population. In particular, it follows that the non-emptiness of $\mathcal{O}$ is a necessary and sufficient condition for population survival. Equally important is the role played by the set $\overline{\mathcal{O}}$ in shaping the long-time dynamics. Indeed, when $\overline{\mathcal{O}} \neq \emptyset$ but $\mathcal{O} = \emptyset$, we nevertheless observe that

$$\max_{y\in\Omega_y} I_R(t,y) = 0 \quad \forall\, t \in [0,T], \tag{3.88}$$

which formally resembles the survival case. However, in this regime, a positive limit mass $N(t) > 0$ would necessarily imply a negative I_R, ultimately leading to a contradiction with (3.88). The key step lies in equation (3.84), where the last equality stems precisely from the fact that no $y \in \Omega_y$ satisfies $g(y) > 0$. Finally, the distinction between *fast* and *slow* extinction arises from the different rates of decay: in the former case ($\overline{\mathcal{O}} = \emptyset$) the mass $N_\varepsilon(t)$ decays exponentially in ε, while in the latter ($\overline{\mathcal{O}} \neq \emptyset$) it only decays as $o(\varepsilon)$, with an asymptotic rate that may be considerably slower.

3.5 Main results of numerical simulations

In this section, we present several numerical results illustrating the evolution of the system described in (3.44) under three distinct scenarios. The main purpose of these tests is to provide a numerical validation of the convergence results established in Section 3.4.2, and to analyse how the qualitative properties of the net growth term influence the overall dynamics of the solutions. In particular, we consider the following representative configurations:

- **Scenario 1:** $\overline{\mathcal{O}} = \emptyset$, where a fast extinction of the agent population is expected;
- **Scenario 2:** $\mathcal{O} = (a,b)$, so we expect the population to proliferate only within this interval;
- **Scenario 3:** $\mathcal{O}$ is given by the union of multiple intervals, leading to the emergence of multiple specialised subpopulations.

The key discriminating element among the different tests is the *mortality function* $\kappa(y)$, while all other functions and parameters are kept identical across simulations to ensure comparability. The analysis focuses on the impact of its profile on the system

TABLE 3.2: Parameters used in the numerical simulations of

Parameter	Description	Value
Ω_x	Nutrient trait domain	$[-1, 1]$
Ω_y	Agent trait domain	$[-1, 1]$
Δx	Trait mesh size for the nutrient	10^{-2}
Δy	Trait mesh size for the agents	10^{-2}
Δt	Time step	10^{-3}
$\overline{\alpha}$	Nutrient regeneration rate	0.25
χ	Units of nutrient needed for proliferation	4
Γ	$\|\|\gamma\|\|_{L^1}$	1
ε	Scaling parameter for the asymptotic regime	10^{-1}, 10^{-2}, 10^{-3}

dynamics, through the study of the sign of the function $g(y)$ introduced in 3.61. Results are reported for three different values of the parameter ε, allowing us to observe convergence towards the steady state as ε decreases and highlight how the saturation and extinction dynamics of the two populations evolve at rates consistent with the chosen scaling parameter. In detail, we present results for a *slow* time scale, $\varepsilon = 10^{-1}$, for a *moderately fast* time scale, $\varepsilon = 10^{-2}$, and for a *fast* time scale, $\varepsilon = 10^{-3}$.
To isolate the influence of the mortality function from that of other parameters, all remaining coefficients are kept constant across simulations (numerical values are listed in Table 3.2). We fix the rate $\alpha \equiv \overline{\alpha}$ as constant and define the function γ as

$$\gamma(x) := \frac{\Gamma}{C_\gamma}\left(e^{-15(x+0.5)^2} + e^{-15(x-0.5)^2}\right), \tag{3.89}$$

where $\Gamma := ||\gamma||_{L^1}$ and $C_\gamma > 0$ is a normalisation constant. The choice of a sum of two Gaussian profiles for the nutrient distribution allows us to explore how the presence of two maxima in γ does not necessarily entail the selection of two distinct dominant traits in the population n. Then we also have the kernels β and η for which holds $\eta(x, y) = \chi\beta(x, y)$ with $\chi > 1$, $\chi \in \mathbb{N}$. We choose functions that increase the likelihood of interactions between agents and nutrients characterised by similar traits. Specifically, the model assumes that a nutrient unit with trait x is more *appealing* to an agent with trait y the closer the two values are, leading to functions that decrease with the distance $|x - y|$:

$$\eta(x, y) := \frac{1}{C_\eta} e^{-5(x-y)^2}, \qquad \beta(x, y) = \frac{1}{\chi}\eta(x, y), \tag{3.90}$$

where C_η is the normalisation constant.
Finally, for the initial conditions $n^0(y)$ and $s^0(x)$ reported below, we choose the same functions for the three tests, except for the initial masses, which are adjusted

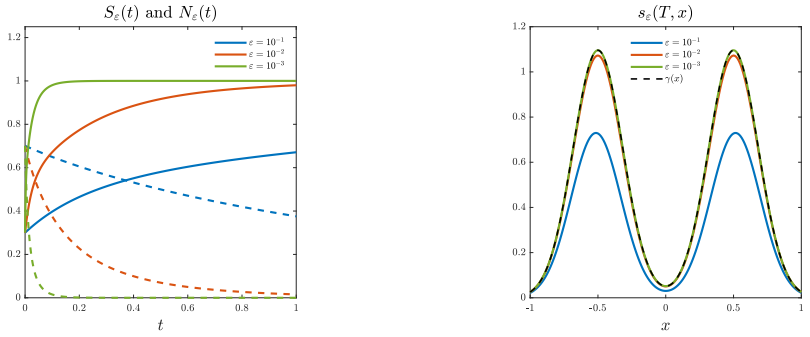

(a) (b)

FIGURE 3.2: **Panel (a)** Time evolution of the total masses of nutrients, $S_\varepsilon(t)$ (solid lines), and agents, $N_\varepsilon(t)$ (dashed lines), computed for the three values of ε listed in Table 3.2. The nutrient population saturates at $\Gamma = 1$, while the agent population vanishes, $N_\varepsilon(t) \to 0$, in agreement with Lemma 3.7. For initial data we chose $N(0) = 0.7$ and $S(0) = 0.3$ **Panel (b)** Comparison between the substrate distribution $s(t,x)$ at the final time $t = T$ (solid lines) and the function $\gamma(x)$ (black dashed line), representing its limiting profile as $\varepsilon \to 0$. Simulation parameters are listed in Table 3.2.

to emphasize the distinct macroscopic behaviours of the system depending on the test:

$$n^0(y) = N(0)\frac{e^{-2y^2}}{C_n}, \qquad s^0(x) = S(0)\gamma(x), \tag{3.91}$$

where C_n is the normalisation constant.

3.5.1 Extinction regime

In this first scenario, we analyse the case in which $g(y) < 0$ for all $y \in \Omega_y$, and consequently $\mathcal{O} = \emptyset$. According to Lemma 3.7, we therefore expect the population n_ε to go extinct in the long run, while the substrate s_ε approaches a saturation state.

To obtain this configuration, we choose a constant mortality function:

$$\kappa(y) \equiv \overline{\kappa} = 0.1. \tag{3.92}$$

With this choice, and taking into account the definitions of γ in (3.89), β in (3.90), and the parameter values reported in Table 3.2, the set $\mathcal{O}$ is indeed empty. This scenario turns out to be the fastest in reaching equilibrium. By setting a relatively short time horizon, $T = 1$, we observe that the system has already reached a stationary state for the fast and intermediate time scales, whereas the slow scale remains in a transient phase. Finally, for the initial masses we choose $N(0) = 0.7$ and $S(0) = 0.3$. As prescribed by Lemma 3.7, Figure 3.2 shows the extinction of the population of agents and saturation of the nutrients. In the left panel, we see that the total mass of

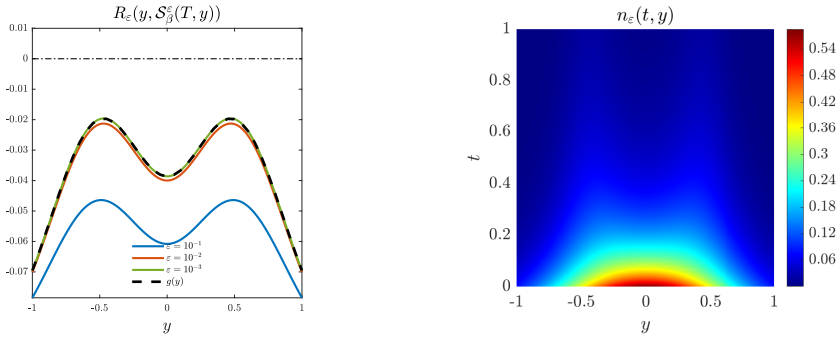

(a) (b)

FIGURE 3.3: **Panel (a)** Comparison between $R_\varepsilon(y, \mathcal{S}^\varepsilon_\beta(T,y))$ (solid lines) and $g(y)$ (dashed line). A clear convergence of the former towards the latter is observed as $\varepsilon \to 0$. The limiting function $g(y)$ remains entirely below the zero threshold (dotted line), confirming that $\mathcal{O} = \emptyset$. **Panel (b)** Full time evolution of the population distribution $n_\varepsilon(t,y)$ with $\varepsilon = 10^{-2}$, which decays to zero for all $t > 0$, consistently with the limit $I_R(t,y) < 0$ $\forall\, t \in [0,T]$. Simulation parameters are listed in Table 3.2.

agents decreases monotonically until it vanishes. In contrast, the nutrient population converges to the saturation value $\Gamma = 1$. The convergence of these trajectories, observed across different rescaling regimes, highlights the robustness of the extinction–saturation mechanism and illustrates how the asymptotic behaviour predicted by the model manifests in finite time. The right panel further corroborates this interpretation, showing that the substrate distribution stabilises into its stationary configuration, consistent with the analytical limit (3.68) obtained for $\varepsilon \to 0$. Hence, the numerical convergence of $s_\varepsilon(t,x)$ towards $\gamma(x)$ not only validates the existence of a steady-state solution but also illustrates how the extinction of agents restores a fully saturated environment.

The results reported in Figure 3.3, Panel (a), compare the net growth rate $R_\varepsilon(y, \mathcal{S}^\varepsilon_\beta(T,y))$, computed at the final simulation time, with the limiting function $g(y)$ that encapsulates its maxima. As ε decreases, the numerical evaluations of R_ε exhibit a clear convergence towards g, confirming the consistency with the asymptotic formulation of the model. Nevertheless, since the limiting profile $g(y)$ lies entirely below the zero threshold, it entails the absence of any viable trait capable of sustaining population persistence. We also observe that the population distribution $n_\varepsilon(t,y)$ for $\varepsilon = 10^{-2}$ (Panel (b)) shows a monotonically decreases for all $y \in \Omega_y$. For $t = T$, the depletion is almost complete in accordance with the mass evolution (Figure 3.2, Panel (a), orange dashed line). This decay behaviour aligns with the condition $I_R(t,y) < 0$ throughout the time interval $[0,T]$, as established analytically.

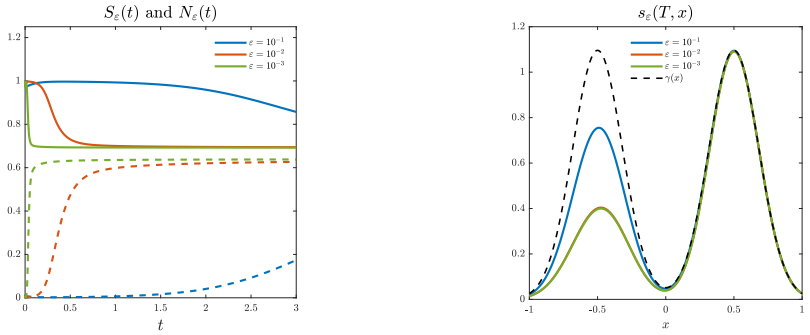

(a) (b)

FIGURE 3.4: **Panel (a)** Time evolution of the total masses of nutrients, $S_\varepsilon(t)$ (solid lines), and agents, $N_\varepsilon(t)$ (dashed lines), for the three time scales corresponding to the values of ε in Table 3.2. The nutrient mass decreases as proliferating agents consume resources and grow to saturation. The fast and intermediate regimes ($\varepsilon = 10^{-3}, 10^{-2}$) reach the steady state within the prescribed time, while the slow one ($\varepsilon = 10^{-1}$) remains transient. **Panel (b)** Comparison between the substrate distribution $s_\varepsilon(t,x)$ at the final time $t = T$ (solid lines) for different ε and its limiting profile $\gamma(x)$ (black dashed line). The depletion of nutrients affects both peaks of the distribution due to the presence of multiple intervals constituting $\mathcal{O}$. Simulation parameters are listed in Table 3.2.

3.5.2 Selection of a single trait

In this second test, we examine the case where $\mathcal{O} = [a,b]$, with $[a,b] \subset \Omega_y$ being a non-trivial interval. In this configuration, we expect to observe the proliferation of individuals whose traits fall within the region of interest $\mathcal{O}$, in particular, selective concentration in the traits that belong to

$$\mathcal{A}(T) = \arg\max_{y\in\Omega_y} I_R(T,y).$$

Indeed, we have $\mathcal{A}(t) \subset \overline{\mathcal{O}}$ for all $t \in [0,T]$, but since the inclusion is strict, Lemma 3.7 does not guarantee survival for all individuals with trait within $\overline{\mathcal{O}}$.

To obtain this configuration, we adopt the following mortality function:

$$\kappa(y) = 0.5 - 0.47\, e^{-5(y+0.6)^2}. \tag{3.93}$$

This choice produces a single maximum point for the function $g(y)$, leading to an interval $\mathcal{O}$ centred around $y = -0.6$. Compared to the previous test, this scenario evolves more slowly; therefore, we set $T = 3$ in order to capture the beginning of the dynamics even for the slowest timescale, corresponding to $\varepsilon = 10^{-1}$. The initial masses are $N(0) = 0.01$ and $S(0) = 0.97$, representing an environment rich in nutrients with limited competition among agents.

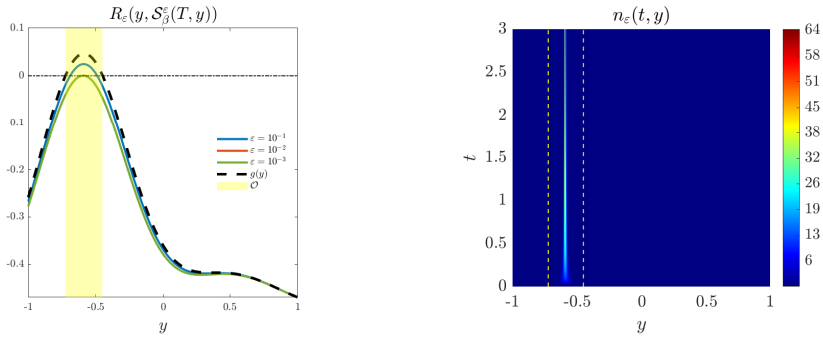

FIGURE 3.5: **Panel (a)** Comparison between $R_\varepsilon(y, \mathcal{S}^\varepsilon_\beta(T,y))$ (solid lines) and $g(y)$ (dashed line). Given the initial condition $s(0,x) = 0.97\gamma(x)$, for small times we have $R_\varepsilon(y, \mathcal{S}^\varepsilon_\beta(T,y)) \simeq g(y)$, while their difference increases as the number of agents grows. The yellow-shaded region corresponds to $\mathcal{O}$. **Panel (b)** Time evolution of the population distribution $n_\varepsilon(t,y)$ for $\varepsilon = 10^{-3}$. The figure highlights the selection of the fittest trait inside the survival region $\mathcal{O}$ (bounded by the yellow dashed lines). Simulation parameters are listed in Table 3.2.

The numerical results illustrated in Figure 3.4 provide a clear quantitative confirmation of the heterogeneous behaviour predicted by the model when the growth region $\mathcal{O}$ is localised around a single trait value. As shown in Panel (a), the total masses of nutrients and agents evolve in opposite directions: the nutrient population gradually decreases due to consumption by reproducing agents, which in turn proliferate and approach saturation. For the fast and intermediate regimes ($\varepsilon = 10^{-3}$ and 10^{-2}), the system reaches equilibrium rapidly, whereas in the slow regime ($\varepsilon = 10^{-1}$), the population dynamics remain in a transient stage. Panel (b) reinforces this interpretation by examining the spatial distribution of the substrate at the final time. The comparison between $s_\varepsilon(t,x)$ and its limiting profile $\gamma(x)$ reveals that nutrient depletion occurs primarily in the left portion of the domain, while the right side remains nearly saturated. This asymmetry mirrors the structure of the set $\mathcal{O}$, concentrated around $y = -0.6$, and is consistent with the non-local coupling induced by the interaction kernels β and η defined in (3.90). Analogous behaviour arises in Figure 3.5, panel (a). Thus, starting from a nutrient distribution close to saturation implies that, for small times, $R_\varepsilon(y, \mathcal{S}^\varepsilon_\beta(T,y)) \simeq g(y)$. As time progresses, however, the discrepancy between the two functions increases, reflecting the progressive loss of mass in the nutrient population. We observe that, over time, $R_\varepsilon(y, \mathcal{S}^\varepsilon_\beta(T,y))$ becomes negative almost everywhere, except for a single point where it remains close to zero—precisely the point where the individuals concentrate (Figure 3.5, panel (b)). In this regime, agents proliferate and persist, but their

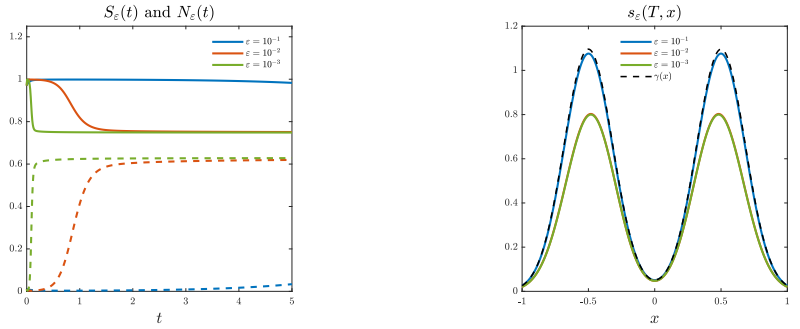

(a) (b)

FIGURE 3.6: **Panel (a)** Time evolution of the total masses of nutrients, $S_\varepsilon(t)$ (solid lines), and agents, $N_\varepsilon(t)$ (dashed lines), for the three timescales corresponding to the values of ε in Table 3.2. The nutrient mass decreases as proliferating agents consume resources and grow to saturation. The fast and intermediate regimes ($\varepsilon = 10^{-3}, 10^{-2}$) reach the steady state within the prescribed time, while the slow one ($\varepsilon = 10^{-1}$) still exhibits the early stage of its evolution even at the final time $T = 5$. **Panel (b)** Comparison between the substrate distribution $s_\varepsilon(t,x)$ at the final time $t = T$ (solid lines) for different ε and its limiting profile $\gamma(x)$ (black dashed line). The depletion of nutrients mainly affects the left region of the domain, consistent with the localisation of the set $\mathcal{O}$ around $y = -0.6$ and with the structure of the interaction kernels β and η in (3.90). Simulation parameters are listed in Table 3.2.

distribution becomes sharply localised around the unique element of $\mathcal{A}(T)$. Together, the two figures demonstrate how heterogeneity in the growth region translates into localised resource depletion and selective proliferation.

3.5.3 Multiple-trait survival

In this final test, we examine a more complex scenario than in the previous two cases. Here, we select a set $\mathcal{O}$ that is not only non-empty but also composed of multiple disjoint intervals contained in Ω_y. The resulting dynamics reveal that the population tends to concentrate around several local maxima, ultimately leading to a final distribution that consists of a sum of Dirac delta functions. It is worth noting that local maxima of $R_\varepsilon(y, \mathcal{S}^\varepsilon_\beta(t,y))$ (and consequently of $I_{R,\varepsilon}(t,y)$) may persist as $\varepsilon \to 0$. However, if these traits do not correspond to global maxima (namely, if $y \notin \mathcal{A}(t)$), they do not survive in the long run. For this simulation, we adopt the following mortality function:

$$\kappa(y) = 0.45 - 0.4\left[e^{-15(y+0.7)^2} + e^{-15y^2} + e^{-15(y-0.7)^2}\right]. \tag{3.94}$$

This function exhibits three global minima at $y_1 = -0.7$, $y_2 = 0$, and $y_3 = 0.7$. Nevertheless, these values do not coincide with three absolute maxima of the fitness

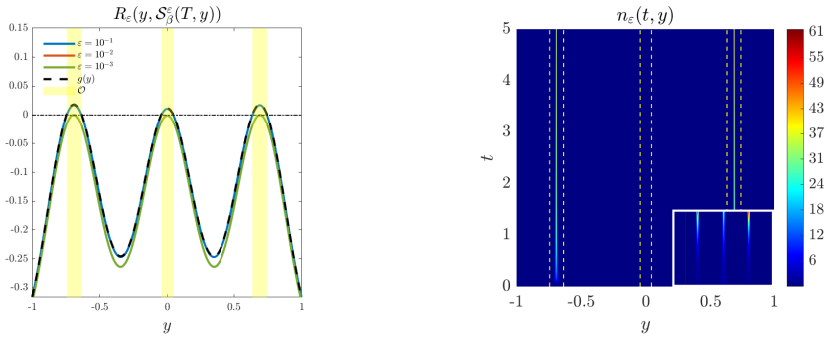

(a) (b)

FIGURE 3.7: **Panel (a)** Comparison between $R_\varepsilon(y, \mathcal{S}^\varepsilon_\beta(T,y))$ (solid lines) for different values of ε, and $g(y)$ (dashed line). Given the initial condition $s(0,x) = 0.97\gamma(x)$, for small times we have $R_\varepsilon(y, \mathcal{S}^\varepsilon_\beta(T,y)) \simeq g(y)$, while their difference increases as the number of agents grows. The yellow-shaded region corresponds to $\mathcal{O}$. **Panel (b)** Time evolution of the population distribution $n_\varepsilon(t,y)$ for $\varepsilon = 10^{-2}$. The figure highlights the selection of the fittest traits inside two of the three survival regions of $\mathcal{O}$ (bounded by the yellow dashed lines).On the other hand, the inset shows an early phase of the dynamics where there is still the presence of a third peak within the middle region of $\mathcal{O}$. Simulation parameters are listed in Table 3.2.

function, since the growth term $\mathcal{S}^\varepsilon_\beta$ does not fully inherit the multimodal structure determined by the peaks of κ. In this case, the dynamics evolve more slowly than in the previous tests: for larger values of ε, the system still appears in an early transient phase even at the final time $T = 5$. The initial masses are the same as in the previous test, namely $N(0) = 0.01$ and $S(0) = 0.97$. Figure 3.7 provides numerical evidence of the selection dynamics arising in the case of a multiple survival sets $\mathcal{O}$. Panel (a) shows the comparison between $R_\varepsilon(y, \mathcal{S}^\varepsilon_\beta(T,y))$ and its limiting profile $g(y)$ for different values of ε. At early stages, the two functions almost coincide, reflecting that the population of nutrients is initially close to saturation. As the system evolves and the number of agents increases, deviations between the two profiles arise for the two fast time scales, signalling the progressive depletion of nutrients in the regions corresponding to higher fitness. The yellow-shaded areas identify the intervals composing $\mathcal{O}$, within which the net growth rate is positive and long-term survival is admissible. However, the evolution also reveals that not all survival intervals persist in the asymptotic regime: although three distinct regions of potential proliferation are initially present, only two maintain a positive population density as the system approaches equilibrium (Panel (b)). Consistent with theoretical predictions, the population $n_\varepsilon(t,y)$ gradually concentrates at $y \in \mathcal{A}(t)$, i.e., where the limit function $I_R(T,y)$ reaches its maximum. The inset highlights an early transient phase of the dynamics, in which a third transient peak still appears in the central portion of $\mathcal{O}$ before being suppressed. This behaviour confirms that, despite the

presence of multiple favourable traits, only those corresponding to global maxima of the effective fitness function contribute to the long-term structure of the population.

3.6 Concluding remarks

In this chapter, we extend the general compartmental framework developed in the previous chapters to a system that describes the interaction between two distinct subsystems: nutrients and consumers. Each subsystem is structured by its own continuous microscopic variable, which captures the heterogeneity among individuals, and is subdivided into compartments corresponding to different stages of their life cycle.

Starting from a stochastic microscopic description, we derive the corresponding mesoscopic model, obtaining a conservative system of five coupled integro-differential equations, one for each compartment. This procedure follows a line of research connecting microscopic agent-based descriptions with mesoscopic and macroscopic integro-differential or partial differential formulations, as developed in kinetic and probabilistic frameworks for structured populations [48, 51, 109, 131]. The formulation obtained preserves the dual conservation property of the total mass and of the two subsystems separately, ensuring a consistent description of the dynamics in which resources and agents belong to different species.

By imposing meaningful simplifications, the system reduces to a pair of integro-differential equations that retain the essential interaction mechanisms. For this reduced model, we establish well-posedness results and analyse the asymptotic behaviour of the solutions. In particular, we identify a survival set $\mathcal{O}$, defined as the region in which the net growth rate of agents is positive, and we prove that the long-term dynamics lead to the extinction of traits outside this region. The analysis, therefore, reveals a clear selection mechanism in accordance with the existing literature [62, 66, 108, 113, 134]. Only traits corresponding to the global maxima of the effective growth rate persist in the limit, while all others vanish.

Numerical simulations explore three representative scenarios, differing in the structure of the survival set $\mathcal{O}$. First, we investigate the case $\overline{\mathcal{O}} = \emptyset$, where the population of agents inevitably becomes extinct while the nutrient pool saturates. Then, we construct a configuration in which $\mathcal{O}$ consists of a single interval, leading to the persistence and concentration of agents around a unique dominant trait. Finally, when $\mathcal{O}$ is the union of multiple disjoint intervals, the population initially spreads across all favourable regions but ultimately concentrates around two globally fittest traits.

These results show that even within a framework based on indirect competition, the survival of the consumer population depends on a selection process in which only certain traits emerge as the fittest, leading to population concentration phenomena around them [59, 62, 115, 122]. At the same time, the results highlight

that environmental conditions may be insufficient to sustain the required level of resource consumption, ultimately leading, at varying rates, to the extinction of the consumer agents.

Chapter 4

Other works and future perspectives

4.1 Introduction

This concluding chapter differs in both nature and purpose from the preceding ones. It does not present established results, but rather gathers a set of reflections, research perspectives, and possible future developments that stem from the models and techniques introduced earlier in the thesis.

Agent-based models have, in fact, proved unexpectedly effective even in new contexts far removed from their classical applications [44, 45, 56, 87, 141], such as those explored throughout this thesis. In particular, several new numerical methods for solving non-convex optimisation problems have been developed based on particle dynamics. The behaviour observed in complex real-world systems, such as swarming, crowd dynamics, and opinion formation, often follows standard rules of cost minimisation. This analogy has naturally motivated the use of tools originally devised for their analysis within the field of optimisation.

These methods fall within the class of metaheuristic algorithms [1, 16, 25, 32, 83], that is, stochastic optimisation schemes designed to find (typically approximate) solutions to problems with non-convex solution spaces, where standard deterministic methods—such as gradient-based algorithms—fail by getting trapped in local minima. Among the most prominent techniques in this family are Ant Colony Optimisation, Genetic Algorithms [69, 78, 104, 146], Particle Swarm Optimisation (PSO) [101, 102, 119, 133], Simulated Annealing [90, 91], and Consensus-Based Optimisation (CBO) [20, 43, 46, 143]. The stochastic nature of their underlying natural counterparts makes these strategies particularly suitable for tackling such classes of problems.

However, in the following, we present a methodological extension of the tools discussed in Chapter 1, exploring their application in a context different from the original bio-mathematical setting. Specifically, we analyse a potential use of these tools

in the framework of non-convex optimisation. By analysing the first qualitative numerical simulations, we highlight the most promising aspects of this approach, as well as the open questions that deserve further investigation. In doing so, we also shed light on the differences that emerge between the discrete particle-based model and its continuous counterpart.

In the final section of this chapter, we will discuss possible future directions and open research avenues that may stem from the developments presented in the first three chapters. Although each of those possesses its own conceptual coherence and internal consistency, several aspects remain open and undoubtedly deserve further investigation and analysis.

4.2 Background

In this first section, we outline some of the main advantages and methodological features of the most widely studied metaheuristic optimisation techniques. This brief overview is intended to orient the reader within the broad and diverse landscape of modern metaheuristic strategies. Such a perspective provides the conceptual background for the following discussion, which focuses more specifically on potential developments directly inspired by the modelling framework presented in this thesis. Obviously, we do not aim to discuss every possible metaheuristic algorithm. Instead, we focus our attention exclusively on those that exhibit the closest conceptual connections with the results developed in the preceding chapters. Particular attention is devoted to CBO methods, which are paving the way toward the theoretical validation of stochastic optimisation algorithms. Their structure naturally allows the integration of the particle-based formulation with its mesoscopic counterpart through a mean-field limit, thereby providing a rigorous analytical bridge between the two levels of description.

4.2.1 Metaheuristic methods

The development of metaheuristic methods dates back to the mid-1970s, when John Holland, in his pioneering work [89], introduced a computational model grounded in probabilistic and biological evolutionary ideas, as an alternative to the deterministic approaches traditionally employed in optimisation — the Genetic Algorithms. In Holland's formulation, the search process follows Darwinian evolutionary principles, and for the first time, genetic mechanisms such as recombination, mutation, and selection were formally defined within a computational framework. The simplicity and flexibility of this approach soon led to the emergence of numerous variants specifically designed to address different classes of optimisation problems (see [78, 100, 146] and the references therein).

In the following decades, considerable attention was devoted to the development of methods of this kind and, more broadly, to stochastic approaches inspired by natural phenomena for solving optimisation problems. In particular, about twenty

years later, Kennedy and Eberhart introduced a socially inspired, population-based optimiser grounded in the concepts of swarm behaviour [102]. The central novel idea of this PSO method was to exploit information sharing, allowing each particle to move not only according to its own experience but also under the social influence of the group. The paradigm shift they proposed, widely applied and subsequently refined, led to the emergence of algorithms that harness collective intelligence rather than relying solely on purely selective mechanisms.

Consensus-Based Optimization (CBO) is a much more recent addition to the family of stochastic optimization algorithms. Introduced in 2017 [132] as a multi-agent, derivative-free method for the global optimisation of high-dimensional problems, it is built upon the key idea of moving a swarm of agents through two complementary mechanisms: a consensus-based drift, which drives alignment towards a common consensus, and a diffusive term, which ensures exploration of the solution space. Unlike PSO, where individuals maintain independent trajectories, in CBO all agents converge towards a common point while continuously exchanging information throughout the process. One of the main advantages of methods like CBO, compared to other meta-heuristics, lies in the possibility of exploiting mean-field techniques to establish convergence results towards global minimiser analytically [8, 43, 46, 143]. Despite their structural simplicity, CBO methods, and their extensions, such as Kinetic-Theory-Based Optimisation (KBO) schemes [20], appear to be robust tools for addressing a wide range of non-convex optimisation problems, which is a property particularly valuable for high-dimensional problems in the context of machine learning.

4.2.1.1 Mean-field interpretation

We recall that for a given $\mathcal{F}$ continuous, nonnegative, and bounded, the task is to find

$$x_* \in \operatorname*{argmin}_{x \in \mathbb{R}^d} \mathcal{F}(x). \tag{4.1}$$

The key feature that characterises these latter methods lies in the assumption that the N agents involved in the search for the minimum are indistinguishable and that their trajectories are driven by a common mean field. These properties, along with the *propagation of chaos* assumption, formally justify taking the limit $N \to \infty$, and allow one to derive analytically tractable mean-field equations. Hence, the time evolution of the positions of agents $X_t^i \in \mathbb{R}^d$, $i = 1, \dots, N$, is governed by a system of stochastic differential equations consisting of a drift term and a diffusion term [132]. Both components are modulated by the distance of each agent from the weighted mean $v_\mathcal{F}$, so that as an agent approaches the minimum, it is attracted towards it and prevented from moving further away. In general, the weighted mean is defined as

$$v_\mathcal{F} = \frac{1}{\sum_i \omega_\mathcal{F}^\alpha(X_t^i)} \sum_i X_t^i \omega_\mathcal{F}^\alpha(X_t^i) \qquad \text{with} \qquad \omega_\mathcal{F}^\alpha(x) = e^{-\alpha \mathcal{F}(x)} \quad \alpha > 0 \tag{4.2}$$

and with this definition, the mean-field limit reads

$$v_{\mathcal{F}} \underset{N\to\infty}{\longrightarrow} \frac{\int x\omega_{\mathcal{F}}^{\alpha}(x)\mathrm{d}\rho_t(x)}{\int \omega_{\mathcal{F}}^{\alpha}(x)\mathrm{d}\rho_t(x)} \tag{4.3}$$

for a suitable Borel probability measure $\rho_t \in \mathcal{P}(\mathbb{R}^d)$ (see [43, 46, 132] for details). Thus, by Laplace's principle [61] we have (see [143, Proposition 1])

$$\lim_{\alpha\to\infty}\left(-\frac{1}{\alpha}\log\left(\int_{\mathbb{R}^d} e^{-\alpha\mathcal{F}(x)}\mathrm{d}\rho(x)\right)\right) = \mathcal{F}(x_*), \tag{4.4}$$

which is the main reason for the choices in (4.2). This result provides the first formal indication of the convergence of the method towards the absolute minimum of $\mathcal{F}$, which is assumed to be unique. The problem, reformulated in the mean-field limit, consists of a single non-linear and non-local Fokker–Planck equation, where both the drift and diffusion terms depend on the global state of the system. From an analytical standpoint, significant progress has been achieved in recent years. Following the first study that established convergence results [43], several contributions have rigorously demonstrated the validity of the propagation of chaos assumption, which is essential to connect the discrete particle-based system to its mean-field counterpart [92]. More recently, quantitative estimates of this propagation have also been obtained [84]. These advances have made it possible to refine global convergence results [76] and to introduce model variants capable of addressing situations in which the cost functional admits a set of global minima, rather than a single minimiser [77].

4.3 An adaptive-dynamics-based optimisation method

In this section, we present our contribution to this framework. We developed a kinetic optimization strategy starting from the biological models introduced in the previous chapters. The connection between the two contexts is quite natural: the success of early metaheuristic models, such as Genetic Algorithms, is rooted in Darwinian principles that underpin evolutionary theory as a whole (namely, recombination, selection, and mutation). At the same time, particle-based models such as PSO and CBO exhibit remarkable connections with kinetic theory, particularly through their characteristic mean-field limits. These observations further reinforce the idea that the multi-scale construction, which has been running throughout this thesis, can also be implemented in this context.
Starting from Chapter 1, we draw the basic intuitions needed to describe the evolution of a population structured by a continuous variable, starting from a particle representation. This type of approach is typical for such models and provides a natural starting point for building a bridge across different levels of description.

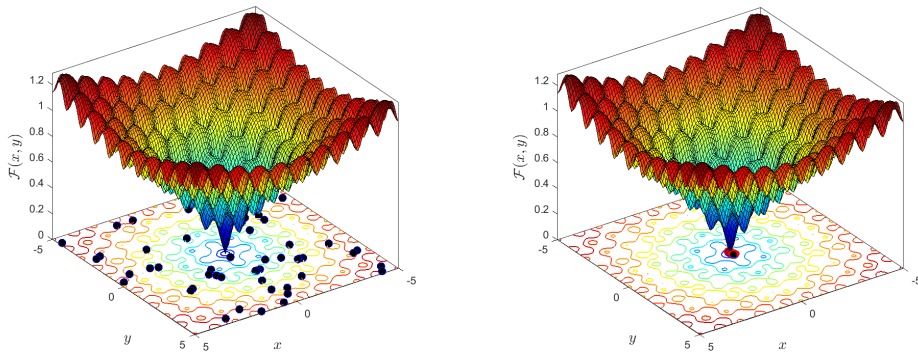

(a) (b)

FIGURE 4.1: Two-dimensional representation of the Ackley function presented in [119], along with its level curves. This function is a classical benchmark in optimisation problems. **Panel (a)** Initial configuration: particles (black and blue dots) are randomly distributed over the two-dimensional domain $\Omega = [-5, 5]^2$. **Panel (b)** Final configuration: particles (red and black dots) have concentrated around the global minimum of the cost function $\mathcal{F}$.

In particular, we analysed the connections between three common representations of structured populations widely discussed in the literature: particle-based models, mesoscopic integro-differential equations (IDEs), and non-local partial differential equations (PDEs). We note that the derivation of the mesoscopic level from the particle dynamics, formalised in (1.11), once again relies on the assumption of *propagation of chaos*. On the other hand, in Chapter 3, although the dynamics involved two interacting subsystems, we observed a convergence behaviour of the population towards an optimum, which in that setting corresponded to the maximum point of the function $g(y)$ ((3.61)). It therefore arises naturally to consider applying the results developed within this theoretical framework to a possible optimisation technique.

4.3.1 Our base model

From system (1.27), considering $\Omega \subset \mathbb{R}^d$ compact, and removing the integral diffusion term (i.e. setting $\mu = 0$), we write:

$$\begin{cases} \partial_t f(t,x) = \big(r(x) - \rho(t)\big) f(t,x), \\ \rho(t) := \displaystyle\int_{\mathbb{R}^d} f(t,x)\,\mathrm{d}x, \quad f(0,x) = f^0(x) > 0 \ \ \forall\, x \in \Omega \end{cases} \tag{4.5}$$

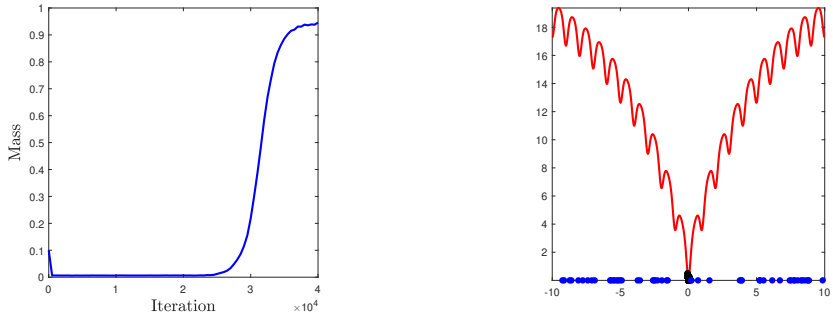

(a) (b)

FIGURE 4.2: **Panel (a)** Normalised number of particles (mass). The figure shows the necessity of imposing a non-extinction constraint to prevent all agents from dying before they have concentrated near the minimum. **Panel (b)** The cost function $\mathcal{F}$ (red solid line) corresponds to the one-dimensional Ackley function introduced in [119], a classical benchmark function for this class of optimisation problems. The black-filled circles represent the agents concentrated around the minimum of $\mathcal{F}$ at the end of the simulation, while the blue ones indicate the positions for the initial batch.

where

$$r \in C(\Omega), \qquad r : \Omega \to \mathbb{R}, \qquad 0 < \underline{r} \leq r(x) \quad \forall\, x \in \Omega. \tag{4.6}$$

In selection models such as system (4.5), where diffusion is absent, individuals tend to concentrate, for large times, at the points of maximum fitness, consistently with an analogue of the Laplace principle introduced in (4.4). If we assume that the maximum of r is attained at a single point x^*, the asymptotic profile of the function f is a Dirac delta concentrated at x^* (see, for instance, [19, 41, 53, 66, 114, 131]). However, analogous results have also been established for problems in which multiple fitness peaks are present [62, 111], yielding steady states characterised by a finite sum of Dirac delta functions, each concentrated at a point

$$x^* \in \underset{x \in \Omega}{\operatorname{argmax}} \left(r(x) \right).$$

Since the continuous model originates from a particle-based formulation, it is reasonable to expect that its discrete counterpart exhibits the same concentration behaviour. In fact, the numerical simulations reported in Section 1.5 show an excellent agreement between the IDE solution and the particle dynamics obtained through Monte Carlo simulations. If our goal is to introduce into the dynamics a cost function to be minimised, it is sufficient to recall that the function r can be defined as

$$r(x) := 1 - \mathcal{F}(x),$$

where the function $\mathcal{F}$ play the role of *death rate*. For this function, the task defined in (4.1) can be reformulated as the search for

$$x^* \in \underset{x\in\Omega}{\operatorname{argmax}}\ r(x) = \underset{x\in\Omega}{\operatorname{argmin}}\ \mathcal{F}(x). \tag{4.7}$$

In this way, it becomes straightforward to identify, even at the microscopic level, where to include this cost term. Indeed, by reconsidering system (1.5), we can define, for the Bernoulli variable $\mathsf{S}^{\mathrm{II}} \in \{0, 1\}$,

$$\text{Prob}\left(\mathsf{S}^{\mathrm{II}} = 1 \,\middle|\, I_t = i,\, V_t = x\right) = \frac{\mathcal{F}(x)\,\Delta t}{1 + \mathcal{F}(x)\,\Delta t}.$$

In this way, the survival probability of each agent is directly modulated by the value of the cost function $\mathcal{F}(x)$, thereby establishing an explicit connection between the life dynamics and the optimisation problem.

The distinctive feature of this model lies in the fact that, unlike traditional particle-based methods, it does not describe agents that move in the parameter space of the objective function by following consensus or direct interaction dynamics. Instead, the particles considered here are agents whose *vital dynamics*, namely, the processes of proliferation and death, are directly governed by the cost function itself, and, to the best of our knowledge, an approach of this kind is currently absent from the existing literature. The agents do not search for the minimum through successive shifts, but rather survive or become extinct depending on the fitness of their trait within that environment, represented by the values of the objective function. Regions of the domain associated with more favourable values (lower $\mathcal{F}$) witness population growth, whereas unfavourable (higher $\mathcal{F}$) areas naturally depopulate. This behaviour leads, in a spontaneous way, to the concentration of the total mass around the points of the global minimum for $\mathcal{F}$, potentially allowing the simultaneous identification of multiple global optima whenever they exist. Nevertheless, this convergence is rigorously guaranteed only in the continuous model, whereas in the particle-based formulation, it can be observed numerically only for a sufficiently large number of particles. Moreover, the absence of diffusion prevents the particles from exploring regions other than those initially occupied. As a consequence, the minimum identified by the system is no longer determined by the global structure of $\mathcal{F}$, but rather by its restriction to the initially populated domain. For instance, as shown in Figure 4.1, Panel (a), at the initial time no particle is located at $(x, y) = (0, 0)$. Without diffusion, the system would therefore be unable to identify the global minimum of the cost function. Obviously, this limitation does not arise in the mesoscopic model derived in (4.5), since the initial condition is chosen to satisfy $f^0(x) > 0$ for all $x \in \Omega$.

Adding diffusion To overcome the exploration limitation discussed above, it is natural to introduce a diffusion term that enables particles to explore regions of the

domain beyond those initially occupied. Such a term, already present in the original formulation of the model introduced in Chapter 1, does not introduce additional analytical difficulties once the corresponding mesoscopic system is derived. However, the nature of convergence changes: in this case, the limiting distribution is no longer a Dirac delta. The presence of spontaneous variations in the phenotypic trait leads instead to an equilibrium distribution centred around the fittest trait, yet characterised by a non-zero variance. In general, the inclusion of diffusion helps to prevent the system from becoming trapped in the minimum identified by the initial batch of particles, although it also makes the identification of the global minimum more challenging. In particle-based methods such as CBO, diffusion is typically modulated through a decaying term that weakens as a particle approaches a minimum, thereby balancing exploration and convergence. At present, however, our construction does not naturally incorporate a similar mechanism, which represents a first avenue for discussion and a possible direction for future implementation of the model. In our simulations, we therefore introduced variance during the initial phase and subsequently let it decay linearly with the number of iterations. Although this strategy does not yet have a formal particle-level formalisation, it serves the practical purpose of enabling sufficient exploration at early stages and progressive concentration around the optimum as the iterations proceed.

Risk of extinction A further interesting aspect concerns the non-conservative nature of the model. Indeed, the total mass may apparently vary in time, since the life of agents is governed by a death-birth mechanism. However, we recall that at the particle level we have two compartments: the first, labelled by the index $i = 1$ is the one that we are investigating and whose trait distribution is governed by a system like the one presented in (4.5), and the other one, labelled by the index $i = 0$ which serves as a reservoir (see Chapter 1, Section 1.1). We noted that if the overall number of particles, including those in the reservoir, is fixed at the initial time, the system remains bounded and cannot experience unbounded growth in the agent population. On the other hand, a different issue may arise. The selection of the optimum occurs as a consequence of the death of individuals associated with disadvantageous traits, that is, those corresponding to high values of $\mathcal{F}$. Although this mechanism resembles others found in the literature [119], the numerical simulations showed that it introduces a distinctive risk that is absent in other classes of models: the possibility of a complete extinction of the agent population, which actually means that all the agents are in the compartment $i = 0$. However, this phenomenon is intrinsic only to the particle-based formulation since, in the corresponding continuous limit, if there exist regions of the domain, which may consist only of isolated points, where extinction is not expected, then the population cannot vanish entirely; instead, it will proliferate only within that subregion. It appears that several factors may contribute to the emergence of extinction dynamics: insufficient initial number of particles, an initial distribution too far from the minimum of the cost function, or a diffusion term too weak to allow effective exploration of the parameter space. In any case, a possible strategy to mitigate this risk is to force a minimum number of particles to remain within the active compartment, in the

expectation that, once the minimum is identified, they will resume proliferation according to the mesoscopic evolution law (Figure 4.2, Panel (a)).

In conclusion, we observe that, among the several aspects that remain open for investigation, two particularly relevant issues concern: the definition of effective stopping strategies and the convergence speed. In its current form, the model does not provide a natural stopping criterion, and the convergence process may be relatively slow, especially in high-dimensional settings. Recent analytical results obtained at the continuous level [111] offer valuable insights into the characterisation of convergence rates and could serve as a theoretical reference for future improvements of the discrete formulation. Incorporating such advances would make it possible to design adaptive mechanisms capable of balancing exploration and convergence more efficiently, thereby enhancing the practical applicability of the method. Overall, although promising, this construction does not yet define a complete algorithm, but it establishes a coherent conceptual framework aligned with evolutionary principles and with the results of the selection-mutation models discussed in the previous chapters. It thus opens the possibility of developing, in the future, a new class of particle-based optimisation algorithms inspired by evolutionary adaptive dynamics.

4.4 Perspectives and future directions

The methodological framework developed throughout this thesis naturally lends itself to a variety of extensions and open research directions. These developments concern both the refinement of the modelling tools introduced in the previous chapters and their possible application to more complex or realistic biological and socio-economic systems.

From structured populations to spatially distributed systems. A natural continuation of the work presented in Chapter 1 consists of extending the proposed approach to populations that, in addition to undergoing proliferation, death, and phenotypic changes, are also spatially distributed. In recent decades, several probabilistic techniques [10, 50, 75, 105] and formal limiting procedures [80, 107, 120] have been developed to connect stochastic agent-based models with deterministic continuous models capable of describing simultaneously the spatial spread and the evolutionary dynamics of phenotype-structured populations. However, while phenotype structuring has been incorporated into kinetic frameworks (see, e.g. [72, 73, 106]), to our knowledge, there is still a lack of derivations rooted in kinetic approaches of the type advanced here. Extending the limiting procedures employed in this work could therefore enable the integration of a wider range of analytical and numerical methods across the agent-based, IDE, and PDE levels, thus advancing the mathematical formalisation of evolutionary dynamics in spatially structured populations.

Demography and epidemiological applications. The general framework presented in Chapter 2 can be further expanded by introducing demographic processes, thereby allowing proliferation and death of individuals in one or more compartments. This would require generalising both the individual-based modelling approach as well as the formal approach employed in this chapter to derive the corresponding mesoscopic and macroscopic models, since both approaches rely on the fact that the total number of individuals in the system is conserved, which would not be the case if demography were incorporated. In the same vein, building for instance on the methods employed in [55, 74, 106], in different application domains, an additional development of this work would be to extend the individual-based modelling approach and the derivation methods employed here to the case where a spatial structure is also included, to then investigate how the interplay between spatial movement and both structuring-variable switching and compartment switching may impact on the evolutionary dynamics of epidemiological systems. Moreover, while the modelling approach presented here is framed in an abstract context to highlight general properties, it would be interesting to apply it to the study of the dynamics of specific infectious diseases. In particular, an additional avenue for future research would be to explore the possibility of estimating the forms of the model functions based on data; for this, techniques similar to those employed in [3, 4, 68] may prove useful. This would enable us to describe specific dynamics of real-world diseases; for instance, we could incorporate the possibility of quarantining an infectious individual with a high viral load by setting their probability of infecting other individuals to zero. This could be of particular relevance for the recent COVID-19 pandemic, and could also be of interest in general for transmissible diseases for which quarantine is a feasible and functioning form of control.

Asymptotic regimes and population heterogeneity. Another promising line of research concerns the analysis of the mesoscopic description provided by the IDE system (2.12). In this regard, it would be interesting to investigate possible limiting regimes and conditions on the model terms under which the population density functions become unimodal or multimodal (i.e. the various compartments become monomorphic or polymorphic). For this, techniques similar to those employed in [6, 23, 62, 97, 111, 131, 134] may prove useful. This would allow for further investigation into the mechanisms and processes underpinning the emergence of inter-individual and intra-compartmental heterogeneity in epidemiological systems.

Further investigation of the two species dynamics It would be of interest to enrich the dynamics described in Chapter 3 by system (3.30) by introducing phenotypic variations capable of capturing mutation phenomena and, consequently, changes in the compatibility between individuals and resources. Although such an extension would not entail a fundamental modification from an analytical standpoint, since it would naturally lead to a *selection–mutation* model [62, 111, 122, 131, 136], it would render the overall representation more accurate and biologically complete. From the viewpoint of asymptotic analysis, an open question concerns

the identification of stability conditions, and in particular the linear stability, of the asymptotic solutions of system (3.30). Such an analysis would complete the theoretical understanding of the model, in analogy with what has been developed in [58, 62, 134].

Periodic environment Another promising research direction involves the description of periodic dynamics. In particular, it would be interesting to consider a time-dependent regeneration rate α, representing the replenishment of nutrients. The choice of keeping the coefficients appearing in the definitions of $\mathcal{P}$ and $\mathcal{Q}$ in (3.6) and (3.7) constant in time is consistent with other models of this kind [21, 110, 117], yet it does not constitute a necessary assumption. The only essential requirement remains their uniform boundedness in time. Introducing this feature would enable the model to account for environmental systems characterised by temporal variability [12, 13, 82, 138], and to realistically describe seasonal nutrient regeneration processes. This would allow, for instance, the investigation of the effects of periodic or pathological variations induced by climatic and environmental changes. Unlike other approaches in the literature [5], this perspective would not model climate-induced mass transport but rather temporary reductions in resource availability, whose effects may be particularly detrimental for traits depending on specific nutrients available only within limited temporal windows.

Bibliography

[1] Emile Aarts and Jan Korst. *Simulated annealing and Boltzmann machines: a stochastic approach to combinatorial optimization and neural computing*. John Wiley & Sons, Inc., (1989).

[2] Lara Abi Rizk, Jean-Baptiste Burie, and Arnaud Ducrot. "Asymptotic speed of spread for a nonlocal evolutionary-epidemic system". In: *Discrete and Continuous Dynamical Systems* 41 (2021), pp. 4959–4985.

[3] Giacomo Albi, Giulia Bertaglia, Walter Boscheri, Giacomo Dimarco, Lorenzo Pareschi, Giuseppe Toscani, and Mattia Zanella. "Kinetic modelling of epidemic dynamics: social contacts, control with uncertain data, and multiscale spatial dynamics". In: *Predicting Pandemics in a Globally Connected World, Volume 1: Toward a Multiscale, Multidisciplinary Framework through Modeling and Simulation*. Springer, (2022), pp. 43–108.

[4] Giacomo Albi, Lorenzo Pareschi, and Mattia Zanella. "Control with uncertain data of socially structured compartmental epidemic models". In: *Journal of Mathematical Biology* 82 (2021), pp. 1–41.

[5] Matthieu Alfaro, Henri Berestycki, and Gaël Raoul. "The effect of climate shift on a species submitted to dispersion, evolution, growth, and nonlocal competition". In: *SIAM Journal on Mathematical Analysis* 49.1 (2017), pp. 562–596.

[6] Matthieu Alfaro and Mario Veruete. "Evolutionary branching via replicator–mutator equations". In: *Journal of Dynamics and Differential Equations* 31 (2019), pp. 2029–2052.

[7] Luís Almeida, Pierre-Alexandre Bliman, Grégoire Nadin, Benoît Perthame, and Nicolas Vauchelet. "Final size and convergence rate for an epidemic in heterogeneous populations". In: *Mathematical Models and Methods in Applied Sciences* 31.05 (2021), pp. 1021–1051.

[8] Stefano Almi, Alessandro Baldi, Marco Morandotti, and Francesco Solombrino. "A general perspective on CBO methods with stochastic rate of information". In: *arXiv preprint arXiv:2507.20029* (2025).

[9] Gary An, Qi Mi, Joyeeta Dutta-Moscato, and Yoram Vodovotz. "Agent-based models in translational systems biology". In: *Wiley Interdisciplinary Reviews: Systems Biology and Medicine* 1.2 (2009), pp. 159–171.

[10] Martín Andrade-Restrepo, Nicolas Champagnat, and Régis Ferrière. "Local adaptation, dispersal evolution, and the spatial eco-evolutionary dynamics of invasion". In: *Ecology letters* 22.5 (2019), pp. 767–777.

[11] Pierre Andries, Kazuo Aoki, and Benoit Perthame. "A consistent BGK-type model for gas mixtures". In: *Journal of Statistical Physics* 106.5 (2002), pp. 993–1018.

[12] Aleksandra Ardaševa, Alexander R. A. Anderson, Robert A. Gatenby, Helen M. Byrne, Philip K. Maini, and Tommaso Lorenzi. "Comparative study between discrete and continuum models for the evolution of competing phenotype-structured cell populations in dynamical environments". In: *Physical Review E* 102.4-1 (2020), p. 042404.

[13] Aleksandra Ardaševa, Robert A Gatenby, Alexander RA Anderson, Helen M Byrne, Philip K. Maini, and Tommaso Lorenzi. "Evolutionary dynamics of competing phenotype-structured populations in periodically fluctuating environments". In: *Journal of mathematical biology* 80 (2020), pp. 775–807.

[14] Aleksandra Ardaševa, Robert A. Gatenby, Alexander R.A. Anderson, Helen M. Byrne, Philip K. Maini, and Tommaso Lorenzi. "A mathematical dissection of the adaptation of cell populations to fluctuating oxygen levels". In: *Bulletin of Mathematical Biology* 82.6 (2020), p. 81.

[15] Hans Babovsky and Helmut Neunzert. "On a simulation scheme for the Boltzmann equation". In: *Mathematical methods in the applied sciences* 8.1 (1986), pp. 223–233.

[16] Thomas Bäck, David B. Fogel, and Zbigniew Michalewicz. "Handbook of evolutionary computation". In: *Release* 97.1 (1997), B1.

[17] Malay Banerjee, Alexey Tokarev, and Vitaly Volpert. "Immuno-epidemiological model of two-stage epidemic growth". In: *Mathematical Modelling of Natural Phenomena* 15 (2020), p. 27.

[18] Maria Vittoria Barbarossa and Gergely Röst. "Immuno-epidemiology of a population structured by immune status: a mathematical study of waning immunity and immune system boosting". In: *Journal of mathematical biology* 71.6 (2015), pp. 1737–1770.

[19] Guy Barles, Sepideh Mirrahimi, and Benoît Perthame. "Concentration in Lotka-Volterra parabolic or integral equations: a general convergence result". In: *Methods and Applications of Analysis* 16.(3) (2009).

[20] Alessandro Benfenati, Giacomno Borghi, and Lorenzo Pareschi. "Binary interaction methods for high dimensional global optimization and Machine Learning". In: *Applied Mathematics and Optimization* 86.1 (2022), pp. 9/1–41.

[21] Emanuele Bernardi, Tommaso Lorenzi, Mattia Sensi, and Andrea Tosin. "Heterogeneously Structured Compartmental Models of Epidemiological Systems: From Individual-Level Processes to Population-Scale Dynamics". In: *Studies in Applied Mathematics* 155.2 (2025), e70091.

[22] Emanuele Bernardi, Tommaso Lorenzi, and Andrea Tosin. "Derivation and quasi-invariant asymptotics of phenotype-structured integro-differential models". In: *arXiv preprint arXiv:2510.15646* (2025).

[23] Emanuele Bernardi, Lorenzo Pareschi, Giuseppe Toscani, and Mattia Zanella. "Effects of vaccination efficacy on wealth distribution in kinetic epidemic models". In: *Entropy* 24.2 (2022), p. 216.

[24] Federico Bianchi and Flaminio Squazzoni. "Agent-based models in sociology". In: *Wiley Interdiscip. Rev. Comput. Stat.* 7.4 (2015), pp. 284–306.

[25] Leonora Bianchi, Marco Dorigo, Luca Maria Gambardella, and Walter J. Gutjahr. "A survey on metaheuristics for stochastic combinatorial optimization". In: *Natural Computing* 8.2 (2009), pp. 239–287.

[26] Marzia Bisi. "Some kinetic models for a market economy". In: *Bollettino dell'Unione Matematica Italiana* 10.1 (2017), pp. 143–158.

[27] Marzia Bisi, Laurent Desvillettes, and Giampiero Spiga. "Exponential convergence to equilibrium via Lyapounov functionals for reaction-diffusion equations arising from non reversible chemical kinetics". In: *ESAIM: Mathematical Modelling and Numerical Analysis* 43.1 (2009), pp. 151–172.

[28] Marzia Bisi, Maria Groppi, and Giampiero Spiga. "Kinetic approach to chemically reacting gas mixtures". In: *Modelling and numerics of kinetic dissipative systems* (2006), p. 85.

[29] Marzia Bisi, Maria Groppi, and Giampiero Spiga. "Kinetic Bhatnagar-Gross-Krook model for fast reactive mixtures and its hydrodynamic limit". In: *Physical Review E—Statistical, Nonlinear, and Soft Matter Physics* 81.3 (2010), p. 036327.

[30] Marzia Bisi and Silvia Lorenzani. "Mathematical models for the large spread of a contact-based infection: a statistical mechanics approach". In: *Journal of Nonlinear Science* 34.84 (2024), pp. 1–44.

[31] Marzia Bisi and Nadia Loy. "Kinetic models for systems of interacting agents with multiple microscopic states". In: *Physica D: Nonlinear Phenomena* 457 (2024), p. 133967.

[32] Christian Blum and Andrea Roli. "Metaheuristics in combinatorial optimization: Overview and conceptual comparison". In: *ACM computing surveys (CSUR)* 35.3 (2003), pp. 268–308.

[33] Ludwig Boltzmann. "Weitere Studien über das Wärmegleichgewicht unter Gasmolekülen". In: *Kinetische Theorie II. WTB Wissenschaftliche Taschenbücher*. Wiesbaden: Vieweg+Teubner Verlag, (1970).

[34] Raul Borsche, Axel Klar, and Mattia Zanella. "Kinetic-controlled hydrodynamics for multilane traffic models". In: *Physica A: Statistical Mechanics and its Applications* 587 (2022), p. 126486.

[35] Thomas Borsoni, Marzia Bisi, and Maria Groppi. "A general framework for the kinetic modelling of polyatomic gases". In: *Communications in Mathematical Physics* 393.1 (2022), pp. 215–266.

[36] Laurent Boudin and Francesco Salvarani. "Opinion dynamics: Kinetic modelling with mass media, application to the Scottish independence referendum". In: *Physica A: Statistical Mechanics and its Applications* 444 (2016), pp. 448–457.

[37] Jean-Baptiste Burie, Ramsès Djidjou-Demasse, and Arnaud Ducrot. "Slow convergence to equilibrium for an evolutionary epidemiology integro-differential system". In: *Discrete and Continuous Dynamical Systems-Series B, American Institute of Mathematical Sciences* 25.6 (2020), pp. 2223–2243.

[38] Stavros N. Busenberg, Mimmo Iannelli, and Horst R. Thieme. "Global behavior of an age-structured epidemic model". In: *SIAM Journal on Mathematical Analysis* 22.4 (1991), pp. 1065–1080.

[39] Giuseppe C. Calafiore, Carlo Novara, and Corrado Possieri. "A time-varying SIRD model for the COVID-19 contagion in Italy". In: *Annual reviews in control* 50 (2020), pp. 361–372.

[40] Àngel Calsina and Sílvia Cuadrado. "Small mutation rate and evolutionarily stable strategies in infinite dimensional adaptive dynamics". In: *Journal of mathematical Biology* 48.2 (2004), pp. 135–159.

[41] Àngel Calsina, Sílvia Cuadrado, Laurent Desvillettes, and Gaël Raoul. "Asymptotics of steady states of a selection–mutation equation for small mutation rate". In: *Proceedings of the Royal Society of Edinburgh Section A: Mathematics* 143.6 (2013), pp. 1123–1146.

[42] Nicolò Cangiotti, Marco Capolli, Mattia Sensi, and Sara Sottile. "A survey on Lyapunov functions for epidemic compartmental models". In: *Bollettino dell'Unione Matematica Italiana* 17.2 (2024), pp. 241–257.

[43] José A. Carrillo, Y.-P. Choi, C. Totzeck, and O. Tse. "An analytical framework for consensus-based global optimization method". In: *Mathematical Models and Methods in Applied Sciences* 28.6 (2018), pp. 1037–1066.

[44] José A. Carrillo, Massimo Fornasier, Jesús Rosado, and Giuseppe Toscani. "Asymptotic flocking dynamics for the kinetic Cucker–Smale model". In: *SIAM Journal on Mathematical Analysis* 42.1 (2010), pp. 218–236.

[45] José A. Carrillo, Massimo Fornasier, Giuseppe Toscani, and Francesco Vecil. "Particle, kinetic, and hydrodynamic models of swarming". In: *Mathematical modeling of collective behavior in socio-economic and life sciences*. Springer, (2010), pp. 297–336.

[46] José A. Carrillo, Shi Jin, Lei Li, and Yuhua Zhu. "A consensus-based global optimization method for high dimensional machine learning problems". In: *ESAIM: Control, Optimisation and Calculus of Variations* 27 (2021), S5.

[47] Nicolas Champagnat, Régis Ferrière, and Sylvie Méléard. "Individual-based probabilistic models of adaptive evolution and various scaling approximations". In: *Seminar on Stochastic Analysis, Random Fields and Applications V: Centro Stefano Franscini, Ascona, May 2005*. Springer. (2005), pp. 75–113.

[48] Nicolas Champagnat, Régis Ferrière, and Sylvie Méléard. "Individual-based probabilistic models of adaptive evolution and various scaling approximations". In: *Seminar on Stochastic Analysis, Random Fields and Applications V: Centro Stefano Franscini, Ascona, May 2005*. Springer. (2008), pp. 75–113.

[49] Nicolas Champagnat, Régis Ferrière, and Sylvie Méléard. "Unifying evolutionary dynamics: from individual stochastic processes to macroscopic models". In: *Theoretical population biology* 69.3 (2006), pp. 297–321.

[50] Nicolas Champagnat and Sylvie Méléard. "Invasion and adaptive evolution for individual-based spatially structured populations". In: *Journal of Mathematical Biology* 55.2 (2007), pp. 147–188.

[51] Nicolas Champagnat, Sylvie Méléard, Sepideh Mirrahimi, and Viet C. Tran. "Filling the gap between individual-based evolutionary models and Hamilton-Jacobi equations". In: *Journal de l'École polytechnique—Mathématiques* 10 (2023), pp. 1247–1275.

[52] Rebecca H. Chisholm, Tommaso Lorenzi, Laurent Desvillettes, and Barry D. Hughes. "Evolutionary dynamics of phenotype-structured populations: from individual-level mechanisms to population-level consequences". In: *Zeitschrift für angewandte Mathematik und Physik* 67 (2016), pp. 1–34.

[53] Rebecca H. Chisholm, Tommaso Lorenzi, and Alexander Lorz. "Effects of an advection term in nonlocal Lotka-Volterra equations". In: *Communications in mathematical sciences* 14.4 (2016), pp. 1181–1188.

[54] Stephane Cordier, Lorenzo Pareschi, and Giuseppe Toscani. "On a kinetic model for a simple market economy". In: *Journal of Statistical Physics* 120.1 (2005), pp. 253–277.

[55] Emiliano Cristiani, Nadia Loy, Marta Menci, and Andrea Tosin. "Kinetic description and macroscopic limit of swarming dynamics with continuous leader–follower transitions". In: *Mathematics and Computers in Simulation* 228 (2025), pp. 362–385.

[56] Felipe Cucker and Steve Smale. "On the mathematics of emergence". In: *Japanese Journal of Mathematics* 2.1 (2007), pp. 197–227.

[57] Mathew P. Dafilis, Federico Frascoli, James G. Wood, and James M. McCaw. "The influence of increasing life expectancy on the dynamics of SIRS systems with immune boosting". In: *The ANZIAM Journal* 54.1-2 (2012), pp. 50–63.

[58] Pierre Degond, Amic Frouvelle, and Gaël Raoul. "Local stability of perfect alignment for a spatially homogeneous kinetic model". In: *Journal of Statistical Physics* 157.1 (2014), pp. 84–112.

[59] Marcello Delitala and Tommaso Lorenzi. "Asymptotic dynamics in continuous structured populations with mutations, competition and mutualism". In: *Journal of Mathematical Analysis and Applications* 389.1 (2012), pp. 439–451.

[60] Rossella Della Marca, Nadia Loy, and Andrea Tosin. "An SIR-like kinetic model tracking individuals' viral load". In: *arXiv preprint arXiv:2106.14480* (2021).

[61] Amir Dembo and Ofer Zeitouni. "Large Deviations Techniques and Applications". In: *Springer Science and Business Media* 38 (2009).

[62] Laurent Desvillettes, Pierre-Emmanuel Jabin, Stéphane Mischler, and Gaël Raoul. "On selection dynamics for continuous structured populations". In: *Communications in Mathematical Sciences* 6.3 (2008), pp. 729–747.

[63] Odo Diekmann. "A beginners guide to adaptive dynamics". In: *Banach Center Publications* 63.1 (2002), pp. 47–86.

[64] Odo Diekmann, Hans J.A.P. Heesterbeek, and Johan A.J. Metz. "On the definition and the computation of the basic reproduction ratio R_0 in models for infectious diseases in heterogeneous populations". In: *Journal of mathematical biology* 28 (1990), pp. 365–382.

[65] Odo Diekmann, Hans J.A.P. Heesterbeek, and Michael G. Roberts. "The construction of next-generation matrices for compartmental epidemic models". In: *Journal of the royal society interface* 7.47 (2010), pp. 873–885.

[66] Odo Diekmann, Pierre-Emanuel Jabin, Stéphane Mischler, and Benoît Perthame. "The dynamics of adaptation: an illuminating example and a Hamilton–Jacobi approach". In: *Theoretical population biology* 67.4 (2005), pp. 257–271.

[67] Giacomo Dimarco, Lorenzo Pareschi, Giuseppe Toscani, and Mattia Zanella. "Wealth distribution under the spread of infectious diseases". In: *Physical Review E* 102.2 (2020), p. 022303.

[68] Giacomo Dimarco, Benoît Perthame, Giuseppe Toscani, and Mattia Zanella. "Kinetic models for epidemic dynamics with social heterogeneity". In: *Journal of Mathematical Biology* 83.1 (2021), p. 4.

[69] Teresa Donateo. "Gli Algoritmi Genetici". In: *Quaderni del Dipartimento di Matematica dell'Università del Salento*. Vol. 2. Dipartimento di Matematica dell'Università del Salento, (2004), pp. 187–203.

[70] Bertram Düring, Daniel Matthes, and Giuseppe Toscani. "A Boltzmann-type approach to the formation of wealth distribution curves". In: *Rivista di Matematica dell'Università di Parma* 8.1 (2009), pp. 199–261.

[71] Bertram Düring and Marie-Therese Wolfram. "Opinion dynamics: inhomogeneous Boltzmann-type equations modelling opinion leadership and political segregation". In: *Proceedings of the Royal Society A: Mathematical, Physical and Engineering Sciences* 471.2182 (2015), pp. 20150345/1–21.

[72] Christian Engwer, Thomas Hillen, Markus Knappitsch, and Christina Surulescu. "Glioma follow white matter tracts: a multiscale DTI-based model". In: *Journal of mathematical biology* 71.3 (2015), pp. 551–582.

[73] Radek Erban and Hans G. Othmer. "From individual to collective behavior in bacterial chemotaxis". In: *SIAM Journal on Applied Mathematics* 65.2 (2004), pp. 361–391.

[74] Gissell Estrada-Rodriguez and Tommaso Lorenzi. "Macroscopic limit of a kinetic model describing the switch in T cell migration modes via binary interactions". In: *European Journal of Applied Mathematics* 34.1 (2023), pp. 1–27.

[75] Joaquin Fontbona and Sylvie Méléard. "Non local Lotka-Volterra system with cross-diffusion in an heterogeneous medium". In: *Journal of mathematical biology* 70.4 (2015), pp. 829–854.

[76] Massimo Fornasier, Timo Klock, and Konstantin Riedl. "Consensus-based optimization methods converge globally". In: *SIAM Journal on Optimization* 34.3 (2024), pp. 2973–3004.

[77] Massimo Fornasier and Lukang Sun. "A PDE framework of consensus-based optimization for objectives with multiple global minimizers". In: *Communications in Partial Differential Equations* 50.4 (2025), pp. 493–541.

[78] Stephanie Forrest. "Genetic algorithms". In: *ACM computing surveys (CSUR)* 28.1 (1996), pp. 77–80.

[79] Martina Fraia, Nadia Loy, and Andrea Tosin. "Linear inelastic kinetic equations modelling the spread of fake news and its interplay with personal awareness". In: *arXiv preprint arXiv:2501.01965* (2024).

[80] Viktoria Freingruber, Tommaso Lorenzi, Kevin J. Painter, and Mariya Ptashnyk. "Trait-structured chemotaxis: Exploring ligand-receptor dynamics and travelling wave properties in a Keller-Segel model". In: *arXiv preprint arXiv:2502.18947* (2025).

[81] Alberto Gandolfi, Andrea Pugliese, and Carmela Sinisgalli. "Epidemic dynamics and host immune response: a nested approach". In: *Journal of mathematical biology* 70 (2015), pp. 399–435.

[82] Jimmy Garnier, Olivier Cotto, Emeric Bouin, Thibault Bourgeron, Thomas Lepoutre, Ophélie Ronce, and Vincent Calvez. "Adaptation of a quantitative trait to a changing environment: new analytical insights on the asexual and infinitesimal sexual models". In: *Theoretical Population Biology* 152 (2023), pp. 1–22.

[83] Michel Gendreau, Jean-Yves Potvin, et al. *Handbook of metaheuristics*. Vol. 2. Springer, (2010).

[84] Nicolai Jurek Gerber, Franca Hoffmann, and Urbain Vaes. "Mean-field limits for consensus-based optimization and sampling". In: *ESAIM: Control, Optimisation and Calculus of Variations* 31 (2025), p. 74.

[85] Maria Groppi and Jacek Polewczak. "On two kinetic models for chemical reactions: comparisons and existence results". In: *Journal of statistical physics* 117.1 (2004), pp. 211–241.

[86] Maria Groppi and Giampiero Spiga. "Kinetic approach to chemical reactions and inelastic transitions in a rarefied gas". In: *Journal of Mathematical chemistry* 26.1 (1999), pp. 197–219.

[87] Seung-Yeal Ha and Eitan Tadmor. "From particle to kinetic and hydrodynamic descriptions of flocking". In: *arXiv preprint arXiv:0806.2182* (2008).

[88] François Hamel, Florian Lavigne, Guillaume Martin, and Lionel Roques. "Dynamics of adaptation in an anisotropic phenotype-fitness landscape". In: *Nonlinear Analysis: Real World Applications* 54 (2020), p. 103107.

[89] John H. Holland. "Adaptation in natural and artificial systems". In: *University of Michigan Press google schola* 2 (1975), pp. 29–41.

[90] Richard A. Holley, Shigeo Kusuoka, and Daniel W. Stroock. "Asymptotics of the spectral gap with applications to the theory of simulated annealing". In: *Journal of Functional Analysis* 83.2 (1989), pp. 333–347.

[91] Richard A. Holley and Daniel Stroock. "Simulated annealing via Sobolev inequalities". In: *Communications in Mathematical Physics* 115.4 (1988), pp. 553–569.

[92] Hui Huang and Jinniao Qiu. "On the mean-field limit for the consensus-based optimization". In: *Mathematical Methods in the Applied Sciences* 45.12 (2022), pp. 7814–7831.

[93] Jisca Huisman and Jarle Tufto. "Comparison of non-Gaussian quantitative genetic models for migration and stabilizing selection". In: *Evolution* 66.11 (2012), pp. 3444–3461.

[94] Giovanni Lo Iacono, Frank van den Bosch, and Neil Paveley. "The evolution of plant pathogens in response to host resistance: factors affecting the gain from deployment of qualitative and quantitative resistance". In: *Journal of theoretical biology* 304 (2012), pp. 152–163.

[95] Hisashi Inaba. *Age-structured population dynamics in demography and epidemiology*. Vol. 1. 1. Springer, (2017).

[96] Hisashi Inaba. "Threshold and stability results for an age-structured epidemic model". In: *Journal of mathematical biology* 28 (1990), pp. 411–434.

[97] Pierre-Emmanuel Jabin and Gaël Raoul. "On selection dynamics for competitive interactions". In: *Journal of mathematical biology* 63.3 (2011), pp. 493–517.

[98] Hildeberto Jardon-Kojakhmetov, Christian Kuehn, Andrea Pugliese, and Mattia Sensi. "A geometric analysis of the SIR, SIRS and SIRWS epidemiological models". In: *Nonlinear Analysis: Real World Applications* 58 (2021), p. 103220.

[99] Panagiotis Kaklamanos, Andrea Pugliese, Mattia Sensi, and Sara Sottile. "A geometric analysis of the SIRS model with secondary infections". In: *SIAM Journal on Applied Mathematics* 84.2 (2024), pp. 661–686.

[100] Sourabh Katoch, Sumit S. Chauhan, and Vijay Kumar. "A review on genetic algorithm: past, present, and future". In: *Multimedia tools and applications* 80.5 (2021), pp. 8091–8126.

[101] James Kennedy. "Particle Swarm Optimization". In: *Encyclopedia of Machine Learning*. Springer, (2010), pp. 760–766.

[102] James Kennedy and Russell Eberhart. "Particle swarm optimization". In: *Proceedings of ICNN'95-international conference on neural networks*. Vol. 4. IEEE. (1995), pp. 1942–1948.

[103] William O. Kermack and Anderson G. McKendrick. "A contribution to the mathematical theory of epidemics". In: *Proceedings of the royal society of london. Series A, Containing papers of a mathematical and physical character* 115.772 (1927), pp. 700–721.

[104] Annu Lambora, Kunal Gupta, and Kriti Chopra. "Genetic algorithm-A literature review". In: *2019 international conference on machine learning, big data, cloud and parallel computing (COMITCon)*. IEEE. (2019), pp. 380–384.

[105] Hélène Leman. "Convergence of an infinite dimensional stochastic process to a spatially structured trait substitution sequence". In: *Stochastics and Partial Differential Equations: Analysis and Computations* 4.4 (2016), pp. 791–826.

[106] Tommaso Lorenzi, Nadia Loy, and Chiara Villa. "Phenotype-structuring of non-local kinetic models of cell migration driven by environmental sensing". In: *arXiv preprint arXiv:2412.16258* (2024).

[107] Tommaso Lorenzi, Fiona R. Macfarlane, and Kevin J. Painter. "Derivation and travelling wave analysis of phenotype-structured haptotaxis models of cancer invasion". In: *European Journal of Applied Mathematics* 36.2 (2025), pp. 231–263.

[108] Tommaso Lorenzi, Anna Marciniak-Czochra, and Thomas Stiehl. "A structured population model of clonal selection in acute leukemias with multiple

maturation stages". In: *Journal of mathematical biology* 79.5 (2019), pp. 1587–1621.

[109] Tommaso Lorenzi, Kevin J. Painter, and Chiara Villa. "Phenotype structuring in collective cell migration: a tutorial of mathematical models and methods". In: *Journal of Mathematical Biology* 90.6 (2025), p. 61.

[110] Tommaso Lorenzi, Elisa Paparelli, and Andrea Tosin. "Modelling coevolutionary dynamics in heterogeneous SI epidemiological systems across scales". In: *Communications in Mathematical Sciences* 22.8 (2024), pp. 2131–2165.

[111] Tommaso Lorenzi and Camille Pouchol. "Asymptotic analysis of selection-mutation models in the presence of multiple fitness peaks". In: *Nonlinearity* 33.11 (2020), p. 5791.

[112] Tommaso Lorenzi, Andrea Pugliese, Mattia Sensi, and Agnese Zardini. "Evolutionary dynamics in an SI epidemic model with phenotype-structured susceptible compartment". In: *Journal of Mathematical Biology* 83.6 (2021), p. 72.

[113] Alexander Lorz, Tommaso Lorenzi, Michael E. Hochberg, Jean Clairambault, and Benoît Perthame. "Populational adaptive evolution, chemotherapeutic resistance and multiple anti-cancer therapies". In: *ESAIM: Mathematical Modelling and Numerical Analysis* 47.2 (2013), pp. 377–399.

[114] Alexander Lorz, Sepideh Mirrahimi, and Benoît Perthame. "Dirac mass dynamics in multidimensional nonlocal parabolic equations". In: *Communications in Partial Differential Equations* 36.6 (2011), pp. 1071–1098.

[115] Alexander Lorz and Benoît Perthame. "Long-term behaviour of phenotypically structured models". In: *Proceedings of the Royal Society A: Mathematical, Physical and Engineering Sciences* 470.2167 (2014), p. 20140089.

[116] Nadia Loy and Andrea Tosin. ""Boltzmann-type equations for multi-agent systems with label switching". In: *Kinetic and Related Models* 14.5 (2021), p. 867.

[117] Nadia Loy and Andrea Tosin. "A viral load-based model for epidemic spread on spatial networks". In: *Mathematical Biosciences and Engineering* 18.5 (2021), pp. 5635–5663.

[118] Nadia Loy and Andrea Tosin. "Essentials of the kinetic theory of multi-agent systems". In: *arXiv preprint arXiv:2503.11554* (2025).

[119] Jingcheng Lu, Eitan Tadmor, and Anil Zenginoglu. "Swarm-based gradient descent method for non-convex optimization". In: *Communications of the American Mathematical Society* 4.17 (2024), pp. 787–822.

[120] Fiona R. Macfarlane, Xinran Ruan, and Tommaso Lorenzi. "Individual-based and continuum models of phenotypically heterogeneous growing cell populations". In: *arXiv preprint arXiv:2202.06583* (2022).

[121] Medicina per Tutti. *Tessuto pigmentato*. Accesso: 13 agosto 2025. 2025. URL: `https://www.medicinapertutti.it/argomento/tessuto-pigmentato/`.

[122] Sepideh Mirrahimi, Benoît Perthame, and Joe Y. Wakano. "Direct competition results from strong competition for limited resource". In: *Journal of Mathematical Biology* 68.4 (2013), pp. 931–949.

[123] Dragoslav S. Mitrinovic, Josip E. Pecaric, and Andreas M. Fink. "Inequalities involving functions and their derivatives". In: *Mathematics and its applications, Kluwer Academic Publishers, Dordrecht-Boston-London* (1991).

[124] Kenichi Nanbu. "Direct simulation scheme derived from the Boltzmann equation. I. Monocomponent gases". In: *Journal of the Physical Society of Japan* 49.5 (1980), pp. 2042–2049.

[125] National Cancer Institute. *Layers of the Skin*. Accesso: 13 agosto 2025. 2025. URL: `https://training.seer.cancer.gov/melanoma/anatomy/layers.html`.

[126] Suzanne M. O'Regan, Thomas C. Kelly, Andrei Korobeinikov, Michael J.A. O'Callaghan, and Alexei V. Pokrovskii. "Lyapunov functions for SIR and SIRS epidemic models". In: *Applied mathematics letters* 23.4 (2010), pp. 446–448.

[127] Lorenzo Pareschi and Giovanni Russo. "An introduction to Monte Carlo method for the Boltzmann equation". In: *ESAIM: Proceedings*. Vol. 10. EDP Sciences. (2001), pp. 35–75.

[128] Lorenzo Pareschi and Giovanni Russo. "Time relaxed Monte Carlo methods for the Boltzmann equation". In: *SIAM Journal on Scientific Computing* 23.4 (2001), pp. 1253–1273.

[129] Lorenzo Pareschi and Giuseppe Toscani. *Interacting multiagent systems: kinetic equations and Monte Carlo methods*. OUP Oxford, (2013).

[130] Benoît Perthame. "Mathematical tools for kinetic equations". In: *Bulletin of the American Mathematical Society* 41.2 (2004), pp. 205–244.

[131] Benoît Perthame. *Transport equations in biology*. Springer Science & Business Media, (2006).

[132] René Pinnau, Claudia Totzeck, Oliver Tse, and Stephan Martin. "A consensus-based model for global optimization and its mean-field limit". In: *Mathematical Models and Methods in Applied Sciences* 27.01 (2017), pp. 183–204.

[133] Riccardo Poli, James Kennedy, and Tim Blackwell. "Swarm intelligence". In: *Particle Swarm Optim* 1.1 (2007), pp. 33–57.

[134] Camille Pouchol and Emmanuel Trélat. "Global stability with selection in integro-differential Lotka-Volterra systems modelling trait-structured populations". In: *Journal of Biological Dynamics* 12.1 (2018), pp. 872–893.

[135] Ilya Prigogine and Fred C. Andrews. "A Boltzmann-like approach for traffic flow". In: *Operations Research* 8.6 (1960), pp. 789–797.

[136] Gaël Raoul. "Exponential convergence to a steady-state for a population genetics model with sexual reproduction and selection". In: *arXiv preprint arXiv:2104.06089* (2021).

[137] Gaël Raoul. "Macroscopic limit from a structured population model to the Kirkpatrick-Barton model". In: *Bulletin des Sciences Mathématiques* (2025), p. 103697.

[138] Lionel Roques, Florian Patout, Olivier Bonnefon, and Guillaume Martin. "Adaptation in general temporally changing environments". In: *SIAM Journal on Applied Mathematics* 80.6 (2020), pp. 2420–2447.

[139] Paul D. Sniegowski and Philip J. Gerrish. "Beneficial mutations and the dynamics of adaptation in asexual populations". In: *Philosophical Transactions of the Royal Society B: Biological Sciences* 365.1544 (2010), pp. 1255–1263.

[140] Horst R. Thieme. "Spectral bound and reproduction number for infinite-dimensional population structure and time heterogeneity". In: *SIAM journal on Applied Mathematics* 70.1 (2009), pp. 188–211.

[141] Giuseppe Toscani. "Kinetic models of opinion formation". In: *Communications in Mathematical Sciences* 4.3 (2006), pp. 481–496.

[142] Andrea Tosin and Mattia Zanella. "Kinetic-controlled hydrodynamics for traffic models with driver-assist vehicles". In: *Multiscale Modeling and Simulation* 17.2 (2019), pp. 716–749.

[143] Claudia Totzeck. "Trends in consensus-based optimization". In: *Active Particles, Volume 3: Advances in Theory, Models, and Applications*. Springer, (2021), pp. 201–226.

[144] Pauline Van den Driessche and James Watmough. "Reproduction numbers and sub-threshold endemic equilibria for compartmental models of disease transmission". In: *Mathematical biosciences* 180.1-2 (2002), pp. 29–48.

[145] Vladimir M Veliov. "On the effect of population heterogeneity on dynamics of epidemic diseases". In: *Journal of mathematical biology* 51.2 (2005), pp. 123–143.

[146] Darrell Whitley. "A genetic algorithm tutorial". In: *Statistics and computing* 4.2 (1994), pp. 65–85.